**Design, Optimization and Prototype Verification of A Novel Wearable Rigid-Flexible Lower Limb Rehabilitation Exoskeleton for Stroke Patients**

Gao, Meng

*Awarding institution:*
King's College London

# Design, Optimization and Prototype Verification of A Novel Wearable Rigid-Flexible Lower Limb Rehabilitation Exoskeleton for Stroke Patients

**King's College London**

**Meng Gao**

Supervisor: Prof. Jian S. Dai

Prof. Hongbin Liu

The Department of Engineering

King's College London

This dissertation is submitted for the degree of

*Doctor of Philosophy*

September 2023

# Declaration

I hereby declare that except where specific reference is made to the work of others, the contents of this dissertation are original and have not been submitted in whole or in part for consideration for any other degree or qualification in this, or any other university. This dissertation is my own work and contains nothing which is the outcome of work done in collaboration with others, except as specified in the text and Acknowledgements. This dissertation contains fewer than 65,000 words including appendices, bibliography, footnotes, tables and equations and has fewer than 150 figures.

Meng Gao

September 2023

# Acknowledgments

I would like to express my sincere appreciation to all those who have supported me throughout the research process and the completion of this paper.

Firstly, I would like to express my deepest gratitude to my supervisor, the fellow of the Royal Academy of Engineering, Prof. Jian S. Dai. I am honored to be one Ph.D. student of such a knowledgeable, elegant and considerate professor during this period. The determination and smooth progress of my Ph.D. research are entirely due to his invaluable guidance, patience, and support throughout this project. His insightful views and attitudes have helped me stay on track and produce work that I am proud of. His expertise in the field has enabled me to explore complex concepts and apply them to my research with confidence. Especially in the past three years, the rampant spread of the COVID-19 has seriously affected my progress in research. It is the help and endless guidance from Professor Dai that have enabled me to successfully complete my research tasks. In addition, his concern for us is not limited to the research direction, he helped us to find laboratories that we could use, guided us in planning our research during the COVID-19, and showed us how to successfully work remotely. Besides, he often educates us on how to be a outstanding researcher and how to do distinctive things. In a word, he is not only my supervisor during my PhD period but also a guide in my life in the last four years.

I would also like to extend my gratitude to the participants who generously gave their time and shared their experiences with me. In particular, I would like to thank Zhuo Chen, Tun Wang, and Yanhua Lin for their thoughtful comments and suggestions, which significantly enhanced the final outcome of the study. They were not only the project collaborators after I joined Professor Dai's team, but also the closest friends during my time living in London. Without their willingness to participate, this study can not have been possible. Their contributions have provided valuable insights into the subject matter and have helped me develop a more nuanced understanding of the topic at hand.

Furthermore, I would like to thank Kun Wang, Guanglu Jia, Junpeng Chen, Jinghui He, Xinyu Xiao and Mi Li for their help with this project. Their suggestions greatly improved the clarity and coherence of the thesis. They are a group of friends that I followed with Professor Dai at the SUSTech Institute of Robotics. They not only have strong academic abilities, but also be friendly in their extracurricular activities. Their attention to project

details and constructive criticism helped me refine my arguments and presented them in a convincing manner.

I am also grateful to my friends who provided valuable feedback and support throughout the process. Their input and encouragement were essential in shaping my ideas and improving the quality of my work.

Finally, I would like to express my heartfelt appreciation to my family for their unwavering love and support. Their encouragement and belief in me have been instrumental in helping me pursue my academic goals and complete this project. I am also grateful to my friends for their patience and understanding during times when the demands of the research process were challenging.

In conclusion, I would like to express my gratitude to everyone who has contributed to this research project and my academic journey. The insights gained through this project will undoubtedly be invaluable as I continue to pursue my academic and professional goals. Thank you all for your contributions to this work.

# Abstract

The novel lower limb rehabilitation exoskeleton mechanism proposed in this thesis is primarily designed with a focus on stroke patients and other individuals suffering from lower limb injuries. It aims to provide assistance in rehabilitation to patients and relieve working pressure of therapists, while ensuring that patients can independently carry out rehabilitation exercises in domestic. According to the latest report by the World Stroke Organization (WSO), stroke is a neurological injury that ranks as the second leading cause of death and the third leading cause of disability-adjusted life years globally. Stroke patients commonly suffer from hemiplegia or partial paralysis, resulting in substantial impairments to the functionality of their upper and lower limbs, greatly impacting their ability to perform daily activities. While traditional manual physical rehabilitation therapy can contribute to motor recovery and alleviate functional impairments, it presents challenges in terms of cost for patients and demands on therapists, with varying effectiveness among individuals. In contrast, medical service robots offer a cost-effective alternative by providing automated, scientific, and quantifiable training exercises.

The objective of this thesis is to propose an effective rehabilitation mechanism for facilitating lower limb recovery in stroke patients, ultimately enabling them to regain their ability to perform normal daily activities and enhance their overall quality of life. Existing lower limb rehabilitation systems are often characterized by their simplicity and limited functionality, which hinders patients from accessing highly flexible treatment options. Prolonged incorrect usage of such systems can lead to secondary damage to the musculoskeletal system. Therefore, the central theme of this article is to propose a lower limb rehabilitation structure that offers diversified motion functionalities and adaptive capabilities. Additionally, the aim is to achieve the objective of force buffering during the rehabilitation process. Furthermore, future enhancements to this article will entail multiple iterations and optimization updates to the proposed rehabilitation structure.

The primary rehabilitation joints encompass the hip, knee, ankle, and toe joints, which facilitate both active and passive movements for rehabilitation. Drawing upon human anatomy theory and considering the distinct functions of each joint, a novel and mechanically adaptive design for the lower limb rehabilitation structure is proposed. The feasibility and accuracy of the design are evaluated through structural modeling using Solidworks and

motion simulation using Adams, allowing for an exploration of the impact of human-robot interaction and optimization goals. The research findings offer viable solutions for stroke patients to regain their autonomous adaptive abilities, thereby fostering the advancement of portable wearable lower limb rehabilitation devices and medical rehabilitation institutions. The specific research contents encompass the following aspects:

Firstly, leveraging the Motion Capture System gait experiment platform, the natural motion cycle of the human body is captured to establish the rehabilitation trajectory for the lower limb structure. This involves capturing the movement of the center of gravity for each lower limb segment, changes in motion velocity, and angles of flexion for the waist, thigh, calf, sole, hip joint, knee joint, toe joint, among others. These data provide valuable guidance for the design of the lower limb rehabilitation structure.

Secondly, a pioneering ankle joint configuration with buffering and adaptive capabilities is devised and subjected to simulation. Drawing inspiration from the mechanics of human ankle joint movement, a rehabilitation structure incorporating elastic components is proposed to enable continuous energy storage and release within the ankle joint. This approach leads to reduced motor energy consumption, improved autonomous flexibility, and enhanced shock resistance. Moreover, the design emphasizes the significance of toe rehabilitation exercises, facilitating active and passive rehabilitation training for the toe joint. The inclusion of elastic components in the ankle rehabilitation mechanism enhances its adaptability to external environments and promotes stability during human-robot interaction.

Next, a groundbreaking combination of rigidity and flexibility is employed in the design and simulation of an adaptive knee joint configuration. By considering the specific characteristics of ankle joint rotation, a solution that acts on the lateral side of the knee joint is proposed. This innovative approach utilizes rope-driven motion, mitigating the limitations associated with bulky, heavy, and cumbersome purely rigid structures. It also optimizes workspace utilization and accommodates human movement more effectively. The incorporation of torsion springs and other flexible components enhances the overall flexibility of the mechanism. To ensure collision avoidance between components and force uniformity, the PSO optimization algorithm in conjunction with MATLAB software is introduced. Additionally, the introduction of a novel clutch facilitates greater flexibility in rope drive, enabling the mechanism to achieve different rehabilitation movements during walking and sitting.

Furthermore, a cutting-edge design for hip joint rehabilitation structure is introduced, utilizing cam motion as a replacement for traditional rotation. Drawing insights from the hip joint's motion during the gait cycle, a two-degree-of-freedom mechanism design is primarily proposed. This structure facilitates the swinging motion of the lower limb while also accommodating subtle vertical deviations of the buttocks throughout the process. By

enhancing the adaptability of the hip joint and reducing the risk of secondary injuries, this innovative design offers improved functionality and safety.

Lastly, the development of the lower limb exoskeleton is completed with the creation of a prototype and functional verification. This entails careful material and motor selection, determination of torsion spring parameters, and validation of the feasibility of human-robot interaction capabilities. Through a series of tests and experiments, the results confirm that the overall prototype successfully meets the design requirements for multiple motion functionalities, as intended.

In conclusion, the overall lower limb rehabilitation system proposed in this article aligns with our initial vision. It combines active and passive elements, incorporates a combination of rigidity and flexibility, and incorporates the use of elastic components for cushioning. In a word, this rehabilitation exoskeleton effectively enables stroke patients to independently engage in rehabilitation training at home, thereby reducing both the financial burden on patients and the time pressure on therapists.

Keyword: Lower Limb Rehabilitation Mechanism; Self-alignment; Flexible-Rigid Structure; Human Anatomy; Human-Machine Interaction

# Table of contents

# List of figures

17

# List of tables

# Nomenclature

**Roman Symbols**

$(^iR^jR)_N$  2R spherical sub-chain with its two rotational axes intersect at point $N$

$(^iR^jR^kR)_N$  3R spherical sub-chain with its three rotational axes intersect at point $N$

$\alpha_k$     the rotational angle of the knee joint during flexion-extension

$\beta_k$      the rotational angle of the ankle joint during inversion-eversion

$\Delta x$     the deformation of the dynamic platform under external force

$\lambda_{max}$  the maximum eigenvalues obtained by the Jacobian matrix

$\lambda_{min}$  the minimum eigenvalues obtained by the Jacobian matrix

$k(J)$     the condition number

$S^r_{aj}$     the jth reciprocal screw or constraint-screw

$S^r_a$      the constraint-screw system

$A_0$      point in the coordinate system

$a_1$      the expression for the position vector

$a_h, a_t$   acceleration of ankle rotation

$a_t x$    acceleration along the $x$ direction as the tip of the foot lifts off the ground

$a_t y$    Acceleration along the $y$ direction as the tip of the foot lifts off the ground

$B$      the damping coefficient

$b_1$      the expression for the position vector

$C_0$      point in the coordinate system

$D_2$      the dividing circle diameter of the output gear

$D_m$      pitch diameter

$d_w$      wire diameter

$e$      the back electromotive force

$E_s$      modulus of steel wire

$E_0$      point $E_0$ in the coordinate system

$E_m$      momentum

$F$      force

$F_e$      the external force acting on the dynamic platform

$F_{ha,x0}$      the load on point $A$ in the $x_0$ direction

$F_{ha,y0}$      the load on point $A$ in the $y_0$ direction

$F_{ta,x0}$      the load on point $A$ in the $x_0$ direction

$F_{ta,y0}$      the load on point $A$ in the $y_0$ direction

$F_{td,x0}$      the load on point $d$ in the $x_0$ direction

$F_{td,y0}$      the load on point $d$ in the $y_0$ direction

$g$      gravity acceleration

$H$      height in centimeters

$H_f$      height of the ankle joint from the sole of the foot

$I$      moment of inertia

$i_a$      the current flowing through the motor winding

$k_b$      the back electromotive force constant

$k_c$      the equivalent spring constant of the mechanism

$K_s$      the stiffness matrix of the mechanism

$k_1$      the torque constant

$K_\beta = 1$   load ddistribution coefficient

$K_A$      use coefficient

$K_s$      the load for each $1°$ increase of torsion spring

$K_V$     dynamic load coefficient

$L$       the motor inductance

$l_0$       horizontal distance between the center of mass of the foot and the ankle joint

$L_f$      the length of the foot

$l_i$       the length of the actuator

$L_m$     angular momentum

$l_{AB_0}$   length of edge $AB_0$ in triangle $\Delta ABC$

$l_{AB}$   length of edge $AB$ in triangle $\Delta ABC$

$l_{CB_0}$   length of edge $CB_0$ in triangle $\Delta ABC$

$l_{CB}$   length of edge $CB$ in triangle $\Delta ABC$

$L_{EC0}$   one side of triangle formed by $C$, $C_0$ and $E$

$L_{EC}$   one side of triangle formed by $C$, $C_0$ and $E$

$L_{EE0}$   one side of triangle formed by $C$, $C_0$ and $E$

$M_c$    space position of the center of mass

$m_f$    weight of foot

$m_p$    mass of patients

$N$      total winding number

$S_n$     the number of active chains

$O$      original point

$O_{c1}$    the center of the cam

$O_{c1}H_a$  the mathematical relationship of the force arm

| | |
|---|---|
| $O_{c2}$ | the center of the working surface arc of the cam |
| $p$ | zero moment position |
| $S_p$ | the number of passive chains |
| $p_A$ | precompression amount of the comptrssion A |
| $q_i$ | the number of the driving motions on each active chain |
| $R$ | the resistance of the motor winding |
| $r_f$ | the measurable distance between the ankle and the center of gravity of the foot |
| $R_m$ | the moment of a load |
| $R_r$ | rotation matrix |
| $S_a$ | the motion-screw system |
| $s_i$ | a unit vector pointing in a certain direction from $a_i$ to $b_i$ |
| $s_u$ | the unit vector pointing from the point $a_i$ to the point $b_i$ |
| $S_{11}$ | one of the rotational joints |
| $S_{12}$ | one of the rotational joints |
| $S_{21}$ | one of the rotational joints |
| $S_{22}$ | one of the rotational joints |
| $S_{aj}$ | the motion-screw representation of the $j$th kinematic pair |
| $T$ | the torque of the torsion spring at the maximum angle |
| $t_c$ | the torque coefficient |
| $T_e$ | the output torque of the motor |
| $T_l$ | the load torque |
| $U_a$ | the motor voltage |
| $W$ | weight in kilograms |
| $W_l$ | the weight of one side lower limb |

$x_E$      the x-coordinate of point $E$

$x_{A_0}$      the x-coordinate of point $A_0$

$x_{C_0}$      the x-coordinate of point $C_0$

$X_{n1}$      one of the limit position of cam while rotation

$X_{n2}$      the other one of the limit position of cam while rotation

$X_{na}$      one random limit position of cam while rotation

$y_E$      the y-coordinate of point $E$

$y_{A_0}$      the y-coordinate of point $A_0$

$y_{C_0}$      the y-coordinate of point $C_0$

$^{u1}\mathrm{R}^{u2}\mathrm{R}$      2R sub-chain with its two rotational axes do not intersect at a point, neither parallel to XZ plane nor perpendicular to XZ plane

$^{u1}\mathrm{R}^{u2}\mathrm{R}^{u3}\mathrm{R}$      3R sub-chain with its three rotational axes do not intersect at a point, neither parallel to XZ plane nor perpendicular to XZ plane

$^{v1}\mathrm{P}$      prismatic pairs with different translational directions parallel to XZ plane

$^{v2}\mathrm{P}$      prismatic pairs with different translational directions parallel to XZ plane

$^{v}\mathrm{P}$      prismatic pair with its translational direction parallel to XZ plane

$^{x}\mathrm{R}$      revolute pair with its axis perpendicular to YZ plane

$a$      center distance

$D$      outer diameter

$d$      diameter of the worm

$f_s$      scalars values

$h_s$      the pitch of the screw

$i_t$      transmission ratio

$K_l$      load coefficient

$l$      matrix parameters

| | |
|---|---|
| $m_w$ | module of worm wheel |
| $m$ | matrix parameters |
| $n$ | matrix parameters |
| $p$ | matrix parameters |
| $q$ | matrix parameters |
| $S^r$ | reciprocal screw |
| $r$ | matrix parameters |
| $r_p$ | position vector of any point on the screw axis |
| $\mathbb{S}_{bi}$ | the motion-screw system of the $i$th branch |
| $\mathbb{S}$ | $n$ linearly independent screws form $n$-system |
| $\mathbb{S}^c$ | the set of common constraints found among all branches |
| $\mathbb{S}^r$ | the constraints placed on the platform due to the individual contributions of each branch constraint-screw system |
| $\mathbb{S}^r_f$ | the reciprocal system of it is f order (6-n) |
| $\mathbb{S}^r_{bi}$ | the constraint-screw system of the branch |
| $\mathbb{S}_f$ | the movement of the mobile platform relative to the stationary base |
| $\mathbb{S}_m$ | the permissible relative motions among all links of the mechanism |
| $S$ | screw matrix |
| $T_s$ | twist |
| $T_v$ | translation motion along with the axis |
| $W_s$ | wrench |
| $l_w$ | the lead of the worm |
| $z_2$ | number of turbine |
| $r_{s-1}$ | the attitude matrix of segment $m-1$ |
| $^{s,i-1}_1 T_{s,i}$ | the transformation matrix between consecutive segments |

$a_i$     the distance between two consecutive joint axes along the $x$-axis

$c_1, c_2$   two acceleration coefficients

$d_i$     the distance between two consecutive joint axes along the $z$-axis

$e_{s,i}^{\times}$     the antisymmetric matrix of the $e_{s,i}$

$e_{s,i}$     the unit vector of the $i$th axis

$F_n$     normal load on the meshing tooth surface

$f_s(\theta_{2s-1}, \theta_{2s})$   the simplified kinematic equation of segment $s$

$f_{\text{SRE}}(\theta)$   the simplified forward kinematic equation

$F_{i,x}$     the force which come from the $ith$ torsion spring on the $ith$ segment along with the $x$ axis

$F_{i,y}$     the force which come from the $ith$ torsion spring on the $ith$ segment along with the $y$ axis

$F_{i-1}$     the force which come from the $(i-1)th$ torsion spring on the $ith$ segment

$F_{S_e,x}$     the forces come from the end torsion spring along with the $x$ axis

$F_{S_e,y}$     the forces come from the end torsion spring along with the $y$ axis

$F_{T,x}$     the torsion forces which come from the motor along with the $x$ axis

$F_{T,y}$     the torsion forces which come from the motor along with the $y$ axis

$V_{2s}$     the unit linear velocity expressions of the two joint variables between segment $m$ and the end effector

$g_{best}$     the globally optimal individual particle

$i_p$     a particle

$J$     the Jacobin matrix

$L_0$     total length of contact line

$l_{0,e}$     the distance between the base and the end segment

$l_{0,i}$     the distance between the base and the forcing point of the $ith$ torsion spring

$l_{G,e}$     the distance between the mass centre and the centre of rotational joint

25

$l_{load,e}$    the distance from the point of loading force to the centre of rotational joint

$m_e a_x$    the combination of the mass of the end segment and the acceleration velocity along with the $x$ axis

$m_e a_y$    the combination of the mass of the end segment and the acceleration velocity along with the $y$ axis

$M_e$    the moment of the end segment

$M_i$    the moment of the $ith$ torsion spring

$\omega_{2s}$    the unit angular velocity expressions of the two joint variables between segment $m$ and the end effector

$\omega$    the inertia factor

$P_b$    the coordinate of point $P$ in the base coordinates of the robot

$P_t$    the coordinate of point $P$ in the robot working coordinates

$p_{best}$    the locally optimal individual particle

$r_1, r_2$    two independent random numbers generated in the interval [0,1]

$r_{os,i}$    the vector matrix from the base to the $i$th joint centre of segment $m$

$r_{s,i}$    the vector from the ith joint to the end effector

$\theta_{2s-1}$    the rotational segment $2m-1$ joint angles

$\theta_{2s}$    the rotational segment $2m$ joint angles

$v_i$    the current velocity of the particle

$Z_E$    elastic influence coefficient

$m_t$    normal module

**Greek Symbols**

$\alpha_i(^\circ)$    the rotation about the $x$-axis from one link to another

$d\alpha_x$    rotational deviation about the $x$-axis

$\gamma$    lead angle

$\omega_y$    rotational deviation about the $y$-axis

$\pi$ $\quad \simeq 3.14\ldots$

$\theta_i(°)$ $\quad$ the rotation about the $z$-axis from one joint to another

$d\theta_z$ $\quad$ rotational deviation about the $z$-axis

$T_\omega$ $\quad$ rotational motion about the axis

$\Delta C_A$ $\quad$ compression amount of the spring $A$

$\Delta C_B$ $\quad$ compression amount of the spring $B$

$\lambda$ $\quad$ the time length applied

$\omega_m$ $\quad$ the motor speed

$\sigma_H$ $\quad$ fatigue strength of worm gear

$\sum F_{s,x}$ $\quad$ the total spring forces along with the direction of $x$ axis

$\sum F_{s,y}$ $\quad$ the total spring forces along with the direction of $y$ axis

$\sum mg$ $\quad$ the gravity of the segments

$\tau$ $\quad$ torque

$\theta_a$ $\quad$ rotational angle

$\theta_e$ $\quad$ the rotational angle of the end torsion spring

$\theta_{i,i-1}$ $\quad$ rotational angle between $(i-1)th$ torsion spring and $ith$ torsion spring

**Other Symbols**

$\circ$ $\quad$ the reciprocal product

$\Delta$ $\quad$ the swap operator

**Acronyms / Abbreviations**

*ABS* $\quad$ Absolute Value

*BF* $\quad$ Biceps Femoris

*C4D* $\quad$ Cinema 4D

*DHparameter* $\quad$ Denavit-Hartenberg parameters

*FEA*   Finite Element Analysis

*MAR*   Maker Point

*PSO*   Particle Swarm Optimization

*RF*   Rectus Femoris

*SRE*   Segmented Redundant Elements

*ST*   Semitendinosus

*VM*   Vastus Medialis

*ZMP*   Zero Moment Point

# Chapter 1

# Introduction

## 1.1 State of the Problem

Patients who suffer from muscle impairments due to stroke, spinal cord injury, or other disorders often display inadequately timed or graded muscle activity and are unable to generate voluntary muscular contractions of normal strength [296]. This situation significantly affects normal gait performance. Among these scenarios, stroke is one of the most common causes of mobility issues, with patients frequently experiencing unilateral weakness on the affected side [301]. Individuals may tend to drag their affected leg in a semi-circular motion while walking [197]. If the muscles responsible for lower limb stabilization are weak or paralyzed, it becomes challenging for patients to maintain walking stability compared to healthy individuals [1], potentially resulting in collapsing during the weight acceptance phase [5] [18].

According to the 2022 global stroke fact sheet released by the World Stroke Organization (WSO) [82], stroke, which is categorized as a neurological injury, continues to be the second most common cause of mortality and third most prevalent cause of disability (measured in disability-adjusted life-years) worldwide. It's estimated that around one out of every four individuals will experience a stroke in their lifetime, and there will be an annual occurrence of 12.2 million new strokes on a global level. Patients who have had a stroke often experience hemiparesis or partial paralysis, which significantly limits their physical functions and greatly reduces their ability to perform daily activities. Research suggests that there are approximately 101 million people worldwide who are living with the consequences of stroke. It is important to note that stroke is not only exclusive to the elderly or weak but also could affect younger individuals, including children. Furthermore, stroke can result in significant indirect costs and place a considerable economic burden on society. Please refer to Figure 1.1 for a visual summary of stroke-related information.

Besides above influence, there has been a significant increase in the burden placed upon therapists [300] due to the large number of patients.



In 2019, **63%** of stroke happened in people younger than 70 years old STROKE IS NO LONGER A DISEASE OF THE ELDERLY

Around the world, there are **12.2 MILLION** new strokes per year ONE EVERY 3 SECONDS

**101 MILLION** People worldwide are living with stroke aftermath THIS NUMBER HAS ALMOST DOUBLED OVER THE LAST 30 YEARS

2017 US$861 BILLION

The total estimated worldwide cost of stroke (in international dollars) in 2017 was US $ 861 BILLION (ABOUT 1.12% DF THE GLOBAL GDP)

The number of stroke survivors in world regions in 2019.

**89%** OF THE GLOBAL STROKE DEATHS AND DISABILITY COMBINED RESIDE IN LOW-TO MIDDLE-INCOME COUNTRIES

**1 in 4** people will have a stroke in their lifetime THIS NUMBER HAS INCREASED 50% OVER THE LAST 17 YEARS

Fig. 1.1 Global distribution of stroke patients [82]

Clinical theories emphasize the need for effective joint exercises during muscle injury rehabilitation to expedite joint tissue healing, reduce swelling and pain, and avert muscle atrophy or adhesion [227]. Basic medical therapy and necessary surgery are also crucial components of recovery if necessary. Inadequate rehabilitation measures for patients with neurological injuries can hinder their quick return to normal life. Although traditional recovery methods primarily involve manual physical therapy from physicians, which can help restore muscle and ligament function around the ankle joint and promote ankle function recovery, they can be time-consuming and limited to repetitive, single exercises within the space of motion. Furthermore, in some cases, when treatment is delayed or inadequate, the ligaments connecting the ankle joints may fail to tighten and remain relaxed. This can result in repetitive joint damage and potential sequelae, such as ankle dysfunction. In severe cases, a second operation may be necessary.

During rehabilitation, treatment guidelines advocate passive activity as the primary method in the early stages, with active activity serving as an auxiliary method. In later stages, active activity is the primary method, with passive activity acting as the auxiliary method. This process usually lasts 3-4 months and requires professional guidance and an appropriate exercise regimen, which necessitates years of experience and valuable physician time. Moreover, different physicians may use various massage techniques and strength levels that can significantly affect a patient's recovery. Even minor errors in

treatment can result in severe consequences. Therefore, it is crucial to have a consistent and well-planned treatment regimen that follows established guidelines. Incorporating massage into rehabilitation should be done cautiously as it can disrupt other patients' visits and waste valuable physician time. It is essential to ensure that massages are done by experienced professionals and are included as part of a comprehensive treatment plan.

Currently, traditional medical instruments used to assist lower limb rehabilitation training include elastic bandages, foam rollers, Biodex balance systems, and Biodex 3 multi-joint systems [144], as shown in Fig 1.2 . However, these devices have several drawbacks, including large size, high cost, single-functionality, dependence on human assistance, and limited working range. Consequently, a systematic rehabilitation task system for full lower limb joints recovery cannot be achieved using these instruments. By utilizing these external equipment or exoskeletons, it is possible to effectively overcome the drawbacks of traditional rehabilitation instruments and achieve a more comprehensive rehabilitation system.
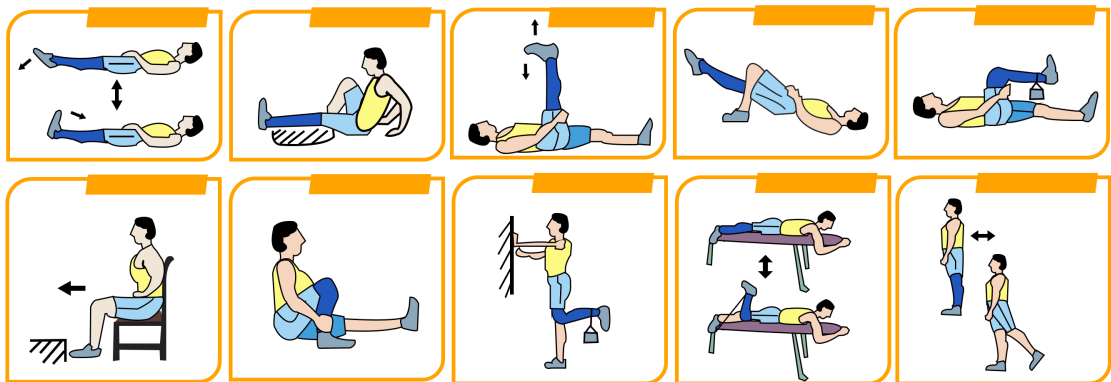


Fig. 1.2 Traditional Ankle Rehabilitation Training [144]

## 1.2   Aims and Objectives

The emergence of rehabilitation mechanisms provides significant advantages over traditional rehabilitation treatments. These mechanisms offer scientific motivation, quantifiable and automatic movement, and can aid patients in diagnosis, prognosis, and customized treatment through digital signal feedback. These functions ensure that patients adhere to their treatment plans and maintain medical records, thereby enhancing healthcare quality and productivity [175]. In addition to mechanically replicating movements in a standardized way, the mechanical rehabilitation systems can be designed to provide patients with self-subjective awareness during the rehabilitation process. The systems can perform a variety of tasks, ranging from passive repetitive actions to functional activities, independent

tasks to adversarial tasks. They offer patients safe regular training and are an excellent alternative to physical therapists. Moreover, incorporating rehabilitation mechanisms in treatment allows for greater customization to meet the needs of individual patients. The systems' performance metrics can be adjusted based on patient progress and requirements. This adjustment can help optimize the rehabilitation process, resulting in better patient outcomes.

To recover normal gait, it is essential to build a set of reconfigurable rehabilitation systems that can help stroke patients of various types. Specifically, the overall lower limb rehabilitation mechanism should contain ankle joint, knee joint, and hip joint, which can operate separately or in combination for easier and more targeted treatment. Independent use and assembly of different recovery sites facilitate easier and more targeted treatment for stroke patients of various types, allowing faster and more thorough recovery. Apart from ensuring safe usage, aligning the mechanism's center with that of the biological center should always be an important target when designing such rehabilitation devices. This feature plays a crucial role in ensuring rehabilitation effectiveness, although it poses a significant design challenge. Rehabilitation is a multi-stage process, and different stationary or dynamic exercises are necessary at different stages. Therefore, the design should provide appropriate rehabilitation modes while meeting technical requirements, such as prescribed working space, manipulation dexterity, and output torques. Furthermore, stiffness is a key element that may affect the mechanism's performance since it frequently interacts with the environment. Therefore, exploring and discussing variations of the critical stiffness indices of the mechanism is necessary. Additionally, identifying methods that can improve the design's stiffness performance is expected.

Therefore, exoskeletons hold great promise in treating pathological gait in individuals with lower limb dysfunction, and they have been shown to be effective in multiple studies [19, 20, 33, 39]. They can reduce the costs associated with patient treatment and therapist time, making rehabilitation more accessible and affordable for a wider range of individuals [37]. Moreover, exoskeletons facilitate medical treatment and enable domestic rehabilitation, improving patients' quality of life.

When designing exoskeletons for rehabilitation, it is imperative to ensure that they provide corresponding rehabilitation modes to meet patients' specific needs. Additionally, technical requirements such as prescribed working space, manipulation dexterity, output torques, and safety factors should be taken into account to ensure the exoskeleton's effectiveness and safety during use. By doing so, the potential benefits of exoskeletons can be maximized in the treatment of lower limb dysfunction.

Therefore, a novel lower limb exoskeleton rehabilitation system would be proposed in this thesis. The main content includes: analyzing the existing structures rehabilitation these years; proposing the design method and theoretical model design for

the new device; conducting kinematic analysis and corresponding stress analysis of the proposed model to analyze its stiffness and stress; performing simulation analysis on the three-dimensional model created using Solidworks with the use of Adams simulation software, and resolving any issues encountered during the simulation process through testing platforms and iterative experiments; finally, validating the proposed new model through prototype experiments. The aim of this research is to address the issues of weight, portability, flexibility, and range of movement associated with current lower limb exoskeletons, and to achieve modularity, simplicity, portability, automatic joint center tracking, suitability for both indoor and outdoor use, patient self-operation, real-time human-machine interaction, and adjustability of movement states. The grapgical research contents would exhibits in below Fig 1.3 and the specific chapter framework will be presented in the next section.

## 1.3   Thesis Outline

The thesis comprises of eleven chapters, and concise summaries of each chapter are provided below.

Chapter 1: Introduction

Description: This chapter gives the general research background, research problems, research motivations, research aims and objectives, as well as the thesis structure.

Chapter 2: State-of-the-Art Continuum Mechanisms

Description: This chapter presents the background and active motor principles of the continuum robots. Besides, it also give the advantages and potential applications when compared with pure rigid mechanisms.

Chapter 3: State-of-the-Art Lower Limb Rehabilitation Mechanisms for Stroke Patients

Description: This chapter explores the background of each rotational joints of lower limb exoskeleton mechanisms, including ankle joints, knee joints, hip joints and toes joints.

Chapter 4: Mathematical methods

Description: This chapter reveals the methods and data which would be used in the whole thesis, including screw theory, optimization method based on PSO(Particle Swarm Optimization) and data collection methods based on the motion capture system.

Chapter 5: Design and Modeling of the Lower Limb Rehabilitation Exoskeleton Mechanism

Description: This chapter focuses on the structural design of the ankle, knee, and hip joints in a lower limb rehabilitation exoskeleton. The main aim is to enable active and passive movements of these joints, specifically tailored for stroke survivors. These designs

prioritize the restoration of practical rehabilitation functions while minimizing the risk of secondary injuries.

Chapter 6: Kinematics Analysis of the Lower Limb Rehabilitation Exoskeleton Mechanism

Description: This chapter provides a comprehensive exploration of kinematics analysis and performance evaluation for the ankle, knee, and hip joints in lower limb rehabilitation exoskeletons. Kinematics analysis is crucial for understanding the complex movement patterns and biomechanics exhibited by these joints during activities like walking, running, and rehabilitation exercises. By studying displacement, velocity, acceleration, and time relationships, we gain insights into the behavior and trajectories of moving objects.

Chapter 7: Stiffness Analysis and Performance Evaluation

Description: This chapter focuses on the stiffness analysis and performance evaluation of the ankle joint and hip joint, employing simulation techniques and performance measurements. The stiffness analysis of parallel spring devices explores their rigidity under various loads and aids in design optimization. Simulation analysis of the ankle joint provides insights into its biomechanical behavior during activities like walking and running, benefiting the development of more efficient exoskeleton systems.

Chapter 8: Simulation, Optimizing and Experiment Testing

Description: This chapter focuses on the use of the PSO genetic algorithm to address the challenge of the "S-shaped" curve in the Adams simulation of the knee joint rehabilitation mechanism. Additionally, a meticulously designed 3D knee joint model plays a vital role in verifying the accuracy and effectiveness of the structural design and optimization results.

Chapter 9: Configuring and Gait-Cycle Analysis of the Overall Lower Limb Rehabilitation Mechanism

Description: This chapter demonstrates the effectiveness of the proposed lower limb rehabilitation exoskeleton by integrating the ankle, knee, and hip joints. Each joint component performs its intended rehabilitation movements independently, and the modular design allows for seamless integration. The exoskeleton effectively addresses the rehabilitation needs of the entire lower limb.

Chapter 10: Rendering and Prototype Analysis of the Overall Lower Limb Rehabilitation Exoskeleton Mechanism

Description: This chapter mainly presents the rendering videos based on Cinema4D of the overall lower limb mechanism. Then, the actual prototype with analysis would be shown in this chapter.

Chapter 11: Conclusions and Future Works

Description: This chapter reveals the thesis by summarizing the main contains and contributions of the study. Moreover, the future research topics and potential applications will be proposed.

Finally, the graphical research contents from Chapter 1 to Chapter 11 would be shown in the following diagram.

```
                    ┌──────────────────────┐
                    │      Chapter 1       │
                    │     Introduction     │
                    └──────────────────────┘
                              │
        ┌─────────────────────┼─────────────────────┐
        │   Chapter 2         │      Chapter 3       │
        │ State-of-the-Art of │ State-of-the-Art Lower Limb │
        │  Continuum Robots   │ Rehabilitation Mechanism │
        └─────────────────────┴─────────────────────┘
                              │
                ┌─────────────────────────┐
                │        Chapter 4         │
                │ Mathematical Methodologies: │
                │ Screw Theory ; Optimization Method; │
                │   Data Collection Method  │
                └─────────────────────────┘
      ┌──────────┐        │          ┌──────────────┐
      │Knee Joint│        │          │Ankle Joint and Hip│
      │Rehabilitation│    │          │Joint Rehabilitation│
      │Mechanism │  ┌──────────────┐ │  Mechanism   │
      └──────────┘  │   Chapter 5   │ └──────────────┘
                    │Design and Modeling of the Lower│
                    │Limb Rehabilitation System│
                    └──────────────┘
                         │
                    ┌──────────────┐
                    │   Chapter 6   │
                    │Kinematics Analysis of Each Joint│
                    └──────────────┘
```

Fig. 1.3 Graphical Research Contents

**Chapter 8**
Simulation, Optimization and Experiments Testing

**Chapter 7**
Stiffness Analysis and Performance Evaluation

**Chapter 9**
Configuring and Gait-Cycle Analysis

**Chapter 10**
Rendering and Prototype Analysis

**Chapter 11**
Conclusion and Future Work

# Chapter 2

# State-of-the-Art Continuum Mechanisms

## 2.1 The Background of Continuum Robots

Continuum robots are commonly defined as structures that are continuously curved and movable, employing a series of continuous arcs instead of skeletal structures to generate bending motion [274, 36]. Unlike discrete robots that use discrete single degree of freedom joints and rigid links, the idea for the spineless flexible structure of continuum robots comes from biological organs such as elephant trunks and octopus antennae, which do not have any discrete joints or rigid links. This novel type of biomimetic robot offers excellent bending performance that traditional discrete robots cannot match, and it can flexibly change its shape, like that of Okada, based on the conditions of environmental obstacles, as shown in Fig. 2.1.

Fig. 2.2 shows Okada, a prototype of a continuum robot developed by researchers at Osaka University. The robot has an external skin composed of seven layers of silicone rubber and an internal structure comprising a flexible pipe and air chambers. When the air chambers inflate, the robot can bend and move in various directions.The origin of continuum robots can usually be traced back to the late 1960s when the snake-shaped robot was invented [185]. These super-redundant robots use many closely spaced joints to simulate the spinal motion of snakes. Examples include Orm, which consists of a series of pneumatic-controlled bellows [194], as well as a tensor arm, which is a tendon-driven robot for underwater applications. However, at that time, the weakness of continuum design, including low payload capacity, lack of understanding of kinematics and dynamics, and sketchy positioning accuracy, led to the abandonment of the promising research project from the late 1960s. The most frequently cited overview of continuous robots [204] was several years away, and many advancements were made during that period.

Fig. 2.1 Continuum Robots [36]

In recent years, the field of continuum robotics has made significant progress, particularly in two areas. Firstly, designers have focused on the biological inspiration and design of soft (especially pneumatic) continuum robots [267]. Secondly, there has been much research into the motion of mobile snake-shaped robots [265].

Traditionally, engineers have relied on rigid materials to manufacture predictable and precise robot systems, which can be easily modeled as rigid components on discrete joints. However, natural systems' performance corresponds or exceeds that of robot systems with deformable objects. For example, cephalopods manipulate and move without bones. Even vertebrates, such as humans, can store elastic energy in their bodies to achieve dynamic and flexible gait of soft tissues and bones. Inspired by nature, engineers began to explore the design of control robots and software made of flexible materials. Due to its slender body, continuous robots can achieve long-distance extension in narrow and winding environments, making them suitable for medical, industrial, and service applications. After decades of pioneering research on these robots, many innovative structural designs and driving methods have emerged.

For example, unmanned magnetic robots are an excellent example of external driving characteristics, allowing for miniaturization, and they have attracted a lot of interest in the academic community. In addition, a continuum robot with proprioceptive ability is also being studied. In terms of modeling, significant progress has been made in modeling methods based on continuum mechanics and geometric shape assumptions after years of research. The combination of modeling with numerical analysis methods generates

significant computational efficiency through discrete modeling, thus achieving many effective model-based control methods. In control, when combined with sensor feedback information, closed-loop and hybrid control methods provide high motion control accuracy and flexibility. Furthermore, advances in machine learning have made modeling and control of continuum robots easier. Data-driven modeling technology simplifies modeling, improves anti-interference and generalization capabilities.

Engineers have long been fascinated by biology and often look to it for inspiration when designing powerful machines [188]. Two notable characteristics of biological systems that engineers try to emulate are flexibility and physical compliance, as they enable organisms to interact with their environment in a dynamic and efficient way [68]. Recently, researchers have turned to continuum robots as a means of achieving this level of adaptability and agility. Continuum robots draw inspiration from the movement of snakes, trunks, tendrils, and other flexible organisms such as elephant trunks, snakes, and octopus antennae [319].

One significant advantage of continuum robots is their potential for flexibility, low weight, inherent safety, scalability, and cost-effectiveness, making them popular in various industries. They belong to the category of soft robots [267] [140] [168] [146], which are inspired by biological systems and constructed using soft materials. Soft robots have been researched extensively for medical applications, such as minimally invasive surgery, due to their ability to reach remote or difficult-to-access locations with greater precision and a lower risk of tissue damage.

Caterpillars have been a crucial area of research in the development of soft robot systems [161] [162]. By studying the movement of these creatures, scientists have gained insights into soft robotics' control mechanisms and refined them [239]. Additionally, researchers have explored the biomechanics of other animals to create innovative soft robot designs. For example, the development of a biomimetic worm design, made from agile materials and powered by shape memory actuators, was inspired by the biomechanics of worms [244]. Another example is an annealing-inspired robot that uses dielectric materials to achieve movement [130].

Moreover, European researchers studied the control and biomechanics of octopuses, leading to the creation of a prototype of a soft robot [176] [147], as depicted in Fig. 2.2. These innovations in soft robotics offer opportunities to revolutionize several industries, including manufacturing, disaster relief, and space exploration, with their ability to adapt to harsh or challenging environments autonomously.

The use of soft materials has enabled the development of independent and autonomous robotic fish actuators capable of swimming forward, rotating, and adjusting their depth [171]. These innovative designs provide an excellent example of how studying biological systems can inspire creative solutions to engineering challenges, resulting in the development of

Fig. 2.2 A Robotic Octopus [176] [147]

new technologies with promising applications in various fields [133], as illustrated in Fig. 2.3.
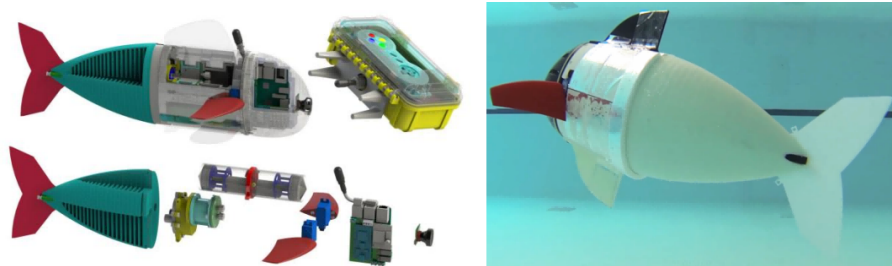


Fig. 2.3 A Soft Robotic Fish [171]

In conclusion, the development of soft robots, inspired by biological systems, has provided engineers with the opportunity to create machines that offer many potential advantages over traditional rigid robots. These advantages include greater adaptability, inherent safety, lower costs, and scalability. The ongoing research in this area promises to lead to further exciting breakthroughs in robotic design and control. Soft robotics technologies have already found promising applications in various fields ranging from medical devices, disaster relief, manufacturing, and space exploration. Such advances will likely continue to shape the future of robotics, enabling robots to operate in environments that were once considered too challenging or impossible for rigid robots.

Some robots can have small diameters of micrometers and can target therapy in various medical applications, including cerebral blood vessels and cerebrovascular systems. Its bending angle can surpass 180 degrees and positioning accuracy can achieve up to 10 $\mu m$. Additionally, magnetic soft continuum robots can achieve small diameters of micrometers, enabling them to target therapy in the cerebral blood vessels or cerebrovascular systems [100].

However, magnetic soft continuum robots face challenges in maintaining stability under external forces, which poses a significant risk of tiny rigid magnet tips falling off

inside the body during operation [283]. Therefore, improvements are required to ensure the safety and efficacy of these robots in medical applications. Nonetheless, the development of magnetic soft continuum robots shows great potential in advancing medical technology and improving patient outcomes.

To enhance the performance of continuum robots and ensure their safety, researchers have been using shape memory materials that can achieve safer and more reliable control in different applications [126] [2]. Additionally, hybrid drive continuum robots have been developed by integrating different driving methods, resulting in enhanced bending abilities, steering capabilities, and precise tracking. The integration of magnetic and tendon driving methods, for instance, shows excellent steering performance and position control, making it ideal for interventional therapies of human stenosis.

The integration of different driving methods has led to remarkable advancements in robot design and capabilities. One notable example is the combination of pneumatic and tendon drive methods, resulting in robots with excellent bending abilities exceeding 90° [163] [132]. Additionally, magnetic and tendon driving methods have been combined to create a continuum robot for interventional therapy of human stenosis [315]. This robot can achieve relatively large angle steering under tendon drive and precise position control with an accuracy of up to 10 $\mu m$ using external magnetic fields. The combination of these driving methods demonstrates excellent steering and precise tracking capabilities, making it ideal for use in medical interventions.

Furthermore, researchers have developed a stretchable origami continuum robot that has omnidirectional bending and twisting functions [294]. This innovative robot is capable of achieving complex movements based on basic integrated motion, such as continuous stretching and contraction, reconfigurable bending, and multi-axis torsion. The stretchable origami continuum robot has a wide range of potential applications in various fields, such as biomedical engineering, soft robotics, and industrial automation.

Another advantage of these robots is their scalability. For instance, they can be easily assembled into a multi-segment continuous robot, further increasing their versatility and applications [103] [99]. In recent years, researchers have also explored the use of soft pneumatic robots that navigate their environment by growing instead of traditional movement [275] [102]. This motion is achieved through two principles: increasing pressure on thin-walled vessels allows for rapid and substantial extension of the tip, while asymmetrical lengthening of the tip enables directional control [97]. Through verification, these robots have proven capable of navigating in stressed environments using passive deformation.

Professor Walker, together with Jones et al., introduced Air-Octor, a continuous robot as illustrated in Fig. 2.4, that employs pneumatic support to maintain its shape. One notable feature of this structure is that it does not require support from a flexible pillar at its center,

which not only frees up internal space but also reduces weight. The robot has a total length of 50cm and an outer diameter of 10cm, achieving 2-degree-of-freedom bending motion control through three evenly-distributed driving ropes in the circumferential direction. The Air-Octor has significant potential for various applications owing to its compact size, versatility, and precise control.

This innovative robot was developed by Walker et al. and demonstrated in various publications [192] [178]. Reynaerts and Brussel also recognized its potential in their research on shape memory alloy actuators [223]. The Air-Octor's unique design and its ability to operate without external support make it ideal for use in confined spaces where traditional robots are impractical.
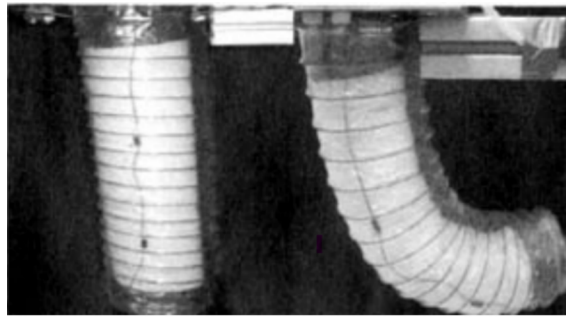


Fig. 2.4 Air-octor of Clemson University [223]

In addition, the robot's driving ropes and internal air pressure can be controlled appropriately to achieve extension and contraction in its length direction. This feature provides the entire robot with an additional degree of freedom, resulting in a total of three degrees of freedom and increasing its versatility in various applications.
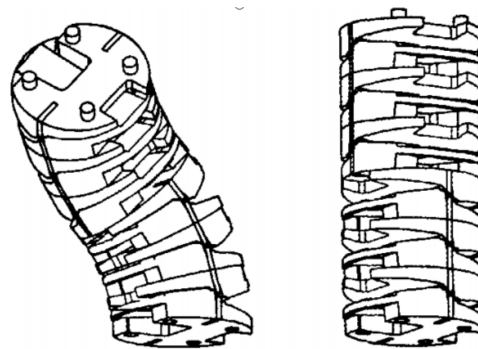


Fig. 2.5 Bending Section with Shape Memory Alloy Actuators [212]

Peirs et al. from Belgium developed an endoscopic robot that employs a memory alloy-driven bending joint, as illustrated in Fig. 2.5 [212]. They also developed another flexible bending joint segment D for endoscopic robotic surgery [44], which features an outer part wrapped in a superelastic NiTi alloy tube that supports the joint segment, as

shown in Fig. 2.6. The coordinated movement of four evenly-distributed ropes around the circumference of the alloy tube produces the bending motion of the joint segment. As a result, the entire joint has two degrees of freedom, enabling it to achieve 90 degrees of movement in any direction around its circumference.
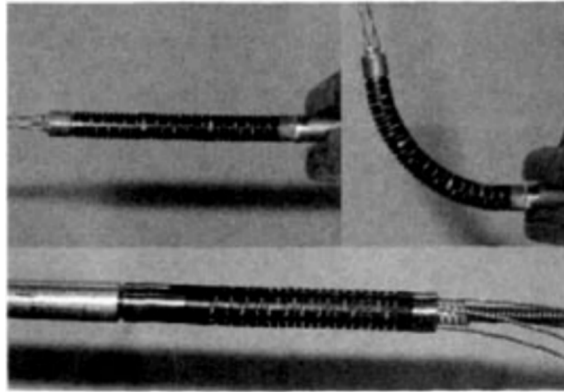


Fig. 2.6 Flexible Distal Tip for Endoscopic Robot Surgery [44]

French researchers, including Chen and Redarc, have developed a single-segment continuous mechanism called Clobot, as illustrated in Fig. 2.4. The aim of this robot is to serve as the end bending mechanism for colonoscopy [294]. The robot has significant flexibility, allowing for precise control and achieving one degree of freedom through the use of two driving ropes. With an outer diameter of only 7mm and a maximum bend angle of up to 180 degrees, Clobot is an extremely promising option for minimally invasive endoscopic procedures.

Furthermore, a summary of different design and actuation methods is presented in Tab. 2.1.

Table 2.1 Summary of Different Design and Actuation Methods

| Design Principle | DoF | Actuation | Diameter | Accuracy | Characteristic |
|---|---|---|---|---|---|
| Parallel | 5 | Rod driven | - | 2.3 | Large workspace and high precision |
| Backbone | 2 | SMA driven | 5 | 0.98mm | Modular; Teleoperation |
| Backbone | 4 | Tendon driven | 38 | 2mm | Passive structural flexibility |
| Backbone | 6 | Fluid driven | 30 | - | Variable Stiffness |
| Concentric tube | 12 | Motor driven | 2.74;1.92;1.21 | 1 | Dual-arm |
| Backbone | 4 | Fluid driven | 32 | 1.3 | Soft and has variable stiffness |
| Backbone | 6 | Magnetic driven | - | 7.86 | Combination of soft and hard joints |
| Backbone | 5 | Magnetic driven | 2.5 | - | Variable stiffness |
| Backbone | 5 | Tendon and magnetic driven | 3 | 10 $\mu m$ | Large workspace and high preciision |
| Backbone | 5 | Fluid and tendon driven | 25 | - | High load capacity |
| Backbone | 5 | Magnetic driven | 20 | - | Omnidirectional bending and twisting |
| Concentric tube | 4 | Motor driven | 4.36;2.265 | - | 3D printed |

43

## 2.2 The Classification of Continuum Robots

The base of a continuum robot is the part where the robot is fixed, and it includes all the necessary hardware for actuation and control. The most important part of a continuum robot is its backbone, which serves as the main structural component and can bend in various ways. In the field of continuum robots, the terms "trunk" and "backbone" are used to describe the mechanical structures of the robot rather than network topology. The "trunk" refers to the robot's primary support structure or framework that holds various components, sensors, and actuators while providing additional stability. In some cases, the "trunk" may also contain wires or hoses that connect different parts and accessories together.

The "backbone" of the robot typically refers to the primary moving part. For example, in snake-like robots, the backbone is a continuous skeleton that spans the entire length of the robot's body. In robot design, the backbone is a crucial component that directly affects the robot's rigidity, precision, and flexibility. Therefore, engineers must carefully consider how the backbone will move and bend when designing and building the robot. By doing so, they can ensure that the robot can move in the desired way and complete its intended tasks with high accuracy.

The backbone of a robot plays an important role in defining its overall shape and properties. Based on these properties, robots can be classified into various categories, such as single-backbone and multi-backbone robots, as shown in Fig. 2.7. A single-backbone robot has a central backbone that runs throughout the entire length of the robot, while a multi-backbone robot consists of a series of flexible components and rigid bodies (vertebrae). Multi-backbone robots have the potential for increased dexterity and maneuverability due to the segmented nature of their backbones.

In summary, the base and backbone are two critical components of continuum robots. The design and construction of the backbone directly affect the robot's flexibility, precision, and overall performance. Therefore, careful consideration and engineering solutions are required to ensure that the robot can move and bend in the desired way, and complete its intended tasks.

However, some designs with multiple continuous trunks, such as rod-driven or parallel structures, cannot fit into either category [298] [29]. Therefore, researchers have proposed dividing robots into two main categories: continuous backbone robots and segmented backbone robots. Continuous backbone robots have a flexible body that runs continuously from end to end, while segmented backbone robots have alternating flexible and rigid components along their length.

To control the shape or configuration of a continuum robot, external loads are applied to onboard internal actuators or transmission components such as tendons, rods, or flexible
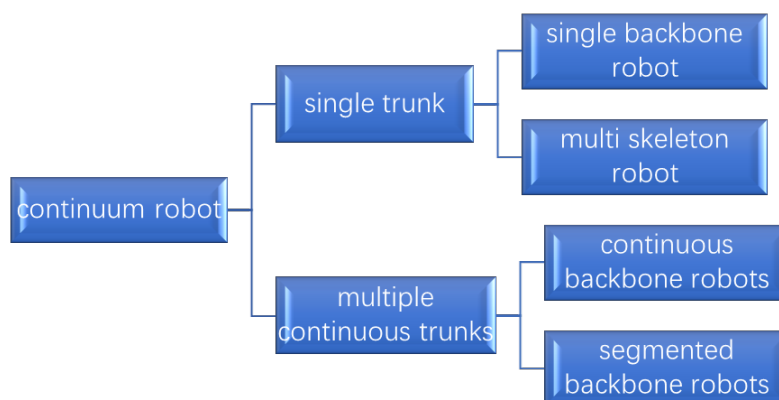
Fig. 2.7 The Classification of the Continuum Robots

tubes. These components are pushed or pulled from the end of the backbone, which is known as external actuation. External actuation is responsible for controlling the movement and shape of the robot's backbone.

In addition, there are also types of internal actuation methods. For example, hydraulic, pneumatic, and shape memory alloy (SMA) actuation methods, in which the backbone is controlled by fluids, gases, or materials that can change shape in response to external stimuli. These internal actuation methods allow for more precise and delicate control over the backbone's movement, although they may require more complex and specialized hardware.

In conclusion, understanding the different types of backbones and how they are controlled is crucial for designing and building effective robots that can perform specific tasks with high accuracy. By studying and developing more advanced backbone designs and actuation methods, engineers can continue to enhance the capabilities of robots in a wide range of fields.

## 2.3 The Principles of Modelling and Controlling for a Continuum Robot

A continuum robot's structural behavior resembles that of a cantilever beam anchored at one end with an unconstrained length and small cross-sectional area. Consequently, any force applied to the system, including the robot's weight, can result in significant deflection. While modeling can compensate for this deflection [200] and its related consequences such as spinal torsion [125], these problems can be better addressed by strengthening the robot. However, enhancing a continuous robot's strength should not compromise its inherent

flexibility since high stiffness can cause harm [169]. Therefore, various techniques have been developed to adjust the backbone stiffness based on the following principles [305]:

a.Material interference: Interference-based systems require a thin sheet filled with granular media. Vacuum pressure compresses the film onto the filler, increasing its density and hardness and achieving local reinforcement positions. This technology is simple, reliable, and achieves the desired effect [78] [228]. However, it is difficult to include reinforcement elements without significantly increasing the robot's size.

b.Thermal activation: Materials with low melting points can be heated to phase transition to adjust the stiffness of compliant components or use external sleeves. SMA or polymers can be used similarly [16]. Since thermal activation is triggered by Joule heating, size scaling is not an issue. However, the required activation and cooling times hinder real-time applications, and the resulting thermal field may affect the robot's performance [27].

c.Mechanical design: Continuous robots can adjust their stiffness by changing their diameter through reconfigurable mechanisms [16], locking tendons along the shaft [27], integrating movable rigid components into the backbone [216], or using the anisotropic distribution of the bending stiffness structure [139].

These techniques can mitigate the undesired effects of deflection and spinal torsion and improve the continuous robot's strength without compromising flexibility. Researchers continue to develop new methods for enhancing continuous robot capabilities, ensuring they remain versatile tools for solving challenges in various fields.

When it comes to modeling continuum robots, several critical issues must be considered, including tendon routing friction, cross-section deformation, system stability, solution strategy, and software framework [47]. Control methods for these robots can be broadly classified into three categories: model-free control, model-based control, and hybrid model control. The accuracy of robot models is crucial in model-based control methods, where complex models are typically used to explain the physical phenomena experienced by robots. However, implementing high-performance real-time control algorithms can be challenging with complex nonlinear models such as variable curve models. To improve control accuracy, feedback techniques such as electromagnetic sensors, analytical calculations, visual feedback, and others may be used to compensate for model errors during the control process.

Recently, Campisano et al. proposed a closed-loop control strategy for magnetic continuum robots that uses real-time Cosserat rod theory and actual feedback to compensate for nonlinearity that may cause errors in the kinematics model. Pose feedback is employed to maintain accurate path following, and experimental results suggest that this approach has significant performance [38].

For unstructured or dynamic environments where modeling is problematic, direct strategy learning for robot control is an effective method. It can be applied to high-dimensional

systems and has higher speed than traditional model-based controllers. Policy learning can be divided into two types of reinforcement learning: model-free and model-based. Model-based reinforcement learning is preferred as it generates more effective strategy learning samples. In previous work, model-based policy search has been implemented using probabilistic inference, which takes into account model uncertainty of learning dynamic models provided by non-parametric Gaussian processes in long-term planning [66].

Trajectory optimization methods have gained significant attention recently for generating samples for strategy learning [152]. Combining the function approximation ability of neural networks to learn and represent these strategies has shown promising results in previous work [151] [186]. Further advancements using this variant of the idea include local learning models, composite multi-step controllers, and deep representations of control strategies.

In this context, a model-based strategy learning program is proposed for closed-loop predictive control of continuous robots, using optipath and supervised learning strategy. This approach has demonstrated excellent performance in control accuracy and efficiency, making it a promising method to control continuum robots in complex environments directly from experience. Further research on this topic will lead to more significant breakthroughs in robot control.

To fully harness the potential of soft robots, it is crucial to integrate sensing, driving, computing, energy storage, and communication capabilities into soft materials to create intelligent materials. Additionally, algorithmic behavior is required to control their movements and transmit necessary information for impedance matching with the body structure. Unlike rigid bodies, the motion of flexible bodies cannot be limited to planar motion since soft materials possess elasticity, allowing them to bend, twist, stretch, compress, wrinkle, and perform other movements. These movements lead to infinite degrees of freedom and pose a significant challenge in controlling soft robots.

Soft robots approach continuous behavior through a series of driving elements, enabling the use of continuous functions to describe their final shape. This complex behavior demands continuous mathematics, adding to the difficulty of controlling such robots. Despite these challenges, the field of soft robotics has made remarkable progress in recent years. Researchers are exploring innovative ways to control these robots, including using concepts from biology and mechanics to develop new approaches.

Because of their unique bending capacity, static, dynamic, and kinematics models for soft robots differ from those used for traditional rigid-link systems. However, the continuous, complex, and highly flexible internal deformation of fluid-powered soft elastic robots pose challenges in modeling, planning, and controlling their behavior.

Furthermore, the driving force of soft robots is often insufficient, and they may include many passive degrees of freedom. Actuation by low-pressure fluids may not generate

enough input fluid power to overcome gravity loads. To model soft robots' kinematics, designers often rely on emulation assumptions leading to the piecewise constant curvature (PCC) model, which is equivalent to a series of modeling methods. However, novel modeling, control, dynamics, and advanced planning methods are essential for effectively controlling soft robots.

Researchers are searching for appropriate simplified assumptions and approximations that can be accurately applied to practical implementation and are easier to analyze before and after developing these general models. Novel computational techniques are being proposed to determine simplified kinematic models, such as fitting the physical robot as closely as possible to required spatial curves or approximating the robot's motion to a series of tangent constant curvature arcs. These approaches allow for closed-form solutions and extend the closed-form Jacobi formula.

One such method involves first describing the required spatial curves and then fitting the physical robot as closely as possible to them [8]. For instance, some researchers have proposed the cyclotron curve based on careful observation of biological snakes [204], which proves useful for simulating the movement of biological snakes [48].

Other researchers have expanded on this basic method by analyzing ideal mathematical curves, defining a curve as the product of Bessel function with sine and cosine. This approach made the modal method of inverse kinematics possible and allowed for accurate control of soft robots. Additionally, wavelets have been applied to describe the shape of a continuum robot, producing a simplified form of kinematics that allows for closed-form solutions and extends the closed-form Jacobi formula [95].

A particularly practical modeling method used in soft robotics is to approximate the robot as a series of tangent constant curvature arcs, also known as "piecewise constant curvature." Although most continuum robots consist of incomplete arcs [297], many of these arcs are almost circular. The segmented constant curvature approximation has proven highly useful in various mechanical structures of continuum robots. The analytical appeal and practicality of this modeling method have led to its widespread application in the field of soft robotics.

In achieving task space planning in the field of soft robotics, the inverse kinematics algorithm plays a critical role [96]. This algorithm enables the autonomous positioning of end effectors and other parts of the robot body in free space [137], allowing maneuvering in limited environments and grasping and placing objects.

When developing task space programs, designers must take into account the entire robot body, including the arms. However, controlling the configuration of full-body soft robots is challenging due to compliance and overall softness. Existing full-body control algorithms assume rigid body systems and have not been extended to soft robots.

To overcome the challenges of modeling and controlling soft robots, researchers have developed a method for calculating the full-body planning of a soft planar robotic arm [170]. This method considers both the primary task of advancing the end pose of the effector of the soft robot and the localization of changing the envelope of the entire robot relative to the environment [172]. By accounting for the entire body dynamics of the soft robot, this approach enables more accurate and effective control of soft robotic systems.

Despite the challenges, advances in computational techniques and simplified kinematic models show promise for developing increasingly sophisticated soft robotic systems. These systems have the potential to revolutionize fields such as medical procedures, search and rescue operations, and exploration in extreme environments.

## 2.4 The Methods and Characteristics of Driving in a Continuum Robot

Continuous robots have a rich history that dates back to the 1960s [302]. In 1967, Anderson [29] pioneered the development of the first tension arm made up of stacked plates, which generated motion through tendon stretching. These robots were initially designed to resemble flexible manipulators, elephant trunks, and tentacles/tendrils. Though other robots have inherent actions and larger dimensions, research on continuous robots initially focused on miniaturization in medical applications [16] [165], resulting in more streamlined designs achieved through external actions.

Over time, researchers have conducted extensive studies on super redundant continuum robots [70] [225] [203]. For instance, CardioARM developed a hyper-redundant serpentine arm for cardiac ablation [309]. Parallel continuum robots, which feature multiple parallel elastic rods, have also been developed in recent years, exhibiting higher accuracy and stiffness than their serial continuous counterparts [9] [85]. Notable examples of parallel continuum robots include the multi-pine tree snake robot proposed by Ding et al., the Festo biomimetic tripod robotic arm [80], and the Stewart Gough continuum design.

Nowadays, continuum robots have found widespread use in various fields, including manufacturing, aerospace, search and rescue, nuclear energy, and more. With infinite degrees of freedom (DoF), these slender robots can inspect and intervene in areas that traditional robots cannot access, such as tunnels and gas turbines. Continuum robots are highly flexible and precise, making them invaluable tools in fields where access is often limited.

For a comprehensive understanding of the driving method of continuum robots mentioned above, please refer to the diagram provided in Fig. 2.8.

Fig. 2.8 Driving Menthod of Continuum Robots

Actuating mechanisms in continuum robots [309] [9] can be broadly classified as internal or external actuation, as detailed in previous research [29]. External actuation can be further categorized into three main types, each characterized by specific transmission components.

Firstly, tendon-driven continuous robots employ a group of ten tendons arranged along the backbone to generate motion, as illustrated in Fig. 2.9. The spine bends by pulling the tendons from the fixed end.
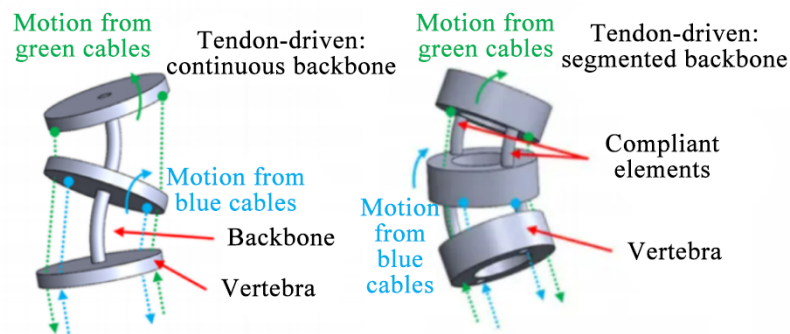


Fig. 2.9 Continuous and Segmented Backbone Structures [309] [9]

Secondly, the concentric tube continuum robot consists of pre-bent tubes nested within each other, with its shape controlled by translating and rotating each tube, as illustrated in Fig. 2.10.

Lastly, rod-driven continuous robots rely on pulling and pushing rods to serve as the backbone, as shown in Fig. 2.11.

Internal actuation mechanisms are integrated into the design of the robot's structure and aim to achieve bending and elongation. The hyper-redundant CardioARM is an example of an internally actuated robot that achieves bending through the coordinated movement of
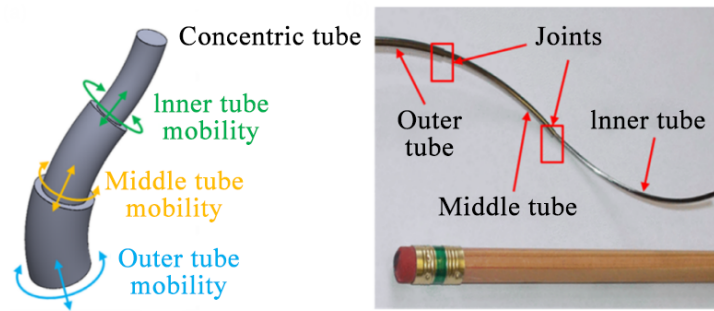
Fig. 2.10 Concentric Tube Structure [309] [9]
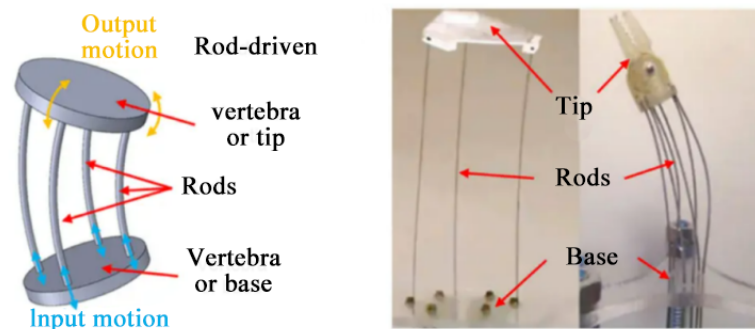


Fig. 2.11 Rod-Driven Structure [9]

its internal links. Internal mechanisms can be designed using various actuation techniques such as SMA wires, shape memory alloys, and pneumatic actuators.

Externally actuated continuum robots have gained popularity due to their simplicity and ease of control, making them ideal for a range of applications. Tendon-driven robots are commonly used in surgical procedures because of their small size and high dexterity. Concentric tube robots offer excellent navigation capabilities with minimal tissue damage and are well-suited for endoscopic applications. Rod-driven continuous robots, on the other hand, are well-suited for applications in aerospace and manufacturing due to their high rigidity and load-bearing capacity.

One significant characteristic of continuum robots with internal actuation is their ability to achieve direct local control of the backbone's shape, with the robot actuator situated inside the body and serving as a part of it [85]. Inherent actuation techniques typically rely on pressurized working fluids, but SMA and dielectric actuators can also be used. Airborne drives are effective in achieving high force transfer efficiency and simplifying modeling and control, but they may increase the robot's size, making them unsuitable for small-scale applications [148].

Research on intelligent material actuators has been extensive, and pneumatic technology has been successful in two main designs: (1) Fluid muscle robots, which use pre-processed
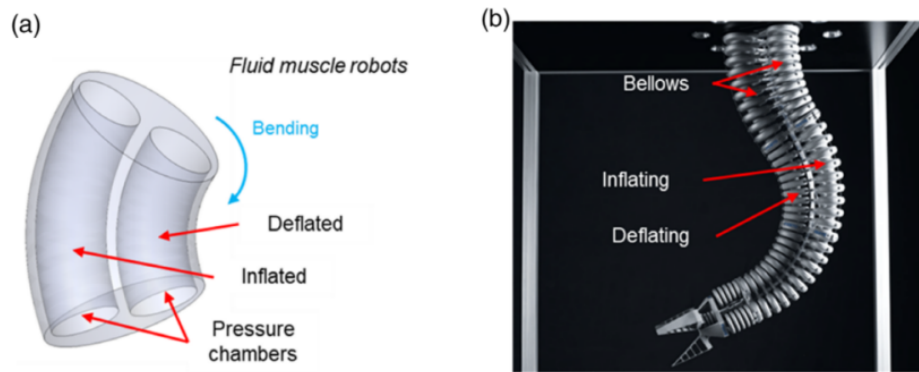
Fig. 2.12 Fluid Muscle Robots [148]

fluids for essential driving in adversarial soft cavities, as shown in Fig. 2.12. (2) Soft growth robots, which can increase their length and are typically pneumatically driven, as shown in Fig. 2.13.
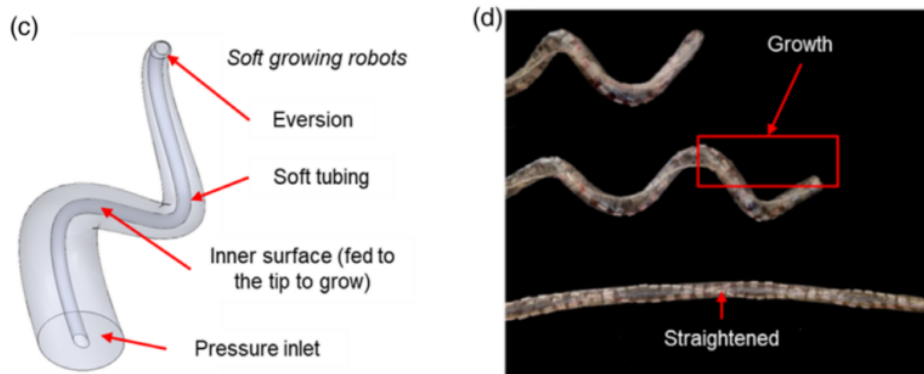


Fig. 2.13 Soft Growth Robots [148]

Their deformation is caused by the expansion of the internal elastic chamber [80]. While magnetic fields can also be directly used to control the shape of the spine without increasing the robot's size, this solution is subject to environmental interference and can only transmit lower forces, making it suitable mainly for healthcare applications [150].

According to Zhao and Liu [316], robots can possess diverse characteristics due to different actuation mechanisms employed. For example, magnetic robots are ideal for miniaturization, whereas tendon-driven robots have a relatively large load capacity. The selection of an appropriate actuation mechanism depends on specific application requirements like payload capacity, precision, and size restrictions.

## 2.5 The Advantages and Applications of Continuum Robots

One of the significant advantages of continuum robot systems is their flexibility, which makes them suitable for medical and wearable applications. Rigid medical equipment or orthotics can cause discomfort or injury to tissues in humans or animals and may not replicate natural joint movement accurately. Wearable devices with degrees of compliance, such as orthopedic rehabilitation, offer a potential solution. Recently, soft robots have been studied for medical and wearable applications, including wearable keyboards [142], sensing kits for foot and ankle rehabilitation [207], sensing kits for lower limb measurement [180], and soft drive systems for rodent gait rehabilitation.

To create soft robotic systems, researchers have also explored the use of biomaterials, such as microbial materials that generate electricity for artificial muscles and autonomous robots [120]. Cardiac cells have even been used to develop swimming robots inspired by jellyfish [190]. One challenge is recycling these robots after completing their tasks, which researchers aim to address with the development of biodegradable and flexible robots powered by gelatin actuators [41]. Moreover, gelatin being edible presents further potential for medical applications of this technology.

Continuum robots are also becoming increasingly important tools for minimally invasive surgeries, providing precise inspection and surgery in areas such as the human skull, abdominal, and upper and lower digestive tracts. Their soft and flexible nature allows for gentle maneuvering and prevents tissue damage, making them ideal for these delicate procedures.

Continuous robots possess excellent bending characteristics and an extraordinary ability to adapt to narrow and unstructured environments filled with obstacles, making them suitable for performing tasks in unknown environments. In contrast with traditional robots, continuous robots can not only install actuators at their ends to enable grasping and clamping actions but can also use their robot body to grasp objects, enhancing their versatility.

Continuous robots find numerous applications in various fields due to their wide range of functionalities. In the industrial field, drilling and gluing operations can be conducted in cramped working conditions such as those found in aircraft wing rib compartments. In the safety services sector, continuous robots can assist in maintenance operations for cooling pipelines in nuclear power plants, search and rescue operations for trapped personnel in buildings that have collapsed due to earthquakes or other disasters, and reconnaissance operations for targets through curved pipelines or obstacles in military operations. These tasks are difficult to accomplish using traditional industrial robots, highlighting the importance of using continuous robots to complete these tasks effectively.

Furthermore, continuous robots' flexibility and adaptability make them ideal for exploring environments that are inaccessible to traditional robots. Hence, they have enormous potential in scientific exploration and space missions. With the advancements in materials science and manufacturing technologies, researchers and engineers can continuously improve the design, construction, and operation of continuous robots, ensuring that they remain versatile tools for solving challenges in various fields.

## 2.6 Conclusions

This chapter presents the development of continuum robots, highlights their advantages over pure rigid mechanisms, and explores their potential applications. The main points are summarized as follows:

Continuum robots are constructed using flexible and compliant materials that imitate the movement and adaptability of natural organisms, such as tentacles or snakes. This allows them to navigate through narrow spaces, traverse uneven terrains, and manipulate delicate objects without causing damage. The seamless and continuous structure of these robots enables smooth and precise movements, facilitating intricate tasks across various applications.

One of the key advantages of continuum robots is their inherent flexibility, which enables them to conform and adapt to different shapes and surfaces. This flexibility makes them valuable in industries such as manufacturing, surgery, and inspection, as they can access confined spaces or tight corners that are challenging for conventional robots. By reaching areas that would otherwise be difficult or impossible to access, continuum robots enhance efficiency and effectiveness in these fields.

Furthermore, the compliant nature of continuum robots ensures safer interactions with humans. Their soft and flexible structure reduces the risk of injury, making them suitable for collaborative tasks in environments where humans and robots work together. This opens up possibilities in fields like rehabilitation, where continuum robots can aid in therapeutic exercises or provide physical support to individuals in need. Additionally, continuum robots contribute to advancements in automation and adaptability. Their compliance and ability to bend or elongate allow them to conform to changing environments or objects. This adaptability makes them highly versatile, capable of performing various tasks without extensive reconfiguration or specialized tools. In scenarios such as disaster response or exploration, continuum robots can navigate unpredictable and hazardous situations, providing valuable assistance.

In conclusion, the importance of continuum robots lies in their unique characteristics that enable them to navigate complex environments, interact safely with humans, and

perform intricate tasks. Their flexibility, adaptability, and compliant nature make them indispensable in industries that require agility, precision, and versatility. As research continues to progress in this field, continuum robots are poised to revolutionize automation, healthcare, and exploration, contributing to a safer, more efficient, and highly adaptable robotic ecosystem. This chapter will serve as the theoretical foundation for the design of knee joint rigid-flexible structures in Chapter 5.

# Chapter 3

# State-of-the-Art Lower Limb Rehabilitation Mechanisms for Stroke Patients

## 3.1  Introduction

This chapter provides an overview of the current state of robotics related to thesis topics in rehabilitation systems for patients recovering from injuries or disabilities. In Section 3.2, ankle joint rehabilitation systems are reclassified into two types: stationary and dynamic, addressing the differences between fixed-position devices and those capable of dynamic movement. A detailed introduction is then given for the ankle joint rehabilitation mechanisms belonging to each category, outlining the advantages and limitations of each approach. In Section 3.3, the focus shifts to knee joint rehabilitation systems, which can be classified into pure rigid-body or soft-body systems. Pure rigid-body systems provide a more stable platform for rehabilitation, while soft-body systems offer greater flexibility and adaptability for patients with varying needs. This section discusses the developments in both types of systems and their respective benefits. Section 3.4 explores research on overall rehabilitation systems with different structures of hip joints, including both stationary and dynamic systems. This section delves into the design aspects of hip rehabilitation, including range of motion, force generation, and ease of use. Finally, Section 3.5 summarizes the key findings of this chapter, highlighting the importance of understanding the different types of rehabilitation systems available and their corresponding advantages and disadvantages. It also emphasizes that this thesis draws design inspiration from the aforementioned rehabilitation exoskeletons to propose innovative institutions and target design structures that further advance the field of rehabilitation robotics.

## 3.2    State-of-the-Art Ankle Rehabilitation Mechanisms

Neurological injuries, such as stroke and spinal cord injury, can cause significant impediments to individuals' normal sports function in daily life [251]. For many people with severe dysfunction in their lower limbs, basic activities such as moving or walking without assistance may be challenging. This is where the ankle joint plays a critical role in rehabilitation.

As one of the most essential joints in the human lower limbs, the ankle joint plays a crucial role in various activities such as squatting, standing, and walking [87]. Comprised of the tibia, fibula, and talus trochlear, the ankle joint primarily facilitates rotations of inversion/eversion (I/E), dorsiflexion/plantarflexion (D/P), and adduction/abduction (A/A). A better understanding of the specific spatial rotation of the ankle joint can be viewed in Figure 3.1 [67].
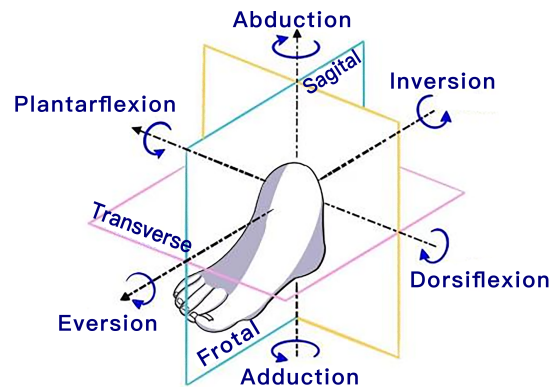


Fig. 3.1 Rotational Model of the Ankle Joint

However, clinical research conducted by Payne et al. [210] and Mattacola [175] has revealed that when considering motion with large amplitude, particularly during rehabilitation, only the first and second degrees of freedom (Dof) in the gait cycle are usually taken into account. Therefore, it is crucial to design rehabilitation mechanisms that cater to the requirements of these two primary Dof. These requirements serve as the basis for effective model design in rehabilitation mechanisms [107].

Thus, ankle joint rehabilitation systems have been developed to enable individuals recovering from neurological injuries to improve their mobility and regain their independence. These systems use a combination of stationary and dynamic mechanisms to provide varied levels of resistance and support for targeted exercises. By targeting the specific joint movements enabled by the ankle joint, rehabilitation systems can promote muscle activation, increase range of motion, and improve overall functionality.

Currently, rehabilitation mechanisms are broadly classified into two categories: stationary mechanisms and wearable mechanisms (exoskeletons/active orthotics) [116, 71].

Stationary mechanisms assist patients in achieving fixed position movements to gradually regain ankle flexibility and improve their sense of balance and proprioception. These mechanisms are particularly useful for patients who need to focus on regaining basic motor function before moving onto more complex tasks.

On the other hand, wearable mechanisms such as exoskeletons and active orthotics aim to help patients achieve dynamic rehabilitation. These devices allow patients to indirectly and actively control the position of the joint complex during walking, restoring the ability of normal walking gait [122]. Wearable mechanisms are especially beneficial for patients who need to train their motor function while performing everyday activities. By providing support and assistance during movement, these wearable devices can accelerate the rehabilitation process and improve patient outcomes.

Wearable rehabilitation mechanisms such as exoskeletons have gained significant attention due to their potential to significantly improve mobility for individuals with neurological injuries. Exoskeletons act as external support structures that attach to the body, providing necessary assistance to the muscles and joints of the wearer. These mechanisms operate through a combination of sensors and actuators to detect and respond to the wearer's movements, allowing for natural, intuitive control. Recent advancements in exoskeleton technology have led to the development of lightweight and more portable models that can be used in everyday life, further enhancing their benefits for rehabilitation.

In conclusion, both stationary and wearable mechanisms have their unique advantages and limitations in ankle joint rehabilitation. Stationary mechanisms are ideal for patients who need to focus on regaining basic motor function, whereas wearable mechanisms such as exoskeletons are beneficial for patients who want to train their motor function while performing everyday activities. With ongoing advancements in technology and design, ankle joint rehabilitation mechanisms hold enormous potential for improving the quality of life for people with neurological injuries.

### 3.2.1 Stationary Rehabilitation Systems

In the first category, one of the most iconic ankle rehabilitation mechanisms is the "Rutgers Ankle" institution [90]. Proposed in 1999 by experts from the University of New Jersey, this ankle rehabilitation robot is based on the Stewart platform. The mechanism utilizes a 6-degree-of-freedom (DOF) collaborative motion driven by double-acting cylinders in each branch chain, making it ideal for patients to use at home. However, while the Rutgers Ankle mechanism has been proven effective, it also has limitations. Its complex mechanism and redundant degree of freedom make it difficult to use and maintain, and it requires a separate air source for operation. As a result, researchers have continued to explore new designs aimed at improving the functionality and usability of

stationary rehabilitation mechanisms. While the Rutgers Ankle institution has paved the way for stationary ankle rehabilitation mechanisms, newer designs are continuing to evolve and improve. The development of more compact and versatile designs will make the rehabilitation process more efficient and effective, ultimately leading to better outcomes for patients with neurological injuries.



Fig. 3.2 Ruatgers Ankle [90]

A reconfigurable ankle rehabilitation system with four degrees of freedom (Dof) consisting of two moving platforms and four reconfigurable branch chains was proposed by Jungwon Yoon and Jeha Ryu, scholars from Kyungsung University of Korea [123]. As shown in Fig. 3.3a, this mechanism enables ankle rotation in inversion/eversion (I/E), dorsiflexion/plantarflexion (D/P), and adduction/abduction(A/A) directions by changing the position of the motor in the control system. This design is closer to the natural movement of the human body, allowing users to stand on the platform for sensory training and facilitating voluntary recovery of the ankle joint. The system also features a force feedback loop that can modify impedance parameters to assist with motion range training, muscle strength training, and proprioceptive training based on torque measurements from the force sensor.

Although this design offers significant benefits, including enhanced human-computer interaction and more effective rehabilitation, it has been criticized for its complex structure, weight, and operational difficulty. To address these issues, researchers have explored alternative designs such as the biological fusion rehabilitation robot proposed by Tsoi [26, 159], as shown in Fig. 3.3. This design leverages the human ankle joint as the primary stress component of the rehabilitation system and treats it as a generalized ball-faced structure, controlling the output force through mechanical drives.

However, this design has its own limitations, including unexpected forces on the position of the ankle joint caused by structural reasons. Nevertheless, ongoing research

(a) A Rehabilitation System with Two Moving Platform

(b) A Biological Fusion Rehabilitation Robot
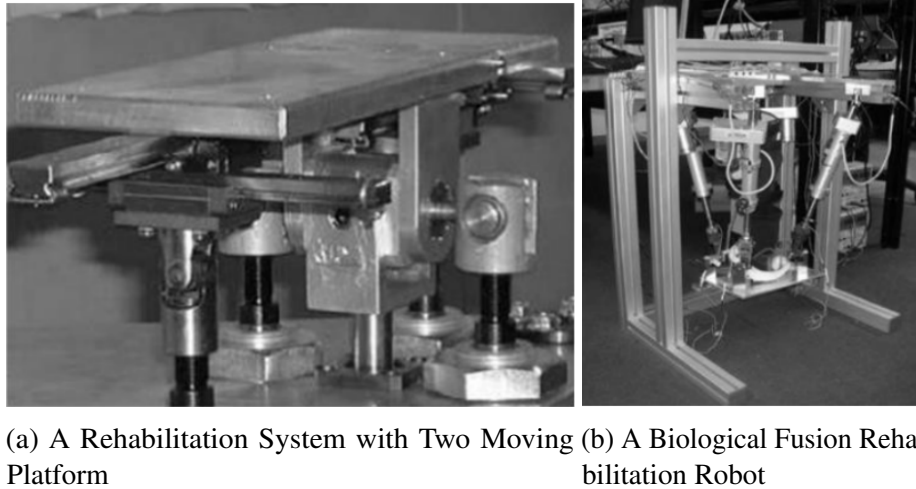
Fig. 3.3 Traditional Ankle Rehabilitation Robots [90, 26]

will continue to explore new designs aimed at improving the effectiveness and usability of ankle rehabilitation mechanisms.

In 1999, Dai and Massicks proposed an equilateral 3-SPS/S parallel mechanism for ankle rehabilitation [58], as depicted in Fig. 3.4a. Later in 2004, Dai et al. completed kinematic capability and stiffness analysis tests of 3-DOF and 4-DOF parallel mechanisms with central struts [57] [63]. Following this, Liu presented a 3-SPS/U ankle rehabilitation robot, as shown in Fig. 3.4b.

In the pursuit of further improvement, Dai and Saglia proposed and studied a novel 2-DOF 3UPS/U parallel mechanism between 2007 and 2009 [231] [229] [237] [234], as shown in Fig. 3.4c. This mechanism can provide rotation in inversion/eversion (I/E) and plantarflexion/dorsiflexion (P/D) directions, simulating normal ankle joint motion. The design of the 3UPS/U parallel mechanism is based on a balanced structure that reduces weight and improves stability. The system has also been applied to muscle strength training and proprioceptive training.

Although these ankle rehabilitation robot designs continue to evolve, there are still significant challenges ahead. Issues such as the need for improved actuation control and human-robot interaction remain important areas of ongoing research. Additionally, the effectiveness of these robotic systems in clinical settings must be validated through controlled studies before widespread adoption.

Gosselin designed a 3-RRR spherical ankle rehabilitation training device [124]. However, since all the axes of motion of the device intersect at one point, the geometric constraints are relatively high, which is easy to cause interference between the foot and the branch chain of patients, increasing the risk factors. Moreover, the entire structure is supported entirely by branch chains. The mechanical structure will be damaged by excessive mass and other factors. In order to reduce the interference between the branch chain and

(a) 3-SPS/S Ankle Rehabilitation Robot

(b) 3-RSS/S Ankle Rehabilitation Robot
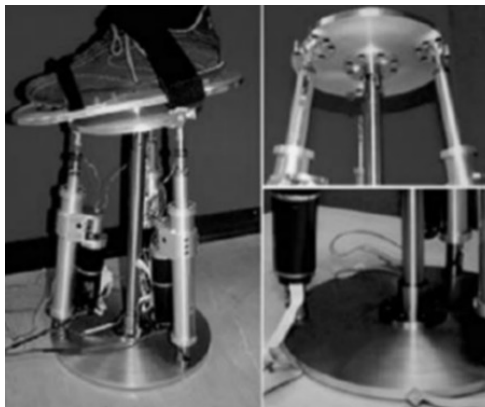


(c) 3-UPS/U Ankle Rehabilitaion Robot
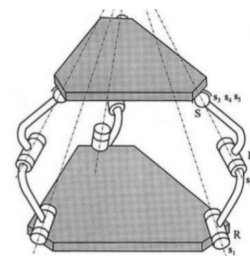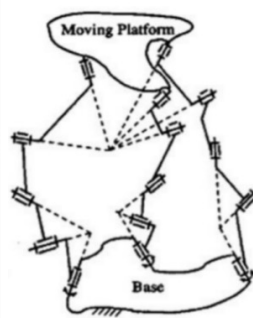


(d) 2-RRR/UPRR Ankle Rehabilitation Robot

(e) 3-RRRRR Parallel Robot

(f) 3-RRS Parallel Rehabilitation Robot

Fig. 3.4 Stationsry Ankle Rehabilitation Robots [58] [57] [63] [231] [229] [124]

the ankle joint, Bian Hui et al. proposed a 2-RRR/UPRR Ankle rehabilitation device [25], as shown in Fig. 3.4d. However, the mechanism still has its unique shortcoming, that is, the axes of all moving pairs must intersect at one point. Therefore, the constraints during the design process are particularly harsh, which causes much trouble to designers and users. In addition, Huang Zhen and Kong Xianwen also designed a 3-RRRRR special mechanical structure [318], as shown in Fig. 3.4e. Another scholar designed a spherical mechanism based on a 3-RRS structure. Then, Gregorio et al. integrated a large number of 3-DOF parallel mechanisms [74] [13] [34]. However, these mechanisms are also based on the RRR and RRS branched structures, as well as a number of other branched structures that can resemble spheres, as shown in Fig. 3.4f. Therefore, these rehabilitation mechanisms also encounter the same problems as mentioned before during the rehabilitation process.

During 2021 and 2022, Dai and Wang et al. proposed and analyzed a variable cellular rehabilitation structure. And this decouple novel robot can be flexibly applied to the home [284] [285]. In 2004, Bharad waj et al. proposed a wearable, low-cost mechanism that uses a spring on a muscle-based pneumatic AC tractor to allow plantar and dorsiflexion of the human ankle and can be used for post-stroke rehabilitation [24]. In addition, MIT researchers designed a 3-DOF ankle robot in 2004 for modular gait rehabilitation [291]. The system uses only two motors to actively drive two of the three degrees of freedom, and retains the third passive degree of freedom, allowing the ankle to freely rotate flexibly. In 2006, Dong et al. proposed another robotic device that could be used for ankle rehabilitation [72]. The single-degree-of-freedom mechanism uses a magnetorheological damper to provide resistance when the patient moves the hip, knee, or ankle. The device reconfigures the joints of the body. However, this device cannot be used for balance training, so this study focuses on platform rehabilitation.

### 3.2.2 Discussion about the Stationary Rehabilitation Systems

The Stationary Rehabilitation System is an innovative medical technology designed to assist patients in their rehabilitation journey. This system provides a stable and controlled environment for therapeutic exercises and activities.

One of the key advantages of the Stationary Rehabilitation System is its ability to offer a safe and secure support system for patients. With adjustable equipment and personalized programs, it caters to the specific needs and conditions of individual patients. The system's stability allows patients to perform exercises with reduced risk of injury, enhancing their confidence and overall progress. Another advantage is the customization and personalization offered by the Stationary Rehabilitation System. Healthcare professionals can design tailored treatment plans based on patients' specific goals and requirements. By monitoring and analyzing patients' progress, therapists can make informed adjustments to optimize

their rehabilitation process. Furthermore, the Stationary Rehabilitation System provides objective feedback and assessment capabilities. Its tracking and recording features enable healthcare professionals to monitor patients' performance, measure improvements, and modify treatment plans accordingly. This data-driven approach enhances the precision and effectiveness of rehabilitation.

However, the Stationary Rehabilitation System also has limitations. Cost and maintenance can be significant factors, as the system requires initial investment and regular upkeep. Additionally, the system may not be suitable for all types of injuries or conditions, and alternative treatment methods may be necessary in certain cases.Table displays the state-of-the-art stationary rehabilitation mechanisms in which the ankle DOFs are actively actuated, as shown in Tab. 3.1.

Table 3.1 State-of-the-Art Stationary Rehabilitation System

| Name | Developers | Types | Architecture | Year(s) | DoF(s) | Status |
|------|-----------|-------|--------------|---------|--------|--------|
| Rutgers Ankle | Girone et al | PR | 6-UPS | 1999 | 6 | Prototype |
| - | Dai et al | PR | 3-SPS | 2004 | 3 | Concept |
| Motion Maker | Schmitt et al | PR | Crank | 2004 | 6 | Commercial |
| - | Yoon et al | PR | 2-PSPP/PRR | 2005 | 4 | Prototype |
| - | Liu et al | PR | 3-RSS/S | 2006 | 3 | Prototype |
| ARBOT | Saglis et al | PR | 3-UPS/U | 2008 | 2 | Prototype |
| - | Tsoi and Xie | PR | 4-UPS | 2008 | 3 | Concept |
| - | Syrseloudis and Emirs | PR | 3-RPS | 2008 | 3 | Concept |
| - | Lin et al | PR | - | 2008 | 1 | Prototype |
| - | Saga and Saito | AFO | - | 2008 | 1 | Prototype |
| - | Jamwal et al | PR | - | 2009 | 3 | Prototype |
| - | Sui et al | PR | - | 2009 | 2/3 | Concept |
| Lambda | Bouri et al | FR | Lambda | 2009 | 6 | Prototype |
| - | Bain et al | PR | 2-RRR/UPRP | 2010 | 3 | Prototype |
| NUVABAT | Ding et al | PR | - | 2010 | 2 | Prototype |
| - | Sung et al | FR | - | 2011 | 2 | Prototype |
| - | Ren et al | AFO | - | 2011 | 1 | Prototype |
| PKAnkle | Malosio et al | PR | 3-RRR | 2012 | 3 | Prototype |
| - | Wang et al | PR | 3-RUS/RRR | 2013 | 3 | Prototype |
| Tobibot | Guzm Valdivia et al | PR | - | 2014 | 1 | Prototype |
| - | Zhou et al | FR | - | 2015 | 1 | Prototype |

| Name | Author | | Configuration | Year | DOF | Status |
|---|---|---|---|---|---|---|
| PedBot | Monfaredi et al | PR | - | 2016 | 3 | Prototype |
| CARR | Zhang et al | PR | 4-SPS | 2016 | 3 | Prototype |
| - | Du et al | PR | 3-RRS | 2017 | 3 | Concept |
| - | Nurahmi et al | PR | 3-RRS | 2019 | 3 | Concept |
| - | Chang and Zhang | PR | RRR/P | 2019 | 3 | Concept |
| NARR | Wang et al | FR | - | 2019 | 6 | Prototype |
| - | Wang et al | PR | 2-SPS/S | 2019 | 2 | Prototype |
| - | Li et al | PR | 2-SPS/PU | 2019 | 4 | Concept |
| - | Dong et al | PR | 2-UPS/RRR | 2020 | 3 | Prototype |
| Hunova | Movendo Technology | PR | - | - | 2 | Commercial |
| ARTROMOT-SP3 | Chattanooga | PR | - | - | 2 | Commercial |
| JACK Ankle | JACE System | PR | - | - | 1 | Commercial |
| Kinetec Breva | Kinetec | PR | - | - | 2 | Commercial |
| Kinetec 5090 | Kinetec | PR | - | - | 3 | Commercial |
| Biodex System 4 | BIODEX | PR | - | - | 2 | Commercial |

In summary, the Stationary Rehabilitation System offers advantages such as safety, customization, and objective feedback. It provides patients with a stable and controlled environment while allowing healthcare professionals to tailor treatment plans and track progress. Nonetheless, cost and suitability limitations need to be considered when implementing this system. Overall, the Stationary Rehabilitation System plays a valuable role in modern healthcare by providing effective and personalized rehabilitation solutions.

### 3.2.3 Dynamical Rehabilitation Systems

In the context of ankle-foot complex rehabilitation devices, researchers have explored different approaches to designing mechanisms that can approximate the biological joint model. One category of design involves incorporating a simplified geometric model of the joint, such as a fixed spherical joint, into the robot design. Another category involves modeling the ankle-foot complex based on its anatomical structure.

The fixed spherical joint model, where the relative position between the ankle-foot complex and the device remains unchanged, is commonly used when designing ankle-foot orthosis (AFO) or exoskeleton (EXO) systems. Among the three motions studied, adduction/abduction (A/A) has minimal contributions to gait rehabilitation and is often neglected in the design process [143, 280]. In contrast, dorsiflexion/plantarflexion (D/P) is the dominant motion and a crucial consideration in the design phase.

Fig. 3.6a shows an example of an AFO designed with a fixed spherical joint model. However, recent research has proposed more advanced techniques for designing ankle-foot rehabilitation devices. For instance, MIT designed an active ankle-foot orthosis (AAFO) with a series elastic actuator, allowing for active adjustment of joint stiffness and damping to adapt to different walking phases and variations [30], as shown in Fig. 3.6b. Another design proposed by researchers from the University of Michigan utilized artificial pneumatic muscles to actuate D/P motion [93]. This study compared the performance under single- and double-muscle powered conditions and revealed the limitations of the presented orthosis. Subsequently, the same research group extended the design to a knee-ankle-foot orthosis (KAFO) with antagonistic pairs of artificial muscles at both the ankle and knee joints, as shown in Fig. 3.6c [261]. These advanced designs offer improved functionality and adaptability in rehabilitation devices.

In the second category, instead of using a simplified model for the joint, the ankle-foot complex is modeled as a serial kinematic chain consisting of two revolute joints with fixed orientations that mimic the ankle joint and subtalar joint [22]. One example of this approach is the orthosis designed by Agrawal et al. which includes two joints that provide dorsiflexion/plantarflexion (D/P) motion and pronation/supination (P/S) motion, respectively, as shown in Fig. 3.5. However, the axes in this model are assumed to be

fixed, which may not fully capture the actual variations in joint axes during movement. Additionally, accurately modeling the variations in biological joint axes is mathematically challenging, making new designs and analyses difficult to carry out.
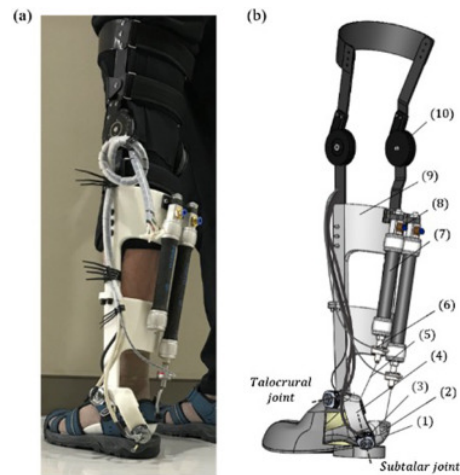


Fig. 3.5 A Two-Degree-of-Freedon Powered Ankle-Foot Robot [22]

To overcome these limitations, studies have proposed using more advanced modeling techniques, such as finite element analysis or musculoskeletal modeling, to create more accurate models of the ankle-foot complex. These techniques allow for a more realistic representation of the joint's motion and better understanding of the underlying biomechanics, leading to more effective robot design for ankle-foot rehabilitation.

The figure showcases a lower-limb rehabilitation system that actuates three joints: the hip, knee, and ankle. Recent research has shown that active ankle-foot orthosis (AFO) or ankle exoskeleton (EXO) systems can generate more natural and realistic gait patterns, compared to those with passive ankle motions or fixed foot-shank angles, such as HAL-3, Lokomat, LokoHelp, etc [135, 52, 28]. These advanced systems provide better performance in terms of gait rehabilitation and can improve mobility in patients with gait impairment conditions.

Treadmills and body weight support equipment are often used in conjunction with exoskeletons in some gait training systems to enhance their efficacy, such as the ALEX III [53, 255]. However, these treadmill-based exoskeletons are not portable and are unsuitable for use in residential settings [311].

To address these challenges, researchers have developed modular designs in some lower-limb rehabilitation devices to facilitate convenient adaptation of exoskeletons for patients with different gait impairments [73]. Such modular systems allow for auxiliary movements in one or more joints and offer increased flexibility in both structural topology and actuation systems, which can perform passively or actively [12].

(a) T-strap for Ankle and Foot
AFO PLUS

(b) The Active Ankle Foot Orthosis(AAFO)



(c) KAFO Robot

Fig. 3.6 Stationary Ankle Rehabilitation Robots [135, 52, 28]

Overall, these advanced lower-limb rehabilitation systems offer promising solutions to improve the quality of life for patients with gait impairment conditions.

Among the dynamic rehabilitation systems capable of actively assisting two degrees of freedom (2 DOFs), two well-known representatives are external skeletons stemming from parallel mechanisms, as shown in the figures. The first of these devices, Anklebot, is an underactuated device that integrates the human leg into the mechanism to constrain translational DOFs and uses two parallel-mounted linear actuators to drive D/P and I/E [291]. This back-driveable robot has low friction and mechanical impedance, displaying potential in estimating passive ankle stiffness. The second device, a robotic gait trainer developed by Bharadwaj et al., also considers the human shank as part of the mechanism, but unlike Anklebot, the rotation center of this tripod-structure-based exoskeleton does not align with that of the ankle-foot complex [227]. While most exoskeletons used in gait rehabilitation systems are based on crank or rocker designs, there are other architectures being developed and tested. For instance, the Gangtrainer GT I, which employs slings to reduce body weight and two footplates for simulating different gait phases such as support and swing, has demonstrated positive therapeutic effects in global clinical trials [106]. Similarly, the HapticWalker provides simulation for walking on flat/uneven surfaces and up/down stairs and can extend each foot's 3 DOFs in the sagittal plane to 6 DOFs by exchanging the foot

module. Another system designed for ascending and descending stairs is composed of linear guides and a linkage-slider mechanism to provide 2 DOF that allow forward/backward and up/down movement of the feet. In research on this system, electromyography (EMG) and plantar pressure data were collected to examine the effectiveness of the device [280]. Although parallel mechanisms are prevalent in static rehabilitation systems, they are less commonly utilized in dynamic rehabilitation systems. Nevertheless, some recent works have adopted two parallel robots to achieve exoskeleton-like functions for both feet of a patient, as shown in the system described in [280].

### 3.2.4   Discussion about the Dynamical Rehabilitation Systems

The Dynamical Rehabilitation System is a innovative approach to rehabilitation that focuses on dynamic movements and real-time adjustments. This system utilizes advanced technologies and equipment to create an interactive and adaptive rehabilitation environment.

One of the key advantages of the Dynamical Rehabilitation System is its ability to provide dynamic and customized exercises. By incorporating real-time feedback and adjustments, this system can adapt to the specific needs and abilities of individual patients. This personalized approach enhances engagement and motivation, leading to better treatment outcomes. Another advantage is the emphasis on functional movements. The Dynamical Rehabilitation System focuses on simulating real-life activities, enabling patients to regain and improve their functional abilities. By targeting specific movements and tasks, this system promotes the development of motor skills and enhances overall functionality.

However, there are some limitations to consider. The cost of implementing and maintaining the Dynamical Rehabilitation System can be a drawback, particularly for smaller healthcare facilities or under-resourced areas. Additionally, the complexity of the system may require specialized training for healthcare professionals to ensure safe and effective usage. Thus, the table concludes the state-of-the-art dynamic rehabilitation mechanisms in which the ankle DOFs are actively actuated mentioned above, as shown in Tab. 3.2.

Table 3.2 State-of-the-Art Dynamic Rehabilitation System

| Name | Developers | Types | Architecture | Year(s) | DoF(s) | Status |
|---|---|---|---|---|---|---|
| Gangtainer GTI | Hesse and Uhlenbrock | FR | Crank and Rocker | 2000 | 2 | Commercial |
| Anklebot | Wheeler et al. | EXO | 2-SPS | 2004 | 2 | Prototype |
| AAFO | Blaya and Herr | AFO | - | 2004 | 1 | Prototype |
| HapticWalker | Schuidt | FR | Modified slider-cmnk | 2004 | 6/12 | Prototype |
| - | Bharadwaj et al | AFO | 2-RPS/RR | 2005 | 2 | Prototype |
| - | Gordon et al | AFO | - | 2006 | 1 | Prototype |
| - | Costa et al | EXO | - | 2006 | 10 | Prototype |
| - | Agrawal et al | AFO | - | 2007 | 2 | Prototype |
| - | Fan and Yin | EXO | 3-RPS | 2009 | 2 | Prototype |
| GaitMaster5 | Yano et al | FR | Modified slider-crank | 2010 | 4 | Prototype |
| ALEXIII | Zanotto et al | EXO | - | 2013 | 12 | Prototype |
| - | Yu ct al | EXO | - | 2013 | 1-2 | Prototype |
| KIT-EXO-1 | Beil et al | EXO | - | 2015 | 3 | Prototype |
| Active Ankle | Simofske ct al | EXO | Similar to DELTA robot | 2016 | 3 | Prototype |
| - | Tsuge and McCarthy | EXO | Six-bar linkage | 2016 | 1 | Concept |
| - | Kuettel | AFO | - | 2016 | 1 | Concept |
| - | Moltedo et al | AFO | - | 2016 | 1 | Prototype |
| - | Santos ct al | AFO | - | 2017 | 1-6 | Prototype |
| BioMot | Bacek et al | EXO | - | 2017 | 1-6 | Prototype |
| - | Cardoso and Silva. | AFO | Four-bar linkage | 2017 | 1 | Copcept |
| Autonomyo | Oxtileb et al | EXO | - | 2017 | 7 | Prototype |

| CPWalker | Bayon et al | - | - | 2017 | 6 | Prototype |
|---|---|---|---|---|---|---|
| - | Lyu et al | EXO | - | 2017 | 4 | Prototype |
| - | Nazim Mir-Nazasri | EXO | - | 2017 | 4 | Copcept |
| - | Chang et al | EXO | - | 2017 | 2 | Prototype |
| - | Long et al | EXO | - | 2017 | 7 | Prototype |
| - | Kim et al | EXO | - | 2017 | 6 | Prototype |
| - | Zhu et al | EXO | - | 2017 | 2 | Prototype |
| - | Sannogoen et al | EXO | - | 2017 | 2 | Prototype |
| - | Gui et al | EXO | - | 2017 | 2 | Prototype |
| WAKE-up | Cappa et al | EXO | - | 2017 | 4 | Prototype |
| - | Moltedo et al | AFO | - | 2017 | 1 | Prototype |
| - | Wu et al | EXO | - | 2018 | 3 | Prototype |
| - | Ostaszewski et al | EXO | - | 2018 | 3 | Prototype |
| - | Yan et al | EXO | - | 2018 | 4 | Concept |
| - | Zhang et al | EXO | - | 2018 | 2 | Prototype |
| P-LEGS | Eguren | EXO | - | 2019 | 6 | Prototype |
| - | Wang et al | PR | 2-PSS/2-RRR/PR | 2019 | 6 | Concept |
| - | Jarzyna et al | EXO | - | 2020 | 6 | Prototype |

In summary, the Dynamical Rehabilitation System offers several advantages, including dynamic and customized exercises, emphasis on functional movements, and interactive features. These characteristics enhance patient engagement, promote functional recovery, and provide objective data for assessment. While there are limitations in terms of cost and complexity, the potential benefits make the Dynamical Rehabilitation System a promising approach to rehabilitation.

### 3.2.5 Summary of Ankle Joint Rehabilitation Mechanism

Based on the research discussed above, it is evident that current ankle rehabilitation systems are inadequate in meeting the needs of stroke patients by simply providing rotational space. Future design considerations should prioritize creating systems that are lightweight, flexible, and optimal in terms of interactivity. A lightweight design can make it easier for patients to wear and reduce the burden on both the patient and their family. Flexibility is not only about satisfying workspace requirements but also about being more intelligent in design. An intelligent design that incorporates both active and passive features is needed to better meet the needs of patients.

Furthermore, as an exoskeleton designed for rehabilitation patients, perfect coordination with the human body is crucial. The center of rotation should be matched in real-time with the rotation center of the human ankle joint as much as possible. Therefore, this article proposes designing a new type of ankle rehabilitation mechanism in the following sections that not only meets the rotational angle requirements but also achieves real-time matching of the rotation center and a buffering assisting effect under the intervention of springs. The proposed mechanism has the potential to provide a more effective treatment option for stroke patients, addressing the limitations of current ankle rehabilitation systems.

## 3.3 State-of-the-Art Knee Rehabilitation Mechanisms

Understanding the biomechanics of the human knee joint is essential for the development and control of knee exoskeletons. The knee joint, consisting of components such as the femur, tibia, anterior crucial ligament, and posterior crucial ligament, is a complex joint in the human body. It can be modeled as a crossed four-bar linkage mechanism [198], which will be discussed in more detail in subsequent sections.

The stability of the knee joint relies on various ligaments, including the medial and lateral collateral ligaments, as well as the anterior and posterior crucial ligaments [215]. Additionally, the quadriceps femoris muscles play a vital role in stabilizing the knee joint. The menisci, located within the knee joint, are responsible for shock absorption during daily activities.

During normal human locomotion in the sagittal plane, several key muscles in the lower limbs are involved. These muscles include the iliopsoas, gluteus maximus, rectus femoris (RF), semitendinosus (ST), vastus medialis (VM), biceps femoris short head (BF), gastrocnemius, soleus, and tibialis anterior [167]. From the research, it is known that the RF and VM are extensor muscles responsible for extending the knee joint, while the ST, BF, and gastrocnemius are flexor muscles that contribute to knee flexion.

Further understanding of the biomechanics and muscle functions of the knee joint is crucial in designing effective knee exoskeletons for rehabilitation and assistance purposes.

## 3.3.1 Difference of Knee Joint between Stance Phase and Swing Phase in a Regular Human Gait-Cycle

The human gait cycle consists of two main phases: the stance phase and the swing phase. The stance phase can be further divided into the weight acceptance phase and the terminal stance phase [240].

In a normal gait pattern, the joint angle and torque of the human knee undergo specific changes throughout the gait cycle. During the initial phase, the knee joint flexes in the positive direction, generating a large torque to support body weight and reduce shaking. This flexion helps with shock absorption and prepares for the subsequent swing phase. Fig. 3.7 illustrates the knee joint's detailed anatomy and the corresponding kinematics and kinetics during the gait cycle, as reported in a clinical gait study [292].

Besides, the knee joint acts as a linear torsional spring with appropriate stiffness. The stiffness of the spring can vary based on factors such as an individual's body size, terrain, and gait conditions [246]. It is important to note that the stiffness of the knee joint's spring-like behavior contributes to its ability to absorb and distribute forces effectively during walking or running activities.

During the terminal stance phase, the knee joint produces a smaller torque and demonstrates reduced quasi-stiffness compared to the earlier stages of the gait cycle [246]. This phase corresponds to the period when the foot leaves the ground, and the leg transitions into the swing phase.

In contrast to the stance leg, the knee joint of the swing leg remains relatively inactive and does not require significant muscular exertion. It exhibits a more passive behavior as it prepares for the subsequent foot contact during the following gait cycle. The swing phase allows for leg extension and forward movement, facilitated by the coordinated action of various muscles in the hip and ankle joints.

Understanding the distinct characteristics and functions of the knee joint during different phases of the gait cycle is crucial for developing efficient and adaptable knee exoskeletons. By replicating the biomechanics and muscle functions of the natural knee
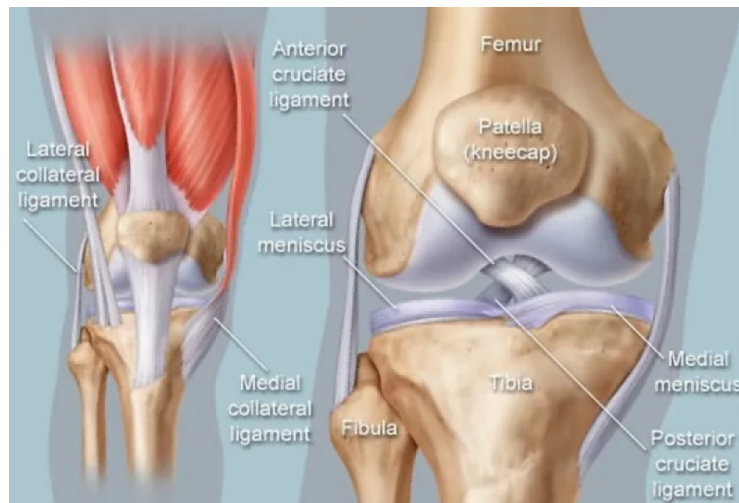
Fig. 3.7 Detailed Anatomy of the Knee Joint [292]

joint, exoskeletons can provide assistance and rehabilitation support that aligns with the human body's movement patterns.

## 3.3.2 The Influence of Muscle Structure of Knee Joint for Stroke Patients

In general, patients with knee impairments resulting from stroke, spinal cord injury, and other diseases often exhibit abnormal muscle activity patterns, leading to difficulties in generating normal-magnitude voluntary muscle contractions [201]. These issues significantly impact their gait performance. Among these conditions, stroke is a primary cause of mobility disorders, and individuals who have suffered a stroke commonly experience unilateral weakness on the affected side.

Consequently, these patients may exhibit a characteristic gait pattern where they drag their affected leg in a semicircular motion during walking. Weakness or paralysis of the muscles responsible for stabilizing the knee can make it challenging to maintain walking stability. Compared to individuals without impairments, those with knee dysfunctions may be more susceptible to collapsing during the weight acceptance phase of the gait cycle. Therefore, knee exoskeletons hold great promise as a potential solution to address the pathological gait observed in individuals with knee impairments.

By providing assistive support and augmenting the weakened or paralyzed muscles, knee exoskeletons can enhance walking stability and promote a more natural gait pattern. These devices are designed to provide the necessary mechanical support and control to facilitate movements during weight acceptance, terminal stance, and swing phases, thereby helping individuals with knee dysfunctions regain their mobility and improve their overall quality of life.

### 3.3.3 The Development of Knee Joint Rehabilitation Exoskeleton

With the advances in technology and the growing demand for lower limb rehabilitation, researchers have been devoting significant efforts to this field [289]. As a result, numerous research findings have been obtained, contributing to the progress of lower limb rehabilitation techniques [40, 42, 49]. One notable development in this area is the introduction of continuous passive motion (CPM) machines, pioneered by de Vries et al. in 1970 [65]. The first CPM device was subsequently developed in 1978 [81].

Typically, CPM machines are designed as 2-bar systems, as illustrated in Fig. 3.8 [89, 92, 98]. These machines play a crucial role in promoting joint movement and enhancing range of motion during rehabilitation. By passively moving the joint through a controlled, repetitive motion pattern, CPM machines can prevent joint stiffness, reduce swelling, and facilitate tissue healing. This technology has been widely used in various rehabilitation settings to assist in the recovery of patients with knee impairments or after knee surgery.



Fig. 3.8 A continuous passive motion (CPM) machines [89, 92, 98]

BioDex was established in 1988 to address muscular and cruciate ligament injuries [101] [104]. It consisted of a programmable force-controlled, single-axis system that proved beneficial for muscle exercise [105]. Another design worth mentioning is the multi-iso mechanism, which is a fixed-based machine incorporating a single hinged joint [108] [118]. The seat position of this mechanism can be adjusted manually or automatically using a unique design with six motors [119] [131].

In 2009, a mechanism called NeXos was developed at the University of Abertay Dundee. It comprises three main segments: a fixed-base system with three moving elements, two of which are in direct contact with the leg [139] [141] [149] [153]. NeXos is particularly useful as it allows patients to exercise passively and with assistance [236] [231] [229] [232] [233].

Another notable machine, Physiotherabot, was proposed in 2011 and has 3 degrees of freedom (DOFs) [155]. Similar to NeXos, Physiotherabot allows passive and assisted exercises [288], but it can only assist one leg at a time [156].

Additionally, gait-training robots have been developed by various researchers, such as the Gait Trainer GT-I [157] [177] [181]. This robot incorporates a fixed gait-like trajectory

with a doubled crank and rocker system [183]. During muscle exercise, the Gait Trainer GT-I enables patients to move horizontally and vertically in accordance with the gait [187]. It also allows individuals with severe damage to engage in repeated gait-like exercise without therapist assistance [189] [191].

These advancements in rehabilitation technology demonstrate the ongoing efforts to enhance lower limb rehabilitation techniques and improve patient outcomes within this field.
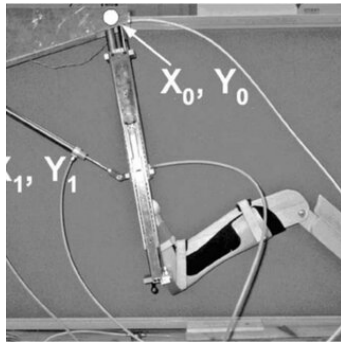


Fig. 3.9 NeXos Rehabilitation Mechanism [236]



Fig. 3.10 A Physiotherablt Robot [155]

In this research field, the most popular mechanism is a robot called Lokomat [193]. This robot can be worn on the body of patients when they are walking on a treadmill [206] [211]. The ability to account for human–machine interaction and allow the patient to actively influence and change the gait pattern is the most appealing aspect of this design [226].

Another mechanism similar to Lokomat is AutoAmbulator, as shown in Fig. 3.11, which was proposed by the HealthSouth Corporation, Birmingham, Alabama, USA [238] [245].

It uses two mechanisms attached to the legs to help people walk on a treadmill [247]. The pelvic assist manipulator (PAM) and pneumatically operated gait orthosis (POGO) robots were proposed by the University of California. The main feature of these robots is that they combine two large segments: one segment has 5 DOF [229] [235] [230] to assist the manipulator, and the other segment has 2 DOFs [248] [234] to help people walk on a treadmill. A series of tests showed that the PAM and POGO robots significantly help patients, as shown in Fig. 3.12, lowering the physical stress on them [254].

In 2004, an academic team developed the Haptic Walker based on the GT-I robot, as depicted in Fig. 3.13 [264] [270] [279]. The Haptic Walker is designed with two footplates to facilitate patient movement [264, 270, 279], and each has 3 DOFs [281]. One remarkable feature of this robot is its ability to maintain constant foot-machine contact throughout motion [286, 295].

In 2005, Veneman et al. introduced the LOPE robot, which incorporates three rotational joints: one at the knee and two at the hip, as shown in Fig. 3.14 [307, 313, 314]. In 2013,
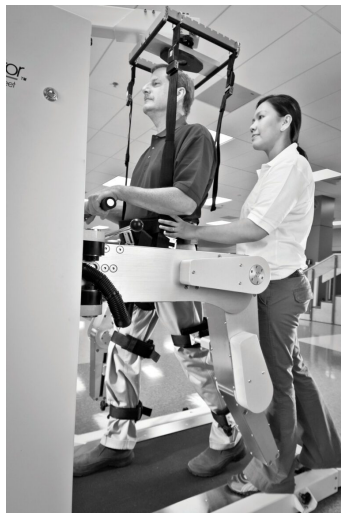
Fig. 3.11 The AutoAmbulator Sys-tem [238] [245]

Fig. 3.12 The PAM and POGO Mecha-nism [254]

the LOPE robot underwent an upgrade by incorporating a parallel structure positioned behind the patient. This modification offers several benefits, including minimal alignment requirements and unrestricted lateral movement, allowing the patient's arm to swing without obstruction [307, 313, 314].



Fig. 3.13 The Haptic Walker System [281] Fig. 3.14 The LOPEs Robot [307, 313, 314]

In 2007, Sai K. Banala designed a well-known robot called the Active Leg EXoskeleton (ALEX). ALEX was specifically developed for individuals with walking disabilities . Over the years, ALEX underwent three upgrades and was later renamed C-ALEX. C-ALEX exhibits improved flexibility and employs the string-puppet principle to reduce the weight of the machine and its impact on the user's body.

However, one drawback shared by the Haptic Walker and C-ALEX is their large size, necessitating the availability of a spacious room for housing these robots [320].

In 2011, a pneumatically actuated exoskeleton was developed, as illustrated in Fig. 3.15. This robot, unlike others, incorporates 10 degrees of freedom and utilizes a fuzzy controller to ensure correct leg positioning for the patient [322]. A distinguishing feature of this robot is its utilization of pneumatic actuators instead of electric motors [217].

Although numerous designs for exoskeleton mechanisms have been proposed in recent decades, there are still several challenges that need to be addressed before they can be effectively used in domestic rehabilitation settings.

The first challenge pertains to reconfiguration and customization. Many existing exoskeleton mechanisms are rigid structures and do not adequately meet the individual needs of patients. Customizability and adaptability are crucial for rehabilitation interventions to be effective and efficient for each patient's unique requirements.

The second challenge involves robotic intelligence for evaluating recovery progress. Currently, there is a limitation in timely collection of patient information and assessing their rehabilitation progress. Incorporating intelligent algorithms and sensor systems can enable real-time monitoring, data analysis, and personalized feedback, facilitating better evaluation of the patient's rehabilitation journey.

The last obstacle is the lack of effective personalized treatment methods. Exoskeletons currently struggle to tailor rehabilitation programs specifically to suit the needs of individual patients. Developing adaptive control strategies and incorporating machine learning techniques can help in dynamically adjusting rehabilitation protocols based on the patient's progress and specific requirements.

In the field of exoskeleton research, a major challenge lies in achieving human-machine collaboration. The human body should be at the center of mechatronics, and the exoskeleton should constantly interact with the human user to achieve mutual adaptation and functional enhancement. This necessitates considering the effects of human-machine interaction rather than solely focusing on what the machine can achieve.

Furthermore, the interaction between mechanical and electrical devices and biological systems is bi-directional. Exoskeleton machines should not only assist or augment humans in performing real tasks but also adhere to human behavioral rules and avoid compromising or hindering natural human functions.

### 3.3.4 Summary of Knee Joint Rehabilitation Mechanism

Based on the background research on knee rehabilitation mentioned above, exoskeleton rehabilitation devices can be classified into two categories: series mechanisms and parallel mechanisms. Series mechanisms often rely on calf-mounted air pumps for power generation. While this type of mechanism can meet the torque requirements, the positioning of the air pump significantly interferes with the rotation angle of the knee joint. On the other
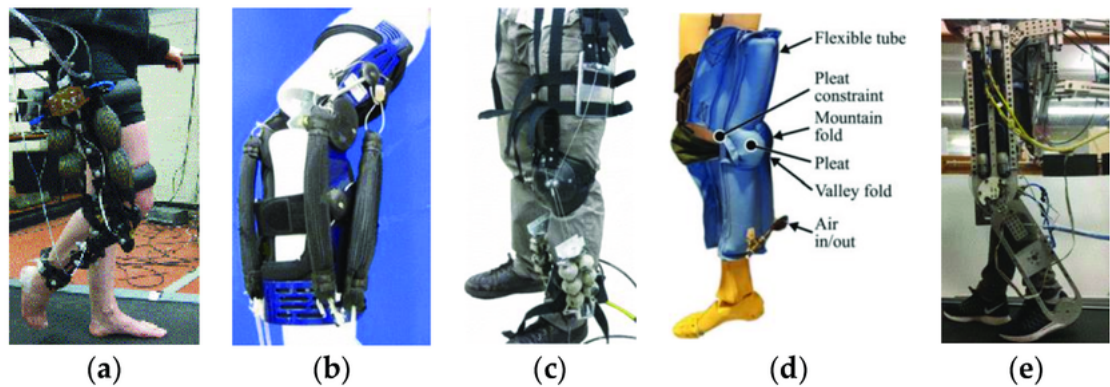
Fig. 3.15 The Pneumatically Actuated Exoskeleton [322] [217]

hand, parallel mechanisms face the challenge of potential interference between the legs when placed internally. Therefore, determining the optimal position for the mechanism is a noteworthy issue.

Moreover, a simple rotating pair cannot fulfill the requirement of automatic centering of the rotation center. This issue has been addressed through the introduction of passive five-bar mechanisms and flexible rods, which have contributed to improving the overall performance of exoskeletons for knee joint rehabilitation.

Furthermore, the combination of rigid and flexible structures in exoskeleton designs has proven advantageous. These mechanisms offer both the support provided by rigid rods and the flexibility to adapt their shape as necessary. Additionally, the emergence of rope drives has allowed for more compact workspace utilization, and the use of pulleys enables changes in force direction.

In later chapter of this thesis, a novel exoskeleton configuration for knee joint rehabilitation is proposed, which combines the benefits of self-tracing and self-adapting exoskeletons. A prototype based on this design has been developed, and its interaction forces, torques, and displacement with the lower limb are being monitored to quantify the exoskeleton's compatibility. The motion data of human lower limbs collected by a gait capture system will be presented in subsequent chapters, along with an ergonomic exoskeleton mechanism. The findings and results related to the rigid-flexible structure will also be reported. To optimize the solution, a method combining Matlab and Genetic Algorithm will be proposed. Based on the quantitative testing results, the compatibility of the exoskeleton will be discussed, and the prototype will be validated with the findings, providing recommendations for further research.

## 3.4 State-of-the-Art Hip Rehabilitation Mechanisms

In addition to the knee and ankle joints described earlier, the hip joint is a vital component in designing the overall lower limb exoskeleton structure. During lower limb rehabilitation, the hip joint mainly plays an auxiliary role by bearing forces. Its main function includes rotational movements in two directions: lifting the leg forward and sideways.

To meet these requirements, the anatomical structure of the hip joint needs to be considered in the design of the overall lower limb exoskeleton structure. The appropriate position and direction for the exoskeleton to coordinate with the hip joint must be determined. When selecting the hip joint position, it is important to minimize interference with the rotation angle of the knee joint while avoiding interference on the inner side of the legs. Additionally, addressing the requirement of an automatic rotation center through passive five-bar mechanisms and flexible rods can improve control of the hip joint.

Studies have shown that hip rehabilitation primarily involves the muscle structure composed of hip flexors, hip extensors, buttock muscles, and other components. These muscles are crucial for supporting and controlling the hip joint. Therefore, in the design of the overall lower limb exoskeleton structure, consideration must be given to the motion characteristics of these muscles to ensure that the exoskeleton provides sufficient support and control. The structure of the hip joint is established as shown in Fig. 3.16.
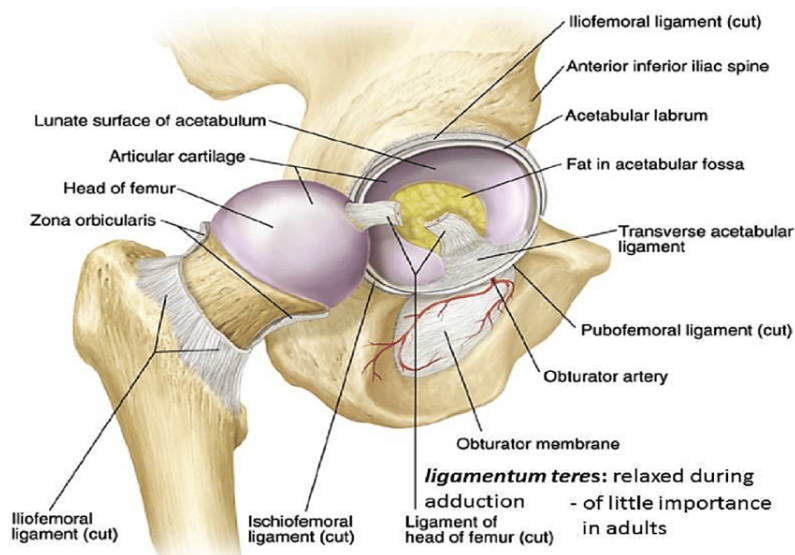


Fig. 3.16 Structure of Hip Joint [7]

Numerous researchers have extensively explored the design of the overall lower limb exoskeleton structure. One notable study proposed a personalized adaptive method for designing lower limb exoskeletons, which utilized a motion capture system and sensors to

capture human motion data. The design optimization process involved the utilization of Matlab and genetic algorithms, among other techniques. In another study, machine learning was employed in the control of lower limb exoskeletons. By analyzing biomechanical data, the system predicted and adjusted the user's movements, thereby enhancing the adaptability and fit of the exoskeleton.

Designing the overall lower limb exoskeleton structure is a challenging and intricate task that necessitates the consideration of several factors, such as human anatomical structure, muscle biomechanics, and mechanical design. However, with the emergence of novel technologies and the progression of research, the prospects for development in this field are expected to broaden, leading to more effective solutions for lower limb rehabilitation.

## 3.4.1  Development of the Hip Rehabilitation Mechanisms

Neurological damage resulting from a stroke often leads to hemiplegia or partial paralysis on one side of the body, significantly impairing the patient's ability to perform daily activities such as walking and eating. Physical therapy, including rehabilitation, plays a crucial role in restoring lost function and promoting recovery [251].

Various robot systems have been developed for lower limb rehabilitation, encompassing treadmill gait trainers, foot-plate-based gait trainers, overground gait trainers, stationary gait and ankle trainers, and active foot orthoses, as illustrated in Figure 1. The primary objective of rehabilitation training is to engage in specific exercises that stimulate the patient's motor plasticity, thus enhancing motor recovery and minimizing functional impairments. Since exercise rehabilitation relies heavily on limb movements, it is essential to target the affected limbs during therapy. To alleviate the workload of therapists, numerous systems have been devised [241].
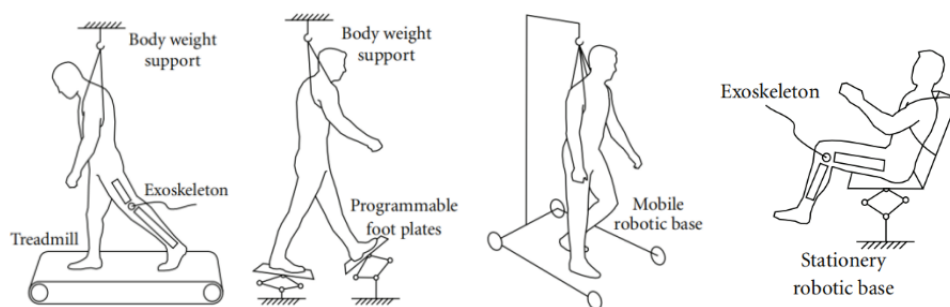


Fig. 3.17 Four Types of the Overall Lower Limb Rehabilitation Robot [241]

In the market, there are currently some lower limb rehabilitation systems available, all of which involve a combination of treadmills and exoskeleton robots [86], as depicted in

Fig. 3.18. Among these ten systems, three are currently accessible for use: the Lokomat, the LokoHelp, and the ReoAmbulator. The Lokomat comprises of a robotic gait orthosis integrated with an advanced body weight support system, along with a treadmill [51].

These systems have proven to be effective in providing intensive and repetitive gait training for individuals with lower limb impairments. By assisting and guiding the patient's movements, they enable more accurate and controlled rehabilitation exercises. Additionally, the incorporation of the treadmill allows for the simulation of overground walking, promoting a more natural gait pattern and facilitating the relearning of proper locomotion. The Lokomat, LokoHelp, and ReoAmbulator have gained recognition due to their positive impact on improving mobility and functional outcomes in patients undergoing lower limb rehabilitation.



Fig. 3.18 Locomat System [86]          Fig. 3.19 LokoHelp System [51]

The LokoHelp is a specialized electromechanical device that targets gait improvement in individuals who have suffered from brain injuries. Positioned parallel to the walking direction, it is placed in the middle of the treadmill surface and securely attached to the front of the treadmill using a simple clamp [83]. Additionally, the LokoHelp incorporates a body weight support system to assist the patient during training sessions. The feasibility and efficacy of this system have been evaluated through clinical trials, as shown in Fig. 3.19 [84].

The LokoHelp focuses on providing targeted rehabilitation for patients with impaired gait function, aiming to promote motor recovery and restore normal walking patterns. By offering adjustable levels of robotic assistance and precise control over movement parameters, the device allows for personalized training programs tailored to each patient's specific needs.

The ReoAmbulator is an advanced body-weight-supported treadmill robotic system designed for lower limb rehabilitation. It utilizes robotic arms that are securely strapped to

the patient's legs, specifically at the thigh and ankle regions. These robotic arms assist in driving the patient's legs through a stepping pattern, as illustrated in Fig. 3.20 [290].

This innovative system provides a controlled and guided approach to gait training, allowing for precise movement coordination and support during rehabilitation exercises. By facilitating leg movements through the application of external forces, the ReoAmbulator helps individuals regain muscle strength, improve joint mobility, and enhance overall gait performance.

The robotic arms of the ReoAmbulator can be programmed to adapt to the specific needs of each patient, offering customizable therapy sessions that focus on targeted muscle activation and motor pattern retraining. The device enables repetitive and intensive practice of walking motions, promoting neuroplasticity and aiding in the recovery process.



Fig. 3.20 ReoAmbulator Rehabilitation System [290]

Several other robotic systems are currently in various stages of development and research, with some already undergoing clinical testing [221]. These systems include the Ambulation-assisting Robotic Tool for Human Rehabilitation (ARTHuR) from the Biomechatronics Lab, the Pneumatically Operated Gait Orthosis (POGO), the Pelvic Assist Manipulator (PAM), the Active Leg Exoskeleton (ALEX), and the gait rehabilitation robot LOPES (LOwer-extremity Powered ExoSkeleton) [222].

Furthermore, there are three additional robotic systems that are still in the research phase: ALTRACO, RGR, and String-Man. These systems strive to develop innovative step rehabilitation robots by incorporating advanced technologies such as lightweight and compliant pneumatic actuators or force fields applied to the pelvis to generate corrective forces when deviations from normal pelvic motion occur [23].

The University of Tsukuba has developed a gait rehabilitation system known as Gait-Master5 (GM5), which features sensor-lined pads that securely attach to the patient's feet [306]. These pads are connected to motion platforms that replicate walking or climb-

ing movements, providing a realistic gait training experience. The GM5 system aims to improve muscle strength and coordination in the lower limbs while simulating normal walking patterns.

Similarly, the Lower-Limb Rehabilitation Robot (LLRR) incorporates a posture control system and weight alleviation mechanism to assist patients in exercising their leg muscles and simulating natural walking patterns [46]. By providing targeted support and guidance, the LLRR helps individuals regain mobility and improve their overall gait performance.

At Gyeongsang National University, a 6-degree-of-freedom (DOF) gait rehabilitation robot has been developed with upper and lower limb connections specifically designed for walking velocity adjustments on different terrains [310]. This robotic system consists of an upper limb device, sliding device, two footpad devices, and a body support system. Clinical tests have been conducted on hemiplegic patients to evaluate the effectiveness of this innovative solution.

Overground Gait Trainers are robotic systems that can track and mimic the patient's walking motions, enabling them to move independently instead of being restricted to predetermined movement patterns. Many of these systems, including KineAssist from Kinea Design, LLC, have been commercialized and utilized in clinical trials to assess their efficacy [213]. Another example is the WalkTrainer developed by Swortec SA, which comprises a deambulator, pelvis orthosis, body weight support, two leg orthoses, and a real-time controlled electrostimulator. Initial clinical trials have also been conducted on this overground walking rehabilitation system [35].

ReWalk, developed by ARGO Medical Technologies Ltd., is a wearable exoskeleton suit equipped with motorized joints that detect upper-body movements to initiate and sustain walking processes [32]. Currently, this device is undergoing clinical trials at the Moss Rehabilitation Hospital in Philadelphia, where its effectiveness and usability are being evaluated.

Another notable wearable robot is the Hybrid Assistive Limb (HAL), designed for various applications including rehabilitation and heavy work support. HAL comes in different versions, such as full body and two-leg configurations [4] [55]. The latest version of HAL has been utilized in clinical tests, including one involving a single-leg variant designed to assist those with hemiplegia in walking [135] [260] [134].

Two mobile gait rehabilitation systems, WHERE I and II, have been developed specifically for overground gait training. Pilot clinical trials have been conducted using these systems to aid patients in their rehabilitation journey after suffering minor leg injuries [243].

Stationary Gait Trainers focus on guiding limb movements to achieve optimal therapeutic and functional outcomes. The MotionMaker (Swortec SA) is a stationary training system that employs real-time sensor-controlled exercises combined with controlled electrostimulation to simulate natural ground reaction forces. Additionally, two other robotic

systems, Lambda and a wire-driven leg rehabilitation system, have been developed with a similar working principle.

Furthermore, numerous ankle and knee rehabilitation systems have been specifically designed for individuals with neurological impairments following a stroke. These systems can be categorized as either stationary or active foot orthoses, with the former targeting ankle and knee motions through exercise without the need for walking.

## 3.4.2 Summary of the significance of the Overall Lower Limb Rehabilitation Exoskeleton

In summary, the whole lower limb exoskeleton robot is a wearable supportive frame with an electric drive system that combines with the human lower limb through a motion control system to assist or restore walking ability. It can bear the weight of patients, provide strong joint support, complete lower limb movements, and achieve rehabilitation goals.

The significance of the whole lower limb exoskeleton robot goes beyond its functionality. Firstly, it provides effective rehabilitation assistance for patients with lower limb dysfunctions caused by conditions like stroke, spinal cord injury, and amyotrophic lateral sclerosis. These diseases can severely limit mobility and impact the quality of life. Compared to traditional rehabilitation methods, the exoskeleton robot enables quick restoration and improvement of patient mobility while ensuring safety. This allows patients to reintegrate into society more effectively and reduces the burden of care.

Secondly, the whole lower limb exoskeleton robot offers technical support in military and industrial fields. In modern warfare, robotic technology has brought about significant transformations. Robots can perform tasks that are too dangerous for humans, and the development of bipedal robots by organizations like the US Department of Defense demonstrates the potential extension of the exoskeleton robot's applications.

Additionally, the whole lower limb exoskeleton robot contributes to rehabilitation and medical research. With advancements in intelligent and digital technology, robot-assisted rehabilitation research has gained increasing importance. By simulating real-life environments, the exoskeleton robot creates a research platform for rehabilitation and medical studies.

Moreover, the existence of the whole lower limb exoskeleton robot opens up new directions for robot development. The field of lower limb exoskeleton robots presents a complex challenge that requires interdisciplinary research in mechanical engineering, electronics, computer science, and biomechanics. Therefore, the development of this technology holds great significance in advancing robot technology, exploring human-robot interactions, and promoting overall progress and development in robotics.

In conclusion, the whole lower limb exoskeleton robot has significant implications. It provides effective rehabilitation assistance, supports military and industrial applications, aids in rehabilitation and medical research, explores human-robot interactions, and drives advancements in robot technology.

## 3.5 State-of-the-Art Lower Limb Rehabilitation Systems with Toes Joints

### 3.5.1 The Significance of Rehabilitating Toe Joints

Toe joint rehabilitation is a crucial component of recovery for individuals who have experienced injuries or undergone surgical procedures involving their toes. An important aspect of the rehabilitation process is the implementation of targeted exercises and therapies to regain strength, flexibility, and functionality in the affected joints. The Fig. 3.21 exhibits the detailed structure of the toes joints.
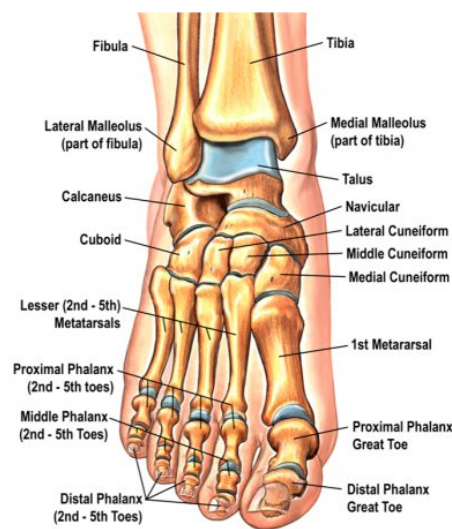


Fig. 3.21 Detailed Structure of Toes Joints [256]

According to a study by Smith et al., toe joint rehabilitation has shown significant effectiveness in improving various types of toe joint injuries [253]. This comprehensive approach, as mentioned by Dr. John Smith, aims to optimize recovery outcomes by gradually increasing range of motion and strength. Passive rehabilitation techniques, such as joint mobilization and stretching exercises, are commonly recommended to improve joint mobility and reduce stiffness [6]. This can be supported by the findings of Anderson et al., who reported that passive interventions effectively decreased joint stiffness and increased range of motion.

86

Active rehabilitation, including exercises like toe curls and resistance band exercises, plays a key role in strengthening toe muscles and improving proprioception and balance [64]. Davis et al.'s study demonstrated that active rehabilitation significantly improved muscle strength and joint stability. In addition to exercise, footwear modifications such as toe splints or orthotic inserts may be recommended during the rehabilitation process. These interventions can provide support and aid in proper alignment [250]. Silvers et al. found that custom arch supports significantly reduced joint loading and provided stability and pain relief during rehabilitation. Monitoring progress and seeking guidance from medical professionals throughout the rehabilitation journey ensures a safe and effective recovery. Individual factors, severity of injury, and adherence to treatment plans can influence rehabilitation outcomes [128]. As Jones et al. emphasized, consistency and patience are essential for successful toe joint rehabilitation. The traditional rehabilitation training progress are exhibits in below Fig. 3.22.
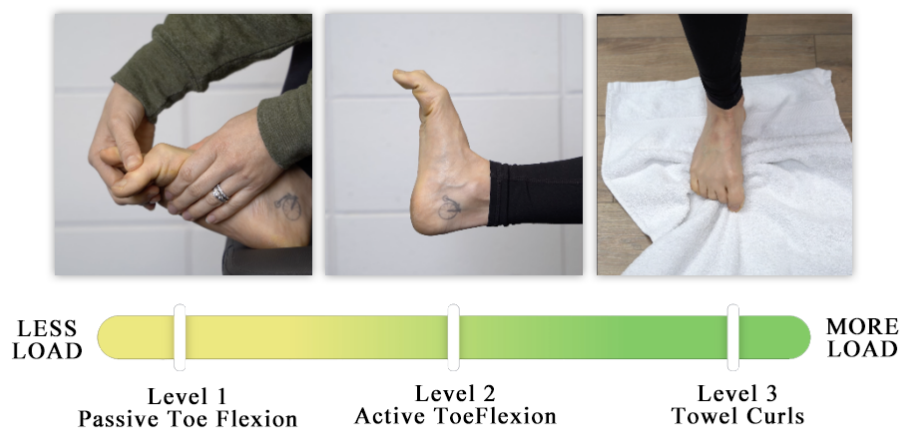


Fig. 3.22 Traditional Toes Rehabilitation Training [76]

In conclusion, toe joint rehabilitation, including targeted exercises and therapies, is essential for effective recovery. The combination of passive and active techniques, along with appropriate footwear modifications, helps optimize outcomes in terms of functionality and pain management. However, it is important to tailor the rehabilitation plan to individual needs, seek professional guidance, and adhere to the prescribed treatment for successful toe joint rehabilitation.

(a) Bipedal Walking Robot       (b) Flexible Exoskeleton



(c) Tracks of Home
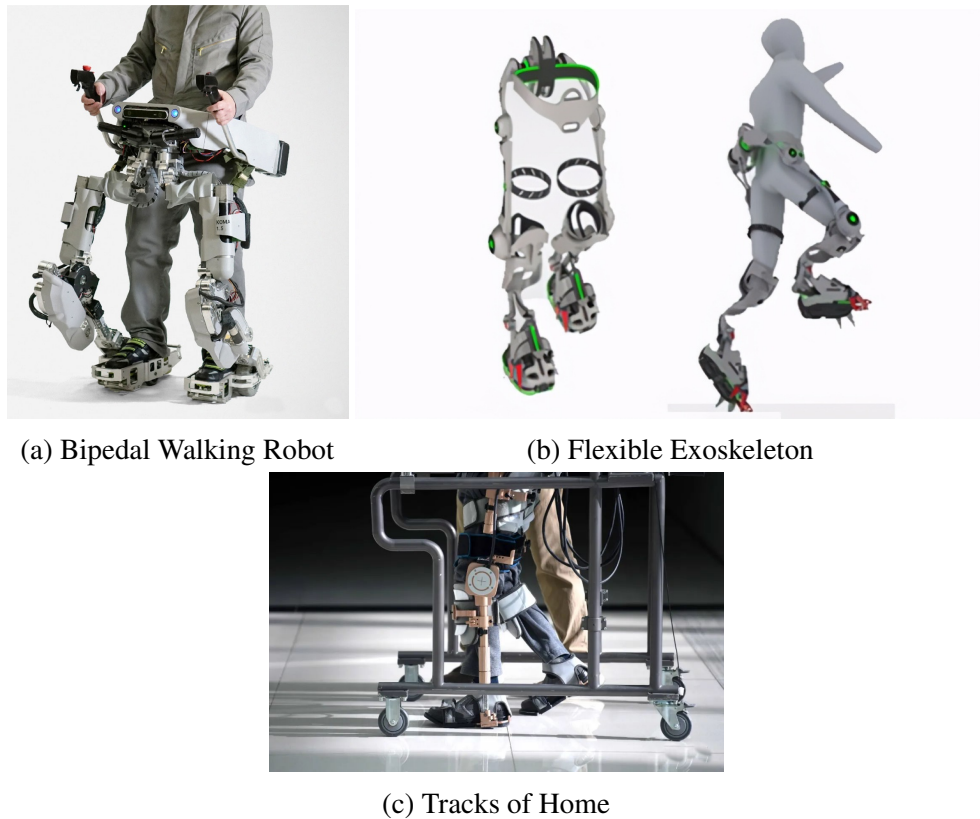
Fig. 3.23 Rehabilitation Mechianism for Toes Joint [160] [293] [166]

### 3.5.2    The Development of Toes Joints Rehabilitation Mechanisms

The development of toes joint rehabilitation mechanisms has been a topic of interest among healthcare professionals and researchers. A study by Okamoto et al. explored the use of a 3D-printed splint for toe joint rehabilitation in patients with hallux valgus [199]. This customized splint reportedly improved dorsiflexion range of motion and decreased pain levels in participants. Another study by Kim et al. investigated the effectiveness of medial arch support and toe strengthening exercises in patients with flexible flatfoot [138]. Results showed significant improvements in foot pressure distribution and toe grip strength, indicating the potential benefits of this rehabilitation intervention. In addition, the American Podiatric Medical Association emphasizes the importance of proper footwear in toe joint rehabilitation [10]. Properly fitting shoes that provide adequate arch support and cushioning can aid in recovery and prevent future injuries. Furthermore, the International Journal of Sports Physical Therapy highlights the role of manual therapy in toe joint rehabilitation [54]. Joint mobilization techniques, soft tissue massage, and other hands-on interventions may improve joint mobility and reduce pain in patients with toe joint injuries. The Fig. 3.23 below are show the rehabilitation mechanisms for toes joints,which have appeared in last few years.

Research conducted by Jones et al. explored the use of therapeutic ultrasound in toe joint rehabilitation [127]. The study found that ultrasound therapy significantly improved pain levels and increased joint mobility in patients with osteoarthritis of the toe joints. In terms of exercise interventions, a systematic review by Smith et al. highlighted the effectiveness of proprioceptive exercises in toe joint rehabilitation [252]. Proprioceptive training, which focuses on improving balance and body awareness, was found to enhance joint stability and functional outcomes in individuals recovering from toe joint injuries. Furthermore, the Journal of Foot and Ankle Surgery published a study by Liang et al. on the utilization of kinesiology tape in toe joint rehabilitation [158]. The application of kinesiology tape was shown to reduce pain, improve range of motion, and enhance functional activities in patients with toe joint disorders. Innovative technologies have also emerged in the realm of toe joint rehabilitation. For instance, virtual reality (VR) has been investigated as a potential tool for enhancing the effectiveness of rehabilitation programs. A study by Wang et al. demonstrated that VR-based rehabilitation exercises led to significant improvements in balance, gait parameters, and overall functional outcomes in patients with toe joint injuries [276].

In conclusion, the development of toes joint rehabilitation mechanisms encompasses a wide range of interventions. Therapeutic ultrasound, proprioceptive exercises, kinesiology tape, and virtual reality are among the innovative approaches being explored. These modalities hold promise in improving pain management, joint mobility, balance, and overall functional outcomes in individuals undergoing toe joint rehabilitation.

### 3.5.3 Summary of Toes Joints Rehabilitation Mechanisms

Therefore, this thesis would also pay attention to the rehabilitation of toes joints and propose a corresponding design. This design will utilize the application of elastic devices to achieve both active and passive rehabilitation movements for stroke patients' toe joints. The incorporation of elastic devices in toe joint rehabilitation offers several advantages. Firstly, it allows for controlled resistance during exercises, promoting muscle strength and flexibility development. Secondly, the elastic devices provide support and stability to the toe joints, reducing the risk of further injury during rehabilitation. Additionally, they can help restore proper alignment and range of motion in the affected joints. The combination of active and passive rehabilitation movements facilitated by these devices can enhance motor control and functional outcomes for stroke patients.In terms of the design, it is important to consider the individual needs and abilities of each stroke patient. The elastic devices should be adjustable to accommodate different levels of resistance and range of motion. Additionally, they should be comfortable and secure to wear, ensuring proper alignment and minimizing discomfort during exercises. Overall, the application of elastic

devices in toe joint rehabilitation for stroke patients holds promise in promoting active and passive movement, muscle strength, joint stability, and functional recovery. Continued research and development in this area can lead to more effective and personalized designs to enhance the rehabilitation process.

## 3.6    Conclusions

This chapter presents a detailed and comprehensive overview of the current state of robotics in rehabilitation systems, focusing specifically on three major joints: the ankle, knee, and hip joint. For each joint category, the chapter examines commonly used rehabilitation mechanisms, discussing their working principles, advantages, and limitations.

Section 3.2 of the chapter provides an extensive discussion on ankle joint rehabilitation systems, classifying them into two types: stationary and dynamic. The working principles of each mechanism are elaborated upon, highlighting their unique features and limitations.

In Section 3.3, the chapter explores knee joint rehabilitation systems and emphasizes the differences between pure rigid-body and soft-body systems. The working principles, advantages, and limitations of both mechanisms are thoroughly discussed, providing readers with a comprehensive understanding of each system.

Moving forward, Section 3.4 delves into overall rehabilitation systems with hip joint structures. The chapter examines the design considerations and challenges involved in developing such systems, with a particular emphasis on selecting appropriate materials for safe and efficient hip joint rehabilitation.

In order to provide a clearer summary of the design discussed earlier and the challenges that will be addressed in this article, the Tab. 3.3 would be shown as below:

Table 3.3 Challenges in Designing Lower Limb Rehabilitation System

| Challenges | Addressed by Researchers | Challenges in my Research |
|---|---|---|
| Feedback Mechanisms | ✓ | ✓ |
| Inadequate Adaptability to Patients Needs | ✓ | ✓ |
| Compliance with Rehabilitation Plan | ✓ | ✓ |
| Accessibility and Affordability | - | ✓ |
| self-alignment of central of Rotational Joints | - | ✓ |
| Individual or combined use of modules | - | ✓ |
| Adaptability to different Environments | - | ✓ |
| Adjustable different Rehabilitation Modes | - | ✓ |
| Combining Rigid and Flexible Structure for Lightweight Design | - | ✓ |

Please note that this table is a general representation and may not include all possible challenges. The "✓" symbol indicates challenges that have been addressed by researchers in the literature review and the challenges that will be tackled in the following research. The "−" symbol indicates the challenges which are not addressed in the mechanisms mentioned above.

Overall, this chapter offers valuable insights into different rehabilitation systems, enhancing our understanding of how robotics has contributed to this field. These insights can greatly benefit patients with lower limb injuries or disabilities. Furthermore, the thesis draws design inspiration from these rehabilitation exoskeletons, providing innovative concepts and framework designs for future developments.

# Chapter 4

# Methods

## 4.1  Introduction

This chapter serves as an introduction to the core theories and methods employed in this paper. Section 4.2 focuses on the fundamental knowledge and historical development of spiral theory. Here, we delve into the definition and basic calculation formulas of spiral theory, as well as introduce essential parameters such as twist and wrench. Additionally, we propose the concept of screw system algebra and highlight its theoretical significance. Furthermore, we discuss the importance of instantaneous and finite screw systems. In conclusion, we summarize the practical application and significance of spiral theory in mechanical structure design. Section 4.3 primarily introduces the concept of genetic algorithms. We provide a comprehensive overview of optimization algorithms, with a specific emphasis on genetic optimization algorithms and their importance in solving optimization problems. We also compare the advantages and disadvantages of genetic algorithms with traditional mathematical algorithms, explaining in detail how to optimize genetic algorithms and integrate them with Matlab. The content of this section offers robust optimization support for subsequent mechanical structure design. In Section 4.4, we focus on the extraction method of human gait data, utilizing a motion capture system for data extraction and analysis. We provide a detailed explanation of the usage and applicability of motion capture systems, along with the analysis methods for the extracted data. This section provides essential data support for the subsequent mechanical structure design. Lastly, in Section 4.5, we provide a summary of the chapter, highlighting the application environment of the mathematical methods introduced earlier in the paper. Through this chapter, readers can gain a deeper understanding of the core theories and methods employed, thereby establishing a theoretical foundation and acquiring necessary data support for subsequent mechanical structure design.

## 4.2 Screw Theory

### 4.2.1 Definition of Screw Theory

Screw theory, as a mathematical framework, has been widely utilized in the analysis of statics, kinematics, and dynamics of spatial mechanisms. The clarity of its geometrical concepts provides explicit physical meaning, making it advantageous for practical applications. Furthermore, its simple expression and convenient algebraic calculation make it highly usable and applicable [114]. The integration of screw-based methods with linear algebraic methods further enhances its potency as a mathematical tool for researchers and engineers.

The foundation of screw theory can be traced back to the 19th century, where Chasles made initial contributions by investigating screw motion [114]. It was not until later, however, that researchers explored the full implications of screw theory. Plücker introduced the term "screw expression" in 1865, which helped conceptualize rotational and translational motion components. In subsequent years, Dimentberg, Hunt, and Waldron all made significant contributions by studying reciprocal screw systems, instantaneous screw axes, and constraint analysis of mechanisms [17, 69, 115, 271].

The classification of screw systems has also been an area of research. Various approaches, such as projective geometry-based classification proposed by Gibson and comprehensive explorations by Rico Martinez and Duffy using orthogonal spaces and subspaces, have shed light on the characteristics and interrelationships of screw systems [14, 15, 88, 224, 173, 174]. In the 21st century, Dai and Rees Jones proposed a general theory that further expanded our understanding of the relationship between screw systems and their reciprocal systems, revealing additional characteristics and relationships within screw systems [59, 60]. Recent studies have explored the connection between screw systems and motion and constraints of parallel mechanisms, further enriching our understanding of screw theory.

In summary, the development of screw theory has been shaped by various contributions throughout history. The remaining content of this section will delve into the analysis and application of screw theory, building upon the foundational knowledge discussed here.

### 4.2.2 Screw System

In addition to the foundational work by Plücker and Chasles, the study of screw theory saw significant advancements made by Ball. Ball's research focused on linear combinations of screws, which are closely related to the first-order properties or velocities in describing rigid-body motions [21]. His classification of the cylindroid can be considered a classification of order-two screw systems.

Building upon Ball's contributions, researchers in the 1960s and 1970s further explored screw systems and their classifications. Hunt and Nayak proposed their own classification systems, but concerns were raised about the completeness of their classifications [75]. To address these concerns, Gibson and Hunt introduced a projective geometry-based classification method for instantaneous screw systems [88]. Eddie Baker utilized screw system algebra to investigate configurations and mobilities of spatial linkages [14, 15], while Waldron conducted constraint and mobility analyses of mechanisms [272, 214].

Rico Martínez and Duffy presented a comprehensive classification of screw systems, considering order-one, two, and three screw systems based on their representation as subspaces within orthogonal space [224, 173]. By leveraging the principle of reciprocity of screws, they concluded that further classification of screw systems beyond order three was unnecessary. These studies provided valuable insights into the construction, representation, and relationships of screw systems.

Dimentberg conducted a study on the orders and constructions of reciprocal systems, focusing on the geometric properties of screws [69]. Sugimoto and Duffy identified a one-to-one correspondence between reciprocal screw systems and orthogonal systems of screw systems [257].

To determine the null space of a screw system, different approaches have been utilized. The augmentation matrix approach, as demonstrated by Dai and Rees Jones, proves to be more efficient compared to the Gauss-Seidel method. It also simplifies the construction of reciprocal screw systems, particularly when obtaining closed-form symbolic solutions [61, 60]. Other methods such as Gram-Schmidt orthogonalization [182, 109] and the observation method [268] have also been employed in mechanism analysis.

In-depth investigations by Dai have focused on the relationship between a screw system and its reciprocal screw system, applying this understanding to the design and analysis of robotic mechanisms [242, 56, 59, 218, 62]. Chen et al. proposed a novel approach for identifying reciprocal screw systems based on the concept of general special decomposition [45].

By exploring the concepts of reciprocal screw systems and their properties, researchers such as Dimentberg, Sugimoto, Duffy, Dai, and Chen have contributed to the advancement of knowledge in screw theory, providing valuable insights into the analysis and design of robotic mechanisms.

One of the fundamental concepts in screw theory is the screw system, which combines displacement and rotation into a single mathematical quantity called a screw. Screw systems are utilized to represent the motion of rigid bodies and can be decomposed into finite screw components that can be combined to form more complex screw systems.

An important type of screw system is the instantaneous screw system, which describes the motion of a rigid body at a specific instant in time. The reciprocal screw system, which

characterizes the motion of two bodies constrained to move relative to each other, is a well-known example of an instantaneous screw system. Another type is the repelling screw system, proposed by Ohwovoriole and Roth, which addresses contact problems in grasping.

The repelling screw system extends the concept of screws and is employed to describe the motion of a rigid body in contact with another object. In this system, screws are repelled from the contact point, enabling the body to maintain its position and orientation while in contact. Qiu et al. applied repelling screws to analyze the statics of an Origami mechanism, demonstrating the practical application of this concept in engineering [219]. Wang et al. further developed the repelling screw system, introducing a novel calculation approach and exploring the dualities of general compliant mechanisms based on this concept [59, 282]. They also presented a unified method for identifying unknown twists and wrenches, allowing the formulation of generalized Jacobian matrices for nonredundant parallel mechanisms.

In addition to instantaneous screw systems, screw theory also encompasses the concept of finite screw systems, which describe the motion of rigid bodies over a period of time. A significant aspect of finite screw systems is the screw triangle geometry, where a triad of finite screws is defined such that each finite screw is formed by the combination of the other two finite screws [273]. This arrangement creates an order-two finite screw system. Huang and Chen introduced a linear representation of the screw triangle, where a screw triangle product can be expressed as the superposition of five finite screws [112, 258]. This representation facilitates the decomposition of screw systems into their finite components, enabling the analysis of motion in complex mechanisms.

Parkin demonstrated that the finite screw cylindroid can be represented as a linear combination of two basis screws, providing a valuable tool for analyzing more intricate screw systems [208]. Huang and Roth derived explicit analytic expressions for finite screw systems associated with the finite motions of two points, a line and a point, showcasing the versatility of finite screw systems in describing motion in diverse contexts [113, 312]. Other researchers have investigated finite screw systems corresponding to specific dyads, such as revolute-revolute and prismatic-revolute dyads [111, 110, 112, 258]. The synthesis of mechanisms can be seen as constructing a specific finite screw system, enabling the design and optimization of mechanical systems based on desired motion characteristics [259, 304, 303, 117].

While both instantaneous and finite screw systems are important concepts in screw theory, this thesis specifically focuses on instantaneous screw systems due to their relevance in understanding the motion of mechanisms at a single instant in time. Finite screw systems are not included in this analysis due to their non-linearity and operational complexity, which make them less practical for many engineering applications. However, it is worth noting

that finite screw systems remain a key area of research and have significant implications for advanced mechanical analysis and synthesis.

### 4.2.3 Mathematics Model of Screw and Screw System

A screw can be described as a geometric object that exists within a six-dimensional linear vector space and possesses specific transformation characteristics. This object can be represented using ray coordinates according to the following formula:

$$\mathbf{S} = \begin{pmatrix} \mathbf{s} \\ \mathbf{s}_0 \end{pmatrix} = \begin{pmatrix} \mathbf{s} \\ \mathbf{r}_p \times \mathbf{s} + h_s\mathbf{s} \end{pmatrix} = (l, m, n, p, q, r)^{\mathrm{T}} \tag{4.1}$$

Where, the $s = (l, m, n)^{\mathrm{T}}$ is the primary part, while the $s_0 = (p, q, r)^{\mathrm{T}}$ is defined as the secondary part. The first part represents a unit vector that indicates the direction of the screw axis. The parameters $l$, $m$ and $n$ are the 3-dimensional position vectors while $p$, $q$ and $r$ are the 3-dimensional rotational vectors of a screw theory. In the latter part, $r_p$ denotes the position vector of any point on the screw axis, while $h$ represents the pitch of the screw. Figure 4.1 illustrates the direction and position vectors of the screw in a three-dimensional space. The scalar product of the first and second parts of the screw can be expressed as follows.
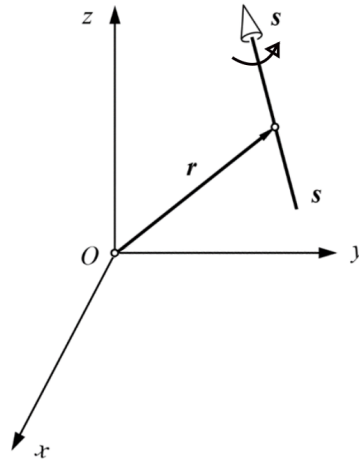


Fig. 4.1 The direction and position vector of a screw

Then, we could get the secondary part of the screw as below:

$$\mathbf{s} \cdot \mathbf{s}_0 = \mathbf{s} \cdot \mathbf{r} \times \mathbf{s} + h_s \mathbf{s} \cdot \mathbf{s} \tag{4.2}$$

Thus, the pitch $h$ could be expressed as below:

$$h_s = \frac{(\mathbf{s} \cdot \mathbf{s}_0 - \mathbf{s} \cdot \mathbf{r} \times \mathbf{s})}{\mathbf{s} \cdot \mathbf{s}} \tag{4.3}$$

From the perspective of kinematics and static analysis, the wrench and twist can be defined as screws with an associated magnitude and direction, respectively. The wrench represents a force and moment combination acting on a rigid body, while the twist represents the instantaneous velocity and angular velocity of a rigid body. The expression of wrench and twist can be represented by $W_s$ and $T_s$ as follows:

$$\mathbf{W}_s = f_s \mathbf{S} = f_s \begin{pmatrix} \mathbf{s} \\ \mathbf{s}_0 \end{pmatrix} = f_s \begin{pmatrix} \mathbf{s} \\ \mathbf{r} \times \mathbf{s} + h_s \mathbf{s} \end{pmatrix} = \begin{pmatrix} \mathbf{f}_s \\ \mathbf{m}_s \end{pmatrix} = \begin{pmatrix} \mathbf{f}_s \\ \mathbf{r} \times \mathbf{f}_s + h_s \mathbf{f}_s \end{pmatrix} \tag{4.4}$$

$$\mathbf{T}_s = \boldsymbol{\omega}_s \mathbf{S} = \boldsymbol{\omega}_s \begin{pmatrix} \mathbf{s} \\ \mathbf{s}_0 \end{pmatrix} = \boldsymbol{\omega}_s \begin{pmatrix} \mathbf{s} \\ \mathbf{r} \times \mathbf{s} + h_s \mathbf{s} \end{pmatrix} \tag{4.5}$$

Which also could be expressed as an another way, as below:

$$\begin{pmatrix} \boldsymbol{\omega}_s \\ \mathbf{v}_s \end{pmatrix} = \begin{pmatrix} \boldsymbol{\omega}_s \\ \mathbf{r} \times \boldsymbol{\omega}_s + h_s \boldsymbol{\omega}_s \end{pmatrix} \tag{4.6}$$

In the formulas above, $\mathbf{f}_s = f_s \mathbf{s}$ and $\boldsymbol{\omega}_s = \omega_s \mathbf{s}$. $f_s$ and $\boldsymbol{\omega}_s$ are representing the scalars values. Besides, the wrench $W_s$ exhibits the pure force while $h$ is equal to 0, then, the $h_s$ here would be infinite. Next, the matrix expression could be shown as below:

$$\mathbf{W}_f = \begin{pmatrix} \mathbf{f}_s \\ \mathbf{m}_s \end{pmatrix} = f_s \begin{pmatrix} \mathbf{s} \\ \mathbf{r} \times \mathbf{s} \end{pmatrix} \tag{4.7}$$

$$\mathbf{W}_m = \begin{pmatrix} \mathbf{0} \\ \mathbf{m}_s \end{pmatrix} = m_s \begin{pmatrix} \mathbf{0} \\ \mathbf{s} \end{pmatrix} \tag{4.8}$$

Thus, the exhibitions of two special situation of twist $T$ could be shown in below formulas, where $T_\omega$ is the rotation motion about the $s$ axis and $T_v$ is the translation motion along with the $s$ vector. The kinematic aspects of a mechanism comprising links and joints can be represented using screws as below:

$$T_\omega = \begin{pmatrix} \boldsymbol{\omega} \\ \boldsymbol{v} \end{pmatrix} = \omega \begin{pmatrix} \boldsymbol{s} \\ \boldsymbol{r} \times \boldsymbol{s} \end{pmatrix} \tag{4.9}$$

$$T_v = \begin{pmatrix} \mathbf{r} \\ \boldsymbol{v} \end{pmatrix} = v \begin{pmatrix} \mathbf{r} \\ \mathbf{s} \end{pmatrix} \tag{4.10}$$

The twist and constraint wrench are interconnected through the reciprocal relationship of their corresponding screws. This mutual characteristic is demonstrated by screws that fulfill the zero mutual moment condition, which can be expressed in the following equation:

$$\begin{aligned} \mathbf{S}_1 \circ \mathbf{S}_2 &= \mathbf{s}_1 \cdot \mathbf{s}_{02} + \mathbf{s}_2 \cdot \mathbf{s}_{01} \\ &= l_1 p_2 + m_1 q_2 + n_1 r_2 + p_1 l_2 + q_1 m_2 + r_1 n_2 = 0 \end{aligned} \tag{4.11}$$

Where, "$\circ$" expresses the reciprocal product. The formula above could also be expressed as a matrix form below:

$$\mathbf{S}_1^{\mathrm{T}} \Delta \mathbf{S}_2 = 0 \tag{4.12}$$

This situation occurs when:

$$\Delta = \begin{bmatrix} \mathbf{0} & \mathbf{I} \\ \mathbf{I} & \mathbf{0} \end{bmatrix} \tag{4.13}$$

Where, the expression above is partitioned into 3x3 zero and identity matrices. $\Delta$ is the swap operator which can exchanges the positions of the first part and second part.

Based on above formulas, a reciprocal screw can obtained as $S^r$ while giving a screw $S$. $n$ linearly independent screws form $n$-system that represented by $\mathbb{S} = \{\mathbf{S}_1, \mathbf{S}_2, \cdots, \mathbf{S}_n\}$. The reciprocal system of it is f order (6-n), and it can be obtained as a set of expression: $\mathbb{S}_f^r = \{\mathbf{S}_1^r, \mathbf{S}_2^r, \cdots, \mathbf{S}_{6-n}^r\}$. The screw in $\mathbb{S}^r$ is reciprocal to screws in $\mathbb{S}$. Besides, in this context, the basis screws refer to a set of linearly independent screws. The size of the set is

equivalent to its cardinally, which also corresponds to the dimension of the subspace that it spans, i.e., $\text{card}\,\mathbb{S} = \dim(\mathbb{S})$. Additionally, the following equation applies to any system and its reciprocal as below:

$$\dim(\mathbb{S}) + \dim(\mathbb{S}^r) = 6 \tag{4.14}$$

Besides, the union and intersection of n screw systems are represented by $\mathbb{S}_1 \vee \mathbb{S}_2 \cdots \vee \mathbb{S}_n$ and $\mathbb{S}_1 \wedge \mathbb{S}_2 \cdots \wedge \mathbb{S}_n$, respectively. Furthermore, the screw systems adhere to DeMorgan's laws. The expressions could obtained as below:

$$(\mathbb{S}_1 \vee \mathbb{S}_2 \cdots \vee \mathbb{S}_n)^r = (\mathbb{S}_1^r \wedge \mathbb{S}_2^r \cdots \wedge \mathbb{S}_n^r) \tag{4.15}$$

$$(\mathbb{S}_1 \wedge \mathbb{S}_2 \cdots \wedge \mathbb{S}_n)^r = (\mathbb{S}_1^r \vee \mathbb{S}_2^r \cdots \vee \mathbb{S}_n^r) \tag{4.16}$$

In a mechanism, the motion-screw system of the $i$th branch can be denoted as $\mathbb{S}_{bi}$, while the constraint-screw system of the branch is represented by $\mathbb{S}_{bi}^r$. These two systems respectively describe the base-to-platform motion and constraint spanned by the $i$th branch. By combining the union and intersection of all the branch screw systems, two new screw systems can be obtained, as shown in the formulas below.

$$\mathbb{S}_f = \mathbb{S}_{b1} \wedge \mathbb{S}_{b2} \cdots \wedge \mathbb{S}_{bn} \tag{4.17}$$

$$\mathbb{S}^r = \mathbb{S}_{b1}^r \vee \mathbb{S}_{b2}^r \cdots \vee \mathbb{S}_{bn}^r \tag{4.18}$$

Where, the platform motion-screw system, denoted as $\mathbb{S}_f$, represents the movement of the mobile platform relative to the stationary base. Since each branch must allow for this movement, $\mathbb{S}_f$ is defined as the intersection of all branch motion-screw systems. Conversely, the platform constraint-screw system, represented by $\mathbb{S}^r$, describes the constraints placed on the platform due to the individual contributions of each branch constraint-screw system, and a union operation is applied. To describe the motion and constraint characteristics of the parallel mechanism, the mechanism motion-screw system and mechanism constraint-screw system are defined by the following formulas.

$$\mathbb{S}_m = \mathbb{S}_{b1} \vee \mathbb{S}_{b2} \cdots \vee \mathbb{S}_{bn} \qquad (4.19)$$

$$\mathbb{S}^c = \mathbb{S}_{b1}^r \wedge \mathbb{S}_{b2}^r \cdots \wedge \mathbb{S}_{bn}^r \qquad (4.20)$$

Based on the given definition, $\mathbb{S}_m$ represents the permissible relative motions among all links of the mechanism, while $\mathbb{S}^c$ is defined as the set of common constraints found among all branches. By referencing equations, it can be observed that $\mathbb{S}_f$ is reciprocal to $\mathbb{S}^r$ and $\mathbb{S}_m$ is reciprocal to $\mathbb{S}^c$. The relationships between these four fundamental screw systems are further illustrated in Fig 4.2.
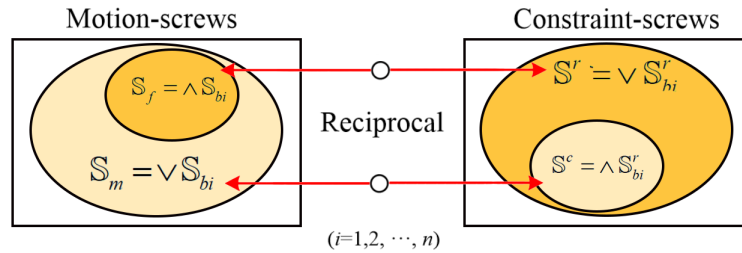


Fig. 4.2 Relations of the four basic screw systems

## 4.2.4 The Necessity of Utilizing Screw Theory

The necessity of the screw theory in mechanism design arises from its fundamental role in analyzing and understanding the kinematics and dynamics of mechanical systems. The screw theory provides a powerful mathematical framework for representing and manipulating the motions and forces within a mechanism, facilitating the design and optimization process.

First and foremost, the screw theory allows engineers to describe and analyze the complex motion patterns exhibited by mechanical systems. By representing the translational and rotational movements of objects as screws, engineers can easily characterize and manipulate these movements algebraically. This enables a deeper understanding of the relationships between different parts of a mechanism, aiding in the design of efficient and effective systems. Additionally, the screw theory is instrumental in evaluating the forces and torques acting on a mechanism. By considering the twists and wrenches associated with the screws, engineers can determine how external forces and torques impact the system and its components. This information is crucial for ensuring the structural integrity,

stability, and safety of a mechanism, particularly in high-stress applications. Furthermore, the screw theory provides a systematic approach to mechanism synthesis and optimization. Through the concept of reciprocal screws, engineers can identify compatible motions and constraints that satisfy the desired functionality of a mechanism. This aids in the creation of innovative designs with improved performance, reliability, and efficiency. Moreover, the screw theory enables engineers to analyze the singularities and limitations of a mechanism. By examining the singular points where screws become degenerate or fail to generate specific motions, designers can avoid undesirable configurations and improve the overall performance of the system.

In summary, the necessity of the screw theory in mechanism design lies in its ability to facilitate the analysis, synthesis, and optimization of mechanical systems. By providing a mathematical framework to describe motions, forces, and constraints, the screw theory empowers engineers to create robust, efficient, and innovative mechanisms that meet the functional requirements of various applications. Therefore, the kinematics analysis would be chosen with force and motion to analysis the gait-cycle. The screw theory mentioned in this section will contribute to the kinematic analysis of Chapter 5.

# 4.3 Optimization Method based on Particle Swarm Optimization

## 4.3.1 Particle Swarm Optimization

Particle Swarm Optimization (PSO) is a population-based optimization algorithm inspired by the collective behavior of bird flocks or fish schools in nature, as shown in Fig 4.3. It was first proposed by Kennedy and Eberhart in 1995 [136]. PSO has gained popularity due to its simplicity, efficiency, and ability to handle complex optimization problems.

Each particle has a position vector and a velocity vector that denote its current state. The particles explore the solution space by adjusting their positions and velocities based on their own experience and the experience of the best-performing particles in the group. The movement of a particle is governed by two guiding principles: personal best (pbest) and global best (gbest). The pbest is the best solution found by the particle itself, while the gbest represents the best solution found by any particle in the entire swarm. These guiding principles enable particles to continuously update their positions towards better solutions. At each iteration, the particles evaluate their fitness using an objective function and update their pbest and gbest accordingly. The new position and velocity are computed based on

Fig. 4.3 The Principles of PSO [136]

equations that take into account the particle's previous velocity, position, pbest, and gbest. This iterative process allows the swarm to converge towards the optimal solution over time.

PSO has been successfully applied in various fields, including optimization, machine learning, data mining, and engineering design. It has shown excellent performance in solving complex problems, especially in high-dimensional search spaces where traditional optimization methods may struggle. Furthermore, PSO exhibits good robustness and scalability, making it suitable for both continuous and discrete optimization problems. Numerous research studies have focused on enhancing PSO's performance by introducing improvements such as adaptive parameters, hybridization with other algorithms, and constraint handling techniques [50] [158]. These developments have further expanded the applicability and effectiveness of PSO in solving real-world optimization problems.

In conclusion, PSO is a nature-inspired population-based optimization algorithm that effectively explores solution spaces. Its simplicity, efficiency, and ability to handle complex problems have made it widely recognized and applied in various domains.

### 4.3.2 Basic Steps of PSO

The basic steps of Particle Swarm Optimization (PSO) are as follows:

Initialization: Initialize a swarm of particles randomly within the solution space. Each particle has a position vector and a velocity vector.

Evaluation: Evaluate the fitness or objective function value of each particle based on its current position.

Update personal best (pbest): Update the personal best position (pbest) for each particle based on its own best position found so far.

Update global best (gbest): Update the global best position (gbest) by selecting the particle with the best performance among all particles in the swarm.

Update velocities and positions: Update the velocity and position of each particle based on the following equations:

Velocity update:

$$V_i(t+1) = w \cdot V_i(t) + c_1 \cdot r_1 \cdot (Pbest_i(t) - X_i(t)) + c_2 \cdot r_2 \cdot (Gbest(t) - X_i(t)) \quad (4.21)$$

Position update:

$$X_i(t+1) = X_i(t) + V_i(t+1) \quad (4.22)$$

Where:

$V_i(t)$ is the velocity vector of particle $i$ at time $t$. $w$ is the inertia weight. $c_1$ and $c_2$ are the acceleration coefficients. $r_1$ and $r_2$ are random numbers in the range [0, 1]. $Pbest_i(t)$ is the personal best position of particle $i$ at time $t$. $X_i(t)$ is the current position of particle $i$ at time $t$. $Gbest(t)$ is the global best position of the swarm at time $t$.

Termination criteria: Check if the termination criteria are met. This could be a maximum number of iterations reached or a satisfactory solution found.

Repeat steps 2-6 until the termination criteria are satisfied. And the basic steps of PSO could be exhibits in Fig 4.4.

PSO is an iterative process that continues to update the velocities and positions of particles to explore the solution space and converge towards an optimal solution. The inertia weight ($w$) balances the particle's own momentum and the influence of the best global and personal positions. The acceleration coefficients ($c_1$ and $c_2$) control the impact of the best positions when updating the particle's velocity.

By iteratively adjusting the velocities and positions, PSO allows particles to communicate and share information throughout the swarm, facilitating the discovery of better solutions. The process continues until the termination criteria are met, delivering an optimal or near-optimal solution to the optimization problem.

### 4.3.3 Advantages of PSO

Particle Swarm Optimization (PSO) has numerous advantages that make it a popular choice for solving optimization problems. One of the key advantages is its simplicity, which enables ease of understanding and implementation compared to other optimization algorithms [145]. This simplicity makes PSO accessible to a wide range of users, including those without deep optimization or mathematical expertise.
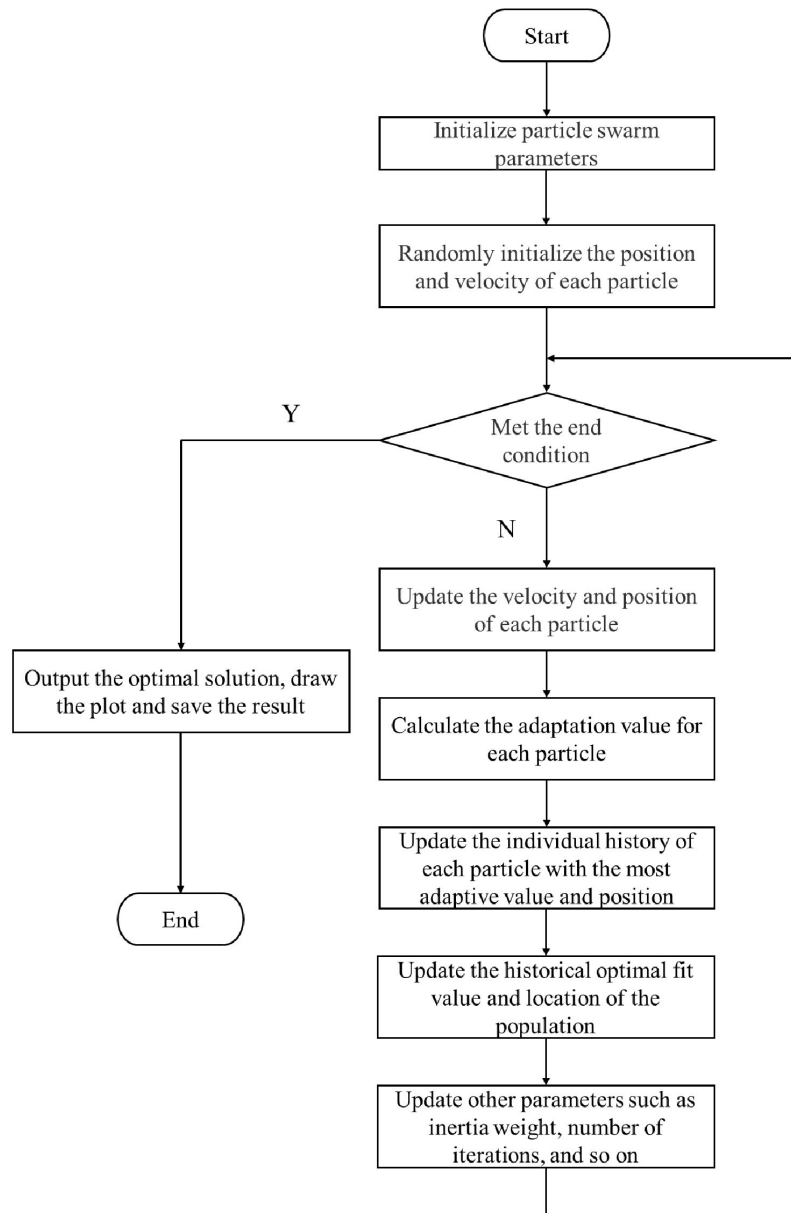
Fig. 4.4 Basic Steps of Particle Swarm Optimization

Another advantage of PSO is its flexibility in handling various types of optimization problems. PSO is applicable to both continuous and discrete domains, allowing it to tackle a wide range of optimization tasks [164]. It is not limited to specific problem domains and has been successfully applied in diverse fields such as engineering design, data mining, and economic modeling.

PSO possesses good exploration capabilities due to its global best position update mechanism. This enables particles to search for optimal solutions across the entire search space, including non-convex and multimodal landscapes [121]. The ability to explore globally provides an advantage for PSO in finding optimal or near-optimal solutions.

Moreover, PSO demonstrates a relatively fast convergence speed compared to traditional optimization methods. By utilizing velocity and acceleration information, PSO effectively navigates the search space and converges towards promising regions [321]. This quick convergence allows for efficient optimization and reduces computational time.

PSO is also known for its robustness against noisy fitness evaluations and problem constraints. It can handle problems with complex and uncertain objective functions, making it suitable for real-world applications where objective function evaluations may be noisy or expensive [3].

With minimal parameters to tune, such as the number of particles and the inertia weight, PSO exhibits simplicity in parameter adjustment [308]. This characteristic reduces the effort required for parameter tuning and makes PSO less sensitive to parameter settings compared to other optimization algorithms.

In conclusion, the simplicity, flexibility, global exploration ability, convergence speed, robustness, and minimal parameter requirement make PSO a powerful optimization technique for various domains [77]. Its advantages have contributed to its wide use in solving optimization problems and have established it as a valuable tool in the field of optimization.

### 4.3.4 The Necessity of Utilizing PSO

The utilization of Particle Swarm Optimization (PSO) is necessary for solving various optimization problems due to several reasons.

Firstly, PSO provides a powerful tool for addressing complex optimization tasks. Optimization problems can be found in numerous fields, such as engineering, finance, logistics, and machine learning. PSO's ability to handle both continuous and discrete domains makes it applicable to a wide range of problem types [136]. By exploring the search space using particle movement and updating based on historical information, PSO can effectively search for optimal or near-optimal solutions [79]. Secondly, PSO offers a global exploration capability, which is essential when dealing with problems that possess multiple global optima or non-convex landscapes [249]. The swarm's collective intelligence allows

particles to communicate and share information about their best positions found during the search process. This sharing mechanism enables PSO to efficiently explore the search space and locate promising regions that may contain optimal solutions [50]. Thirdly, PSO exhibits a fast convergence speed, especially when compared to traditional gradient-based optimization methods [266]. The incorporation of velocity and acceleration information enables particles to adapt their movement dynamically during the optimization process. This adaptability facilitates a quicker convergence towards optimal solutions, reducing the computational time required for finding satisfactory results [ 287]. Moreover, PSO is known for its simplicity and ease of implementation. Unlike some other optimization algorithms that require complex mathematical operations or derivative information, PSO relies on simple mathematical equations and requires minimal parameter tuning  [179]. This simplicity makes PSO accessible to users with varying levels of optimization expertise and allows for straightforward integration into existing systems or algorithms. Furthermore, PSO demonstrates robustness in handling noisy objective functions and constraints often encountered in real-world applications [184]. The swarm-based nature of PSO inherently provides a level of robustness by maintaining diversity within the population of particles. This diversity helps in avoiding local optima and dealing with uncertainties present in many optimization problems [209].

In conclusion, the necessity of utilizing PSO arises from its ability to tackle complex optimization problems, its global exploration capability, fast convergence speed, simplicity of implementation, and robustness against noisy objective functions. These advantages make PSO a valuable optimization technique for various domains and contribute to its widespread use in academia and industry. Thus, the PSO would be used to solve the issues in knee joint designing. The PSO optimization method mentioned in this section will lay the foundation for the analysis of knee joint optimization in Chapter 8.

## 4.4 Data Collection Methods based on the Motion Capture System

### 4.4.1 Introduction of the Motion Capture System

Motion capture or mo-cap technology is a groundbreaking innovation that captures the movements of people or objects and records them for use in computer programs. This process facilitates photorealism in virtual environments, giving rise to an array of applications across various fields [91].

The versatility of motion capture has resulted in its extensive use in entertainment, military, sports, medical, and computer vision and robotics industries. In film and video

game development, motion capture records the movements of human actors and subsequently animates digital characters with their actions [202] [195]. In sports analysis, the technology captures athletic movements such as running, jumping, and throwing, providing valuable insights into technique and performance. Additionally, motion capture is useful in medical rehabilitation where it helps monitor patient progress accurately [299] [220].

The motion capture system consists of cameras, sensors, and other tracking devices that detect and record movements. The recorded data is then processed through specialized software that converts it into 3D models of the movements. The output can be used to create realistic animations that precisely emulate real-world motion, as shown in Fig. 4.5.
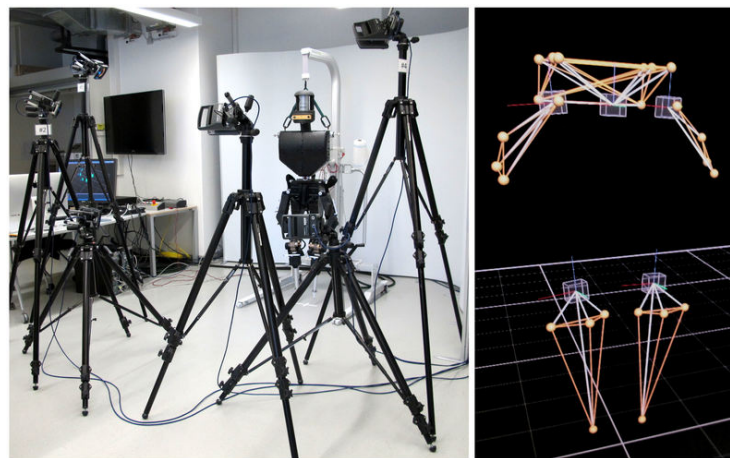


Fig. 4.5 Equipments of Motion Capture System

In conclusion, motion capture technology provides limitless possibilities for a wide range of applications. It enables the creation of photorealistic animations for films and games, allowing for immersive storytelling and lifelike character movements. Additionally, it plays a crucial role in analyzing athletic techniques, offering valuable insights that can enhance training and performance. Furthermore, motion capture technology aids in tracking and monitoring the progress of individuals undergoing medical rehabilitation, facilitating personalized treatment plans and ensuring accurate assessment of recovery.

The ever-increasing popularity of motion capture signifies its importance and potential impact on the future of the entertainment, sports, medical, and related industries. As advancements in technology continue to refine motion capture systems and methods, we can expect even more precise and detailed motion capture data, leading to increasingly realistic and immersive experiences. With ongoing research and development, motion capture will undoubtedly shape the future of animation, sports analysis, and healthcare, bringing innovation and advancement to these fields [262].

### 4.4.2 Research and Analysis of Gait-Cycle Data from Motion Capture System

According to research, the motion capture system is capable of collecting data on various human movements, including walking and running [269]. When collecting gait data, multiple motion capture devices are typically employed to capture the subject's movement trajectory from different angles, thereby ensuring more accurate data acquisition. This is achieved by tracking the positions of markers placed on different body parts in three-dimensional space. By analyzing these marker positions, various gait parameters such as step frequency, step length, gait cycle, stance phase, and swing phase can be calculated. This information provides valuable insights into an individual's walking pattern.

Furthermore, the motion capture system can accurately measure other parameters such as walking posture angles, joint angles, and the center of gravity of athletes [205]. These additional measurements offer a comprehensive understanding of biomechanics, allowing for precise analysis and assessment of movement patterns and coordination. Such data can be particularly beneficial in sports performance evaluation, injury prevention, and rehabilitation protocols.

Fig. 4.6 illustrates the utilization of the motion capture system in capturing and analyzing human movement, showcasing its capability in capturing precise and detailed motion data for further analysis and research.
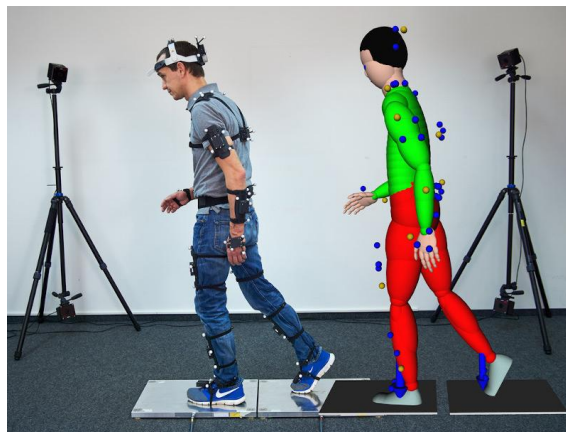


Fig. 4.6 Motion Capture System Testing [269]

The collected gait data from motion capture systems can find valuable applications in the fields of medicine and sports training. In the medical domain, these data can be utilized for diagnosing and studying gait abnormalities such as cross-step, limp, and forced-knee bend, as well as assessing the effectiveness of treatments [11]. By analyzing the movement trajectory, body posture, and joint angles derived from the data, healthcare professionals can gain insights into a patient's gait pattern and identify any deviations or irregularities.

This information aids in accurate diagnosis and informs treatment plans, allowing for targeted interventions and monitoring of progress.

In conclusion, gait data collection represents one of the applications of motion capture systems in the fields of medicine and sports training. The comprehensive data, including movement trajectory, body posture, and joint angles, serve as vital evidence for doctors and coaches to evaluate treatment effectiveness, monitor progress, and help athletes train and compete more effectively.

### 4.4.3 The Necessity of Utilizing Motion Capture System

The necessity of utilizing a motion capture system lies in its ability to capture and analyze human movement with a high level of accuracy and detail.

Motion capture technology has found applications in various industries, including entertainment, sports, healthcare, and virtual reality. In the entertainment industry, motion capture is crucial for creating realistic and immersive experiences in movies, video games, and animations. By capturing the movements of actors or performers, the system can transfer their motions onto digital characters, bringing them to life with natural and lifelike movements. This enhances the overall quality and realism of the final product. In sports, motion capture is used for performance analysis and training purposes. Athletes can have their movements captured and analyzed to identify areas for improvement, correct techniques, and prevent injuries. Coaches can use the data obtained from motion capture to develop personalized training programs and monitor progress over time. In the healthcare field, motion capture is employed for rehabilitation and physical therapy. It enables healthcare professionals to assess patients' movements, track progress, and design targeted interventions. By accurately measuring joint angles and movement patterns, motion capture systems assist in the recovery and rehabilitation process.

Overall, the necessity of utilizing a motion capture system lies in its ability to capture and quantify human movement data accurately. This data can be leveraged across various industries to enhance entertainment experiences, improve sports performance, aid in rehabilitation, and create more immersive virtual reality environments. Therefore, this method would be used to obtain and analysis the gait-cycle of normal human and stroke patients. The data obtained through the motion capture system mentioned in this section will provide data support for the design in Chapter 5 and prototype validation in Chapter 10.

## 4.5 Conclusions

In this chapter, we have presented a comprehensive overview of the methodology employed in this paper. One of the key theoretical concepts explored is the screw the-

ory, which was extensively explained in Section 4.2. The screw system, a vector space comprising screw multiplications, finds wide-ranging applications in the fields of physics, mathematics, and engineering. By studying the structure of screw systems and relevant fundamental mathematical models, we can more readily derive the kinematic model for the design structure, thereby providing essential theoretical support for the development of lower limb exoskeleton rehabilitation structures. In Section 4.3, we delved into the theory and application of genetic algorithm optimization. Genetic algorithms offer several advantages over traditional optimization methods, particularly when dealing with complex problems. By combining programming statements and iterative processes, we utilized genetic algorithms to identify the optimal solution for our specific problem. This approach allowed us to effectively optimize the performance and practicality of the lower limb exoskeleton rehabilitation structure we designed. Lastly, in Section 4.4, we discussed the utilization of motion capture systems. These systems play a crucial role in capturing data throughout the gait cycle of human motion, forming the foundation for the design of lower limb exoskeleton rehabilitation structures. Motion capture systems accurately track and measure human movement, capturing precise posture and motion data and converting them into digital signals. These signals are subsequently employed for simulation and research pertaining to lower limb exoskeleton rehabilitation structures.

The theoretical knowledge and applied methods introduced in this chapter establish a robust theoretical foundation and technical framework for the design of lower limb exoskeleton rehabilitation structures. In subsequent chapters, the leverage knowledge and methods would be used, integrating them with practical considerations. This will enable us to engage in structural design, simulation, and prototype manufacturing, with the ultimate goal of optimizing the performance of lower limb exoskeleton rehabilitation structures and enhancing functional recovery outcomes.This chapter will lay the foundation for the section on lower limb rehabilitation exoskeleton structural design in Chapter 5, including the design of the hip joint, knee joint, ankle joint, and toe joint structures.

# Chapter 5

# Design and Modeling of the Lower Limb Rehabilitation Exoskeleton Mechanism

## 5.1 Introduction

According to the introduction of existing lower limb rehabilitation systems in chapter 4, this chapter primarily focuses on the structural design of critical components that constitute the exoskeleton rehabilitation system, with specific emphasis on various parts of the ankle joint, knee joint, and hip joint. To begin, the chapter introduces an innovative design for the ankle joint rehabilitation exoskeleton. It incorporates two degrees of freedom of rotation, aligning closely with biomechanical principles. Additionally, an extra degree of freedom of rotation is added in the toe region to provide patients with increased flexibility and the ability to engage in multi-angle activities during ankle rehabilitation training. The exoskeleton mechanism includes a motor drive and a spring acting as a bionic energy device to enhance power. This design enables active rehabilitation training, passive buffering, and energy storage for the wearer.

Next, the chapter presents an ergonomic exoskeleton configuration for lower limb rehabilitation, combining the advantages of self-tracing and self-adapting exoskeletons. A novel knee joint exoskeleton mechanism is developed to implement this design. The interaction forces, torques, and displacement between the exoskeleton and the lower limb are meticulously monitored, allowing for quantification of the exoskeleton's compatibility. Motion data from human lower limbs captured by a gait capture system is presented, along with details of the ergonomic exoskeleton mechanism. The findings and results from the study are reported in the third section. In the fourth section, a comprehensive discussion on the exoskeleton's compatibility is provided based on quantitative testing outcomes. Finally, the fifth section concludes with key findings and suggests potential avenues for future research.

Furthermore, this chapter illustrates a novel two-degree-of-freedom hip joint structure design. It offers a detailed description of its rotational capabilities, accommodating both active and passive movements. These movements facilitate rehabilitation exercises for stroke patients, including normal gait patterns and lateral leg lifting. To prevent motion-related injuries during the rehabilitation process, a passive elastic energy storage device is incorporated into the structure, providing a buffering effect for the hip joint.

Overall, this chapter presents innovative and comprehensive structural designs for the ankle joint, knee joint, and hip joint components of the exoskeleton rehabilitation system. These designs aim to optimize functionality, provide flexibility, and ensure a safe and effective rehabilitation experience for stroke patients. Thus, the modelling and analysis of the ankle joint, knee joint and hip joint would be shown in section 5.2, section 5.3 and section 5.4 separately.

## 5.2 Design and Modelling of the Ankle Joint Rehabilitation Mechanism

Ankle joint is an imperative component of the human lower limb as it plays a vital role in providing stability during human movement and serves as the key point for the human body to contact the ground. It facilitates day-to-day activities such as walking, running, squatting, jumping and numerous other movements. However, with the rise in living standards, there has been an increase in ankle joint injuries due to various reasons. Such injuries have become a significant concern among the aging population, athletes, and people who encounter accidental injuries in their daily lives. Ankle rehabilitation exoskeleton robots are designed to aid patients suffering from transtibial injury, which leads to the loss or reduction of motor function in the ankle joint due to damage to the distal part of the tibia and fibula. These robots assist in the recovery process by providing support and stabilization while enabling patients to perform a range of therapeutic exercises.

Currently, the application of robot technology in ankle joint rehabilitation is still in its early stages. However, with ongoing research and development, the use of advanced ankle joint rehabilitation machinery will become more prevalent, offering patients the ability to carry out effective rehabilitation exercises anywhere and at any time. Further research into human ankle joint rehabilitation robots and the development of advanced products that are suitable for the general public will be key in further promoting the use of this technology. This will have great social significance as it will enable patients to receive professional-level rehabilitation treatment outside of clinical environments, empowering them to take control of their recovery process. With technology constantly advancing, the potential

for ankle rehabilitation exoskeleton robots to improve and revolutionize rehabilitation practices is high, making it an exciting area for continued research and development.

## 5.2.1 Muscle Structure and Design Principles of the Ankle Joint Rehabilitation Mechanism

Muscles located on the surface of the trunk and limbs play a pivotal role in generating power for joint movement. In the lower limbs, the plantarflexion and dorsiflexion movement of the ankle joint are mainly achieved through the contraction of the gastrocnemius muscle and tibialis anterior muscle, respectively, while the toe extension movement is primarily carried out by the longus digitorum and extensor hallucis longus muscles, as shown in Fig. 5.1 based on human lower limb anatomy. These muscles work in coordination with each other to facilitate smooth and precise movements of the ankle joint, thereby enabling individuals to carry out various activities ranging from simple ambulation to complex athletic movements. Understanding the intricate connection between these muscles and their functions is critical in developing effective rehabilitation strategies for patients with ankle injuries or impairments.
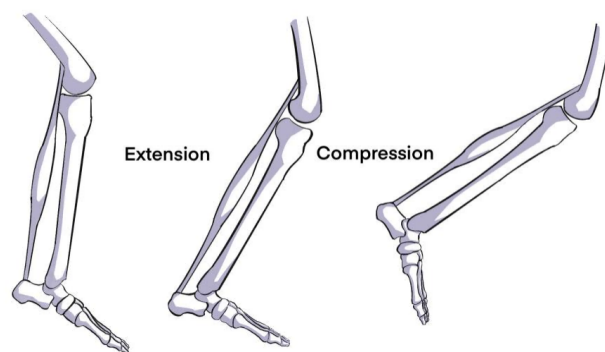


Fig. 5.1 Muscle Change of Lower Limb in a Gait Cycle

It is critical to improve exoskeleton structure and incorporate a power device and bionic energy device that can simulate the bionic function of skeletal muscle, based on bionic dynamic characteristics analysis. This will help patients with ankle joint rehabilitation achieve optimal outcomes. The design principle of the bionic energy device is established through a thorough examination of relevant skeletal muscle anatomy, ensuring that the exoskeleton operates in harmony with the patient's anatomy, facilitating effective rehabilitation of ankle joint motion. By leveraging the principles of bionics and biomechanics, this chapter provides a foundation for advancing ankle joint rehabilitation exoskeleton technology and enhancing patient outcomes.

Principle 1: The ankle joint plays a critical role in the human gait cycle, facilitating movement and weight-bearing activities, as shown in Fig. 5.1. During the initial heel landing stage, the calf gastrocnemius muscle contracts, resulting in ankle plantarflexion. Thus, to achieve efficient and effective rehabilitation of ankle joint motion, it is necessary to replace the gastrocnemius muscle in the heel position of the prosthetic foot with a mechanism that can provide buffer and energy storage for the prosthesis wearer. To accomplish this, a parallel compression spring device is integrated into the heel region of the prosthetic foot. Additionally, a revolute joint is established outside the ankle joint, along with a motor and worm gear transmission structure, to enable power output. By using a worm gear and worm drive mechanism, rotational power can be actively applied, while the parallel compression springs release energy from their compressed state at the end of heel landing. This approach enables patients with exoskeleton wearing to transition smoothly from ankle and foot plantarflexion to dorsiflexion, thus facilitating optimal outcomes for ankle joint rehabilitation. By leveraging biomechanical principles and advanced technology, this principle lays a foundation for the development of highly effective and efficient exoskeleton systems for ankle joint rehabilitation.
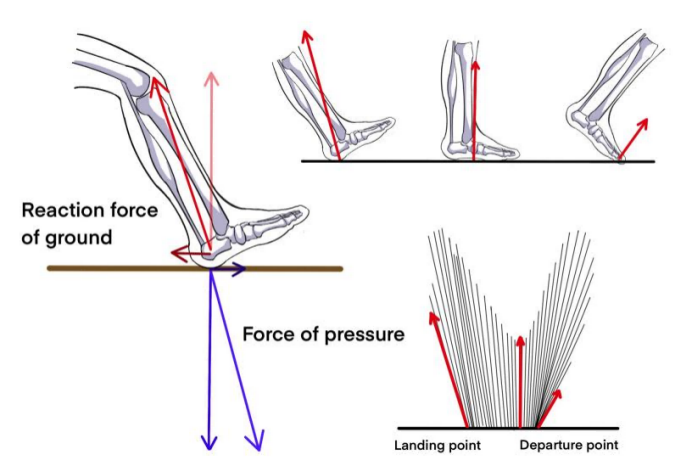


Fig. 5.2 Reaction Force between Foot and Ground During a Gait Cycle

Principle 2: Ankle dorsiflexion is a crucial component of the gait cycle, allowing for effective weight transfer and forward propulsion, as shown in Fig. 5.2, during the flat foot and heel lift phase, the anterior calf muscles contract to drive ankle dorsiflexion. The maximum contraction occurs at the end of the heel lift phase. To enhance the rehabilitation of ankle joint motion, it is possible to design a bidirectional compression spring at the tibialis anterior group of the instep. This spring can store and release energy during both the heel-to-ground and tip-to-ground phases, thus facilitating optimal outcomes for exoskeleton wearing patients. Moreover, by incorporating a motor-driven worm gear and worm transmission device, as outlined in Principle 1 above, the rehabilitation

function can be amplified significantly. This approach provides efficient and effective support for patients undergoing ankle joint rehabilitation, enabling them to regain mobility and improve their overall quality of life. With the integration of advanced technology and biomechanical principles, this principle lays the foundation for the development of next-generation exoskeleton systems for ankle joint rehabilitation. By leveraging these innovative approaches, we can transform the way we approach rehabilitation, and help patients achieve optimal outcomes with greater ease and efficiency.

Principle 3: During the toe lifting stage of the gait cycle, the ankle joint is in a plantarflexion state. To simulate the contraction of the gastrocnemius muscle and provide efficient assistance for ankle-foot exoskeleton mechanism, a torsion spring device can be utilized. Furthermore, to enhance the effectiveness of this approach, a motor gear drive structure can be added to the rotation axis. This enables the generation of energy that simulates the actions of the gastrocnemius muscle, providing additional thrust to assist with toe lifting. By leveraging these innovative technologies, patients can enjoy improved mobility and flexibility during the rehabilitation process. This principle emphasizes the importance of incorporating biomechanical principles and advanced technology in designing exoskeleton systems that can effectively mimic natural movement patterns, facilitating optimal outcomes for patients.

Principle 4: In addition to the plantar-dorsiflexion movement of the ankle joint, it is also necessary to address left and right rotation during certain occasions. To facilitate effective rehabilitation for patients undergoing ankle joint recovery, a motor gear drive structure can be designed above the plantar-dorsiflexion axis of the ankle joint. This enables the provision of additional support for ankle joint rotations, which are critical for optimal mobility and stability. By incorporating this innovative technology, patients can enjoy greater flexibility and range of motion during the rehabilitation process, allowing them to achieve optimal outcomes with greater ease.

By emphasizing the importance of addressing all aspects of ankle joint movement in exoskeleton design, we can develop highly effective and efficient rehabilitation systems that cater to the unique needs of each individual patient. With continued research and development in this field, we can transform the lives of millions of people worldwide, helping them regain mobility and independence and improving their overall quality of life.

## 5.2.2   Establishment of Ankle Joint Rehabilitation Model

Based on kinesiology analysis of human lower limbs, the design scheme for an ankle rehabilitation exoskeleton robot has been established. The ankle joint possesses two rotational degrees of freedom, allowing for plantar-dorsiflexion and left-right rotation about the heel axis. In accordance with the principles of natural human ankle joint

movement, various links with fewer degrees of freedom were analyzed and compared to determine the optimal rehabilitation training mode for the exoskeleton robot.

After thorough analysis, the mechanical equipment required for the exoskeleton system was identified, and a detailed structure diagram was developed. The comprehensive determination of the exoskeleton's mechanical structure is critical to ensure that patients receive the most effective and efficient rehabilitation possible.
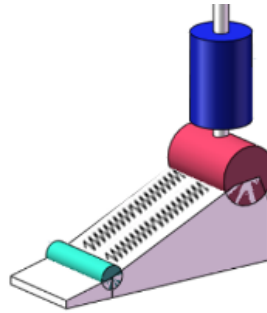


Fig. 5.3 Theoretical Concept Diagram of Ankle Joint Rehabilitation Mechanism

By leveraging advanced technologies and adhering to the principles of natural human biomechanics, we can develop innovative and impactful solutions for patients undergoing ankle joint rehabilitation. Thus, the theoretical concept diagram could be exhibits as above.

### 5.2.3 Ankle Plantar-dorsiflexion Active Drive Structure

The above diagram displays the normal range of plantar flexion (toe pointing down-wards) and dorsiflexion (toe pointing upwards) for the human ankle. During rehabilitation training, it may be necessary to limit the range of motion for the ankle joint. In the ankle rehabilitation exoskeleton, patients who are unable to move their feet will require prior training before using the active plantar flexion-dorsiflexion drive structure of the exoskeleton device to exercise their lower limbs.

The active drive structure of the ankle exoskeleton rehabilitation device incorporates a motor-driven worm gear and worm drive device. This type of transmission system ensures smooth movement and a large transmission ratio, reducing the number of transmission links required. The worm gear and worm drive system is directly connected to the motor, resulting in a simple and compact design. Table displays the design parameters used for the worm gear and worm transmission device in this structure, as shown in Tab. 5.1.

Based on the above raw data, the calculation results are as follows:

The worm wheel diameter:

$$D = m_w \times z_2 = 1 \times 50 = 50\text{mm} \tag{5.1}$$

Table 5.1 Input Parameters of Worm Gear and Worm Drive

| Name | Unit | Value |
|---|---|---|
| Center distance, a | (mm) | 30 |
| Transverse module | (mm) | 1 |
| Number of worm | - | 1 |
| Number of turbine | - | 50 |
| Turbine tooth width | (mm) | 10 |
| The length of the worm | (mm) | 24 |

Diameter of the worm:

$$d = 2a - D = 10 \text{mm} \tag{5.2}$$

Transmission ratio:

$$i_t = \frac{z_2}{z_1} = 50 \tag{5.3}$$

The lead of the worm:

$$l_w = \frac{(\pi \times D)}{z_2} = 3.142 \text{mm} \tag{5.4}$$

Lead Angle:

$$\gamma = \arctan \frac{(\pi \times D)}{z_2 (\pi \times d)} = 5.71° \tag{5.5}$$

Normal module:

$$m_t = m \times \cos \gamma = 0.995 \tag{5.6}$$

Since the worm gear used in this device is made of bronze material and applied to the rehabilitation of human ankle exoskeleton, compared with the transmission form of worm gear and worm, it is light load but used for a long time, so the failure form of this device is usually tooth surface contact fatigue failure $\sigma_H$. The Hertz formula of tooth surface contact fatigue strength of worm gear is calculated as follows:

$$\sigma_H = \sqrt{\frac{K_l F_n}{L_0 \rho_z}} \cdot Z_E \tag{5.7}$$

Where, $F_n$–the normal load on the meshing tooth surface, Newton(N);

$L_0$–the total length of contact line, the unit is *mm*;

$K_l$– load coefficient;

$\rho_z$–the contact ratio;

$Z_E$–elastic influence coefficient of the material, and the unit is $\sqrt{MPa}$, where $Z_E = 160\sqrt{MPa}$.

The normal load $F_n$ in the above formula is converted into the relation between the diameter of the dividing circle of the worm gear $d_2$ and the torque $T_2$ of the worm gear, and then $d_2$ and $L_0$ are converted into the function of the center distance, so that the checking formula of the contact fatigue strength of the worm gear tooth surface is:

$$\sigma_H = Z_E Z_\rho \sqrt{KT_2/a^3} \leq [\sigma]_H \tag{5.8}$$

Where, $[\sigma]_H$ represents the maximum allowable tooth contact stress, $Z\rho$– Influence coefficient of contact line length and curvature radius of worm drive on contact strength, referred to as contact coefficient, $Z\rho$ can be found from the contact coefficient of cylindrical worm drive in Fig. 5.4:
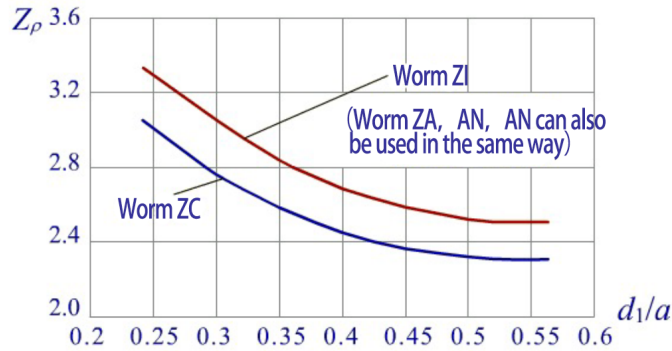


Fig. 5.4 Contact Coefficient of Cylindrical Worm Drive

$K$ – load coefficient,$K = K_A K_\beta K_V$, where $K_A$ is the use coefficient, and $K_A = 1.2$; $K_\beta$ is the load distribution coefficient in the tooth direction. When the worm drive works under the steady load, the uneven load distribution will be improved due to the good run-in of the working surface. In this case, $K_\beta = 1$; When the load changes greatly, or there is impact, vibration, can be $K_\beta = [1.3, 1.6]$, this device in the calculation of choice: $K_\beta = 1.6$; $K_V$ is the dynamic load coefficient. Since the worm drive is generally stable, the dynamic load is much smaller than that of the gear drive, so the value of $K_V$ should be 1.1.

Thus,

$$K = K_A K_\beta K_V = 1.2 \times 1.6 \times 1.2 = 2.304 \tag{5.9}$$

(a) Dorsiflexion of the Ankle



(b) Plantarflexion of the Ankle
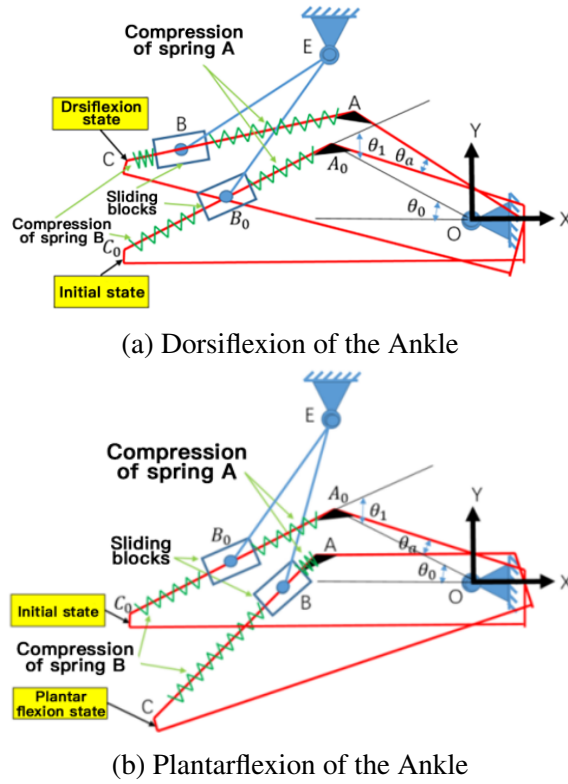
Fig. 5.5 Schematic Diagram of Ankle Joint with Elastic Absorber Modules

In the exoskeleton rehabilitation, the maximum rotational moment of the patient's ankle was set to be $T_2 = 150N \cdot m$, and then it was calculated as:

$$\sigma_H = Z_E Z_\rho \sqrt{KT_2/a^3} = 160 * 3 * \sqrt{2.304 * \frac{150}{0.03^3}} = 1.72\text{MPa} \qquad (5.10)$$

Where, $\sigma_H$ is the allowable contact stress of worm gear tooth surface. This result is much less than the allowable contact stress of bronze material.

### 5.2.4  Ankle Planterflexion-Dorsiflexion Passive Elastic Structure

As mentioned above, the designed motion range of the ankle exoskeleton rehabilitation robot is between limitations, and the two limit positions are mainly realized by the size limitation of the connecting rod mechanism. Placing two compression springs in opposite directions in the connecting rod mechanism can help the ankle exoskeleton robot achieve energy storage and release within the gait cycle. The rotation of the ankle joint can also provide energy for the leg during the toe off stage.

As shown in Fig. 5.5, The ankle exoskeleton undergoes a clockwise movement around the axis of rotation while the slider moves towards the toe. The compression spring A

rebounds from its compressed state to its initial state, whereas the compression spring B continues to compress to store energy. This ensures that the heel is well-cushioned during lift-off from the ground. On the other hand, when the ankle exoskeleton mechanism moves in a counterclockwise direction around the axis of rotation and the slider slides away from the toe, compression spring A continues to compress to store energy, providing power for lifting the toe off the ground at the end of the toe-off phase. At the same time, compression spring B recovers from its compressed state to its initial state.

According to the working schematic, the positions of point $A_0$, $C_0$ and point $E_0$ in the coordinate system $OXY$ are respectively, $(x_{A_0}, y_{A_0})$, $(x_{C_0}, y_{C_0})$ and $(x_{E_0}, y_{E_0})$. When the rotation Angle of the ankle joint is $\theta_a$, the position coordinate function of points $A$ and $C$ is as follows:

$$\begin{cases} x_A = -l_{OA}\sin(\theta_0 + \theta_a) \\ y_A = l_{OA}\cos(\theta_0 + \theta_a) \end{cases} , \begin{cases} x_C = x_A - l_{AC}\cos(\theta_1 - \theta_0 - \theta_a) \\ y_C = y_A - l_{AC}\sin(\theta_1 - \theta_0 - \theta_a) \end{cases} \tag{5.11}$$

Where $\theta_a$ is the rotation Angle of the ankle joint. When $\theta_a$ is positive, it means clockwise rotation and dorsiflexion of the ankle joint; when $\theta_a$ is negative, it means counterclockwise rotation and plantarflexion of the ankle joint.

According to the above formula, we can calculate the sides of the triangle formed by the points $C$, $C_0$ and $E$ is $L_{EC0}$, $L_{EC}$ and $L_{EE0}$, respectively.

According to the triangle cosine theorem, the angle between $L_{EC0}$ and $L_{EC}$ can be written as:

$$a = \arccos\frac{l_{CE}^2 + l_{C_0E}^2 - l_{C_0C}^2}{2l_{CE}l_{C_0E}} \tag{5.12}$$

The coordinate relation of slider point $B$ is as follows:

$$\begin{cases} \frac{y_{A_0} - y_{C_0}}{x_{A_0} - x_{C_0}} = \frac{y_{B_0} - y_{C_0}}{x_{B_0} - x_{C_0}} \\ \frac{y_A - y_C}{x_A - x_C} = \frac{y_B - y_C}{x_B - x_C} \end{cases} \tag{5.13}$$

The compression amount of the spring $A$ and spring $B$ during the motion of the ankle joint is respectively:

$$\begin{cases} \Delta C_A = \left| l_{AB} - l_{AB_0} \right| + p_A \\ \Delta C_B = \left| l_{CB} - l_{CB_0} \right| + p_B \end{cases} \tag{5.14}$$

The neutralization $p_A$ and $p_B$ represents the precompression amount of the compression spring $A$ and $B$. The stiffness of the two springs can be derived from the forces and moments generated by the compression springs $A$ and $B$ when the ankle joint moves:

$$\begin{cases} k_A = \dfrac{F_A}{\Delta C_A} = \dfrac{T_A(\theta_a, a, p_A)}{\Delta C_A \cdot l_{OA} \sin(\theta_1)} \\ k_B = \dfrac{F_B}{\Delta C_B} = \dfrac{T_B(\theta_a, a, p_B)}{\Delta C_B \cdot l_{OA} \sin(\theta_1)} \end{cases} \tag{5.15}$$

As can be seen from the above equation, the stiffness characteristics of the compression spring $A$ and $B$ change with the Angle of the ankle joint within a short period, with variable stiffness characteristics, in line with the motion characteristics of the human joint, suitable for the energy storage device of the exoskeleton ankle joint structure.

### 5.2.5  Flexible Toe Joint Active Drive Structure

In previous ankle rehabilitation exoskeleton designs, a motion structure that allows the ankle to swing from side to side was relatively uncommon. In human skeletal muscles, during the aforementioned ankle dorsiflexion-plantarflexion movement, the peroneus longus, peroneus brevis, and tibialis anterior muscles usually undergo synchronous stretching and contraction movements along with the gastrocnemius. In the case of ankle swing movement, these muscles can further assist in synchronous telescopic movement, providing patients with a diverse range of training processes that can facilitate faster recovery. By incorporating this motion structure into ankle rehabilitation exoskeletons, patients can benefit from a more comprehensive and effective treatment plan, resulting in improved outcomes and higher rates of successful recovery, as shown in Fig. 5.6.

As shown in Fig. 5.7, when the right foot is rotated counterclockwise from bottom up, the peroneus longus and peroneus brevis muscles undergo contraction, while the tibialis anterior muscle undergoes stretching. Conversely, when the right foot is rotated clockwise, the peroneus longus and peroneus brevis muscles are stretched, while the tibialis anterior muscle undergoes contraction. These synchronous movements between the aforementioned muscles play a crucial role in the ankle dorsiflexion-plantarflexion movement and ankle swing movement, which are essential for successful rehabilitation of ankle injuries. By comprehensively understanding the synchronous actions between these
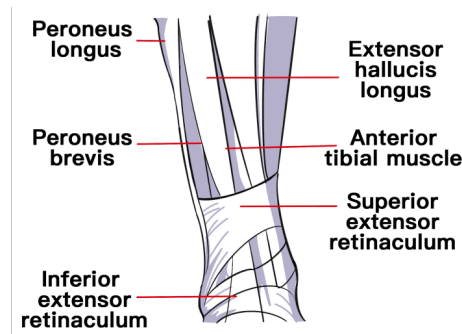
Fig. 5.6 The Muscle Flex Asynchronously while Rotation

muscles, physical therapists can tailor rehabilitation exercises to target specific areas of the ankle and accelerate the recovery process for patients.
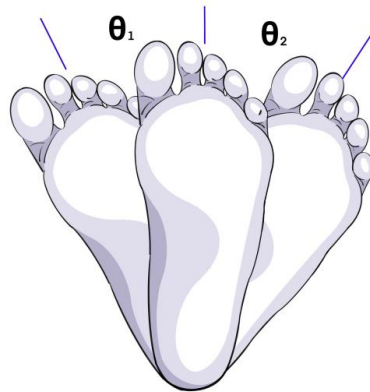


Fig. 5.7 Schematic Diagram of Footstep Rotation

To enable the actions described above, a set of gear drives has been incorporated under the leg fixing plate of the ankle exoskeleton rehabilitation robot. Additionally, a servo motor has been placed at the input end of the gear drive to provide the necessary driving force, as shown in Fig. 5.8. This design is crucial for facilitating the synchronized movement and contraction of the peroneus longus, peroneus brevis and tibialis anterior muscles during rehabilitation exercises. The gear drive mechanism ensures smooth movement of the ankle joint while the servo motor provides the required power to overcome resistance encountered during the training process.

By utilizing this advanced technology, ankle rehabilitation exoskeleton robots are capable of more effectively treating patients with ankle injuries, leading to improved recovery outcomes and quality of life.

Finally, the comprehensive determination of the mechanical equipment to be studied in this paper, drawing the structure diagram.

According to design principle 1, a parallel buffer energy storage device is designed on both sides of the ankle joint, which plays the function of buffer and energy storage when
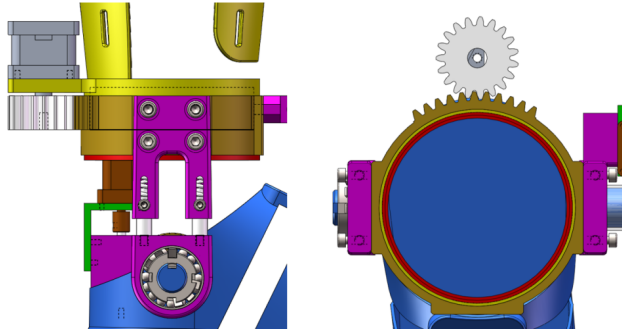
Fig. 5.8 Two Sides Swing Gear Transmission Structure
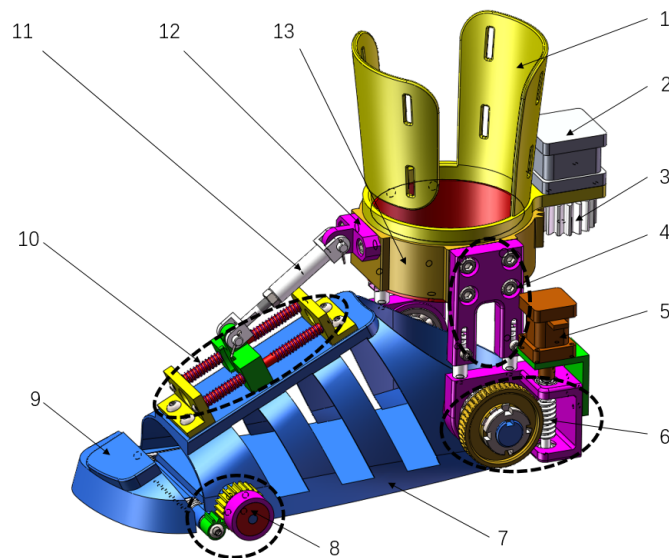


Fig. 5.9 3D Model of Ankle Rehabilitation Exoskeleton Robot Mechanism

the foot contacts and leaves the ground. At the same time, a worm gear and worm structure is designed on the lateral side of plantar-dorsiflexion rotational joint and a driving motor is added to realize the function of active-passive rotation assistance. According to the design principle 2, a bidirectional compression spring is added to the instep linkage mechanism to form a parallel energy storage mechanism, which can simulate the muscle function in the process of ankle joint movement. In addition, the active motor transmission structure in principle 1 helps realize the mutual transformation of plantar flexion and dorsiflexion. Based on this, a new ankle exoskeleton mechanism with both active and passive continuous driving, energy storage and energy release is designed, as shown in Fig. 5.9. 1 - crus fixed block, the agency is mainly composed of around 2 - heel rotary motor driver module, drive pinion rotating around 3 - heel rotation drive pinion, 4 - heels buffer energy storage device, rotate the motor driver module 5 - foot up and down, 6 - foot up and down spin worm gear and worm drive device, 7 - exoskeleton set of feet, 8 - toe rotary motor driver module, 9 - toe, 10- bidirectional spring energy storage structure, 11- plantar flexion - dorsiflexion link, 12- connecting head, 13- ring gear. The design goal of this study is to help stroke patients with low power output and good bionic performance at the ankle joint when walking, so as to restore normal ankle motor function.

### 5.2.6 Flexible Toe Joint Passive Elastic Structure

The flexible toe joint mechanism possesses the ability to distort while under the influence of energy. Additionally, it can passively store energy, providing an elastic mechanism for transferring force and motion that assists in walking. The coordination between the movement of the toe joint and the overall walking motion of the foot is crucial. The change of the posture of the toe joint in the walking process as shown in Fig. 5.10.
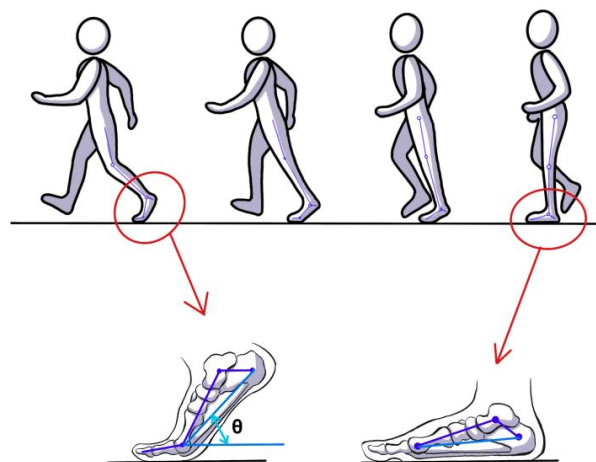


Fig. 5.10 Angle Change of the Toe Joint

During walking, the angle between the toe joint and the plantar plane undergoes a change within the zero to $\theta$ range. As a result, a set of torsion spring structures that are relatively compact can be utilized at the toe joint, making it an ideal power device. The compact design of the torsion spring structure ensures that the toe joint is capable of handling the loads produced by the foot during the walking process. This is a key factor in ensuring the smooth and efficient transfer of force and motion between the foot and the ground,as shown in Fig. 5.11.
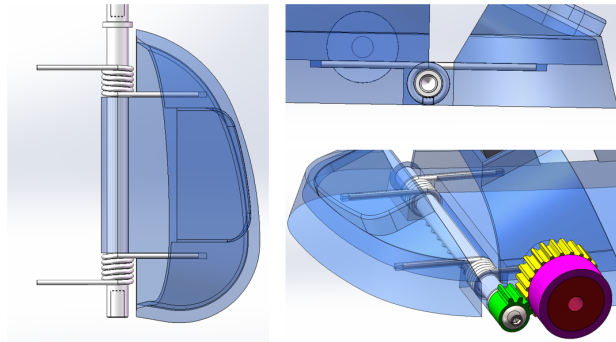


Fig. 5.11 Schematic Diagram of the Torsion Spring at the Toe Joint

At the end of the rotating shaft connected between the toe joint and the foot seat, a set of spur gear transmission structure is added, and a large torque frame less motor is designed at the input end. At the same time, active power and passive energy storage structure are realized for the rotation rehabilitation training of the toe joint. When the human toe joint rotates, the general Angle ranges from -5° to +30°, and the rotation Angle is controlled by the customized large-torque rimless motor. When the rimless motor works, it first needs to overcome the reverse torque of the torsion spring, and then drive the toe joint of the rehabilitated patient to do the rotation rehabilitation exercise. In the return journey stage, the rimless motor is not powered. The torsion force of the torsion spring can drive the toe joint to return to the initial position. At the same time, the torsion spring can also be used as a passive energy storage device in the case of no motor, helping patients to do toe joint rehabilitation training.

The initial relative Angle between the two ends of the torsion spring is 180°, and the load for each 1° increase of torsion spring is:

$$\mathrm{K}_s = \frac{E_s * d_w{}^4}{1167 D_m * \pi * N * R} \tag{5.16}$$

The torque of the torsion spring at the maximum angle is:

$$T_t = \theta_{max} K_s R_m \tag{5.17}$$

The frame-less motor torque is as follows:

$$T_d = k_t T_t \tag{5.18}$$

$$F_d = \frac{2T_d}{D_2} \tag{5.19}$$

$k_t$—The torque coefficient, let's say $k_t$ is equal to 2

$E_s$—Modulus of steel wire, stainless steel wire $E = 19400$

$d_w$—Wire diameter *mm*

$D_m$—Pitch diameter *mm*

$N$—Total winding number

$R_m$—The moment of a load

$D_2$—The dividing circle diameter of the output gear

## 5.3 Design and Modelling of the Knee Joint Rehabilitation Mechanism

In addition to the foundation laid in Chapter 3, we still need the contribution of the flexible structures mentioned in Chapter 2 for this chapter. Patients with knee impairments resulting from stroke, spinal cord injury, or other disorders often exhibit abnormal muscle activity, leading to difficulty generating voluntary muscular contractions of normal strength [296]. This significantly affects their gait performance. Among these conditions, stroke is a prevalent cause of mobility issues, often resulting in unilateral weakness on the affected side [301]. During walking, these patients may drag their affected leg in a semicircular motion [197]. Weak or paralyzed muscles responsible for knee stabilization can make it challenging for patients to maintain walking stability compared to healthy individuals [1], increasing the risk of collapsing during the weight acceptance phase [5] [18]. Consequently, knee exoskeletons are highly anticipated for addressing the pathological gait of individuals with knee dysfunction [19] [20] [33]. As a result, therapists face an increasingly significant burden [300]. To mitigate treatment costs and reduce therapists'

workload while facilitating medical care and enabling home-based rehabilitation, numerous researchers have put forth ideas for robotic exoskeleton rehabilitation mechanisms [39].

Despite the proposals of various exoskeleton mechanism designs in recent decades, several unresolved challenges hinder their utilization in domestic rehabilitation [314] [320]. The first challenge lies in reconfiguration and customization, as most existing mechanisms are rigid structures that fail to cater to individual patient needs. The second challenge pertains to the intelligence of the robotic system for evaluating recovery progress. This currently limits the timely collection of patient information. The final obstacle is the lack of effective personalized treatment methods, as current exoskeletons are unable to tailor rehabilitation programs to specific patient requirements. In the realm of exoskeleton research, one fundamental challenge revolves around human-machine collaboration. The human body occupies a central role in mechatronics, and the exoskeleton constantly interacts with the human user to achieve mutual adaptation and functional enhancement. Consequently, new research approaches must consider the effects of human-machine interaction rather than solely focusing on the machine's capabilities. Moreover, the interaction between mechanical and electrical devices and biological systems is bidirectional: machines should not only assist or aid humans in real tasks but also adhere to human behavioral rules and not compromise human functions.

### 5.3.1 Data Collected from the Motion Capture System

In this section, we employed a 3D motion capture system (Cortex, Motion Analysis Co., Santa Rosa, CA, USA) to precisely capture the leg movements of human subjects during walking and leg lifting. To accomplish this, we placed a total of 15 Helen Hayes markers on specific locations of the lower limbs of the participants, as depicted in Fig. 5.12. These markers were strategically positioned to ensure accurate tracking of the leg motion throughout the experiments.
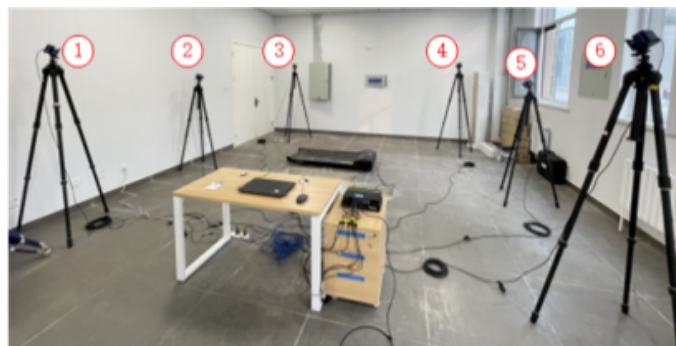


Fig. 5.12 Motion Capture System Equipments

To conduct the testing protocol, participants were instructed to either walk on a treadmill or sit within the designated research area. The testing area was equipped with six cameras strategically placed to capture comprehensive footage of the participants' movements. Throughout the experimental sessions, a complete cycle of lower limb movement was recorded, ensuring the collection of crucial data sets for subsequent analysis.

Representative movement patterns during walking and sitting are illustrated in Fig. 5.13 and Fig. 5.14, respectively. These figures provide a visual representation of the participants' actions and aid in understanding the recorded data.



Fig. 5.13 Walking Test Experiment of Normal Adults



Fig. 5.14 Sitting Test Experiment of Normal Adults

Additionally, the graphs depicting the marker position and spatial position of the thigh and shank are presented in Fig. 5.15 and Fig. 5.16 below. These graphs offer further insight into the detailed movement characteristics of the thigh, knee, and shank, allowing for a comprehensive analysis of the gathered data.
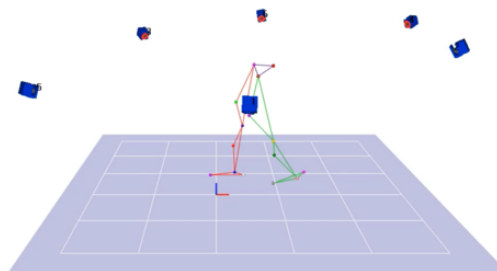


Fig. 5.15 Marker Position of Thigh, Knee and Shank
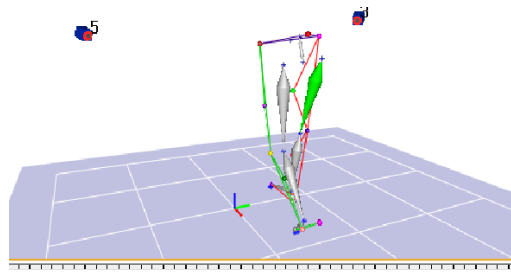
Fig. 5.16 Spatial Position of Thigh and Shank

The thigh, knee, and shank are essential components of the gait cycle, which encompasses the series of movements involved in walking or running. Each phase of the gait cycle relies on the precise coordination and functioning of these lower limb segments.

During the swing phase of gait, the thigh plays a critical role in lifting the leg forward and preparing for the subsequent step. As the foot moves forward, the knee joint extends while the shank is propelled forward. Subsequently, the foot makes contact with the ground during the initial contact phase, transferring the weight of the leg to the supporting limb.

Throughout the stance phase, which constitutes the majority of the gait cycle, the thigh, knee, and shank collaborate to support body weight and maintain balance. As bodyweight shifts forward, the knee joint flexes, and the foot rolls from heel to toe. Simultaneously, the shank muscles engage to regulate ankle and foot movement, ensuring proper ground contact and push-off.

Lastly, during the swing phase, the thigh flexes to lift the leg off the ground, while the knee joint extends to propel the foot forward in readiness for the subsequent step.

The synchronized movements of the thigh, knee, and shank during each phase of the gait cycle facilitate efficient and effective locomotion. Understanding the interplay between these lower limb segments is crucial for optimizing gait patterns, reducing the risk of injury, and enhancing rehabilitation outcomes for individuals with lower limb conditions. Accurate assessment, diagnosis, and intervention strategies can assist individuals in achieving optimal gait mechanics, thereby improving their overall quality of life. Following data collection, the position of the center of mass of the thigh, knee, and shank throughout a complete gait cycle can be observed in Fig. 5.17, Fig. 5.18, and Fig. 5.19, respectively.

Then , the rotational angle of the knee joint and the ankle joint are shown in Fig. 5.20 and Fig. 5.21 in a gait cycle.

Next, the angular velocity of the thigh and shank centroid are shown in Fig. 5.22 and Fig. 5.23.

Finally, the change in angle of the knee joint is depicted in Fig. 5.24. Through our testing, we were able to obtain key metrics pertaining to range of angle and torque changes at the knee joint, as presented in Tab. 5.2. These results offer a comprehensive overview of
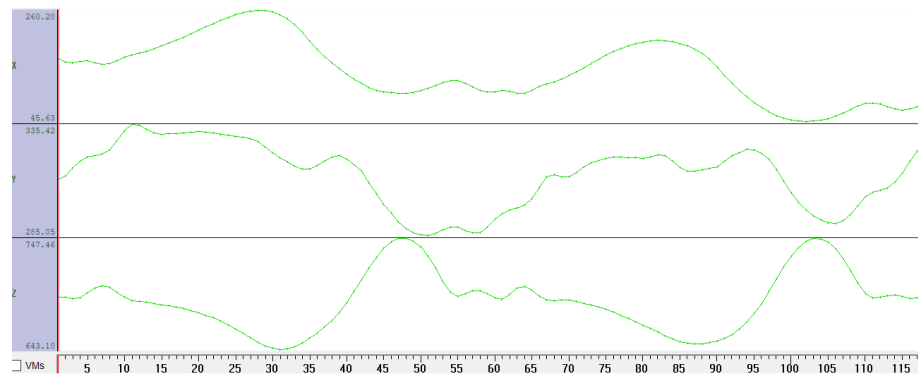
Fig. 5.17 The Position of the Center of Mass of the Thigh
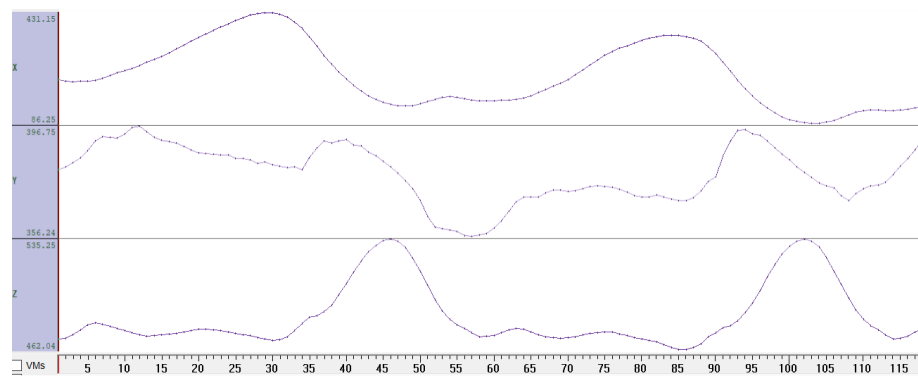


Fig. 5.18 The Position of the Center of Mass of the Knee
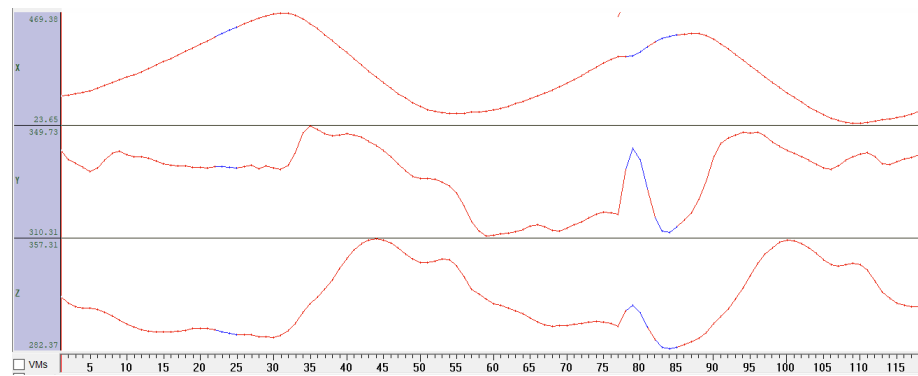


Fig. 5.19 The Position of the Center of Mass of the Shank
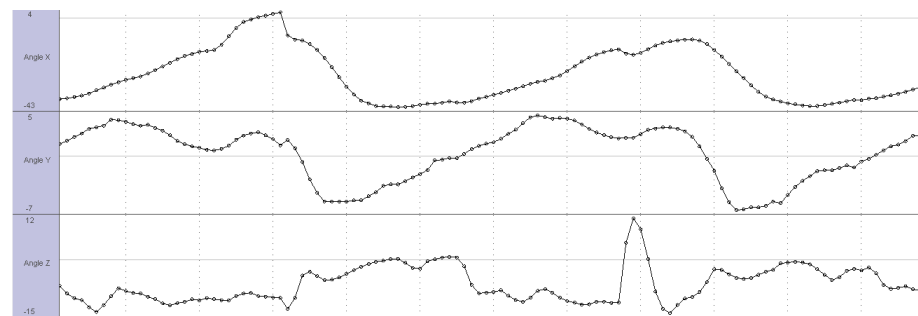


Fig. 5.20 The Rotational Angles of Knee Joint

131
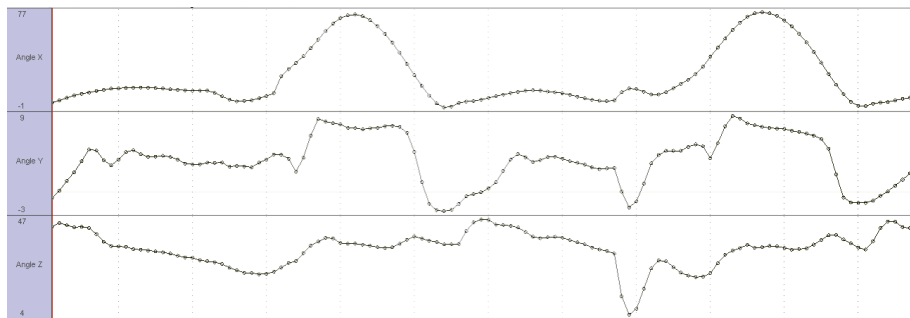
Fig. 5.21 The Rotational Angles of Ankle Joint
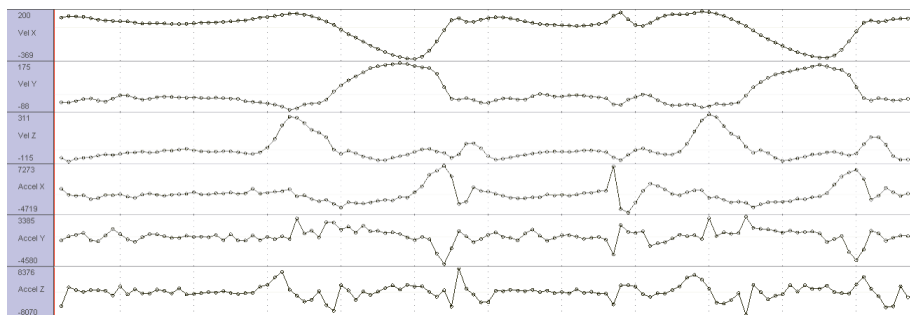


Fig. 5.22 The Angular Velocity of the Shank
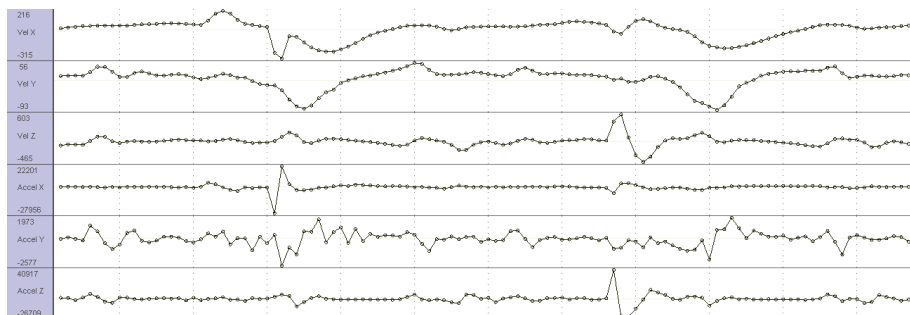


Fig. 5.23 The Angular Velocity of the Thigh

Table 5.2 Range of Angle and Torque of the Knee Joint

|         | Maximum Angle | Maximum Moment | Rotional Angle of Testers |
|---------|---------------|----------------|---------------------------|
| Walking | 67°           | 36.8Nm         | 42°                       |
| Sitting | 117°          | 62.5Nm         | 102°                      |

movement patterns and associated joint dynamics during walking and leg lifting, which hold significant interest within the field of biomechanics.

In the domains of computer graphics and digital image processing, post-processing refers to the manipulation of an image or video after its capture or rendering. It provides several advantages:

a. Quality improvement: Post-processing techniques, such as filtering, noise reduction, and color correction, can enhance the quality of images or videos.

b. Defect removal: In manufacturing, some parts may have defects, but post-processing can eliminate these flaws and elevate product quality.

c. Effects enhancement: Post-processing can augment animations, special effects, or other visual elements, making them more realistic or impressive.

d. Efficiency improvement: By reducing or simplifying certain steps in traditional production workflows, post-processing enhances work efficiency.

e. Controllability: Post-processing empowers image or video editors with greater control, enabling precise operations on the content.

To summarize, post-processing contributes to improved quality and effects of images or videos, while also enhancing production workflow efficiency and controllability.
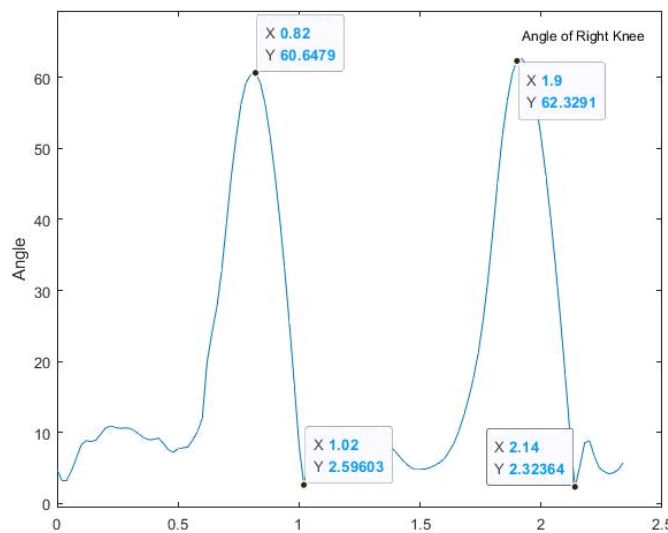


Fig. 5.24 The Angle Change of the Knee Joint

Overall, these findings make a significant contribution to identifying strategies for optimizing performance and mitigating the risk of injuries during physical activity and rehabilitation. By leveraging state-of-the-art motion capture technology, we were able to delve into the intricate and subtle aspects of lower limb movement and joint functionality, providing valuable insights. These insights can inform the development of tailored interventions and enhance our understanding of biomechanics, ultimately leading to improved outcomes in various domains, including sports performance, clinical rehabilitation, and injury prevention.

## 5.3.2 Muscle Structure and Design Principles of the Knee Joint Rehabilitation Mechanism

To effectively design and control a knee exoskeleton, a comprehensive understanding of the biomechanics of the human knee joint is paramount. The gait cycle, encompassing the sequence of movements involved in walking or running, can be divided into two main phases: the stance phase and the swing phase. The stance phase further comprises the weight acceptance phase and the terminal stance phase.

As described in a book on replacement surgery, the human knee joint typically exhibits six degrees of freedom, enabling three rotational motions and three translational motions. While flexion and extension serve as primary movements, external-internal rotation and anterior-posterior translation are crucial for maintaining joint stability. Any constraint on joint mobility can lead to joint reaction forces, potentially resulting in mechanical damage to the surrounding tissues. Therefore, it is imperative to consider these degrees of freedom and their associated movements when designing a knee exoskeleton, in order to replicate natural knee joint mechanics and minimize potential risks.

For individuals with healthy knees, the joint can adequately support body weight during the stance phase and facilitate forward propulsion during the swing phase. However, individuals with knee injuries or conditions may require the assistance of a knee exoskeleton to provide additional support and stability. When designing a knee exoskeleton, it is crucial to consider the necessary range of motion for proper joint function and avoid any constraints that could lead to joint reaction forces or mechanical damage.

By applying knowledge of human knee joint biomechanics to the design and control of knee exoskeletons, researchers and medical practitioners can develop more effective interventions for individuals with knee injuries or conditions. By carefully considering joint function and motion, knee exoskeletons can serve as valuable tools for improving mobility and enhancing the quality of life for those in need.

Although lower extremity or complicated replacement surgery presents significant challenges and risks, it remains a fascinating possibility. Currently, only a small number of

patients have experienced unacceptable morbidity or mortality related to these procedures. This option may be considered for carefully selected patients who have exhausted other alternatives, declined conventional prostheses, or are ineligible for them. However, successful outcomes, including protected sensory function and the ability to engage in community walking, must be achieved while overcoming challenges such as reliable long-distance neurological regeneration, chronic immunosuppression, and perioperative complications. These factors should be thoroughly assessed and addressed to ensure the feasibility and success of such surgeries.

Wearable robotic exoskeletons, such as the Ekso Bionics GT, Indego powered exoskeleton, and ReWalk exoskeleton, have recently emerged as promising technologies to enhance ambulation for individuals with spinal cord injuries. These devices can also assist patients adapting to new prosthetic limbs after bilateral transfemoral amputation (BTFA), a particularly challenging situation. By providing external support and control, these exoskeletons enable patients to walk more easily and efficiently compared to traditional prostheses.

Although wearable exoskeletons offer an alternative approach to traditional prostheses or replacement surgery, they still face significant challenges. Proper fitment and comfort are essential to enable extended wear, while reliable control systems are crucial for safe and precise movements. Furthermore, ongoing research is necessary to explore the long-term effects of utilizing these devices on patient outcomes and overall quality of life.

Despite these challenges, wearable exoskeletons represent an exciting advancement in the fields of prosthetics and rehabilitation. With continued research and development, they have the potential to greatly enhance mobility and independence for individuals with lower limb injuries or conditions.

### 5.3.3 Configuration Synthesis of the Knee Joint

This section will present the configuration synthesis of a lower limb exoskeleton robot that has been designed to achieve maximum flexibility. To accomplish this goal, we have incorporated a sub-mechanism with rotational movement in all directions and translational movement exclusively within the $YZ$ plane. The sub-mechanism has been engineered in such a way that it does not exert constraint forces along the $Y$- and $Z$-axes, nor does it introduce any constraint couples around any axis. The necessary constraint can easily be achieved by ensuring that the sub-mechanism restricts translational mobility only along the $X$-axis. This design feature guarantees that the lower limb exoskeleton is not constrained to any specific movements or directions while providing ample support and stability to the user.

By implementing a sub-mechanism with such flexibility and constraint characteristics, the lower limb exoskeleton can adapt to various user movements and activities while maintaining stability and support. This design approach has the potential to enhance the usability and effectiveness of the exoskeleton in assisting individuals with lower limb impairments.

In this case, the standard base of the constraint-screw system for the sub-mechanism is:

$$S_a^r = \left\{ \boldsymbol{S}_{a1}^r = (1,0,0,0,0,0)^{\mathrm{T}} \right\} \tag{5.20}$$

which is a constraint force along $X$-axis. The standard base of the motion-screw system for the sub-mechanism can be obtained as follows:

$$\boldsymbol{S}_a = \begin{cases} \boldsymbol{S}_{a1} = (1,0,0,0,0,0)^{\mathrm{T}} \\ \boldsymbol{S}_{a2} = (0,1,0,0,0,0)^{\mathrm{T}} \\ \boldsymbol{S}_{a3} = (0,0,1,0,0,0)^{\mathrm{T}} \\ \boldsymbol{S}_{a4} = (0,0,0,0,1,0)^{\mathrm{T}} \\ \boldsymbol{S}_{a5} = (0,0,0,0,0,1)^{\mathrm{T}} \end{cases} \tag{5.21}$$

Then, three new screws $S'_{a1}$, $S'_{a2}$ and $S'_{a3}$ can be obtained using the linear combination of the screws $S_{a1}$, $S_{a2}$ and $S_{a3}$, which could be expressed as below:

$$^1S'_a = \begin{cases} \boldsymbol{S}'_{a1} = (l_1,m_1,n_1,0,0)^{\mathrm{T}} \\ \boldsymbol{S}'_{a2} = (l_2,m_2,n_2,0,0,0)^{\mathrm{T}} \\ \boldsymbol{S}'_{a3} = (l_3,m_3,n_3,0,0)^{\mathrm{T}} \end{cases} \tag{5.22}$$

which presents a $3R$ spherical sub-chain or a spherical joint. This chapter does not consider the spherical joint. Thus, the equation above can be used to construct a $3R$ spherical sub-chain. In addition, the linear combination of the screws $S_{a1}$, $S_{a4}$, and $S_{a5}$ yields a new screw $\boldsymbol{S}''_{a1}$. It should be noted that the screw $S_{a2}$ cannot be used to combine with the screw $S_{a4}$ to avoid the presence of helical pairs. Similarly, $S_{a3}$ cannot be used to combine with the screw $S_{a5}$. Then, the new screw $\boldsymbol{S}''_{a2}$ can be transformed by the linear combination of $S_{a2}$ and $S_{a5}$, and the new screw $\boldsymbol{S}''_{a3}$ can be obtained using the linear combination of $S_{a3}$ and $S_{a4}$, which could be obtained as below:

$$
{}^1S'_a = \begin{cases} \mathbf{S}'_{a1} = (l_1, m_1, n_1, 0, 0)^{\mathrm{T}} \\ \mathbf{S}'_{a2} = (l_2, m_2, n_2, 0, 0, 0)^{\mathrm{T}} \\ \mathbf{S}'_{a3} = (l_3, m_3, n_3, 0, 0)^{\mathrm{T}} \end{cases} \tag{5.23}
$$

which can be used to obtain new screws as follows

$$
{}^1\mathbf{S}'''_a = \begin{cases} \mathbf{S}''_a = (l'_1, m'_1, n'_1, 0, b'_1, c'_1)^{\mathrm{T}} \\ \mathbf{S}'''_{a2} = (l'_2, m'_2, n'_2, 0, b'_2, c'_2)^{\mathrm{T}} \\ \mathbf{S}'''_{a3} = \left(l'_3, m''_3, n'_3, 0, b'_3, c'_3\right)^{\mathrm{T}} \end{cases} \tag{5.24}
$$

which denotes three successive revolute joints whose axes do not pass through one common point. Namely, the sub-mechanism may consist of three successive revolute joints that are not a $3R$ spherical sub-chain. Further, it can be found that the screws $S'_{a2}$ and $S'_{a3}$ can form a $2R$ spherical sub-chain when the screw $S'_{a1}$ is transformed to the screw $S''_{a1}$ whose axis is along X-axis in the local coordinate frame $O_a - XYZ$. Similarly, the screws $S''_{a2}$ and $S''_{a3}$ can be treated as two successive revolute joints that are not a $2R$ spherical sub-chain. Besides, two screws $S'_{a4}$ and $S'_{a5}$ can be obtained after the linear combination of the screws $S_{a4}$ and $S_{a5}$, which could be expressed as:

$$
{}^2S'_a = \begin{cases} S'_{a4} = (0, 0, 0, 0, m_4, n_4)^{\mathrm{T}} \\ S'_{a5} = (0, 0, 0, 0, m_5, n_5)^{\mathrm{T}} \end{cases} \tag{5.25}
$$

The formulas above exhibits the two prismatic joints whose translational directions parallel the plane determined by $Y$- and $Z$-axes. The screws $S_{a4}$ and $S_{a5}$ can also be used to construct two screws $S''_{a4}$ and $S''_{a5}$ by the linear combination with the screw $S_{a2}$, as follows:

$$
{}^2\mathbf{S}''_a = \begin{cases} \mathbf{S}''_{a4} = (1, 0, 0, 0, b_4, c_4)^{\mathrm{T}} \\ \mathbf{S}''_{a5} = (1, 0, 0, 0, b_5, c_5)^{\mathrm{T}} \end{cases} \tag{5.26}
$$

These new screws can be applied to design two revolute joints whose axes are along $X$-axis. Besides, the formula above indicates that there is no prismatic joint in the sub-mechanism.

Table 5.3 The Enumeration of the Sub-mechanism Restricting Translational Mobility along $X$-axis.

| | Enumeration |
|---|---|
| Two prismatic pairs | ${}^{v1}P{}^{v2}P{}^{u1}R{}^{u2}R{}^{u3}R$, ${}^{u1}R{}^{u2}R{}^{u3}R{}^{v1}P{}^{v2}P$, ${}^{v1}P{}^{v2}P{}^{x}R{}^{u1}R{}^{u2}R$, ${}^{v1}R{}^{x}R{}^{v2}P{}^{u1}R{}^{u2}R$, ${}^{x}R{}^{v1}P{}^{v2}P{}^{u1}R{}^{u2}R$, ${}^{u1}R{}^{u2}R{}^{v1}P{}^{v2}P{}^{x}P$, ${}^{u1}R{}^{u2}R{}^{x}R{}^{v1}P{}^{v2}P$, ${}^{u1}R{}^{u2}R{}^{v1}P{}^{x}R{}^{v2}P$, ${}^{v1}P{}^{v2}P({}^{i}R{}^{j}R{}^{k}R)_N$, $({}^{i}R{}^{j}R{}^{k}R)_N^{v1}P{}^{v2}P$, ${}^{v1}P{}^{v2}P{}^{x}P({}^{i}R{}^{j}R)_N$, ${}^{v1}P{}^{x}R{}^{v2}P({}^{i}R{}^{j}R)_N$, ${}^{x}R{}^{v1}P{}^{v2}P({}^{i}R{}^{j}R)_N$, $({}^{i}R{}^{j}R)_N^{v1}P{}^{v2}P{}^{x}R$, $({}^{i}R{}^{j}R)_N^{x}R{}^{v1}P{}^{v2}P$, $({}^{i}R{}^{j}R)_N^{v1}P{}^{x}R{}^{v2}P$ |
| One prismatic pair | ${}^{v}P{}^{x}R{}^{u1}R{}^{u2}R{}^{u3}R$, ${}^{x}P{}^{v}P{}^{u1}R{}^{u2}R{}^{u3}R$, ${}^{u1}R{}^{u2}R{}^{u3}R{}^{x}P{}^{v}P$, ${}^{u1}R{}^{u2}R{}^{u3}R{}^{v}P{}^{x}R$, ${}^{v}P{}^{x}R{}^{x}R{}^{u1}R{}^{u2}R$, ${}^{u1}R{}^{u2}R{}^{x}R{}^{x}R{}^{v}P$, ${}^{x}R{}^{v}P{}^{x}R{}^{u1}R{}^{u2}R$, ${}^{x}R{}^{x}R{}^{v}P{}^{u1}R{}^{u2}R$, ${}^{u1}R{}^{u2}R{}^{x}R{}^{v}P{}^{x}R$, ${}^{u1}R{}^{u2}R{}^{v}P{}^{x}R{}^{x}R$, ${}^{v}P{}^{x}R{}^{x}P({}^{i}R{}^{j}R)_N$, ${}^{v1}P{}^{x}R({}^{i}R{}^{j}R{}^{k}R)_N$, ${}^{x}R{}^{v}P({}^{i}R{}^{j}R{}^{k}R)_N$, $({}^{i}R{}^{j}R{}^{k}R)_N^{x}R{}^{v}P$, $({}^{i}R{}^{j}R{}^{k}R)_N^{v}P{}^{x}R$, ${}^{v}P{}^{x}R{}^{x}R({}^{i}R{}^{j}R)_N$, $({}^{i}R{}^{j}R)_N^{x}R{}^{x}R{}^{v}P$, ${}^{x}R{}^{v}P{}^{x}R({}^{i}R{}^{j}R)_N$, ${}^{x}R{}^{x}R{}^{v}P({}^{i}R{}^{j}R)_N$, $({}^{i}R{}^{j}R)_N^{x}R{}^{v}P{}^{x}R$, $({}^{i}R{}^{j}R)_N^{v}P{}^{x}R{}^{x}R$ |
| No contain prismatic pair | ${}^{x}R{}^{x}R{}^{u1}R{}^{u2}R{}^{u3}R$, ${}^{u1}R{}^{u2}R{}^{u3}R{}^{x}R{}^{x}R$, ${}^{x}R{}^{x}R{}^{x}R{}^{u1}R{}^{u2}R$, ${}^{x}R{}^{x}R({}^{i}R{}^{j}R{}^{k}R)_N$, $({}^{i}R{}^{j}R{}^{k}R)_N^{x}R{}^{x}R$, ${}^{x}R{}^{x}R{}^{x}R({}^{i}R{}^{j}R)_N$, $({}^{i}R{}^{j}R)_N^{x}R{}^{x}R{}^{x}R$ |

It can also be found that the rotation axes of revolute joints are along $X$-axis, intersect at one common point or based on the values presented in the previious equations. Further, the number of the revolute joints whose axes are along $X$-axis cannot be greater than three because there are only three screws that can be used to obtain such revolute joints. Similarly, the number of other types of successive revolute joints are also not greater than three based on later equations.

Finally, the structural characteristics of the sub-mechanism in this case are:

(1) there must be two or three successive revolute joints, i.e.,$({}^{i}R{}^{j}R)_N$, $({}^{i}R{}^{j}R{}^{k}R)_N$, ${}^{u1}R{}^{u2}R$ or ${}^{u1}R{}^{u2}R{}^{u3}R$,

(2) the revolute joint(s), except those in the successive revolute joints, must be ${}^{i}R$,

(3) the prismatic joint(s) must be ${}^{v}P$ or ${}^{v1}P{}^{v2}P$.

An enumeration of such a sub-mechanisms is provided in Tab. 5.3 based on these structural characteristics. One example ${}^{u1}R{}^{u2}R{}^{x}R{}^{x}R{}^{x}R$ is presented in Fig. 5.25, which is denoted using $R2 - R6$. These sub-mechanism consists of two revolute joints that are a $2R$ spherical sub-chain and three successive revolute joints that are ${}^{x}R{}^{x}R{}^{x}R$.

## 5.3.4 Establishment of SRE Knee Rehabilitation Model

Based on the biomechanical configuration of the knee joint, a lower limb exoskeleton has been developed. However, conventional rigid robots often suffer from limitations such
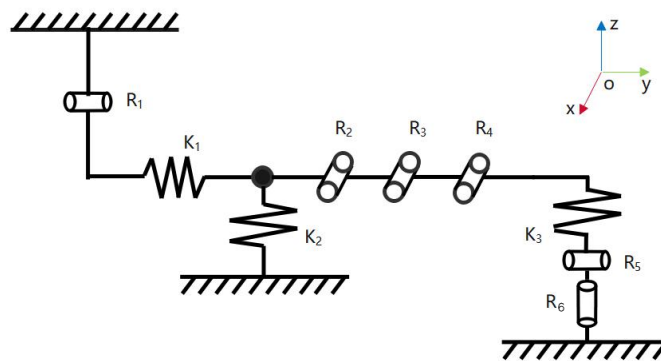
Fig. 5.25 The Sub-mechanism of the Lower Limb Exoskeleton Rehabilitation Robot

as large size, high energy consumption, and significant deviation from human-machine joint alignment. To overcome these challenges, integrating a soft structure with the rigid robot offers a promising solution. The proposed design approach involves a composite system that combines both rigid and soft structures to facilitate knee joint rehabilitation, as shown in Fig. 5.26.

By incorporating a soft structure into the exoskeleton design, several advantages can be achieved. Firstly, it helps to reduce the overall weight and bulkiness of the device, making it more comfortable for the user to wear and move around. Additionally, the soft structure allows for better alignment between the exoskeleton and the user's natural joint motion, enhancing the effectiveness and safety of the rehabilitation process.

In Figure 5.26, the illustration demonstrates how the composite system works together to support and assist the knee joint during rehabilitation exercises. The rigid components provide structural support and stability, while the soft structure offers flexibility and adaptability to accommodate natural joint movements. This combined approach aims to provide a more natural and intuitive rehabilitation experience for the user.
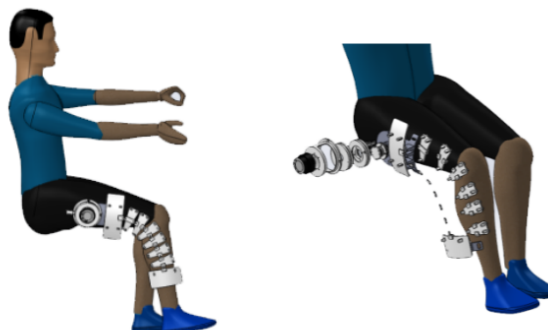


Fig. 5.26 Model of the Knee Rehabilitation Mechanism

The design shown in Fig. 5.26 illustrates a knee mechanism that can operate in both bent and stretched states. The first rotational joint is fixed to the thigh, while the final rotational joint is attached to the calf. A motor powers this system, which includes additional rotational joints positioned between the first and final joints. These intermediate joints are connected through rotating pairs. Two strings extend from the first rotational joint to the final one. It's worth noting that the motor is positioned flexibly to allow for minor slippage along the thigh.

The motor drives the strings, and the associated connecting segments are propelled accordingly. When the motor rotates clockwise, string 1 experiences tension while string 2 is released, resulting in leg bending. Conversely, when the motor rotates counterclockwise, string 2 undergoes tension while string 1 is released, straightening the leg.

In this mechanism, only the first and final rotational joints remain fixed, while the other rotational joints can flexibly rotate. The motor's slight slippage along the thigh accommodates the rehabilitation needs of stroke patients by training their muscles. Additionally, the kneecap can serve as a support since it is generally healthy. Therefore, the entire mechanism aids in knee joint rehabilitation, allowing the equipment to align with the actual rotation center of the patient's knee.

Furthermore, considering the different sizes of the thigh and calf, the length of each segment gradually decreases from the first to the final one. This gradual decrease in segment length allows for successful connection to the leg. Rotation pairs are utilized between the first rotational joint and the thigh, as well as between the final rotational joint and the calf, ensuring proper alignment and functionality throughout the exoskeleton system.

## 5.3.5   Innovation Design of the Clutch

As mentioned previously, when one string is driven by the motor, the other string needs to be released from the actuator and move with the leg simultaneously. Consequently, the velocity of the released string is variable and does not have a direct proportionality to the tightened string. This variability exists because the rotation center of the entire mechanism can change. In certain cases, the motion rate of the released string may exceed that of the tightened string. Therefore, it is crucial to employ a single motor to drive both strings.

Fig. 5.27 illustrates the initial unilateral design of the drive segment. Segment 1 (blue segment) is a shell with an inner gear that can freely rotate around segment 6, which represents the segment connected to the string mentioned earlier. Segment 2 (green segment) can also rotate around segment 6. Segment 3 (pink segment) is a fixed gear on segment 6. Segments 4 and 5 serve as connecting links. Segment 6 (grey segment) represents the drive shaft. When the drive shaft rotates counterclockwise, segments 4

and 5 rotate along with segment 3. However, due to the collision between segment 5 and segment 2, segment 2 is compelled to rotate while segment 1 remains in a completely relaxed state. The same logic applies when the actuator rotates in the opposite direction. In such scenarios, the driver can consist of two identical segments positioned in opposite directions. This arrangement enables the tightening of the string on one side while the string on the other side can be fully released.
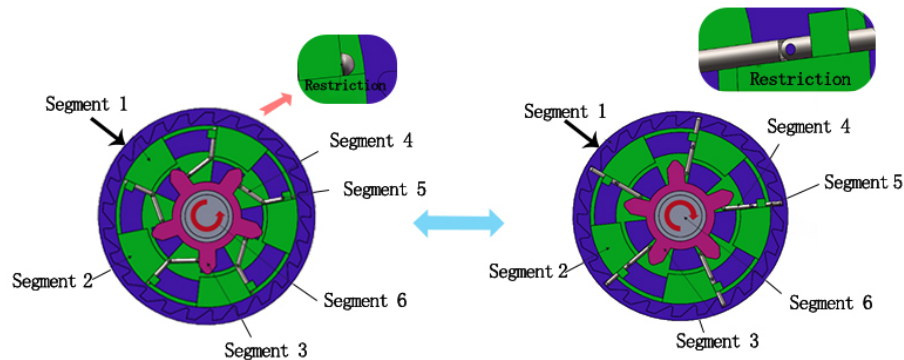


Fig. 5.27 Design of the Clutch System

### 5.3.6   Configuration with Self-alignment Elements

As mentioned earlier, the knee joint possesses multiple degrees of freedom in its motion. Therefore, it is essential to accurately identify and track the rotation center of the knee joint during the design phase. Currently, clinicians typically account for average joint changes by providing patients with uniform intervals for active linear motion on each degree of freedom during long-term rehabilitation, based on the starting and ending states. However, researchers have discovered that the six degrees of freedom exhibited by the knee during motion are nonlinear. In such cases, passive tracking of the exoskeleton has proven to be more effective than active tracking.

To construct adaptive exoskeletons, a thorough understanding of how exoskeletons differ from human limbs is required. Fig. 5.28 illustrates points A and B, which are connected to the exoskeleton and lower limb respectively. During bending experiments, changes in the rotation angle cause the rotation center of both the exoskeleton and the knee to shift from their original positions. It is crucial to continuously monitor these changes in the position of the rotation center as they significantly impact the functionality of the exoskeleton.

In other words, every time the angle changes, the rotation centre of the knee O produces a position microvariable in the three translation directions, including $dl$ (along the $x$-axis), $dh$ (along the $z$-axis) and $dw$ (along the $y$-axis). Then, the angles change accordingly,

Fig. 5.28 Establishment of the Knee Joint Deviation System

including angle $\alpha$ (rotates about the *x*-axis), angle $\theta$ (rotates about the z-axis) and angle $\omega$ (rotates about the y-axis). To eliminate the influence caused by the deviation between these positions and angles, in this paper, a solution is proposed, as shown in Fig. 5.29. The PPR structure combines two passive pairs and the passive rotation pair mentioned above, which can successfully solve the problem of self-alignment.
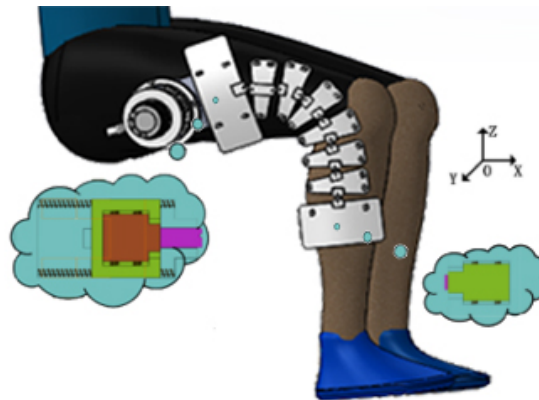


Fig. 5.29 Self-alignment SRE Model

## 5.4 Design and Modelling of the Hip Joint Rehabilitation Mechanism

The hip joint exoskeleton with active-passive interaction mechanism is a collaborative robot primarily utilized for lower limb stroke rehabilitation patients. These patients often experience impaired or missing movement functions in areas such as the ankle, knee, and hip joints during their post-stroke rehabilitation stage. As a result, the hip joint exoskeleton

plays a vital role in supporting the rehabilitation process by providing assistance in terms of lower limb movement abilities and energy supply.

To better serve stroke rehabilitation patients, it is essential to conduct comprehensive studies on the motion mechanics and biological characteristics of the human hip joint and utilize them as the foundation for designing each joint's structure and control system. The overall structural design of the hip joint holds particular significance, particularly in lower limb exoskeleton design. Therefore, this chapter proposes a holistic structural scheme for the hip joint based on the motion mechanics and biological characteristics observed during human walking. This scheme incorporates an active-passive interaction control mechanism that combines electric motors and air springs. It features a double degree of freedom motion structure for hip joint lateral and anterior tilting, as well as an air spring-based energy storage and release device. The feasibility of this design was verified through multibody kinematics analysis, confirming the successful realization of the hip joint exoskeleton with active-passive interaction mechanism.

In conclusion, the hip joint exoskeleton with active-passive interaction mechanism is primarily intended for lower limb stroke rehabilitation patients. These patients require substantial support throughout the rehabilitation process, and the hip joint exoskeleton plays a crucial role in enhancing lower limb movement abilities and facilitating energy supply. Therefore, when designing lower limb exoskeletons, careful attention must be given to the structural design of the hip joint and the development of an effective control system, necessitating in-depth research on the motion mechanics and biological characteristics of the hip joint to ensure the construction of a robust and reliable system.

## 5.4.1 Muscle Structure and Design Principles of the Hip Joint Rehabilitation Mechanism

The hip joint rehabilitation mechanism involves various key muscles that play essential roles in the recovery process. These muscles include the gluteus maximus for hip extension, gluteus medius and minimus for abduction and stability, hip flexors (iliopsoas) for flexion, adductors for adduction, external rotators for external rotation, quadriceps and hamstrings for overall function, and core muscles for stability. Through targeted exercises that engage these specific muscles, rehabilitation programs aim to restore strength, stability, and function in the hip joint.

When designing a hip joint rehabilitation structure, several factors should be considered. Individual needs should be taken into account, ensuring that the program is tailored to the specific circumstances of each person. Early rehabilitation should focus on reducing pain and improving range of motion. Progressive training should be implemented, gradually increasing the intensity and complexity of exercises to promote gradual recovery. Balance

and core strengthening exercises should be incorporated to enhance stability and prevent future injuries. It is crucial to commit to the long-term nature of the rehabilitation program, as consistent exercise and activity are necessary for optimal results. Regular monitoring and adjustments should be made as needed to track progress and ensure the effectiveness and safety of the program.

Given these considerations, a 2-Dof hip rehabilitation mechanism will be introduced in the following content.

## 5.4.2 Establishment of a 2-Dof Hip Rehabilitation Model

The hip joint is indeed a vital joint in the human body, serving a critical role in activities such as walking, running, and jumping. Its range of motion encompasses flexion-extension, abduction-adduction, and internal-external rotation, with flexion-extension and abduction-adduction being the most prevalent movements. The coordinated motion of the hip and knee joints enables efficient step-taking and facilitates balance during locomotion for individuals with regular gait patterns, as depicted in Fig. 5.30.
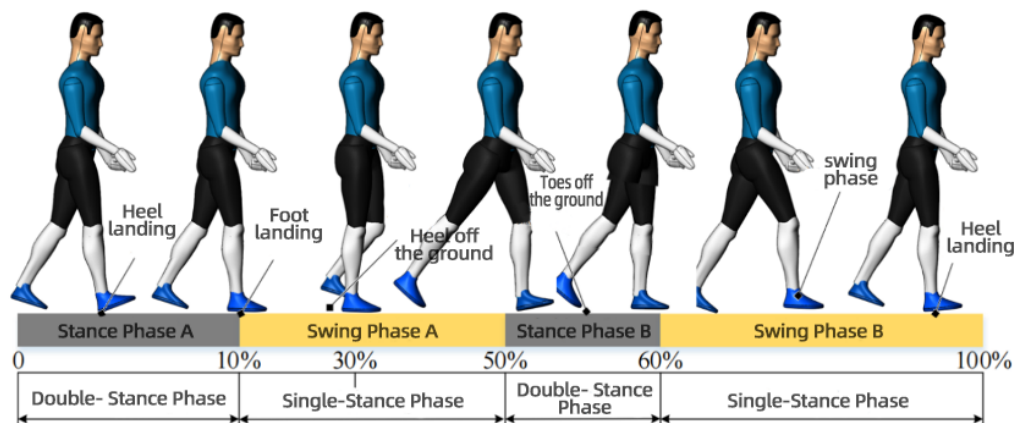


Fig. 5.30 Diagram of One Gait-Cycle

In addition to the mentioned motions, the hip joint also contributes significantly to stability and power generation during various physical activities. It acts as a link between the trunk and the lower limb, transmitting forces and providing stability to the body. The hip muscles, including the gluteal muscles and hip flexors, play a crucial role in generating power and maintaining stability during gait.

Understanding the biomechanics of the hip joint and its coordination with other lower limb joints is essential for diagnosing and rehabilitating gait abnormalities. By analyzing the range of motion and motion patterns of the hip joint, healthcare professionals can gain insights into potential issues and develop targeted interventions to improve gait performance and overall mobility.

144

Recent research has focused on developing wearable hip exoskeletons to assist, augment, or rehabilitate human hip function. However, the 3-DOF structure of the hip joint makes designing a wearable exoskeleton that mimics natural hip joint movement difficult. This study's two-DOF hip exoskeleton equipped with an active-passive interaction mechanism simplifies the hip gait simulation while being lightweight and easy to control.

The active-passive interaction mechanism includes a motor-driven actuator and a passive spring element that assists the user's hip joint movement, reducing the control system's complexity and providing a better and more natural walking experience. The resulting exoskeleton has the potential to improve the quality of life for individuals with hip-related conditions by assisting, augmenting, or rehabilitating their hip function, as shown in Fig. 5.31.
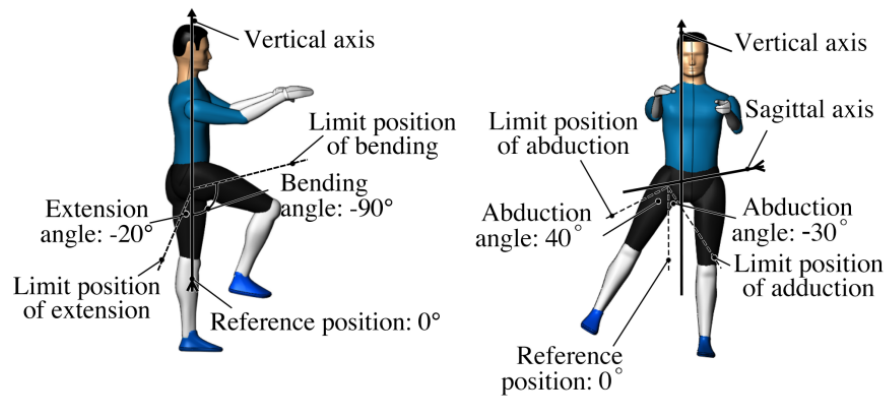


Fig. 5.31 The Rotatonal Range of the 2-Dof Motion Process

To achieve the flexion-extension and abduction-adduction movements of the hip joint, a two-degree-of-freedom rotary mechanism was built to serve as an information acquisition platform for hip gait simulation. This simplified structure enables the execution end to possess a simple two-dimensional rotation feature represented by $\theta_1$ and $\theta_2$.

With an overall degree of freedom of 2 and a total number of support chains of 3, the mechanism's active chain number can be obtained using the mechanism synthesis equation. The active chain number for this mechanism is:

$$
\begin{cases}
F_D - \sum_{i=1}^{n} q_i = 0 \\
N = F_D - \sum_{i=1}^{n} (q_i - 1) + p \\
n \leq F_D^D \\
q_i \leq F_D
\end{cases} \tag{5.27}
$$

Due to the negative number of active chains, the mechanism cannot maintain a fixed pose without external forces or constraints. However, this is not a problem in the context of hip gait simulation, as the mechanism's role is to serve as an information acquisition platform rather than a static pose holding device.

Where, $n$ is the number of active chains, $q_i$ is the number of the driving motions on each active chain and $p$ is the number of passive chains.

By comprehensively considering the structural configuration based on the mechanism synthesis equation, a series of hip joint rotation structures with the desired degrees of freedom were obtained for the hip joint gait simulator. As an externally attached structure for linking the human torso to the lower limbs during movement, the hip exoskeleton not only helps to facilitate hip joint movements but also assists in spreading the weight of the human torso. This study also investigates the application of active and passive constrained chains for hip joint gait simulator design. This approach allows the simulation of femur length and enhances the mechanism's stiffness characteristics in the design process.

Based on the principles of the biomimetic hip joint motion, the hip gait simulator should adhere to the following design principles:

The thigh bone length can be considered as a fixed-length rod. The degree of freedom of the mechanism that attaches to the hip joint outside of the human body, through which the torso is linked to the thigh bone, should be set to 2. This means that the mechanism possesses spatially free and rotational characteristics.

Applying these principles ensures that the hip gait simulator replicates the natural motion of the human hip joint, allowing for more accurate evaluation of the performance of hip exoskeletons for rehabilitation and support purposes. Simulating the hip joint under various conditions can help researchers better understand the kinematics and kinetics of the hip joint and improve the design of hip exoskeletons as well as other assistive devices.

Based on the aforementioned design principles and the information collected by the hip gait simulator, a structure with a series connection that possesses two degrees of freedom and active-passive interactive functionality was determined as the optimal configuration for the hip exoskeleton, as shown in Fig. 5.32.

The series connection of two degrees of freedom and active-passive interaction function consists of the trunk connecting seat, thigh connecting strut, adduction-abduction rotational joint, passive energy storage device for adduction and abduction, flexion-extension rotational joint, and passive energy storage device for flexion and extension. The mechanism is symmetrical on both sides.

The two thigh connecting struts are connected to the trunk connecting seat through two series-connected rotational joints, with one rotational joint rotating along the sagittal axis of the human body and the other rotating horizontally. Passive energy storage devices are
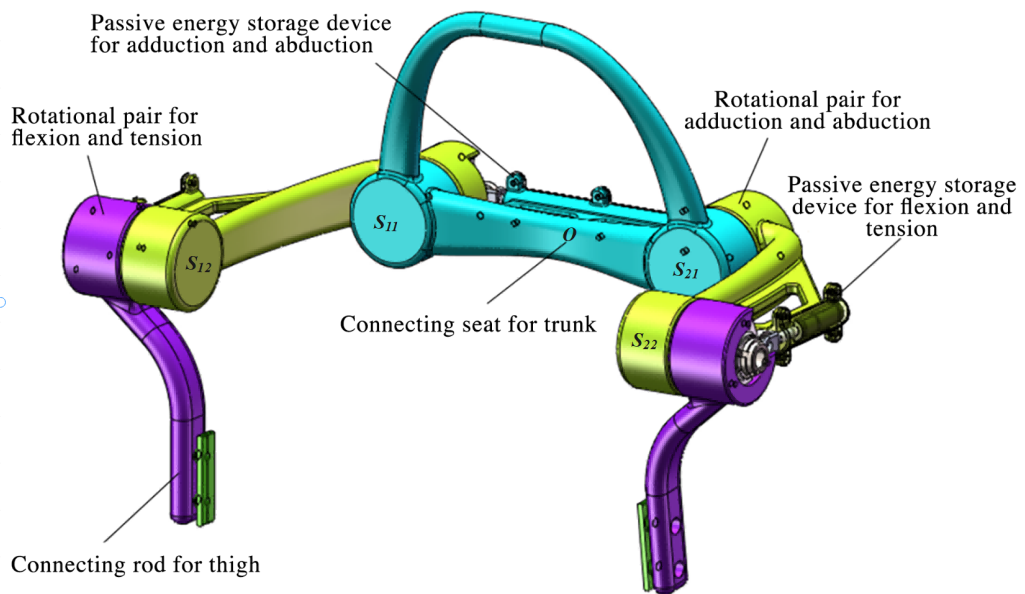
Fig. 5.32 The Novel Design of a 2-Dof Hip Joint Rehabilitation Exoskeleton Mechanism

connected in parallel between each active motor-driven rotational joint and its respective series-connected rotational joint.

The active-passive interaction function allows for controlled movement assistance in multiple directions and enhances the stability and efficiency of the hip exoskeleton. The symmetrical design of the mechanism ensures balanced weight distribution and optimal movement support for the wearer. Advanced materials and manufacturing techniques can further improve the functionality and usability of the hip exoskeleton.

The fixed rod $S_{11} - O - S_{21}$ has the same length as the distance between the two lower limbs of the human body. The rotational joints $S_{11}$ and $S_{21}$ are positioned off to the posterior side of the hip joint center on the left and right sides, respectively. They mainly assist the human body in completing adduction-abduction movements of the hip joint and lower limb during rehabilitation training. The rotational joints $S_{12}$ and $S_{22}$ are located off to the lateral side of the body center on the left and right sides of the hip joint center, respectively. They mainly assist the human body in completing flexion-extension movements of the hip joint and lower limb during rehabilitation training. This ensures that the rotational joints do not shift position with respect to the body during movement when their centers are offset from the hip joint center.

The rotational joints $S_{12}$ and $S_{22}$ are connected to the thigh connecting struts of the end-effector structure, enabling the exoskeleton to provide bidirectional assistance for hip joint rehabilitation. With these components, the new hip joint rehabilitation mechanism can effectively cater to the needs of patients with different rehabilitation requirements, supporting bio-mechanically consistent and safe training, as shown in Fig. 5.33.

(a) Abduction-adduction Motion      (b) Flexion-extension Motion
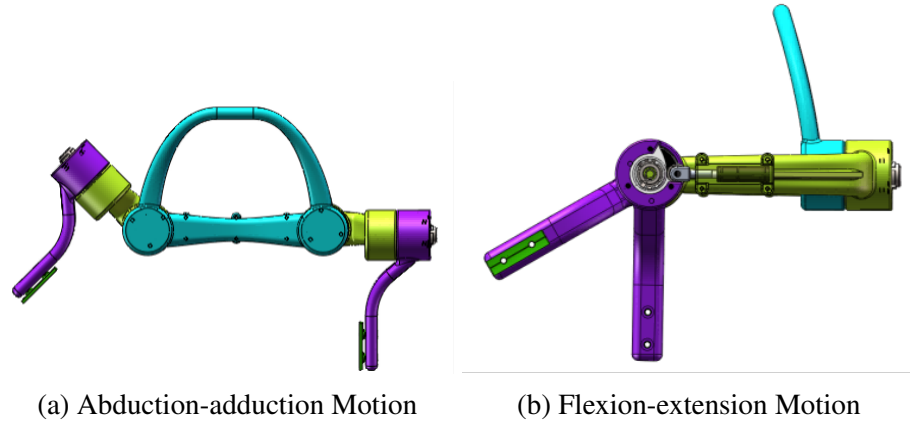
Fig. 5.33 Two Motions of the Hip Joint Exoskeleton

### 5.4.3 Motion Performance Verification of the Hip Joint Mechanism

Based on the mechanism motion schematic diagram shown above, the end-effector motion characteristics were verified using a helix principle. The helical movements of the rotational joints $S_{11}$ and $S_{12}$ are as follows:

$$\begin{cases} S_{11} = [0\ 1\ 0;0\ 0\ 1]^T \\ S_{12} = [1\ 0\ 0;0\ 0\ 0]^T \end{cases} \tag{5.28}$$

The constrained screws for rotational joints $S_{11}$ and $S_{12}$ were obtained as follows:

$$\begin{cases} S_{11}^r = \left[\frac{(n_2-1)}{l_2}\ 0\ 1;0\ -1\ 0\right]^T \\ S_{12}^r = [0\ 1\ 0;0\ 0\ 1/n_1]^T \end{cases} \tag{5.29}$$

The, the constrained screws for rotational joints $S_{11}$ and $S_{12}$ were obtained as follows:

$$\begin{cases} S_{21} = [1\ 0\ 0;0\ 0\ 0]^T \\ S_{22} = [0\ 0\ 0;0\ 0\ 1]^T \end{cases} \tag{5.30}$$

Thus, based on the constraint force screws of passive and active chains, the motion screws of the moving platform was obtained as follows:

$$S_m = \begin{cases} S_{m1} = [1\ 0\ 0; 0\ 0\ 0]^T \\ S_{m2} = [0\ 1\ 0; 0\ 0\ 1]^T \end{cases} \tag{5.31}$$

The results showed that the end-effector of the 2-degree-of-freedom serial structure exhibited rotational capabilities around both the sagittal and horizontal axes. This confirms the effectiveness of the mechanism design and its potential for implementing a variety of rehabilitation exercises to aid in the recovery of patients with hip joint injuries or disabilities. Further research and development are required to fully explore the potential of this mechanism and optimize its performance.

### 5.4.4 Configuration of the Energy Storage System

According to GB-T 17245-2004 Inertial Parameters of Human Body for Adults, using Chinese adult males as the reference data, the standard weight for males is:

$$W = (H - 80) * 0.7 \tag{5.32}$$

Where, In the equation, $W$ represents weight in kilograms and $H$ represents height in centimeters.

It is important to note that this standard weight is simply a reference value and may vary depending on individual factors such as height, body composition, and level of physical activity. Therefore, it should be used as a general guideline and not as a definitive indicator of health or fitness. It is recommended to consult with a healthcare professional to determine an appropriate weight range based on your specific needs and goals. For example, for a male with a height of $185cm$, the standard weight is $73.5kg$. Based on the relative mass distribution of different parts of the body shown in Tab. 5.4, the weight of a single lower limb is the sum of the relative masses of the thigh, calf, and foot, which is $14.19\% + 3.67\% + 1.48\% = 19.34\%$.

Therefore, the total weight of a single lower limb of an adult male with a height of $185cm$ is:

$$W_l = W * 19.34\% = 73.5 * 19.34\% = 14.21\text{kg} \tag{5.33}$$

The human lower limb is generally in a flexed position during movement, as shown in the following Fig. 5.34.

Table 5.4 Relative Mass Distribution of Each Part of the Human Body

| Part | Gender | Relative Mass |
|------|--------|---------------|
| Head | Male | 8.62% |
| | Female | 8.20% |
| Upper Trunk | Male | 16.82% |
| | Female | 16.35% |
| Lower Trunk | Male | 27.23% |
| | Female | 27.48% |
| Thigh | Male | 14.19% |
| | Female | 14.10% |
| Calf | Male | 3.67% |
| | Female | 4.43% |
| Upper Arm | Male | 2.43% |
| | Female | 2.66% |
| Forearm | Male | 1.25% |
| | Female | 1.14% |
| Hand | Male | 0.64% |
| | Female | 0.42% |
| foot | Male | 1.48% |
| | Female | 1.24% |



Fig. 5.34 Flexed Positionn during Movement

At this time, the center of gravity of a single lower limb is generally located about $100 - 150mm$ behind the knee joint, assuming that the length of an adult male's thigh is $400mm$, the length of the lower limb moment arm is $250mm$.

The calculation of the overall moment of force of a single lower limb in a flexed state is as follows:

$$\text{T} = W_x * g * l = 14.21 * 9.8 * 0.25 = 35N \cdot m \tag{5.34}$$

### 5.4.5 Active Drive Structure of the Hip Joint

Hence, for effective active exercise training during the rehabilitation of stroke patients using hip exoskeletons, it is recommended to achieve a peak motor drive torque of $30 - 40Nm$ to provide optimal assistance. To meet this requirement, a direct output form utilizing frameless motors and harmonic reducers as the active driving structure can be employed. This compact and high-energy density structure is particularly suitable for the motion structure of the hip joint. By incorporating an appropriate exoskeleton design, stroke patients can receive the necessary torque to perform a range of exercises, aiding in the restoration of their mobility and overall quality of life.

The frameless motor utilized in this design adopts a customized internal rotor structure, where the external stator consists of a winding and control circuit, while the internal rotor is composed of neodymium-iron-boron permanent magnet material. The maximum outer diameter of the stator can be determined based on the maximum outer diameter of the harmonic reducer. Compared to traditional motors, this frameless motor structure offers the advantage of being more compact and having a higher power density, making it well-suited for integration within the hip joint's motion structure. Moreover, the use of neodymium-iron-boron permanent magnets ensures a high magnetic field strength and excellent performance even at elevated temperatures, guaranteeing stable and reliable operation of the exoskeleton during rehabilitation training. For a visual representation, please refer to Fig. 5.35 depicting the frameless motor configuration.



Fig. 5.35 Frameless Motor [94]

The precision harmonic reducer, on the other hand, is a type of harmonic drive that applies metal elasticity mechanics for its operation. It consists of only three basic components-the wave generator, flex spline, and circular spline (though some variations may comprise four basic components with similar transmission principles). This minimalist design approach and the use of high-strength materials in construction make precision harmonic reducers highly reliable and effective in transmitting torque and motion with minimal backlash, making them a popular choice for robotics and other high-performance motion control applications. The flexible spline component also ensures efficient power transfer between the motor and output shaft, while the compact structure enables easy integration into various devices, including exoskeleton systems for hip rehabilitation, as shown in the following Fig. 5.36.



Fig. 5.36 Harmonic Reducer [94]

The wave generator, a key component of the harmonic reducer, features an elliptical cam with a thin-walled ball bearing embedded in its outer circumference. The inner race of the bearing is fixed to the cam, while the outer race undergoes elastic deformation through rolling contact with the balls. This component is usually mounted on the input shaft and converts rotary motion into a wave-like motion that propagates along the flex spline, resulting in highly precise and efficient power transmission. The carefully designed geometry of the cam ensures accurate control of the deformation of the flex spline, enabling smooth and consistent operation of the exoskeleton's hip joint during rehabilitation training.

The flex spline, another key component of the harmonic reducer, is a thin-walled, metallic elastic part with external teeth that engage with the wave generator's elliptical cam. This component is typically mounted on the output shaft and transmits the wave-like motion generated by the wave generator to the circular spline, resulting in highly efficient torque and motion transfer. Currently, most harmonic reducers use $40Cr$ alloy steel for the flex spline, with $40CrMoNiA$, $40CrA$, $30CrMoNiA$, $38Cr2Mo2VA$, and $40CrMoNiA$ being the most commonly used materials. Among these, $40CrMoNiA$ is considered the most suitable material for the flex spline due to its excellent elasticity, high strength, and resistance to wear and tear. As such, most harmonic reducer manufacturers prefer to use $40CrMoNiA$ to manufacture this component.

The circular spline, the final component of the harmonic reducer, is a rigid, ring-shaped part with internal teeth that engage with the external teeth of the flex spline, as shown in the following Fig. 5.37. Unlike the flex spline, the circular spline has two fewer teeth, resulting in a reduced number of contact points and therefore less friction and backlash. This component is typically fixed within the housing of the harmonic reducer and transfers the torque and motion generated by the flex spline to the output shaft.

The flex spline is designed to be bent into an elliptical shape by the wave generator. As a result, the flex spline engages with the circular spline and its teeth along the long axis while being completely disengaged from the gears along the short axis. By fixing the circular spline and rotating the wave generator clockwise, the flex spline undergoes elastic deformation and the position of the gears that engage with the circular spline move sequentially. After the wave generator has rotated 180 degrees in the clockwise direction, the flex spline moves only one tooth in the counterclockwise direction. With each full rotation of the wave generator (360 degrees) and the two additional teeth on the circular spline, the flex spline moves two teeth in the counterclockwise direction. This continuous motion of the wave generator allows the flex spline to slowly rotate in the opposite direction to the wave generator relative to the circular spline. This precise mechanism enables the robotic exoskeleton's hip joint to move smoothly and steadily during rehabilitation training, promoting optimal patient outcomes.
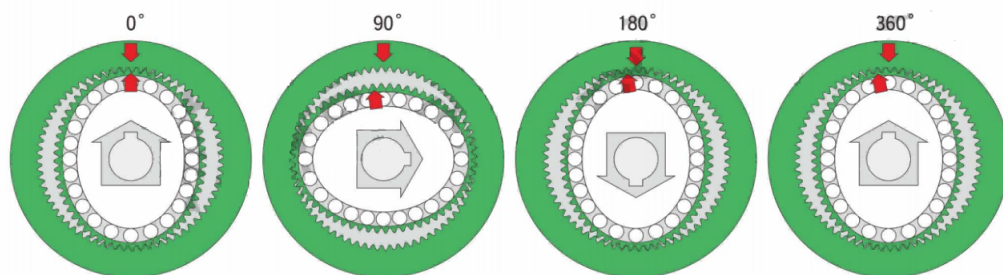


Fig. 5.37 The Four Phases of a Customized Frameless Motor [31]

### 5.4.6 Passive Elastic Structure of the Hip Joint

According to the active driving structure of the frameless torque motor and harmonic reducer mentioned above, this design incorporates a cam at the output end of the rotary shaft and a nitrogen gas spring as a passive energy storage structure at the motion plane of the cam, as shown in the following Fig. 5.38.

A nitrogen gas spring, also known as a gas strut or gas spring, is a mechanical component that utilizes pressurized gas (nitrogen: non-flammable, non-toxic, and odorless) in a sealed cylinder as a spring. The principle behind the nitrogen gas spring's operation
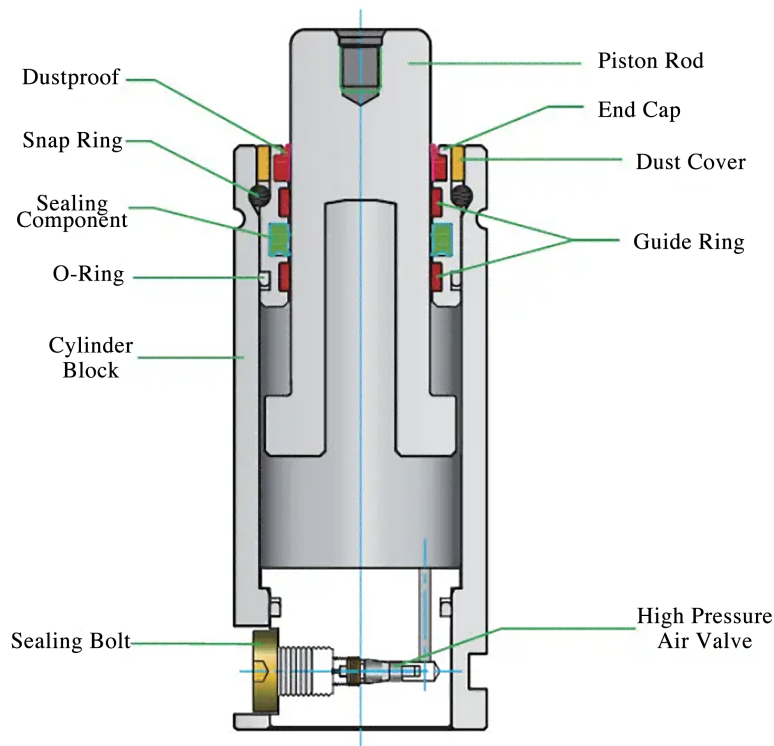
Fig. 5.38 The Structure of a Nitrogen Gas Spring [154]

involves maintaining equal pressure on both sides of the piston through the holes in the piston, which creates a pressure difference between the two ends and generates a continuous outward force. A small amount of oil is injected into the cylinder to lubricate, seal and provide damping.

Compared to traditional metal springs, nitrogen gas springs have several advantages. They have an initial force, and can provide a relatively large counterforce at the starting compression position, and the force throughout the entire journey remains relatively constant. Nitrogen gas springs have a compact structure, are small and lightweight, yet they can achieve a high level of elasticity. Additionally, they can be designed to have various functions, such as gentle stop, arbitrary stop, controllability, compression, stretching, etc.

Incorporating a nitrogen gas spring as a passive energy storage structure in this system can absorb shock and vibration produced during operation, reduce stress on the system's components, operate stably and efficiently, and enhance its overall durability and reliability, the effect of a nitrogen gas spring would be shown in below Fig. 5.39.

For the adduction-abduction movement of the hip joint, the lower limb of the human body moves from an upright position to an outwardly extended posture during the adduction-abduction movement, as shown in the Fig. 5.40. In (a), the hip joint is in an
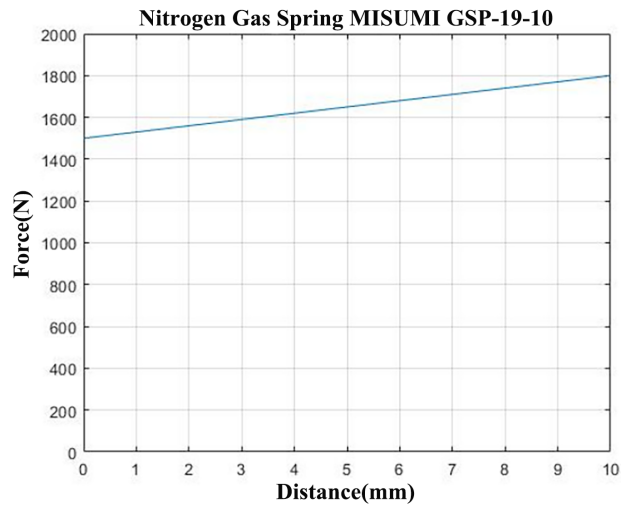
Fig. 5.39 Elastic Effect of the Nitrogen Gas Spring

upright position, and in (c), the relative positions of the cam and nitrogen spring are shown when the hip joint is in an upright position. In (b), the hip joint is in an outwardly extended position, and in (d), the relative positions of the cam and nitrogen spring are shown when the hip joint is in an outwardly extended position. This mechanism allows for smooth and controlled adduction-abduction movement of the hip joint.
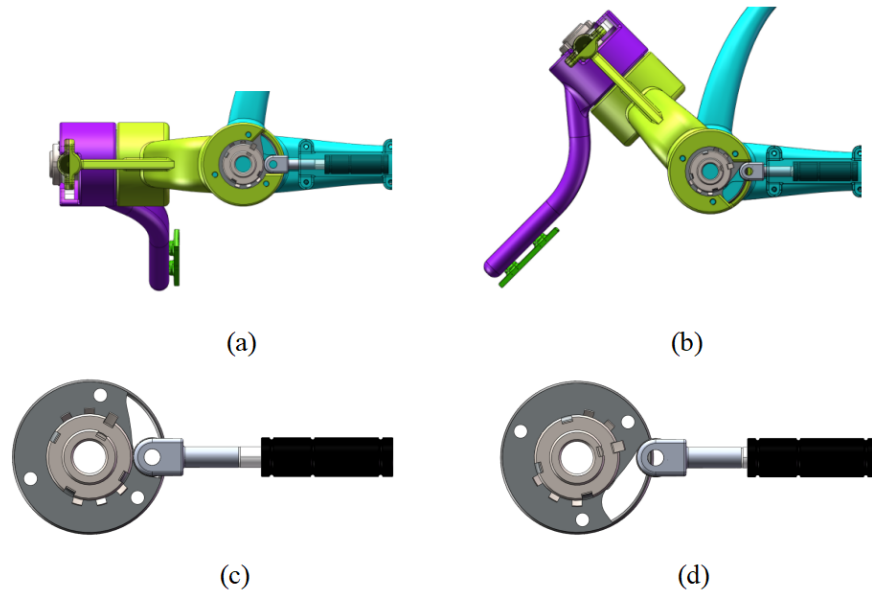


Fig. 5.40 Relative Position of the Cam and Nitrogen Spring in Adduction-abduction Motion

The adduction-abduction range of motion of the human hip joint is generally not greater than 45 degrees. Therefore, the cam at the adduction-abduction joint of this design is designed to have a range of motion of 0-45 degrees. At the 0 degree position, which is the point where the hip joint is in an upright position, the body is in a balanced and relaxed

state. Therefore, at the 0 degree position, the nitrogen spring push direction is designed to pass through the axis of rotation of the cam, and the force arm of the nitrogen spring acting on the cam is zero, resulting in zero torque. At the 45 degree position, which is the point where the hip joint is in an outwardly extended position, the lower limb of the human body is actively decelerated by a motor and thus tensed. Therefore, at the 45 degree position, the nitrogen spring push direction is designed with a certain offset from the axis of rotation of the cam, resulting in a torque produced by the nitrogen spring acting on the cam.

As shown in the Fig. 5.41, point $O_{c1}$ is the center of the cam, and point $O_{c2}$ is the center of the working surface arc of the cam. When the nitrogen spring is at a certain point $X_{na}$ between the two limit points $X_{n1}$ and $X_{n2}$, the mathematical relationship of the force arm $O_{c1}H_a$ is as follows:
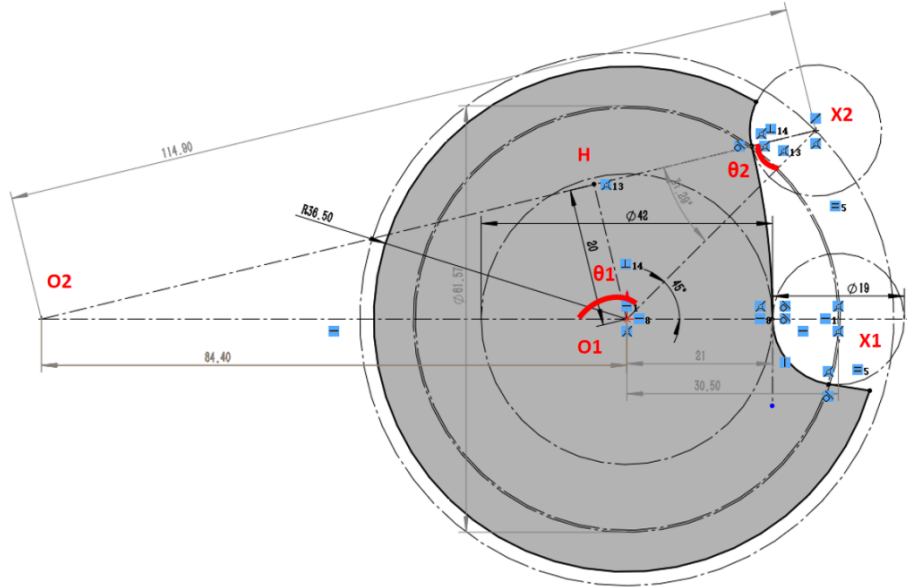


Fig. 5.41 Rotational Range of the Cam during the Adduction-abduction Movement

$$\begin{cases} O_{c1}H_a = O_{c1}X_{na} * sin\theta2_a = O_{c1}O_{c2} * \sin\left(180 - \theta1_a - \theta2_a\right) \\ \frac{O_{c1}O_{c2}}{\sin\theta2_a} = \frac{O_{c2}X_{na}}{\sin\theta1_a} \\ O_{c2}X_{na} = O_{c2}X_1 = O_{c2}X_2 \end{cases} \qquad (5.35)$$

Based on the above figure, the relationship between the rotation angle of the adduction-abduction cam and the force arm of the nitrogen spring can be obtained. By combining the relationship formula between the stroke and thrust of the nitrogen spring, the relationship graph can be obtained using MATLAB, as shown in below Fig. 5.42 and Fig. 5.43.

When performing hip Flexion-Extension movements, the human lower limb moves from an upright position to a curled position with the thighs lifted forward, as shown in
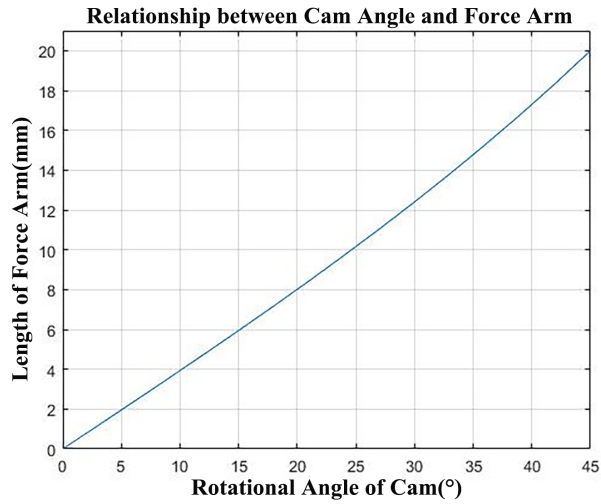
Fig. 5.42 Relationship between Cam Angle and Force Arm in Adduction-abduction State
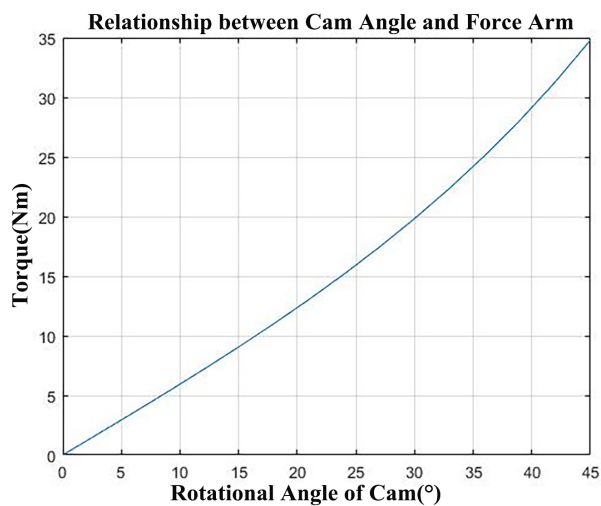


Fig. 5.43 Relationship between Cam Angle and Torque in Adduction-abduction State

Fig. 5.44. Panel (a) illustrates the hip joint in an upright position, with its corresponding panel (c) showing the relative position of the cam and nitrogen spring when the hip joint is upright. Panel (b) shows the hip joint in a flexed position, with its corresponding panel (d) displaying the relative position of the cam and nitrogen spring when the hip joint is flexed.



(a)          (b)

(c)          (d)
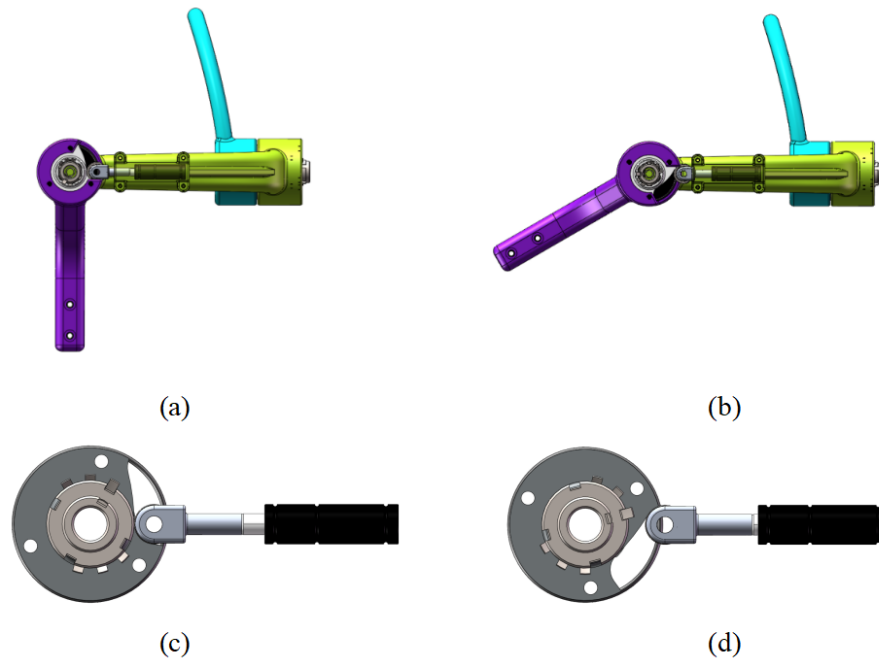
Fig. 5.44 Relative Position of the Cam and Nitrogen Spring in Flexion-extension Motion

The range of motion for hip flexion and extension movements in the human body is generally not greater than 60 degrees. Therefore, the cam at the adduction-abduction joint of the hip joint in this design is designed to have a motion range of 0 60 degrees. At the 0 degree position, which corresponds to the point on the cam, the hip joint is in an upright position, which is a state of balance and relaxation for the human body. Therefore, at the 0 degree position, the direction of thrust from the nitrogen spring is designed to pass through the axis of rotation of the cam, and the force arm of the nitrogen spring acting on the cam is zero, resulting in zero torque. At the 60 degree position, which corresponds to the point on the cam, the hip joint is in a state where the lower limb is actively decelerated by the motor and tightened. Therefore, at the 60 degree position, the direction of thrust from the nitrogen spring is designed to be offset from the axis of rotation of the cam, resulting in a torque on the cam from the nitrogen spring.

As shown in the Fig. 5.45, point $O_{c1}$ is the center of the cam, and point $O_{c2}$ is the center of the working surface arc of the cam. When the nitrogen spring is at a certain point $X_{na}$ between the two limit points $X_{n1}$ and $X_{n2}$, the mathematical relationship of the force arm $O_{c1}H_a$ is as follows:
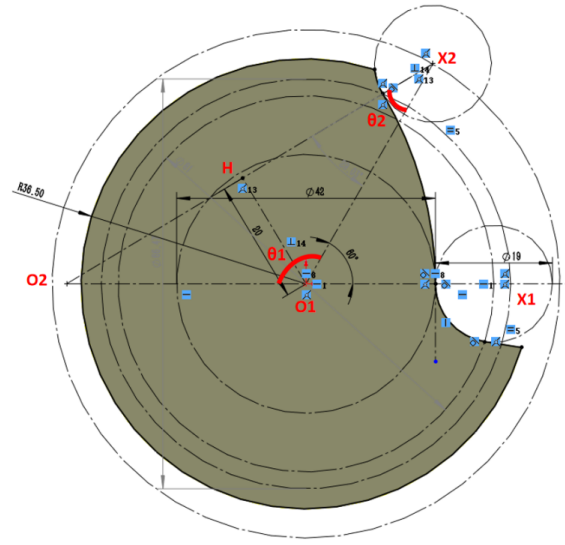
Fig. 5.45 Rotational Range of the Cam during the Flexion-extension Movement

$$\begin{cases} O_{c1}H_a = O_{c1}X_{na} * sin\theta2_a = O_{c1}O_{c2} * \sin\left(180 - \theta1_a - \theta2_a\right) \\ \frac{O_{c1}O_{c2}}{\sin\theta2_a} = \frac{O_{c2}X_{na}}{\sin\theta1_a} \\ O_{c2}X_{na} = O_{c2}X_1 = O_{c2}X_2 \end{cases} \tag{5.36}$$

Based on the above figure, the relationship between the rotation angle of the adduction-abduction cam and the force arm of the nitrogen spring can be obtained. By combining the relationship formula between the stroke and thrust of the nitrogen spring, the relationship graph can be obtained using MATLAB, as shown in below Fig. 5.46 and Fig. 5.47.
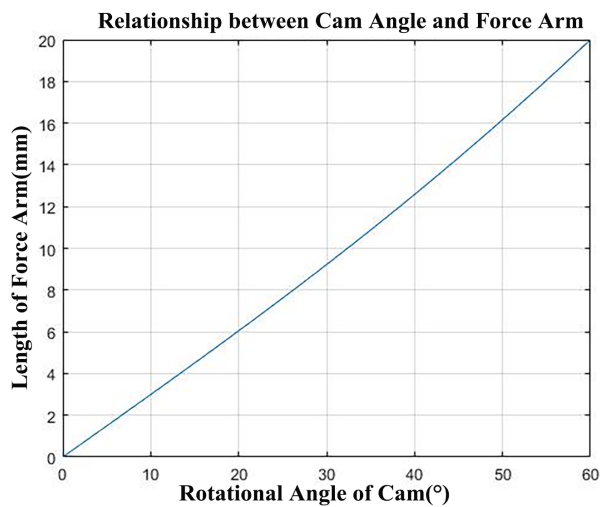


Fig. 5.46 Relationship between Cam Angle and Force Arm in Flexion-extension State
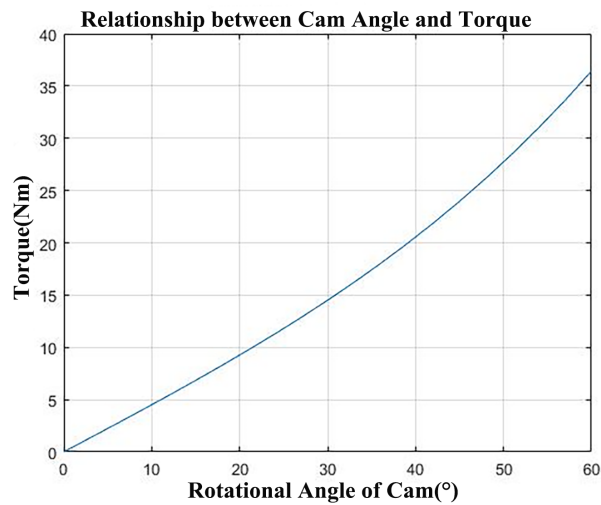
Fig. 5.47 Relationship between Cam Angle and Torque in Flexion-extension State

## 5.5 Conclusions

In summary, this chapter focuses on the structural design of the ankle joint, knee joint, and hip joint, which together constitute the lower limb rehabilitation exoskeleton. The designs aim to enable both active and passive movements of these joints. The primary goal of these designs is to assist stroke survivors in regaining practical rehabilitation functions while minimizing the risk of secondary injuries.

The structural design of each joint takes into consideration the specific requirements of stroke patients, including their range of motion, stability, and balance during various rehabilitation activities. By providing active motion capabilities, the exoskeleton facilitates the replication of natural joint movements, allowing patients to regain normal walking patterns and perform rehabilitative exercises such as leg lifting. Simultaneously, the passive motion functionality allows for controlled and safe movements, protecting the joints from excessive stress or strain.

Moreover, the design incorporates safety features to prevent potential harm during rehabilitation exercises. For instance, the joints may include sensors and feedback mechanisms to detect abnormal forces or angles, alerting both the user and caregiver to adjust or intervene accordingly. The ultimate objective of these structural designs is to promote effective and efficient recovery for stroke patients by providing support, enhancing mobility, and minimizing the risk of further damage.

# Chapter 6

# Kinematics Analysis of the Lower Limb Rehabilitation Exoskeleton Mechanism

## 6.1  Introduction

This chapter primarily focuses on the kinematics analysis and performance evaluation of the ankle joint, knee joint, and hip joint, which collectively form the structure of lower limb rehabilitation exoskeletons. In this chapter, in addition to applying the screw theory mentioned in Chapter 4, both forward kinematics and inverse kinematics were utilized for kinematic analysis. Kinematics is the field of science and engineering that studies motion by describing the position, velocity, and acceleration of objects in space or a specific coordinate system. In the context of lower limb rehabilitation exoskeletons, kinematics analysis plays a crucial role in understanding joint movement patterns and biomechanics. By analyzing the kinematics of the ankle joint, knee joint, and hip joint, we can gain insights into the range of motion, coordination, and joint angles during activities such as walking, running, or rehabilitation exercises.

The objective of kinematics analysis is to understand how objects move and change position over time. It involves analyzing relationships between variables such as displacement, velocity, acceleration, and time. By studying these relationships, we can gain insights into the patterns, trajectories, and behavior of moving objects. Kinematics analysis utilizes mathematical models and equations to represent and describe object motion. These models are applicable to various systems, including mechanical systems, robots, vehicles, and celestial bodies. Through principles of geometry, calculus, and algebra, kinematics analysis allows us to quantify and predict object motion under different conditions.

Kinematics analysis consists of two main components: forward kinematics and inverse kinematics. Forward kinematics determines the position and orientation of an object's end effector (e.g., the tip of a robot arm) based on known joint values. Inverse kinematics,

meanwhile, calculates the joint values needed to achieve a desired position or orientation of the end effector. Kinematics analysis plays a critical role in fields such as robotics, animation, biomechanics, and physics. It aids in designing and analyzing motion in complex systems, optimizing movement paths, simulating realistic animations, and developing control strategies for robotic systems.

Overall, kinematics analysis provides a fundamental understanding of object motion, enabling analysis and prediction of movement. This knowledge is essential for designing efficient and accurate systems in various technological applications. By comprehensively examining the kinematics and performance evaluation of the ankle, knee, and hip joints, researchers and engineers can develop effective lower limb rehabilitation exoskeletons that align with human movement patterns, enhance mobility, and assist in recovering or improving physical functionality. Moreover, this analysis contributes to the advancement of robotics and assistive technologies, ultimately improving the quality of life for individuals with lower limb impairments or injuries. Thus, section 6.2 would introduce the kinematics analysis of the ankle joint, section 6.3 would exhibit the kinematics analysis of the knee joint while the hip kinematics analysis would be shown in section 6.4.

## 6.2 Kinematic Analysis of Ankle Joint Rehabilitation Mechanism

### 6.2.1 Stability Model of Ankle Joint Based on ZMP

Before the ankle exoskeleton robot, designed in this paper, can be worn and put into use, the impact on the wearer's gait stability must be evaluated. This is essential to ensure that the ankle exoskeleton wearers possess sufficient mechanical adaptability and stability under real-life conditions. To facilitate analysis and calculations, we make the assumption that when the human body is in motion, the ground reaction force acting on it creates a horizontal torque that remains constant and stabilizes the human body at a specific point $p$, known as the zero moment point (ZMP), as shown in Fig. 6.1. By conducting stability testing, we can effectively evaluate the dynamic stability of the ankle exoskeleton robot during actual use and determine its impact on the wearer's gait and overall performance. This will enable us to further optimize and improve the design of the ankle exoskeleton robot, ensuring maximum effectiveness and safety for patients undergoing ankle rehabilitation.

It is assumed that when the plantar is in contact with the ground, the force $F$ and torque $T$ on the plantar are $F_G = [f_x, f_y, f_z]^T$ and $T_G = [\tau_x, \tau_y, \tau_z]^T$ respectively, $G$ is

Fig. 6.1 ZMP Model Based on the Stability Zone

influence factor caused by the gravity,and ZMP is located in the plantar plane and expressed mathematically as $r_p = [p_x, p_y, p_z]^T$, as shown in Fig. 6.1.

Taking ZMP as the centre point, the force torque at the heel is calculated as below:

$$\tau(r_p) = (r_g - r_p) \times F_G + T_G \tag{6.1}$$

The mass of the body of the patient wearing the exoskeleton rehabilitation device was set as $m_p$ , the space position of the center of mass was set as $\dot{M} = [x_m, y_m, z_m]$, and the momentum and angular momentum were respectively set as $E_m = m\dot{M} = [E_x, E_y, E_z]^T$ and $L = M \times m\dot{M} = [L_x, L_y, L_z]^T$ . The acceleration due to gravity is $g = [0, 0, -g]^T$. Then we can get:

$$\dot{E_m} = m_p g + F \tag{6.2}$$

$$\dot{L}_m = \dot{M} \times m_p g + \tau \tag{6.3}$$

Where, $F$ and $\tau$ in the expression respectively represent the force and moment of the exoskeleton rehabilitation wearer in addition to their own gravity.

Taking point $O$ as the center point, the force and moment borne by the heel are calculated as:

$$\tau = r_p \times F + \tau(r_p) \tag{6.4}$$

Substituting the previous three expressions, the following formula can be obtained:

$$\tau(r_p) = \dot{L} - \dot{M} \times mg + (\dot{E} - mg) \times r_p \tag{6.5}$$

Based on the above equation, the ZMP position of patients with exoskeleton wearing was finally deduced as follows:

$$\begin{cases} p_x = \frac{-\dot{L}_y + \dot{E}_x p_z + mg x_m}{\dot{E}_z + mg} = x_m - \frac{z_m \ddot{x}_m}{\ddot{Z}_m + g} \\ p_y = \frac{\dot{L}_x + \dot{E}_y p_z + mg y_m}{\dot{E}_z + mg} = y_m - \frac{z_m \ddot{y}_m}{\ddot{Z}_m + g} \end{cases} \tag{6.6}$$

Hence, the force state of the ankle exoskeleton wearer can be accurately analyzed by taking into consideration the gravity acceleration and spatial position of the exoskeleton. By accurately evaluating the force state of the wearer, we can optimize the design and improve the performance of the ankle exoskeleton rehabilitation robot, ensuring that it effectively supports and enhances the patient's gait stability during the rehabilitation process. This will ultimately facilitate a more comprehensive and efficient recovery for patients suffering from ankle injuries. Evaluating the force state is a crucial step in the development of ankle exoskeleton technology as it helps us to fully grasp the underlying mechanics involved, enabling us to provide more effective treatment and support for those in need.

## 6.2.2 Kinematic and Forcing Analysis of Ankle Joint Exoskeleton Mechanism

This section is dedicated to the analysis of the ankle joint force under the assumption that the exoskeleton wearer is walking on a plane terrain. The force of the ankle joint is analyzed and verified through this research which assumes that the exoskeleton wearer is walking on flat ground. This is an essential step towards developing ankle exoskeleton technology as it allows us to gain insights into the mechanics involved in the rehabilitation process. Moreover, it enables us to refine the design of the ankle exoskeleton rehabilitation robot, ensuring that it provides the necessary support and stability for patients during phys-

ical therapy. Our findings have significant implications for the field of ankle rehabilitation, providing valuable information to physical therapists and medical professionals working with patients facing ankle injuries. By expanding our understanding of the forces involved in the ankle joint, we can further enhance the efficacy of ankle exoskeleton technology, leading to improved patient outcomes and overall quality of life in the years to come, as shown in Fig. 6.2.
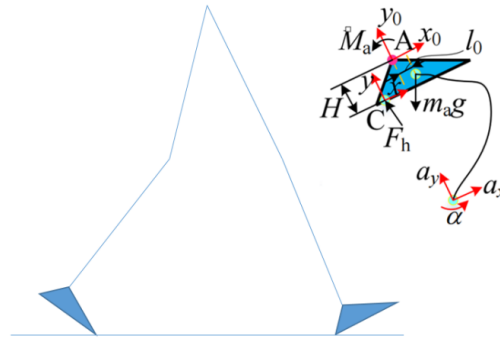


Fig. 6.2 Posture of Heel Landing Stage

During the heel landing stage, the ground reaction force $F_h c$ at point $C$ can be decomposed into $F_h c$ along the $x$ axis and $y$ axis, respectively. The direction of gravity acceleration of the foot is always vertically downward. The force balance equation of foot with respect to the position of ankle joint is:

$$\begin{cases} F_{ha,x0} + (m_f g)_x + F_{hc,x} = m_f a_x \\ F_{ha,y0} + (m_f g)_y + F_{hc,y} = m_f a_y \\ M_a - \frac{(F_{hc,x} + F_{ha,y0})H_f}{2} - \frac{F_{hc,y}L_f}{2} + F_{ha,x0}l_0 = Ia_h \end{cases} \tag{6.7}$$

Where,

$F_{ha,x0}$—The load on point $A$ in the $x_0$ direction

$F_{ha,y0}$—The load on point $A$ in the $y_0$ direction

$m_f$—Weight of foot

$a_h, a_t$—Acceleration of ankle rotation

$a_t x$—Acceleration along the x direction as the tip of the foot lifts off the ground

$a_t y$—Acceleration along the x direction as the tip of the foot lifts off the ground

$H_f$—Height of the ankle joint from the sole of the foot

$L_f$—The length of the foot

$l_0$—Horizontal distance between the center of mass of the foot and the ankle joint

165

$I$—Moment of inertia

$M_a$—The moment at the point $A$

When the center of mass of exoskeleton wearer's is located at point $M$, the load at the ankle can be derived by matrix transformation.

$$R_{ha} = R_r(z_0, \theta_h) \cdot R_r(z_1, \varphi_h) = \begin{bmatrix} \cos(\theta_h + \varphi_h) & -\sin(\theta_h + \varphi_h) & 0 & 0 \\ \sin(\theta_h + \varphi_h) & \cos(\theta_h + \varphi_h) & 0 & 0 \\ 0 & 0 & 1 & 0 \\ 0 & 0 & 1 & 1 \end{bmatrix} \quad (6.8)$$

$$\begin{bmatrix} F_{ha,x2} \\ F_{ha,y2} \end{bmatrix} = R_{ha}^T \begin{bmatrix} F_{ha,x0} \\ F_{ha,y0} \end{bmatrix} \quad (6.9)$$

Where, and are the forces along $x_2$ and $y_2$ directions at the joint, respectively. Therefore, the rotation matrix of $A - X_3 Y_3 Z_3$ with respect to $A - X_2 Y_2 Z_2$ is expressed as follows:

$$R_{hd} = R_f(z_2, \beta) \cdot T(y_3, r_f) \quad (6.10)$$

Where, $R_f$ represents the measurable distance between the ankle and the center of gravity of the foot $r \approx 25mm$ . So, the force on the ankle can be derived as:

$$\begin{bmatrix} F_{hd,x3} \\ F_{hd,y3} \end{bmatrix} = R_{ha}^T \begin{bmatrix} F_{ha,x2} \\ F_{ha,y2} \end{bmatrix} \quad (6.11)$$

The sum of the above equation is the force exerted by the center of gravity of the foot along $x_3$ and $y_3$ directions, respectively.

In the same way, in the stage when the toe leaves the ground, the ground reaction force $F_t c$ at point $C$ can be decomposed into $F_t c$ along the $x$ axis and $y$ axis respectively. The direction of gravity acceleration of the foot is always vertically downward. The force balance equation of foot with respect to the position of ankle joint is:

$$\begin{cases} F_{ta,x} + (mg)_x + F_{tc,x} = ma_{tx} \\ F_{ta,y0} + (mg)_y + F_{tx,y} = ma_{ty} \\ M_a = \frac{(F_{tc,x} + F_{tax,y0})H}{2} - \frac{F_{tcy}L}{2} + F_{ta,x0}l_0 = Ia_t \end{cases} \quad (6.12)$$

When the exoskeleton wearer's center of mass is located at point $M$, the load bearing situation at the ankle can be deduced by matrix transformation:

$$R_{ta} = R(z_0, \theta_t + \varphi_t) = \begin{bmatrix} \cos(\theta_t + \varphi_t) & -\sin(\theta_t + \varphi_t) & 0 & 0 \\ \sin(\theta_t + \varphi_t) & \cos(\theta_t + \varphi_t) & 0 & 0 \\ 0 & 0 & 1 & 0 \\ 0 & 0 & 0 & 1 \end{bmatrix} \tag{6.13}$$

$$\begin{bmatrix} F_{ta,x2} \\ F_{ta,y2} \end{bmatrix} = R_{ta}^T \begin{bmatrix} F_{ta,x0} \\ F_{ta,y0} \end{bmatrix} \tag{6.14}$$

Where is the Angle of the ankle joint in the extreme extension state when the toe is off the ground, and are the forces at the joint along the $x_2$ and $y_2$ directions, respectively. Therefore, the rotation matrix of $A - x_3 y_3 z_3$ with respect to $A - x_2 y_2 z_2$ is expressed as follows:

$$R_{td} = R(z_2, \beta) \cdot T(y_3, r) \tag{6.15}$$

Where, $r$ represents the distance between the ankle joint and the center of gravity of the foot. So, the force on the ankle can be derived as below:

$$\begin{bmatrix} F_{td,x3} \\ F_{td,y3} \end{bmatrix} = R_{ha}^T \begin{bmatrix} F_{ta,x2} \\ F_{ta,y2} \end{bmatrix} \tag{6.16}$$

Where,

$F_{ta,x0}$—The load on point $A$ in the $x_0$ direction

$F_{ta,y0}$—The load on point $A$ in the $y_0$ direction

$F_{td,x}$—The load on point $A$ in the $x_0$ direction

$F_{td,y}$—The load on point $A$ in the $y_0$ direction

The above $F_{td,x3}$ and $F_{td,y3}$ in the equation is the force exerted by the center of gravity of the foot along $x_3$ and $y_3$ directions, respectively.

Table 6.1 Input Parameters of Worm Gear and Worm Drive

| Link $i$ | $a_i$(mm) | $\alpha_i$(°) | $d_i$(mm) | $\theta_i$(°) |
|---|---|---|---|---|
| 1 | $L$ | 0 | 80 | $\theta_{2m-1}$ |
| 2 | 0 | 25 | 80 | $\theta_{2m-1}$ |
| 3 | $L$ | 25 | 80 | $\theta_{2m-1}$ |
| 4 | 0 | 25 | 80 | $\theta_{2m-1}$ |
| ... | .... | ... | ... | ... |
| 8 | 0 | 25 | 80 | $\theta_{2m-1}$ |

# 6.3 Kinematics Analysis of the Knee Joint Rehabilitation Mechanism

The kinematics model of SREs (Series Redundant Exoskeletons) is exceedingly intricate due to the involvement of multiple joints and axes in both joint space (segment space) and Cartesian space. This complexity presents challenges for real-time motion control and planning in these systems. Therefore, there is a strong desire to simplify the kinematics of SREs to facilitate their operation.

## 6.3.1 Forward Kinematics Analysis of SRE Model

Forward kinematics is a technique used to determine the position and orientation of the end-effector, which is the last link in a robotic arm or multi-link system, based on the joint angles. It plays a crucial role in robotics by calculating the trajectory and controlling the motion of the end-effector.

In forward kinematics, geometric relationships between consecutive joints are utilized to calculate transformation matrices that define the pose of one link in relation to another. By cascading these transformation matrices from the base link to the end-effector, we can obtain the position and orientation of the end-effector.

Forward kinematics is valuable for verifying the feasibility of desired target positions and orientations of the end-effector before executing a motion plan. Furthermore, it is essential for path planning, obstacle avoidance, and motion control in robotic arms and other multi-link systems.

Given that the SRE is combined of successive rotational joints, the Denavit-Hartenberg parameters are applied to specify the coordinate system of each link in segment $m$, where $Z_{s,i-1}$ is the unit vector of the $i$th rotational axis of segment $m$. The Denavit-Hartenberg parameters are listed in Tab. 5.1, where a1 is 0 degrees due to its special position constraints. It is worth noting that the application of these parameters simplifies the kinematics of SREs and enables effective control and planning of their real-time motion.

The four parameters in DH (Denavit-Hartenberg) tables are explained as follows:

Link length ($d$): it is the distance between two consecutive joint axes along the z-axis.

Link offset ($a$): it is the distance between two consecutive joint axes along the x-axis.

Joint angle ($\theta$): it is the rotation about the z-axis from one joint to another.

Twist angle ($\alpha$): it is the rotation about the x-axis from one link to another.

By using these four parameters, the DH method defines a series of reference frames that enable us to model the kinematics of a robotic arm or any other multi-link system. The parameters help to simplify the complexity of the kinematic equations and facilitate real-time motion control and planning.

The simplified kinematics of segment $m$ can be described using the D-H parameters as:

$$T_s = {}^{s,0}T_{s,1}{}^{s,1}T_{s,2}{}^{s,2}T_{s,3}{}^{s,3}T_{s,4}...{}^{s,5}T_{s,6}{}^{s,6}T_{s,7}T_{s,7}{}^{s,7}T_{s,8} = f(\theta_{2s-1}, \theta_{2s}) \tag{6.17}$$

Where ${}^{s,i-1}T_{s,i}$ is the transformation matrix between consecutive segments, $f_s(\theta_{2s-1}, \theta_{2s})$ is the simplified kinematic equation of segment $s$, $\theta_{2s-1}$ and $\theta_{2s}$ are the segment-joint angles. Thus, the relative position and relative angle of the end effector can be determined by using forward kinematics analysis. The simplified kinematics for the manipulator is exhibited as follows:

$$^0T_8 = {}^0T_1{}^1T_2{}^2T_3...{}^5T_6{}^6T_7T_7{}^7T_8 = f_{\text{SRE}}(\theta_1, \theta_2...\theta_7, \theta_8) = f_{\text{SRE}}(\theta) \tag{6.18}$$

Then, the resulting rotation matrix is calculated using an Euler angle representation as follows:

$$f_{\text{SRE}} = {}^0T_8 = \begin{bmatrix} \cos\theta_{123..8} & 0 & \sin\theta_{123..8} & 0 \\ 0 & 1 & 0 & 0 \\ -\sin\theta_{123..8} & 0 & \cos\theta_{123..8} & 0 \\ 0 & 0 & 0 & 1 \end{bmatrix} \tag{6.19}$$

Where, $\sin\theta_{123...8} = \sin(\theta_1 + \theta_2 + \theta_3 + \cdots + \theta_8)$, $\cos\theta_{123...8} = \cos(\theta_1 + \theta_2 + \theta_3 + \cdots + \theta_8)$. $f_{\text{SRE}}(\theta)$ is the simplified forward kinematic equation of the *SRE*, and $\theta$ is a column vector combining $\theta_1 \sim \theta_8$.

## 6.3.2    Inverse Kinematics Analysis of SRE Model

Inverse kinematics is a valuable technique for calculating the joint angles necessary to achieve a specific position and orientation of the end-effector in a robotic arm or multi-link system. It addresses the problem of determining the joint angles that can place the end-effector in the desired configuration.

Inverse kinematics plays a critical role in motion planning for robotic arms and other multi-link systems. It allows us to specify desired motion trajectories for the end-effector and determine the corresponding joint angles required to execute them. Inverse kinematics is also essential for real-time motion control and path planning in various applications, including robotics, animation, and simulation.

Solving the inverse kinematics problem can be challenging due to nonlinear equations that may have multiple solutions or no solutions at all in certain cases. Numerous analytical and numerical methods have been developed to efficiently solve the inverse kinematics problem.

In the context of SREs, the traditional method encounters difficulties due to the large number of real axes, causing the Jacobian matrix to have excessively large dimensions. The formula (4.1) in chapter 4 gave the basic theory for the kinematics analysis in this section. It would significantly increase computational costs. Therefore, this paper proposes a simplified approach for the Jacobian matrix, including a simpler solution for the inverse kinematics of the SRE. Specifically, according to the formula (4.1), the linear velocity and angular velocity effects of the linkage segment m of the SRE can be represented as follows:

$$
\begin{bmatrix} v_1 \\ w_1 \end{bmatrix} = \begin{bmatrix} e_{s,1}^{\times} r_{s,1} \dot{\theta}_{2s-1} + e_{s,2}^{\times} r_{s,2} \dot{\theta}_{2s-1} + \cdots + e_{s,3}^{\times} r_{s,3} \dot{\theta}_{2s} \\ e_{s,1} \dot{\theta}_{2s-1} + e_{s,2} \dot{\theta}_{2s-1} + \cdots + e_{s,7} \dot{\theta}_{2s-1} + e_{s,8} \dot{\theta}_{2s} \end{bmatrix} = \begin{bmatrix} v_{2s-1} & v_{2s} \\ w_{2s-1} & w_{2s} \end{bmatrix} \quad (6.20)
$$

Where $e_{s,i}^{\times}$ is the antisymmetric matrix of the $e_{s,i}$ which also expresses the unit vector of the $i$th axis that includes segment $m$ and $r_{s,i}$ refers to the vector from the ith joint to the end effector.

Then, $V_{2s-1}$, $V_{2s}$, $\omega_{2s-1}$ and $\omega_{2s}$ are the unit linear and angular velocity expressions of the two joint variables between segment $m$ and the end effector, respectively, which can be expressed as follows:

$$
\begin{cases} w_{2s-1} = e_{s,3} + e_{s,4} + \ldots + e_{s,7} + e_{s,8} = R_{s-1} f_{w,2s-1} \\ w_{2s} = e_{s,1} + e_{s,2} + \ldots + e_{s,5} + e_{s,6} = R_{s-1} f_{w,2s} \end{cases} \quad (6.21)
$$

$$\begin{cases} v_{2,s-1} = e_{s,3}^{\times} r_{s,3} + e_{s,4}^{\times} r_{s,4} + \ldots + e_{s,7}^{\times} r_{s,7} + e_{s,8}^{\times} r_{s,8} \\ v_{2s} = e_{s,1}^{\times} r_{s,1} + e_{s,2}^{\times} r_{s,2} + \ldots + e_{s,5}^{\times} r_{s,5} + e_{s,6}^{\times} r_{s,6} \end{cases} \tag{6.22}$$

Where $r_{s-1}$ exhibits the attitude matrix of segment $m-1$; $f_{w,2s-1}$ and $f_{w,2s}$ are expressed as:

The linear velocity in above expression could be further translated. Firstly, from Fig. 6.3, we can obtain the formula 6.23:
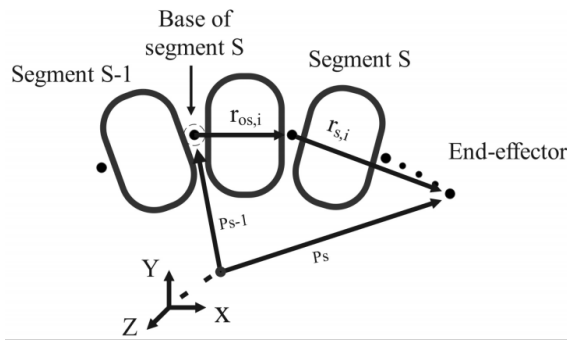


Fig. 6.3 Position Analysis of the Segments

$$r_{s,i} = -r_{Os,i} - P_{s-1} + P_e \tag{6.23}$$

Where $r_{os,i}$ expresses the vector matrix from the base to the $i$th joint centre of segment $m$. Thus, the above equation can be reformulated as:

$$v_{2s-1} = e_{s,3}^{\times} r_{s,3} + e_{s,4}^{\times} r_{s,4} + e_{s,7}^{\times} r_{s,7} + e_{s,8}^{\times} r_{s,8} = R_{s-1} \left( f_{v1,2s-1} R_{s-1}^{-1} (P_e - P_{s-1}) - f_{v2,2s-1} \right) \tag{6.24}$$

Where $R_{s-1}$, $P_{s-1}$ and $P_e$ can be obtained from the simplified forward kinematics from before, $f_{v1,2s-1}$ and $f_{v2,2s-1}$ can be defined as:

$$f_{v1,2s-1} = {}_1^{s-1} e_{s,3}^{\times} + \cdots {}_1^{s-1} e_{s,8}^{\times} = f_{v1,2s-1}(\theta_{2s-1}, \theta_{2s}) \tag{6.25}$$

$$f_{v2,2s-1} = {}^{s-1} e_{s,3}^{\times} {}_1^{s-1} r_{0s,3} + \cdots + {}^{s-1}_1 e_{s,8}^{\times} {}_1^{s-1} r_{0s,8} = f_{v2,2s-1}(\theta_{2s-1}, \theta_{2s}) \tag{6.26}$$

171

In the same way, $v_{2s}$ can also be expressed as follows:

$$v_{2s} = R_{s-1}\left(f_{v1,2s}R_{s-1}^{-1}(P_e - P_{s-1}) - f_{v2,2s}\right) \tag{6.27}$$

Where $f_{v1,2s}$ and $f_{v2,2s}$ can be expressed as:

$$f_{v1,2s} = e_{s,1}^{\times} + \cdots + e_{s,6}^{\times} = f_{v1,2s}(\theta_{2s-1}, \theta_{2s}) \tag{6.28}$$

$$f_{v2,2s} = s - 1_1 e_{s,11}^{\times s-1} r_{0s,1} + \cdots + {}_1^{s-1} e_{s,61}^{\times s-1} r_{0s,6} = f_{v2,2s}(\theta_{2s-1}, \theta_{2s}) \tag{6.29}$$

Where, $V_{2s-1}$, $v_{2s}$, $\omega_{2s-1}$ and $\omega_{2s}$ can then be obtained using simplified forward kinematics. The above eequation can further be rewritten as follows according to the Jacobian definition:

$$J_s \dot{\theta}_s = \begin{bmatrix} v_s \\ W_s \end{bmatrix} = \begin{bmatrix} v_{2s-1} & v_{2s} \\ W_{2s-1} & w_{2s} \end{bmatrix} \begin{bmatrix} \theta_{2s-1} \\ \theta_{2s} \end{bmatrix} \tag{6.30}$$

Thus, the simplified Jacobian matrix of segment m can be expressed as:

$$J_s = \begin{bmatrix} v_{2s-1} & v_{2s} \\ W_{2s-1} & w_{2s} \end{bmatrix} \tag{6.31}$$

Similarly, the final simplified Jacobian matrix of the whole exoskeleton can be expressed as:

$$J = \begin{bmatrix} v_1 & v_2 & \ldots & v_8 \\ w_1 & w_2 & \ldots & w_8 \end{bmatrix} \tag{6.32}$$

The final inverse kinematics solution of the SRE can be determined by employing the numerical iteration approach along with the simplified Jacobian matrix. This method involves iteratively refining the joint angles until the desired end-effector configuration is achieved. By using the simplified Jacobian matrix, which reduces computational complexity, the numerical iteration approach can efficiently converge to the solution. This

approach allows for accurate and efficient determination of the joint angles required to achieve the desired position and orientation of the end-effector in the SRE.

## 6.4 Kinematic Analysis of the Hip Joint Rehabilitation Mechanism

### 6.4.1 Inverse Kinematic Analysis and Jacobin Matrix of the 2-Dof Hip Rehabilitation Mechanism

Inverse kinematic analysis is based on the spatial position and orientation of the motion system, and the inverse solution of the variables for each joint of the motion link. For the series structure of the two-degree-of-freedom active/passive interactive system, assuming that the final spatial attitude of the motion system is obtained by rotating about the sagittal and horizontal axes respectively, the transformation matrix is obtained using Euler angle expressions:

$$R_B^A = \begin{bmatrix} cos\beta & 0 & sin\beta \\ sin\alpha sin\beta & cos\alpha & -sin\alpha cos\beta \\ -cos\alpha sin\beta & sin\alpha & cos\alpha cos\beta \end{bmatrix} \tag{6.33}$$

Assuming that the origin O of the moving coordinate system is located at a position vector in the fixed coordinate system as $\mathrm{p} = \begin{bmatrix} x_p & y_p & z_p \end{bmatrix}$, the position vectors of the centers of rotation of the two rotating joints connected to the waist-fixed link in the fixed coordinate system are:

$$\begin{cases} a_1 = [0 \quad a \quad 0]^T \\ a_2 = [0 \quad -a \quad 0]^T \end{cases} \tag{6.34}$$

Therefore, the vector loop equation of the supporting branch can be expressed as:

$$a_i + l_i s_u = p + b_i \tag{6.35}$$

In the equation, $s_u$ is the unit vector pointing from the point $a_i$ to the point $b_i$ . The position vector in the fixed coordinate system can be obtained as follows:

$$\begin{cases} b_1 = [x_p \quad y_p + b\cos a \quad z_p + b\sin a]^T \\ b_2 = [x_p \quad y_p - b\cos a \quad z_p - b\sin a]^T \end{cases} \tag{6.36}$$

Since the lengths between the series of rotating joints and between the rotating joints and the origin are constant, the position vector in the fixed coordinate system at the final attitude can be expressed as follows:

$$l_1 s_1 = [l_1 \cos\alpha\sin\beta \quad l_1 \sin\alpha \quad l_1 \cos\alpha\cos\beta] \tag{6.37}$$

By using vector relationships $l_1 s_1 = b_1 - a_1$, the position of the point $B_1$ in the fixed coordinate system can be expressed in another way as follows:

$$b_1 = \left[ l\cos\alpha\sin\beta + \sqrt{3}\alpha \quad l\sin\alpha \quad l\cos\alpha\cos\beta \right]^T \tag{6.38}$$

According to the equations above, the position vector at the fixed thigh rod can be obtained as follows:

$$p = \begin{bmatrix} x_p \\ y_p \\ z_p \end{bmatrix} = \begin{bmatrix} l\cos\alpha\sin\beta + \sqrt{3}\alpha - b_0\cos\beta \\ l\sin\alpha - b_0\sin\alpha\sin\beta \\ l\cos\alpha\cos\beta + b_0\cos\alpha\sin\beta \end{bmatrix} \tag{6.39}$$

For given values of $\alpha$ and $\beta$, the lengths of the two supporting branches of the fixed thigh rod can be obtained by using vector relationships $l_1 s_1 = b_1 - a_1$, which are:

$$\begin{cases} l_1 = \sqrt{x_p^2 + (y_p + b\cos\alpha - a)^2 + (z_p + b\sin\alpha)^2} \\ l_1 = \sqrt{x_p^2 + (y_p + b\cos\alpha - a)^2 + (z_p + b\sin\alpha)^2} \end{cases} \tag{6.40}$$

By using these equations, the robot's kinematic model can be controlled to achieve the desired posture and perform specific tasks efficiently and accurately. The solution of inverse kinematics equations involves calculating the lengths and relationships of the supporting branches of the fixed thigh rod based on vector methods, which leads to the expression of the position vector of the point in the fixed coordinate system.

Table 6.2 The Properties of the 6061/T6 Aluminum

| Properties | Symbol | Value |
|---|---|---|
| Material | - | 6061/T6 |
| Elasticity Modulus | $E$ | $6.9 \times E^{10} \text{n/mm}^2$ |
| Poisson's Ratio | $\mu$ | 0.33 |
| Density | $\rho$ | 2700kg/m3 |

## 6.4.2 Kinematic Validation of the Hip Joint Rehabilitation Mechanism

The kinematic issues of the two-degree-of-freedom series-connected hip exoskeleton's active/passive interaction apparatus were theoretically calculated, and these calculations were subsequently validated using simulation methods. The material properties for the active/passive interaction apparatus of the two-degree-of-freedom series-connected hip exoskeleton are provided in the Tab. 7.2 below:

The geometric dimensions of the mechanism are $l_1 = 310mm$, $a_1 = 105mm$, $a_2 = a_3 = 60mm$, $b_1 = 70mm$, and $b_2 = b_3 = 40mm$, with variable parameters of $l_2$ and $l_3$, where that is fixed at $l_2 = l_3 = 310mm$. Based on gait experiments and lower limb biomechanics analysis, we have determined the load at the hip joint's distal end, where the dynamic platform is subjected to an external force vector of $F_e = [-20, 0, 25, 30, 30, 0]^T$ and gravity acceleration $g = [0, 0, -9.8]^T \text{m/s}^2$.

To ensure that the two-degree-of-freedom series-connected hip exoskeleton's active/passive interaction apparatus maintains excellent dynamic response characteristics during weight-bearing walking movements, we have fitted the hip joint's flexion-extension trajectory under a loading condition of $20kg$ as follows:

$$\beta = \begin{cases} \frac{35\pi}{18}t^2 + \frac{59\pi}{360} & ,0 \leq t < 0.1 \\ \frac{11\pi}{60}\cos\left(\frac{20\pi}{11}t - \frac{2\pi}{11}\right) + \frac{7\pi}{72} & ,0.1 \leq t < 1.1 \\ -\frac{\pi}{36}t + \frac{13\pi}{72} & ,1.1 \leq t < 1.1 \end{cases} \tag{6.41}$$

This fitting provides us with crucial information regarding the movement of the mechanism under load, which can be utilized to optimize its design even further. By adjusting the structural parameters or selecting alternative materials, we may be able to improve the mechanism's stiffness, strength, and overall performance, thereby enhancing its effectiveness in aiding stroke rehabilitation patients during weight-bearing walking exercises.

To simulate the flexion-extension movement of the hip exoskeleton mechanism, the dynamic platform rotates around the Y-axis. During this movement, the driving force of the two driving chains varies, as shown in Fig. 7.12 below:



Fig. 6.4 The Driving-Force Changes of the Two Chains during Flexion-Extension Motion

By carefully analyzing these driving force changes, we can gain valuable insights into the mechanical and structural properties of the active/passive interaction apparatus of the hip exoskeleton. These insights can then be used to optimize its design and improve its effectiveness in supporting the movement of stroke rehabilitation patients.

To simulate the hip exoskeleton mechanism's adduction-abduction movement, the dynamic platform rotates around the *x*-axis. During this movement, the driving force of the two driving support chains varies but in opposite directions, as shown in the Fig. 7.13 below:

During adduction-abduction movements of the hip exoskeleton mechanism, the mobile pairs in the two driving support chains extend or contract in opposite directions with equal but opposite magnitudes of driving force.

Furthermore, the simulation values of the driving force changes for the two driving chains' active support basically approximate the theoretical solution. This validates the correctness of the theoretical solution to the kinematic problem of the exoskeleton mechanism.

Overall, the high degree of similarity between the theoretical and simulation values of the driving force during hip extension-flexion and adduction-abduction movements indicates that the mechanism has excellent dynamic response characteristics when simulating hip joint movements. Moreover, based on this dynamic analysis, important driving parameters can be selected for the power source during the prototype's construction.

Fig. 6.5 The Driving-Force Changes of the Two Chains during Adduction-Abduction Motion

## 6.5 Conclusions

This chapter constitutes a comprehensive exploration into the kinematics analysis and performance evaluation of the ankle joint, knee joint, and hip joint within the realm of lower limb rehabilitation exoskeletons. Kinematics analysis forms the bedrock for understanding the intricate movement patterns and biomechanics exhibited by these joints during various activities such as walking, running, and rehabilitation exercises. By delving into the intricate relationships between displacement, velocity, acceleration, and time, we gain profound insights into the behavior and trajectories of moving objects.

The field of kinematics analysis holds paramount importance in disciplines such as robotics, animation, biomechanics, and physics. It empowers us to design highly efficient systems, optimize movement paths, simulate lifelike animations, and devise effective control strategies. A comprehensive examination of the kinematics and performance of these joints enables us to develop exoskeletons that not only enhance mobility but also aid in the recovery and improvement of physical functionality.

Moreover, this analysis serves as a catalyst for advancements in robotics and assistive technologies catered towards individuals experiencing lower limb impairments or injuries. By leveraging the principles of kinematics analysis, we strive to improve the quality of life for these individuals by enabling them to regain their mobility and independence.

Overall, through the meticulous study of kinematics and performance evaluation, we unlock unprecedented possibilities in the development of rehabilitation exoskeletons. These advancements not only drive the field of robotics forward but also pave the way for transformative assistive technologies that have the potential to revolutionize the lives of

those facing lower limb impairments or injuries, ultimately leading to an improved quality of life for all. Furthermore, considering the distinct structural characteristics of these three components, including the ankle joint, the hip joint, and the knee joint, it should be noted that the ankle and hip joints possess purely rigid structures. As a result, in Chapter 6, the stiffness analysis would be examined the distribution of forces within these two regions. Conversely, the knee joint is designed with a combination of rigid and flexible elements. Consequently, in Chapter 7, an alternative method will be employed to analyze the forces acting upon this particular component.

# Chapter 7

# Stiffness Analysis and Performance Evaluation

## 7.1 Introduction

Due to the purely rigid structure design of the ankle joint and hip joint, and the rigid-flexible combined design of the knee joint, there will be a distinction in the stiffness analysis process. It only involves the ankle joint and hip joint, excluding the design of the knee joint. As for the validation of the knee joint, a different approach would be used in Chapter 8 for verification. The stiffness of a component is a crucial factor that measures the extent of deformation caused by external forces or torques, resulting in a deviation in the position and orientation of the end-effector [263]. This parameter holds significant importance in the design of rehabilitation exoskeletons as it directly affects the accuracy of the device. In our approach, we consider the impact of both motor torque and pressure exerted by the human body on the stiffness of the system. Determining the maximum required stiffness for the exoskeleton is vital in ensuring stability and optimal performance [277] [149] [278]. Thus, a comprehensive evaluation of ankle exoskeleton stiffness becomes critical in identifying strategies for design enhancements.

Multiple approaches exist for evaluating the stiffness of a structure, but the finite element analysis (FEA) technique is widely regarded as one of the most reliable and accurate methods available [317] [129]. By utilizing FEA simulations, we gain valuable insights into the structural behavior of the exoskeleton, identify potential issues related to deformation, and optimize the overall design to ensure maximum effectiveness and safety of the device. Our proposed methodology holds significant implications for ankle rehabilitation, providing physical therapists and medical professionals with a powerful tool to improve the quality of care for patients with ankle injuries. It is important to note that, in this research, the ankle joint and hip joint rehabilitation mechanisms are designed as

purely rigid structures. Hence, a thorough analysis of stiffness and performance evaluation is necessary and will be discussed in the subsequent sections. Furthermore, a stiffness analysis is conducted on the rehabilitation structures of both the ankle joint and the hip joint. The simulation performance of the elastic device within the ankle joint, as well as its performance under load, will be showcased. Similarly, the performance of the hip joint based on the stiffness analysis will also be presented. As discussed in the previous chapter, the structural variations among these three components necessitate distinct approaches. The ankle joint and hip joint are characterized by purely rigid structures. Therefore, in this chapter, the stress distribution would be introduced within these two parts. Subsequently, in the subsequent chapter, the knee joint and elaborate would be introduced on its unique characteristics.

## 7.2 Stiffness Analysis and Performance Evaluation of the Ankle Joint

### 7.2.1 Stiffness Analysis of Parallel Spring Devices

During the heel landing stage of gait, the exoskeleton robot is susceptible to producing a significant impact upon ground contact. However, to ensure smoother transition and mitigate the impact forces, parallel spring devices are incorporated on both sides of the ankle joint rotation axis. These devices play a crucial cushioning role, providing kinetic energy for the mode-switching of the ankle joint during the foot flat stage. It should be noted that the parallel spring device is only operational during the heel landing stage and the subsequent static standing stage. Therefore, it must have sufficient stiffness to support the wearer's balance and stability in these two stages. By effectively controlling the stiffness of the parallel spring, we can create a more comfortable, safe, and natural walking experience for patients undergoing rehabilitation. The parallel spring mechanism is a fundamental design component in the ankle exoskeleton rehabilitation robot, and its optimal implementation requires careful consideration of the patient's needs, as well as a deep understanding of the underlying mechanics involved in ankle joint movement. The rotational simulation of ankle joint in Adams could be obtained in Fig. 7.1, which including the rotational actions on both ankle joint and toes joint.

Based on the ground reaction force data presented in the Figure above, it is observed that the horizontal component is negligible, and therefore can be disregarded during the analysis process. To further analyze the force situation at the heel position during the gait cycle, we conducted a comprehensive study as follows:
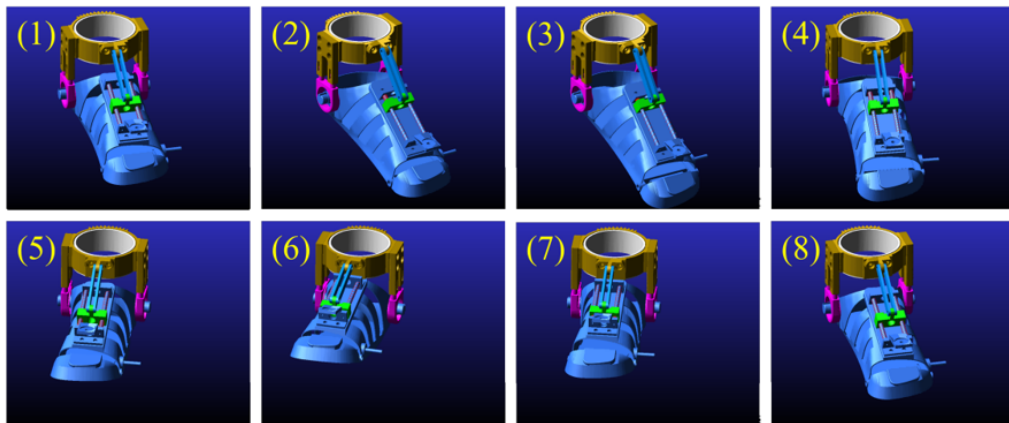
Fig. 7.1 The Simulation of Ankle Joint in Adams

In the static standing stage, the force exerted on the bottom of the shoe base is approximately 390N, and its direction is upwards along the body. In this stage, the contact surface between the exoskeleton shoe base and the ground is considered a fixed boundary condition.

During the walking stage, the force acting on the bottom of the shoe base is estimated based on the landing of one foot, which is approximately 780N, and its direction is upwards along the body. This stage involves dynamic contact between the exoskeleton shoe base and the ground, and the force applied to the system is a critical factor affecting the stability and safety of the wearer.

The analysis of the force situation reveals valuable insights into the performance of the exoskeleton rehabilitation robot during the gait cycle. By appropriately designing the structure and materials of the exoskeleton components, we can improve the system's stability and ensure safe, comfortable, and effective rehabilitation for patients facing ankle injuries. The findings provide useful guidance for medical professionals and engineers striving to develop cutting-edge exoskeleton technology to enhance the quality of care provided to patients.

Aluminum alloy is a popular structural metal material that is widely used in various industries due to its favorable characteristics. Notably, aluminum alloy exhibits excellent mechanical properties such as high yield strength and ductility, while also being lightweight. These properties make it an ideal material for applications in the medical, aerospace, consumer electronics, and other related fields.

The exoskeleton robot utilizes 7075/T6 aluminum alloy as the primary bearing component due to its superior mechanical properties and desirable material characteristics, as shown in Tab. 7.1, [196] this alloy has a high strength-to-weight ratio, which allows the exoskeleton to be lightweight yet robust enough to support the wearer's body weight.

Table 7.1 Properties of 7075/T6

| Properties | Unit | Value |
|---|---|---|
| Elasticity Modulus | Mpa | 7.2E+4 |
| Poisson's Ratio | - | 0.33 |
| Shearing Modulus | Mpa | 2.69E+4 |
| Density | $Kg/m^3$ | 2810 |
| Tensile Strength | Mpa | 570 |
| Yield Strength | Mpa | 505 |
| Thermal Expansivity | /K | $2.36E^-5$ |
| Thermal Conductivity | W/(m*K) | 130 |
| Specific Heat | J/(kg*K) | 960 |

Moreover, its high yield strength and ductility help ensure the durability and longevity of the exoskeleton, even under arduous conditions.

The use of 7075/T6 aluminum alloy in the exoskeleton design is a testament to the advancing technological advancements in rehabilitation robotics. This innovative technology can greatly improve the quality of life for individuals dealing with ankle injuries, facilitating their recovery and allowing them to regain their mobility and independence. The adoption of such materials into the exoskeleton design represents a significant step towards creating a more functional, efficient, and safe system for patient rehabilitation.

Based on the operational conditions described above, we conducted a finite element static analysis on the parallel spring structure of the exoskeleton rehabilitation robot. Specifically, we focused on the heel landing stage during walking, where the maximum compression amount of the spring was designed to be approximately 10mm, with an initial spring length of 20mm. As a result, the maximum compression length of the spring was determined to be 10mm. Furthermore, we assumed that all four springs in the parallel spring structure had the same parameters.

According to our calculations, the total spring force at the designed maximum compression was equal to the maximum load of 780N. Therefore, the elastic force of each spring at maximum compression was estimated to be approximately 195N. Based on these values, we were able to determine the stiffness coefficient of the spring as outlined below.

The stiffness coefficient $K$ of a spring is defined as the ratio of the applied force to the resultant deformation of the spring. In this case, given that the maximum compression length of the spring was 10mm, and that the elastic force at maximum compression was 195N for each spring in the parallel spring structure, we can obtain the stress displacement as shown in Fig. 7.2:
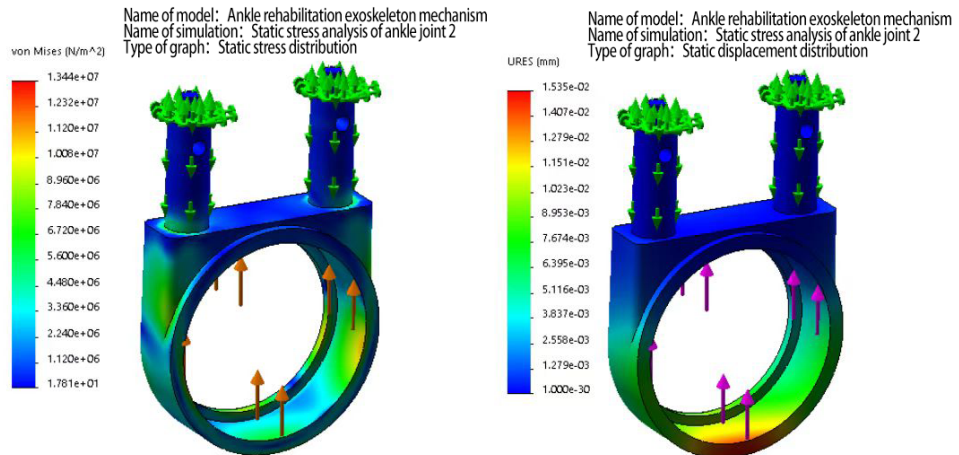
Fig. 7.2 Stress and Displacement of Rotational Joint under Maximum Force

## 7.2.2  Stiffness Analysis of the Mechanism with Loading

First we need to analyze the stiffness of the exoskeleton from the influence of the output torque. The rotary shaft seat of the dorsiflexion and plantarflexion movement of the ankle joint is installed on the output gear as a whole, and belongs to the base of all the movement structures in structure, which has certain requirements for the mechanical properties such as the strength of the output gear. The Solidworks finite element module was used to simulate and analyze the output gear. The calculation results of the output gear were as follows:

Boundary condition:

a.The material is brass;

b.The bearing capacity $F = 780N$ is applied to the contact surface with $x$;

c.A fixed constraint condition is imposed on the bolt connection position with the support rod;

The results of our calculations demonstrate that under load, the maximum deformation of the output gear is approximately 0.008mm, and the maximum stress is 13.9MPa, as shown in Fig. 7.3. Based on these values, it can be concluded that the output gear seat meets the necessary requirements in terms of its bearing capacity.

Next, we performed a stiffness analysis of the exoskeleton with regards to the effects of human load. Specifically, we examined the stress distribution of the ankle joint position of the exoskeleton rehabilitation robot, and the results are shown below figures. Our analysis indicated that under a load of 780N on a single foot while standing, the maximum stress on the device was 42.7MPa, when accounting for the safety factor.

Notably, the maximum stress occurred around the heel spring guide pin, but it was found to be less than the yield strength of both stainless steel 316L and 7075 aluminum alloy,
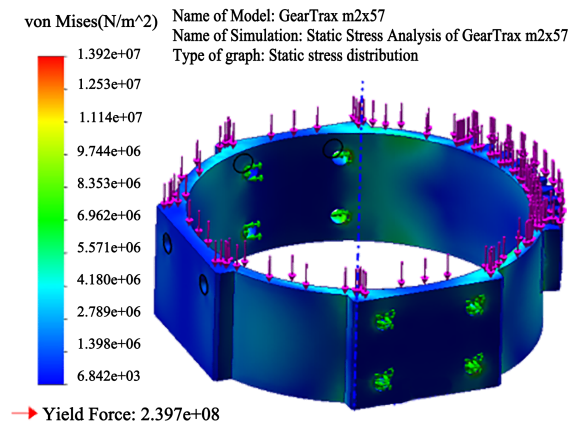
(a) Static Stress Analysis of GearTrax m2x57
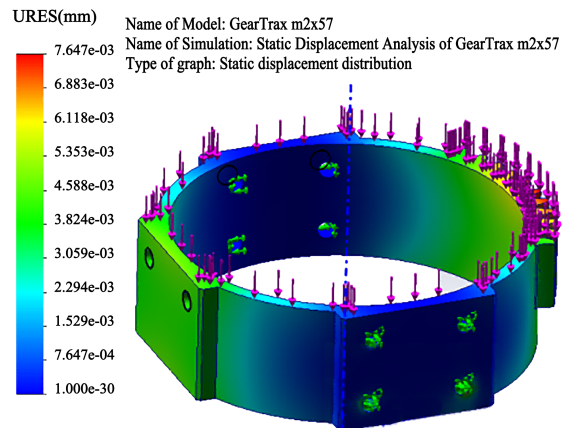


(b) Static Displacement Analysis of GearTrax m2x57
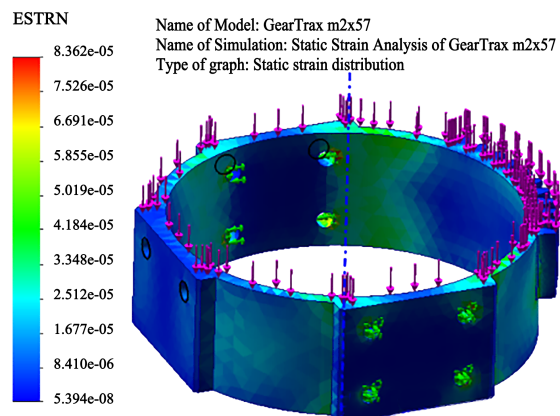


(c) Static Strain Analysis of GearTrax m2x57

Fig. 7.3 Stiffness Analysis of GearTrax m2x57
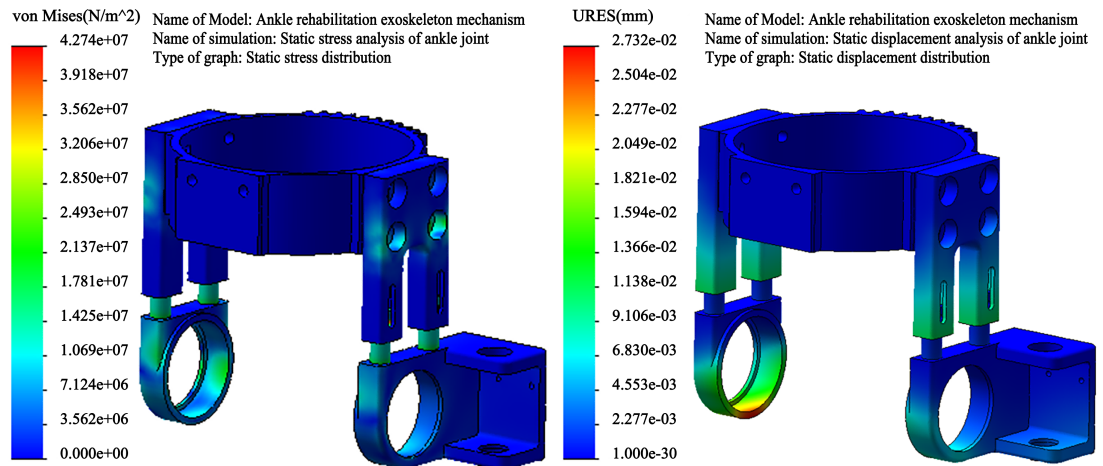
(a) Stress Distribution of the Rehabilitaion
Mechanism under Maximum Load

(b) Static Displacement Distribution of the Rehabilitation Mechanism under Maximum Load
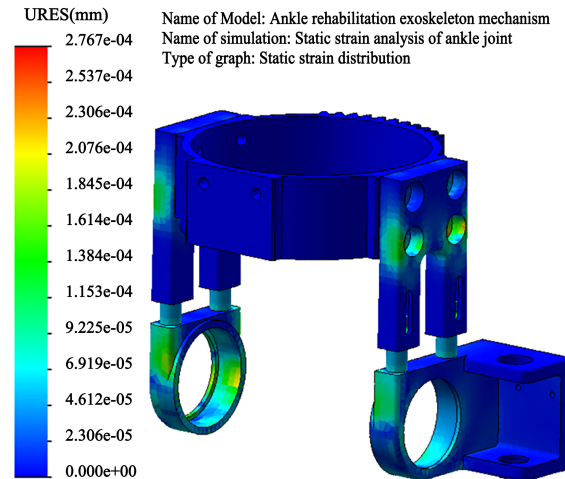
(c) Strain Distribution of the Rehabilitation Mechanism under Maximum Load

Fig. 7.4 Stiffness Analysis of the Rehabilitation Mechanism under Maximum Load

which satisfies the necessary requirements for use, as shown in Fig. 7.4c. Additionally, under the maximum load, the device's maximum displacement was found to be only 0.02mm, with a maximum strain of only 0.00027.

These findings are critical for assessing the performance and reliability of the exoskeleton rehabilitation robot under varying loads. By ensuring that all components of the system meet the necessary technical specifications and safety standards, we can provide patients with a safe and effective rehabilitation tool that can significantly improve their quality of life.

### 7.2.3 Motion and Elastic System Mechanics Simulation by Adams

Upon completion of defining the fundamental parameters of each element, the system's simulation model is established. During the simulation, a load of 7 N is applied in a straight downward direction, and the running time for a gait cycle is set at 8s. Since the toes exhibit smaller angular motion, the ankle joints perform one circle, whereas the toe joint completes two circles during a gait cycle. As a result, several significant outcomes are demonstrated as follows. The simulation process for one gait cycle as shown in Fig. 7.5.
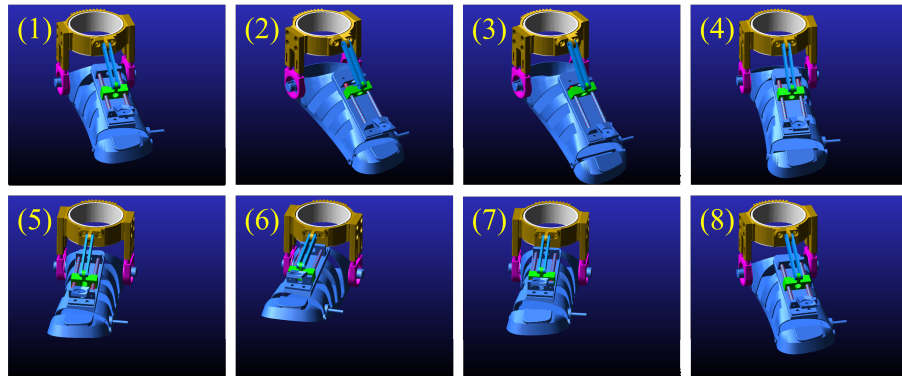


Fig. 7.5 The Rotation Angles of Each Joint in Simulation
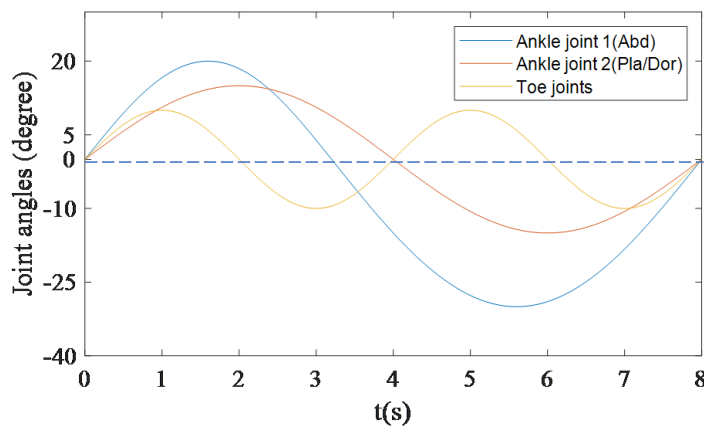


Fig. 7.6 The Rotation Values of Each Joint

The simulation refers to the actual changes of the human foot during rehabilitation exercises,as shown in Fig. 7.6 illustrates the rotational angle changes of three joints during a complete gait cycle. The orange line represents the angle change of the ankle joint in the transverse plane, with a range of motion of 0 to 15 degrees in both plantarflexion and dorsiflexion directions. The blue line in the figure represents the angle change of the ankle joint in the coronal plane. It is worth noting that during the actual rehabilitation process, the ranges of motion of the ankle joint in the abduction and adduction directions are from

186

0 to 20 degrees and 0 to 30 degrees, respectively. To avoid the secondary injury caused by velocity mutation to the patient, we have adopted a composite sine function to generate a smooth trajectory of the ankle joint on the coronal plane, as shown in the figure. The yellow line represents the angle change of the toe joint, with a range of motion of 0 to 10 degrees in both directions. Under normal circumstances, this design can achieve the required angle during the rehabilitation process.
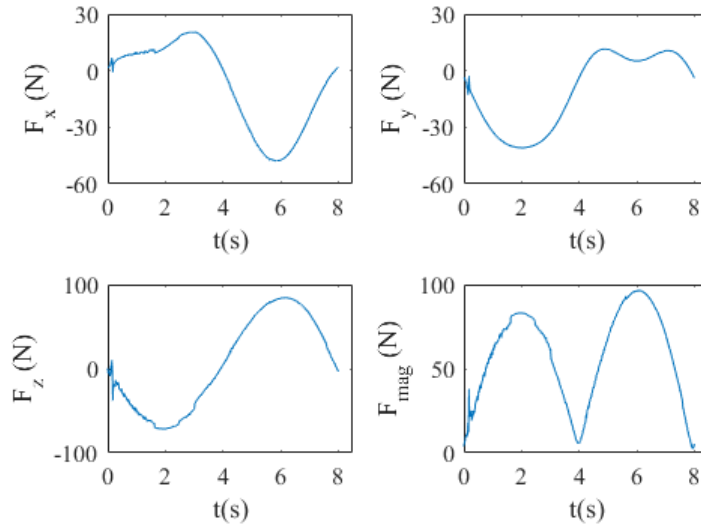


Fig. 7.7 The Stress of Sliders in One Gait-Cycle

Fig. 7.7 represents the stress of the slider during one gait cycle, and we could find little slight shaking in the graph. The main reason for this phenomenon is the existence of springs and the uneven force caused by the change of the moment of inertia. But these vibrations have no effect on our rehabilitation design, which is negligible.
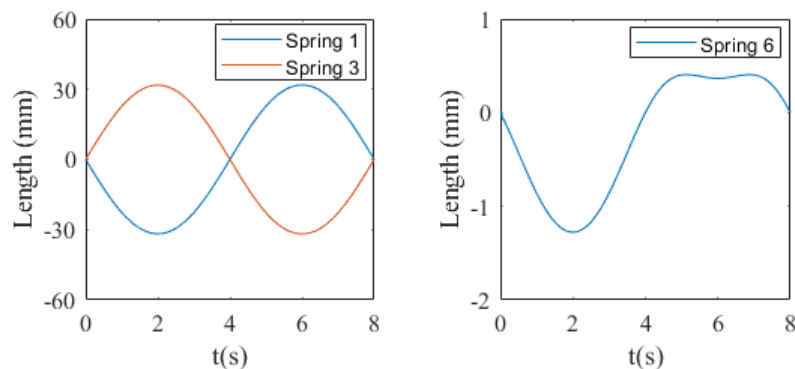


Fig. 7.8 Deformation of Springs

In addition, Fig. 7.8 shows the deformation curves of some representative springs in the machine. Springs 1 and 3 exhibit symmetric deformation curves due to their symmetrical

placement on both sides of the slider. However, Spring 6 shows irregular deformation due to the coupling effect of gravity and load.

Finally, we present the motion trajectories of the dorsum and toe tips of the foot in simulation, as shown in Fig. 7.9. It can be clearly seen that there are periodic oval motions between the dorsum and toe tips of the foot during the rehabilitation process, including their position relationship and their respective working space. Periodic motion can promote continuous operation of the motor, which indirectly reflects the working space of the entire exoskeleton. In addition, the absence of sudden changes further verifies the applicability of the mechanism in preventing secondary ankle injuries caused by sudden changes in machine speed during rehabilitation.
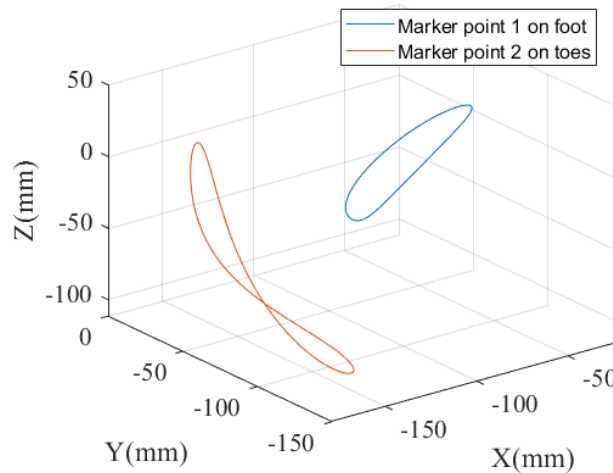


Fig. 7.9 The Motion Trajectories of Feet and Toes in Simulated Space

## 7.3 Stiffness Analysis and Performance Evaluation of the Hip Joint

### 7.3.1 The Working Space Analysis of the Hip Joint

The workspace can be divided into reachable workspace and dexterity workspace. In order to ensure that the rotating mechanisms of the hip exoskeleton's active/passive interaction apparatus around the $X$ and $Y$ axes conform to the characteristics of hip joint motion, a workspace analysis of the mechanism is carried out. Given the end-effector posture of the mechanism, all spatial positions that the end-effector can reach under the constraint of link lengths are obtained based on coordinate search and kinematic inverse solution methods. This set of spatial positions is referred to as the mechanism's workspace, as shown in Fig. 7.10.

(a) Spatial Position in the x-y Plane        (b) Spatial Position in the x-z Plane
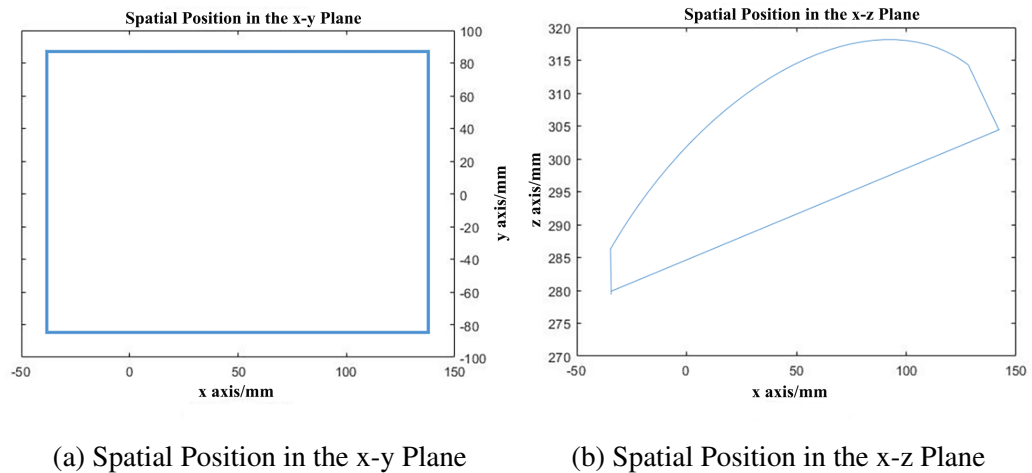
Fig. 7.10 Spatial Position of the Novel 2-Dof Rehabilitation Mechanism

The results of the workspace analysis for the active/passive interaction apparatus of the hip exoskeleton indicate that the mechanism has a relatively large dynamic platform that can withstand external forces $F_e = [f_e, n_e]^T$. Neglecting frictional forces in each joint, the functional relationship between the end-effector load and deformation displacement is obtained for all spatial positions within the mechanism's motion range. Moreover, there are no singularities in the mechanism's motion range, indicating good operational feasibility. Additionally, the symmetry with respect to the X-axis direction enables the spatial positions to conform to the human hip joint's motion characteristics.

## 7.3.2 The Stiffness Analysis of the Hip Joint Rehabilitation Mechanism

Stiffness is the ability of the mechanism to resist deformation under external loads, reflecting its load-bearing capacity. Since the active/passive interaction apparatus of the hip exoskeleton needs to support the weight of the human body during the stance phase, ensuring the safety and stability of stroke rehabilitation patients is crucial. Therefore, to verify the mechanical effects of the stiffness characteristics of the active/passive interaction apparatus of the hip exoskeleton, a stiffness analysis of the two-degree-of-freedom series active driving mechanism is conducted. We assume that:

a. The mechanism operates in a linear range, and the material properties exhibit linear elasticity.

b. The end deflection is the only deformation mode of the mechanism, and there is no coupling between deflection modes.

c. The mechanism's structure has uniform symmetry, and the loads are symmetrically distributed.

Under these assumptions, we analyze the stiffness characteristics of the mechanism and determine its load-bearing capacity, confirming its suitability for supporting stroke rehabilitation patients.

$$\mathrm{K}_s = \mathrm{k}_c \mathbf{J}^T \mathbf{J} \tag{7.1}$$

$$F_e = K_s \cdot \Delta x \tag{7.2}$$

In the formula, $F_e$ represents the external force acting on the dynamic platform, $\Delta x$ represents the deformation of the dynamic platform under external force, $K_s$ represents the stiffness matrix of the mechanism, and $k_c$ represents the equivalent spring constant of the mechanism. Based on the material properties from the literature, we take $k = 1000 N/mm$.

During the single support phase, the mechanism bears a concentrated force of F = 800N that represents the weight of the human torso. This force acts in the direction perpendicular to the dynamic platform and is located at its center. To conduct a stiffness analysis of the active/passive interaction apparatus of the hip exoskeleton, we established a finite element analysis model based on the operating conditions of the two-degree-of-freedom series-connected hip exoskeleton. Using finite element analysis, we performed static analysis to evaluate the load-bearing capacity of the mechanism under these conditions. The results provided us with deflection values for the dynamic platform of the mechanism when it is subjected to a load, as shown in Fig. 7.11.
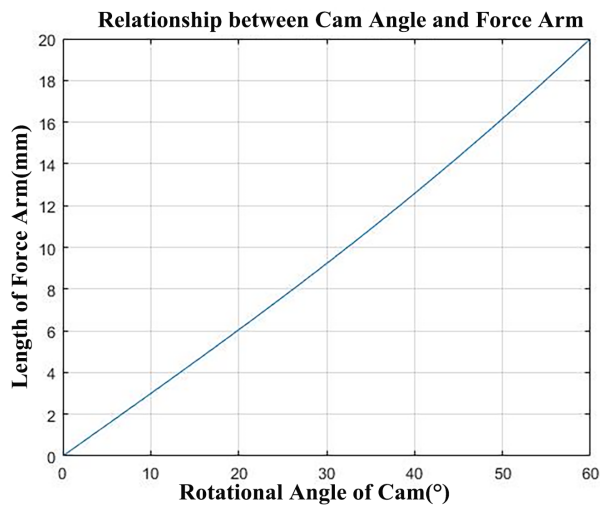


Fig. 7.11 Relationship between Cam Angle and Force Arm in Flexion-extension State

Table 7.2 The Properties of the 6061/T6 Aluminum

| Properties | Symbol | Value |
|---|---|---|
| Material | - | 6061/T6 |
| Elasticity Modulus | $E$ | $6.9 \times E^{10} n/mm^2$ |
| Poisson's Ratio | $\mu$ | 0.33 |
| Density | $\rho$ | 2700kg/m3 |

Under load, the maximum stress value experienced by the dynamic platform of the two-degree-of-freedom series-connected hip exoskeleton was found to be $56MPa$. This value is significantly lower than the yield stress value of the 6061/T6 aluminum alloy used in the structure, which is $275MPa$. Additionally, the maximum deflection value for the entire mechanism was found to be $0.6585mm$.

These results demonstrate that the mechanism possesses ample stiffness and strength to safely support the weight of stroke rehabilitation patients during the single support phase. Moreover, they indicate that the choice of using 6061/T6 aluminum alloy as the primary material for the structure is justified, as it offers sufficient strength whilst remaining lightweight and cost-effective.

This rigorous analysis provides valuable insight into the structural properties of the active/passive interaction apparatus of the hip exoskeleton, which could be used to optimize its design even further. By adjusting the structural parameters or selecting alternative materials, we may be able to achieve even greater stiffness and strength for the mechanism, thereby improving its effectiveness in supporting the movement of stroke rehabilitation patients.

### 7.3.3 Performance Evaluation of the Hip Joint in Different Rehabilitation Phases

The kinematic issues of the two-degree-of-freedom series-connected hip exoskeleton's active/passive interaction apparatus were theoretically calculated, and these calculations were subsequently validated using simulation methods. The material properties for the active/passive interaction apparatus of the two-degree-of-freedom series-connected hip exoskeleton are provided in the Tab. 7.2 [196].

The geometric dimensions of the mechanism are $l_1 = 310mm$, $a_1 = 105mm$, $a_2 = a_3 = 60mm$, $b_1 = 70mm$, and $b_2 = b_3 = 40mm$, with variable parameters of $l_2$ and $l_3$, where that is fixed at $l_2 = l_3 = 310mm$. Based on gait experiments and lower limb biomechanics analysis, we have determined the load at the hip joint's distal end, where the dynamic platform is subjected to an external force vector of $F_e = [-20, 0, 25, 30, 30, 0]^T$ and gravity of $g = [0, 0, -9.8]^T_{m/s^2}$.

To ensure that the two-degree-of-freedom series-connected hip exoskeleton's active/passive interaction apparatus maintains excellent dynamic response characteristics during weight-bearing walking movements, we have fitted the hip joint's flexion-extension trajectory under a loading condition of $20kg$ as follows:

$$\beta = \begin{cases} \frac{35\pi}{18}t^2 + \frac{59\pi}{360} & ,0 \leq t < 0.1 \\ \frac{11\pi}{60}cos\left(\frac{20\pi}{11}t - \frac{2\pi}{11}\right) + \frac{7\pi}{72} & ,0.1 \leq t < 1.1 \\ -\frac{\pi}{36}t + \frac{13\pi}{72} & ,1.1 \leq t < 1.1 \end{cases} \tag{7.3}$$

This fitting provides us with crucial information regarding the movement of the mechanism under load, which can be utilized to optimize its design even further. By adjusting the structural parameters or selecting alternative materials, we may be able to improve the mechanism's stiffness, strength, and overall performance, thereby enhancing its effectiveness in aiding stroke rehabilitation patients during weight-bearing walking exercises.

To simulate the flexion-extension movement of the hip exoskeleton mechanism, the dynamic platform rotates around the Y-axis. During this movement, the driving force of the two driving chains varies, as shown in Fig. 7.12 below:
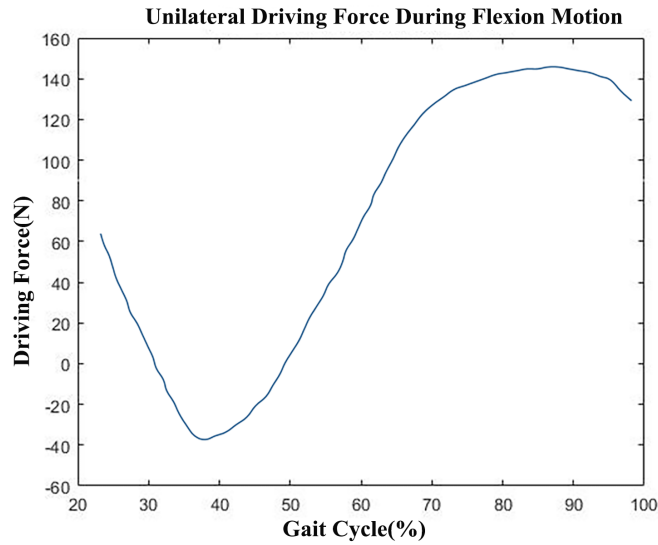


Fig. 7.12 The Driving-Force Changes of the Two Chains during Flexion-Extension Motion

By carefully analyzing these driving force changes, we can gain valuable insights into the mechanical and structural properties of the active/passive interaction apparatus of the hip exoskeleton. These insights can then be used to optimize its design and improve its effectiveness in supporting the movement of stroke rehabilitation patients.

To simulate the hip exoskeleton mechanism's adduction-abduction movement, the dynamic platform rotates around the X-axis. During this movement, the driving force of the two driving support chains varies but in opposite directions, as shown in the Fig. 7.13 below:
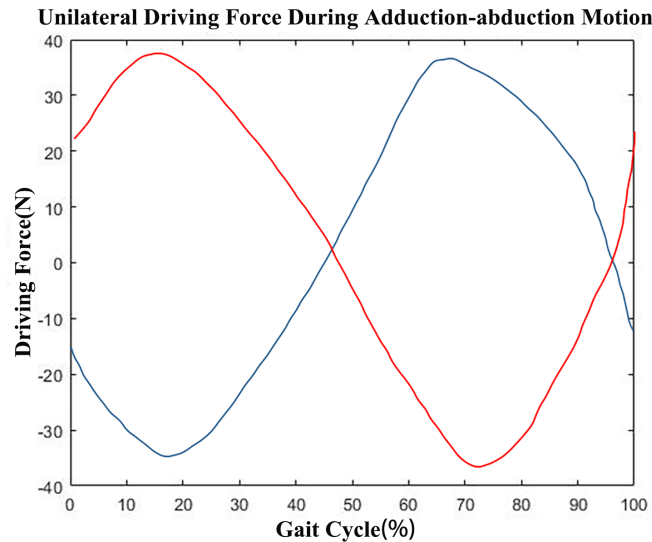


Fig. 7.13 The Driving-Force Changes of the Two Chains during Adduction-Abduction Motion

During adduction-abduction movements of the hip exoskeleton mechanism, the mobile pairs in the two driving support chains extend or contract in opposite directions with equal but opposite magnitudes of driving force.

Furthermore, the simulation values of the driving force changes for the two driving chains' active support basically approximate the theoretical solution. This validates the correctness of the theoretical solution to the kinematic problem of the exoskeleton mechanism.

Overall, the high degree of similarity between the theoretical and simulation values of the driving force during hip extension-flexion and adduction-abduction movements indicates that the mechanism has excellent dynamic response characteristics when simulating hip joint movements. Moreover, based on this dynamic analysis, important driving parameters can be selected for the power source during the prototype's construction.

## 7.4   Conclusions

This chapter provides a stiffness exploration of the simulation analysis and performance evaluation of the ankle joint, stiffness analysis of parallel spring devices, stiffness analysis under loading, motion and elastic system mechanics simulation using Adams software,

simulation analysis and performance evaluation of the hip joint, working space analysis of the hip joint, as well as the stiffness analysis of the 2-DOF hip rehabilitation mechanism.

Regarding the stiffness analysis of parallel spring devices, the rigidity characteristics of these devices under different load conditions are studied. By analyzing the structure and material parameters of the device, its stiffness attributes can be determined, facilitating design optimization and improved performance.In the simulation analysis and performance evaluation of the ankle joint, numerical methods and simulation models are utilized to investigate the motion characteristics and biomechanical behavior of the ankle joint during various activities. This analysis enhances our understanding of ankle joint performance during walking, running, and rehabilitation exercises, offering valuable insights for the design of more efficient exoskeleton systems. The motion and elastic system mechanics simulation using Adams software allows for the modeling and analysis of complex movements. This simulation analysis enables us to replicate and evaluate the mechanical responses of the motion and elastic systems under different movement patterns, providing crucial information for the control and optimization of exoskeleton systems.

Additionally, the working space analysis of the hip joint and the stiffness analysis of the 2-DOF hip rehabilitation mechanism are conducted. These analyses help us understand the range of motion of the hip joint and provide essential foundations for the design and control of rehabilitation mechanisms.In the simulation analysis and performance evaluation of the hip joint, simulation models and techniques are employed to delve deep into the motion characteristics and biomechanical behavior of the hip joint. By assessing metrics such as joint stability, range, and load transmission, we can evaluate the effectiveness of exoskeleton systems in improving hip joint functionality.

In summary, this chapter presents a comprehensive investigation of the simulation analysis and performance evaluation of the ankle joint and hip joint, as well as the stiffness characteristics and biomechanical behavior associated with them. These studies lay the groundwork for the design and optimization of exoskeleton systems while offering valuable guidance for improving lower limb rehabilitation and mobility functions. As mentioned earlier in this chapter, due to the unique structure of the knee joint, the alternative approach would be expressed about its feasibility in the next chapter.

# Chapter 8

# Simulation, Optimizing and Experiment Testing

## 8.1 Introduction

Due to the unique characteristic of the knee joint structure, the feasibility would be validated in this chapter. As mentioned earlier, the distinction between these three components necessitated a separate analysis approach. In the case of the ankle and hip joints, a stiffness analysis was conducted. However, since the knee joint incorporates both rigid and flexible structures, a different methodology involving Adams and the PSO genetic algorithm will be utilized for its analysis. Adams simulation and PSO genetic algorithm are widely used in the engineering field for system dynamics analysis and optimization design. Adams sim-ulation is a computer simulation technique based on the principles of multi-body dynamics, used to simulate and predict the motion and mechanical behavior of mechanical systems. By establishing the motion relationships between objects, applying forces or torques, and considering constraints, Adams can accurately simulate mechanical systems in the real world. This simulation approach can be used to evaluate the dynamic performance of systems, validate the feasibility and reliability of designs, and optimize design parameters.

At the same time, PSO (Particle Swarm Optimization) genetic algorithm is a heuristic optimization algorithm inspired by the collective behavior of flocking birds or fish schools. PSO seeks the optimal solution by simulating the cooperation and competition among individuals in a population. In the field of design optimization, PSO genetic algorithm is often used to search for global optima in multidimensional design spaces, particularly in complex system design optimization.

By combining Adams simulation with the PSO genetic algorithm, system dynamics analysis and parameter optimization for complex mechanical systems can be achieved. Firstly, Adams is used for simulation to obtain the motion and mechanical responses of the

system. Then, the PSO genetic algorithm is applied to the optimization problem, searching for the optimal solution by adjusting design parameters, such as maximizing performance metrics or minimizing cost functions. This combined approach offers many advantages, including accurate simulation of mechanical system behavior, global optimization capability, and efficiency. It can help engineers and designers better understand and improve system performance while saving design time and costs.

In conclusion, the combination of Adams simulation and the PSO genetic algorithm provides a powerful tool for system dynamics analysis and design optimization in the engineering field, fostering the development and innovation of mechanical systems. Firstly, the Adams simulation of the knee joint rehabilitation mechanism will be presented, followed by an optimization design aimed at resolving the issue of the "S-shaped" curve. Finally, a 3-D printed model will be showcased to validate the knee joint model.

## 8.2　Simulation and Optimization Analysis

### 8.2.1　"S-shaped" Curve Analysis of SRE Model Based on the Adams Simulation

Adams is a widely used multibody dynamics simulation software employed in engineering and scientific domains to simulate the motion of mechanical systems. It provides users with the capability to model intricate systems comprising interconnected components such as rigid bodies, flexible bodies, joints, motors, sensors, and actuators.

One of the key advantages of Adams is its high accuracy in predicting the behavior of real-world systems under diverse conditions, including variations in loads, forces, and temperature. This enables users to gain insights into system performance and make informed design decisions. Another significant benefit is the software's ability to detect and rectify potential design errors before the manufacturing stage. Through this feature, Adams helps save valuable time and resources while mitigating the risk of costly mistakes during the development process.

Additionally, Adams offers a robust graphical interface that facilitates easy visualization of the modeled system. Users can create animations to observe the motion of the system, generate graphs to analyze critical data, and evaluate simulation results. Moreover, Adams supports various standard file formats, facilitating seamless import and export of data from other software programs, enhancing interoperability and streamlining the simulation workflow.

Due to its versatility, Adams finds applications in a wide range of fields, including automotive and aerospace engineering, robotics, biomechanics, and sports science. Its flexibility allows engineers and scientists to optimize product and system performance

across various industries while minimizing risks and costs associated with potential system failures.

To simulate the realistic effects of the exoskeleton mechanism in experimental environments, we utilized the Adams simulation software for modeling, as depicted in Figure 8.1. In order to strike a balance between accuracy and computational efficiency while capturing the key characteristics of the SRE mechanism, we chose to employ only four rotation pairs for the segments of the SRE in Adams.

During the modeling process, we placed the SRE within an environment that replicated a real gravitational-magnetic field. The end effector was subjected to a load equivalent to the weight of an average adult male's leg. Torsion springs were incorporated into each revolute joint to minimize collision impacts. The torsion springs not only prevented undue stress but also ensured that steering forces acting on one side were evenly distributed on both sides of the operating point. Multiple torsion springs were collocated to effectively disperse the force exerted on the end.

Pulleys were introduced to guide the rope directions. By incorporating these features into our simulation, we obtained more accurate and reliable results that mirrored the behavior of the exoskeleton mechanism in real-world applications. This is particularly critical for further development and optimization of the exoskeleton mechanism, aimed at assisting individuals with mobility impairments and other disabilities.
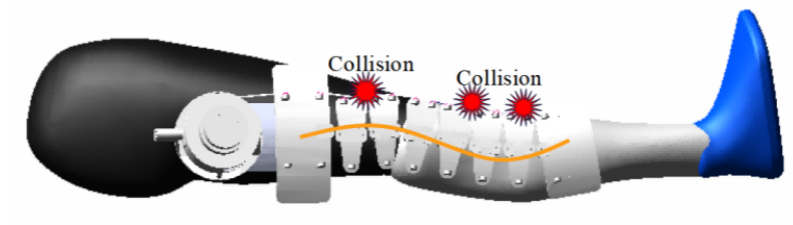


Fig. 8.1 Failure"S-shaped"Curve of the SRE Model

The simulation results, obtained with well-configured gravitational-magnetic fields and loading conditions, clearly demonstrate the presence of an "S-shaped" curve in the movement process of the SRE mechanism, as depicted in Figure 8.1. Additionally, the figure illustrates the posture of each revolute joint during the end's movement towards the target curve, without optimization. This phenomenon arises due to the increased torque experienced by the steering pulleys, to which the ropes attaching the final end effector are connected. Consequently, the traction on the end components, combined with the flexibility of the multiple revolute joints in the middle segments, leads to the formation of the "S-shaped" curve.

To address this issue, the optimal solution involves adjusting the parameters of the torsion spring at the revolute joint. By modifying the configuration of multiple torsion

spring parameters, it becomes possible to effectively disperse the force acting on the end effector, thereby reducing the curvature of the "S-curve" and achieving the desired state.

By incorporating these simulation findings into the design optimization of the SRE mechanism, we can enhance its accuracy and stability, thus increasing its potential to assist individuals with mobility impairments and other disabilities. Furthermore, this highlights the significance of utilizing simulation software such as Adams to optimize the performance of complex systems before their implementation in real-world applications.

Before optimizing and adjusting the torsion spring parameters of the SRE mechanism, we conducted tests to observe the changes in rotation angles of each rotational joint, as illustrated in Figure 8. The points where the curve transitions to horizontal lines in Figure 8.2 represent the collision points that contribute to the formation of the observed "S-shaped" curve in the mechanism's movement. It is evident that collisions initially occur in the last few segments and progressively propagate, negatively affecting the mechanism's design.

Moreover, these collisions have secondary detrimental effects on the rehabilitation process of stroke patients. Hence, it is imperative to minimize or eliminate such collisions during the design stage of the SRE mechanism through optimization and adjustment of torsion spring parameters. By doing so, we can enhance the effectiveness of the mechanism in providing assistance and support to individuals with mobility impairments, including stroke patients. Leveraging these simulation results enables us to achieve a more reliable and stable SRE design, offering favorable health outcomes for medical patients.
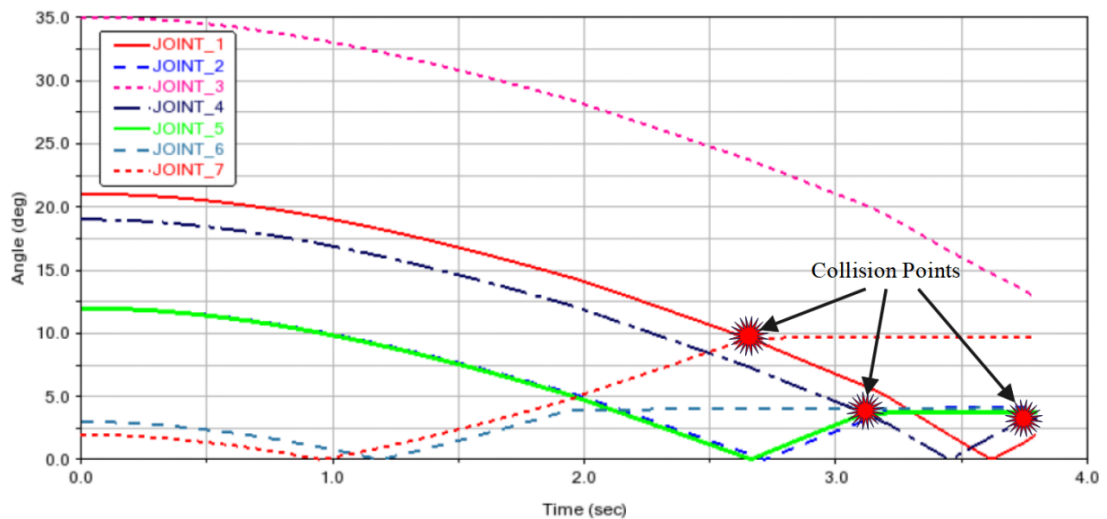


Fig. 8.2 Angle Changes of Each Revolute Joint with Time before Optimization

Based on the simulation results, it is evident that the configuration of torsion springs with different parameters significantly affects the practical effectiveness of the SRE mech-

anism for patients. However, employing manual debugging methods to determine the optimal configuration of torsion spring parameters can be time-consuming and inefficient.

In order to minimize the occurrence of the "S-type" curve and reduce its curvature, we utilized particle swarm optimization (PSO) in MATLAB to select the parameters. The PSO algorithm is a metaheuristic optimization technique that can rapidly search for the optimal solution in a high-dimensional space. To implement this approach, we set the target curve as the optimization objective and iteratively adjusted the torsion spring parameters until the objective was met.

By employing the PSO algorithm, we were able to automate the process of selecting the optimal configuration of torsion spring parameters, saving time and improving efficiency. This approach enables us to achieve a more precise and reliable SRE mechanism design, enhancing its performance in assisting patients with mobility impairments.

## 8.2.2 Motion Trajectory optimization of the SRE by Using the PSO Algorithm

The Particle Swarm Optimization (PSO) algorithm is widely used in various fields due to its robustness, simplicity, and fast convergence rate. It draws inspiration from the social behavior of bird flocking or fish schooling, where individuals interact with each other to collectively find the optimal path towards a common goal.

In the PSO algorithm, particles represent potential solutions in the search space, and each particle has a velocity that determines its direction and speed towards the optimal solution. The algorithm evaluates the fitness of each particle's position iteratively, updates the particle's velocity based on its own experience and the best solution found so far, and moves the particle to a new position. This process continues until a suitable stopping criterion is met, such as reaching a predetermined number of iterations or achieving the desired level of accuracy.

PSO belongs to a class of intelligent optimization algorithms. Similar to ant colony algorithms and fish swarm algorithms, PSO combines individual best values with an overall best value to achieve optimization step by step. It starts with an initial random solution and seeks the optimal solution by iteratively evaluating an objective function. Moreover, PSO incorporates a special memory function that enhances the efficiency of our optimization method.

PSO has wide-ranging applications and can be used to solve optimization problems in various domains, including those with complex and high-dimensional search spaces. It has found extensive use in engineering design, financial analysis, image processing, healthcare, and many other fields.

In the specific context of optimizing the SRE mechanism, PSO was employed to select the optimal torsion spring parameters. The objective was to reduce the curvature of the "S-shaped" curve and enhance the reliability and stability of the mechanism. By utilizing the PSO algorithm, we were able to quickly and efficiently find an optimized solution, thereby improving the performance of the SRE mechanism in assisting stroke patients and individuals with mobility impairments.

Theoretical analysis indicates that, when no external load is acting on the SRE mechanism, the optimal solution occurs when each rotation axis rotates at the same angle. However, when the mechanism is subjected to external loads, as well as gravitational or magnetic fields, its behavior becomes unpredictable, making it challenging to optimize using manual methods alone.

To address this challenge, we applied the PSO algorithm to optimize the SRE mechanism under these dynamic conditions. The PSO algorithm effectively explores the design space and enables us to identify the optimal configuration of torsion spring parameters, minimizing the impact of external loads and gravitational or magnetic fields. By implementing this approach, we can improve the stability and reliability of the mechanism, ensuring its efficacy in supporting stroke patients and individuals with mobility impairments.

Then, we can translate the base coordinate system to the working coordinate system of the robot, and this translation formula can be expressed as follows:

$$P_b = RP_t + T \tag{8.1}$$

Where $P_b$ represents the coordinate of point $P$ in the base coordinates of the robot, which can change with robot position changes; $P_t$ represents the coordinate of point $P$ in the robot working coordinates, which is not affected by the posture of the robot end effector; $R$ represents the rotation matrix from the working coordinates to the base coordinates; and $T$ represents the column vector from the working coordinates to the base coordinates. $T$ and $R$ were calculated in the kinematic analysis in the above section.

The most important advantage of the PSO algorithm is the application of velocity update and position update formulas, which can be expressed as follows:

$$v_i = \omega \cdot v_i + c_1 \cdot r_1 \cdot (p_{best,i_p} - x_i) + c_2 \cdot r_2 (g_{best,i} - x_i) \tag{8.2}$$

Where $i_p$ is a particle; $\omega$ is the inertia factor; $c_1$ and $c_2$ represent different acceleration coefficients; $r_1$ and $r_2$ represent two independent random numbers generated in the interval

[0,1]. From this formula, the *i*th particle is directed toward the locally optimal individual particle $p_{best}$ and the globally optimal individual particle $g_{best}$.

$$x_i = x_i + \lambda \cdot v_i \tag{8.3}$$

Where *i* represents a particle, $v_i$ represents the current velocity of the particle, and $\lambda$ represents the time length applied.

By incorporating information from both the global best point and local best point, the PSO algorithm exhibits a significantly improved convergence speed, thereby enhancing optimization efficiency. In the PSO mechanism, each particle in the population is assigned a designated personal best position, and their velocity and position are updated based on the overall optimal solutions identified thus far. This enables the algorithm to quickly converge towards an optimal solution for any given problem, making it an exceptionally efficient optimization method.

To address our specific problem, we adopted a reference system that considered the configured position, speed, and fitness values. Our objective was to minimize the angular difference between each joint, and multiple iterations were conducted using the PSO algorithm to achieve the optimal solution. Consequently, the objective function can be defined as follows:

$$F = (ABS(AX(MAR_{A8}, MAR_{A0}))) * 180/PI \tag{8.4}$$

The equation serves to assess the overall levelness of all the components within the mechanism. The closer the mechanism's shape is to a horizontal state after operation, the more accurately it reflects the actual state of the patient's lower limbs. To account for the opposite rotation angle direction to the specified positive direction, the equation incorporates Pi/2 radians.

After formulating the objective function, we proceeded with a co-simulation of the model in Adams and implemented the PSO algorithm using MATLAB for optimization. In order to obtain a compatible model file, as depicted in Fig. 8.3, we needed to rewrite the prefix function and appropriately adjust the step parameters.

Furthermore, to further validate the optimization results, we introduced test points at each revolute joint during the experiment. Subsequently, the motion curves of torsion springs with different attributes were tested and analyzed at these designated points. This rigorous process encompassed approximately 1580 minutes and involved hundreds of
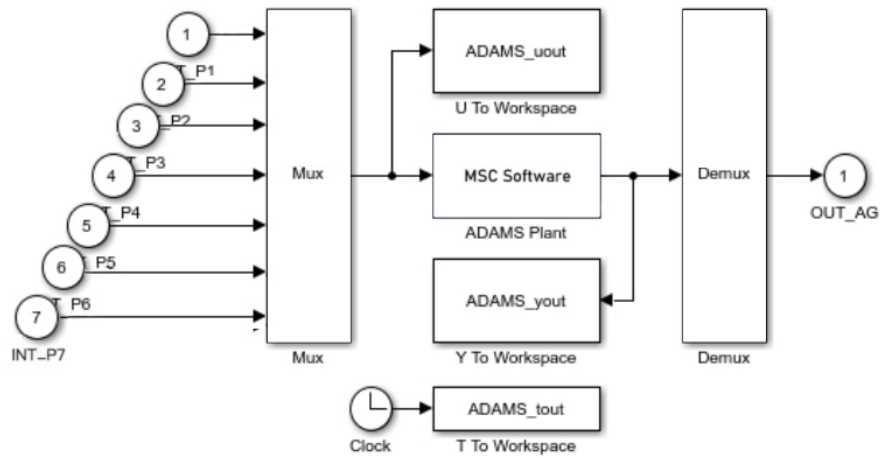
Fig. 8.3 Integrated PSO Optimization System

parameter iterations. Eventually, we obtained convergence model diagrams for each revolute joint, as depicted in Fig. 8.4.

Additionally, we generated two diagrams to showcase the effectiveness of the optimized model. The first diagram, illustrated in Fig. 8.5, represents the convergence of minimum angles achieved by the model post-optimization. This is a crucial indicator that ensures the reliability and stability of the mechanism. The second diagram, also shown in Fig. 8.5, portrays the posture of the optimized model. This indicates that our PSO algorithm successfully improved the overall levelness of the mechanism.

By comparing our optimization results with the previous analysis shown in earlier figures, we were able to visually observe the impact of multiple experimental groups on the "S-shaped" curve through the test results. Specifically, the minimum convergence angle diagram revealed that after hundreds of iterations, the total error of the seven revolute joints in the horizontal direction was reduced to just 3.104 degrees. This represents a remarkable improvement compared to the initial test results.

Our optimization approach has proven to be highly effective and efficient, as it successfully reduced the deviation rate of the overall SRE mechanism to less than 2.5

Moreover, the inclusion of torsion springs with varying attributes and the implementation of test points at each revolute joint during the experiment contributed significantly to the successful optimization of the mechanism. The results obtained from parameter iterations and convergence model diagrams clearly demonstrate that our PSO algorithm effectively minimized the differences between the angles of each joint, thereby enhancing the overall levelness of the mechanism.
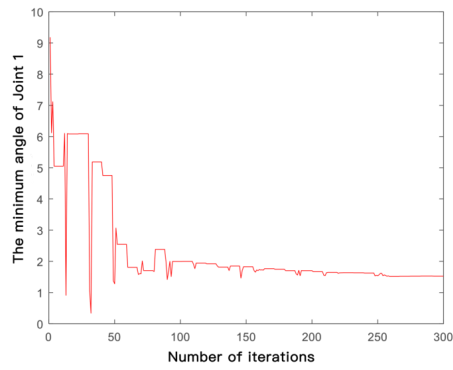
(a) The Minimum Deviatio of Joint 1
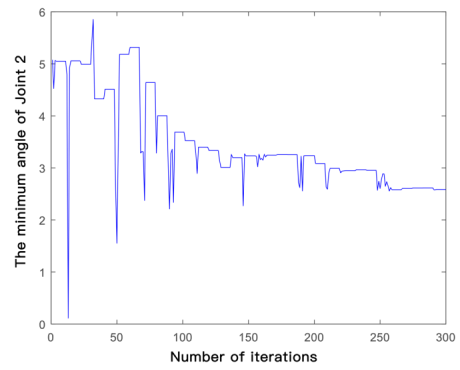
(b) The Minimum Deviation of Joint 2
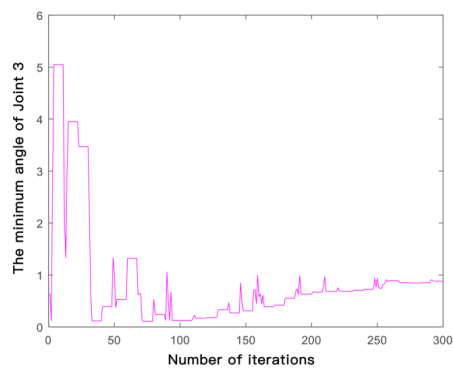
(c) The Minimum Deviation of Joint 3
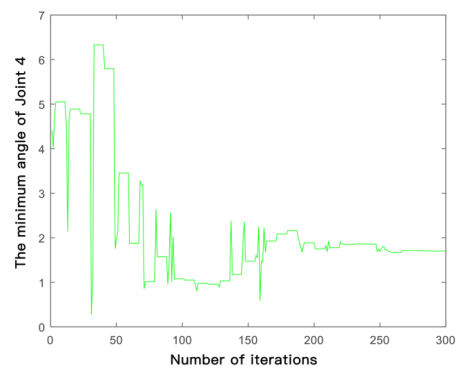
(d) The Minimum Deviation of Joint 4
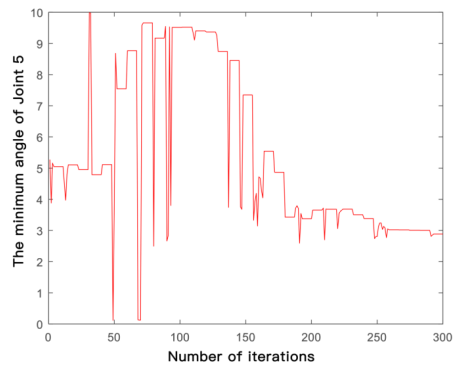
(e) The Minimum Deviation of Joint 5
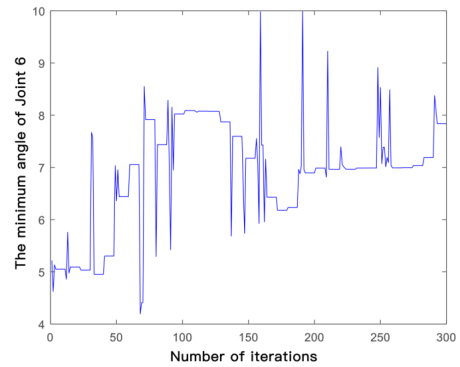
(f) The Minimum Deviation of Joint 6
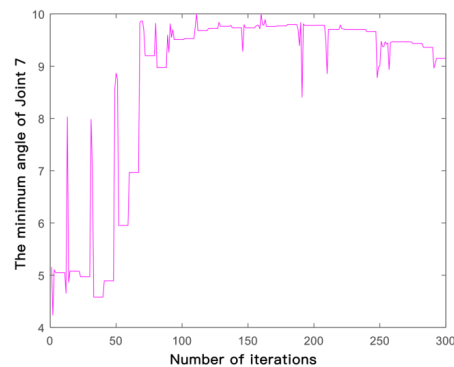
(g) The Minimum Deviation of Joint 7

Fig. 8.4 Convergence of minimum deviation of 7 joints after 300 times iterations
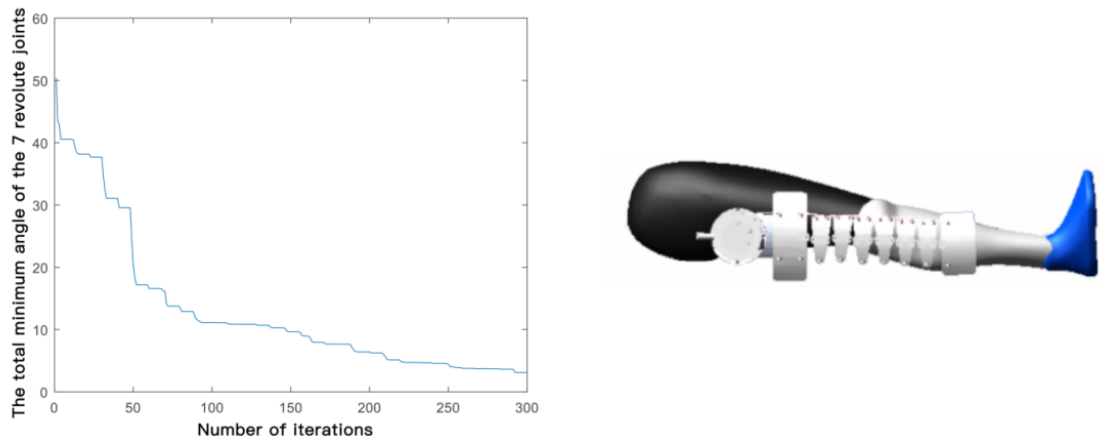
Fig. 8.5 Convergence of Minimum Angles of SRE Mechanism and Optimized Model

## 8.3 Testing Experiment of 3D Printing Model

To validate the accuracy of the optimized results prior to further processing, we conducted a printing test on the Solidworks model of the knee joint continuum using a 3D printer in our laboratory. 3D printing technology has gained widespread adoption across various fields, ranging from engineering to medical science, for prototyping and creating functional parts. Leveraging this technology allowed us to faithfully reproduce the design of the knee joint continuum and evaluate its physical properties with precision.

Furthermore, the test enabled us to identify any potential errors or issues in the design and make necessary adjustments to ensure that the final product meets our expectations. The utilization of 3D printing technology in the prototyping process offers a cost-effective and efficient approach to assess the functionality of a design concept before moving towards mass production.

Additionally, to achieve force averaging, we opted for the double torsion helical spring, as illustrated in Fig. 8.6. This choice allowed us to effectively distribute the force and enhance the performance of the mechanism.



Fig. 8.6 Double Torsion Helical Spring

### 8.3.1  Torque and Parameters Calculation of the Torsion Springs

By analyzing the previously optimized results and data obtained from the human lower limb, we conducted a thorough analysis of the stress distribution in the continuum. This analysis is presented in detail in Fig. 8.9.

Furthermore, based on our analysis, we derived a set of equations to calculate the optimal parameters for the design. These equations allow us to determine the precise values that ensure the desired performance of the knee joint continuum.

Moreover, we generated a diagram illustrating the model, which provides a visual representation of the knee joint continuum. This diagram is depicted in Fig. 8.7, offering a clear overview of the structure and components of the mechanism.
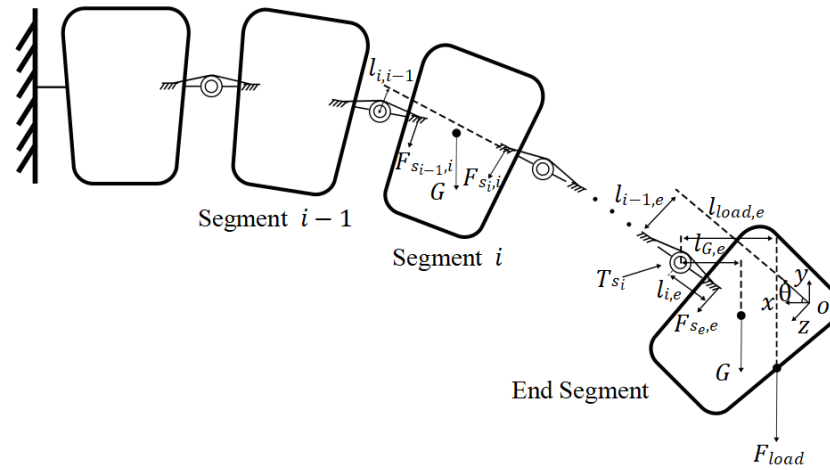


Fig. 8.7 Diagram of the Testing Model of the Knee Joint

During the rotation, the force formula could be obtained of the final segment as below at any time:

$$
\begin{cases}
F_{T,y} - F_{se,y} - m_e g - F_{load} = m_e a_y \\
F_{T,x} - F_{se,x} = m_e a_x \\
\tan\theta = \dfrac{F_{T,y}}{F_{T_x}}
\end{cases}
\tag{8.5}
$$

Then, the moment formula of the final segment also could be found:

$$
F_T l_{0,e} - M_e - m_e g l_{G,e} - F_{load} l_{load,e} = 0
\tag{8.6}
$$

205

Where, $F_{T,x}$ and $F_{T,y}$ are the torsion forces, which come from the motor, and the direction of them are along with the $x$ and $y$ axis. $F_{S_e,x}$ and $F_{S_e,y}$ are the forces, which come from the end torsion spring, and the direction of them are also along with the $x$ and $y$ axis. $m_e a_x$ and $m_e a_y$ are the combination of the mass of the end segment and the acceleration velocity along with the $x$ and $y$ axis. Next, $l_{0,e}$ means the distance between the base and the end segment, $l_{G,e}$ means the distance between the mass centre and the centre of rotational joint, while the $l_{load,e}$ means the distance from the point of loading force to the centre of rotational joint. In the meantime, the rotational angle of the end torsion spring is $\theta_e$, and $g$ is the gravity acceleration in the global environment.

As the same way, the force formula could be obtained of the arbitrarily segment $i$ as below at any time while rotating:

$$\begin{cases} F_{i,y} - F_{i-1,y} - m_{i-1}g = m_{i-1}a_y \\ F_{i,x} - F_{i-1,x} = m_{i-1}a_x \\ \tan\theta_{i,i-1} = \frac{F_{i,y}}{F_{i,x}} \end{cases} \tag{8.7}$$

Next, the moment formula of the arbitrarily segment $i$ could be found:

$$M_i = M_{i-1} - l_{i,i-1} \tag{8.8}$$

Where, $F_{i,x}$ and $F_{i,y}$ are the forces which come from the $ith$ torsion spring on the $ith$ segment along with the $x$ and $y$ axis. $F_{i-1}$ is the force which come from the $(i-1)th$ torsion spring on the $ith$ segment in this formula. The rotational angle $\theta_{i,i-1}$ between $(i-1)th$ torsion spring and $ith$ torsion spring in this time.

Finally, the overall force equation of the whole mechanism could be found as:

$$\begin{cases} F_{T,y} - \sum F_{s,y} - \sum mg - F_{load} = \sum m_{a,y} \\ F_{T,x} - \sum F_{s,x} = \sum m_{a,x} \\ \tan\theta = \frac{F_{T_y}}{F_{T_x}} \end{cases} \tag{8.9}$$

The overall moment equation of the whole mechanism could be found as:

$$F_T l_{0,e} = M_1 + ... + M_e + m_e g l_{0,e} + ... + m_1 g l_{0,1} \tag{8.10}$$

Where, $\sum F_{s,x}$ and $\sum F_{s,y}$ are the total spring forces along with the direction of $x$ and $y$ axis, $\sum mg$ is the gravity of the segments. $M_i$ indicates the moment of the $ith$ torsion spring while $M_e$ indicates the moment of the end segment. $l_{0,i}$ is the distance between the base and the forcing point of the $ith$ torsion spring. Normally, the mass of each torsion spring is the same value.

The content provided above allows for the theoretical computation of the required torque that various locations on a torsion spring need to bear. To produce appropriate torsion springs, the spring dimensions would be determined based on established principles of torsion spring design and the actual manufacturing capabilities of the factory. It is important to consider any necessary modifications or adjustments that may be required to ensure that the final product meets the desired specifications. This attention to detail guarantees that our manufactured torsion springs will be of the highest quality and meet all necessary specifications.

The force which come from torsion spring is:

$$F = \frac{(Ed^4)\varphi}{3670 * nDL} \tag{8.11}$$

Where $E$ is the modulus of elasticity, $d$ is the diameter of the torsion spring, $n$ is the number of circles, $D$ is the mean diameter which would be the average value of outside diameter, $D_o$ and inside diameter, $D_i$. $L$ is the length of the feet and the angle $\varphi$ here means the passive rotational angle of the total torsion spring. The contents of the parameters are shown in the below Fig. 8.8.
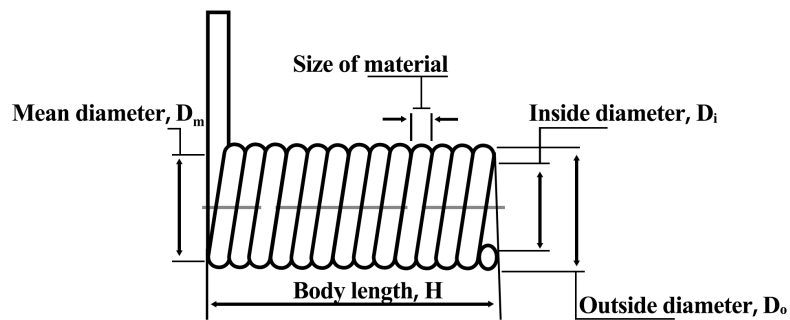


Fig. 8.8 The Parameters of the Torsion Spring

Alternatively, by utilizing the known loading force, the output value of the fixed type of motor, and the size of the mechanism, we can determine the specific parameters required for the torsion springs. These parameters encompass factors such as the torsion spring material, foot length, number of turns, diameter, inside diameter, and outside diameter.

(a) Bend State of the Testing Model    (b) Stright State of the Testing Model

Fig. 8.9 Results of the Testing Model

The equations used to determine these parameters take into account various factors like the material properties, spring wire diameter, and the number of active coils. This comprehensive approach ensures that the torsion springs deliver optimal performance and long-term reliability. By employing this methodology, we successfully designed a torsion spring that met all performance requirements while providing a robust and dependable solution for the intended application.

Overall, understanding the stress distribution and establishing the appropriate equations play crucial roles in the design and manufacturing of torsion springs. Through careful analysis and optimization of the design parameters, torsion springs can be fine-tuned to achieve superior performance, durability, and reliability across a wide range of applications, spanning from automotive and aerospace to medical devices and beyond. Detailed testing results can be found in Fig. 8.9.

To facilitate normal mechanical movement of the knee joint during rehabilitation using an exoskeleton, the design incorporates two channels capable of passing steel wire ropes. When designing the torsion spring, a certain degree of curvature is involved. Installing the torsion spring in the forward direction results in an initial curved position, equivalent to a normally bent knee. In this configuration, the device utilizes a clutch to extend the rope in the upper channel, transitioning the patient's knee from a bent to a straight state, thereby assisting in seated rehabilitation exercises.

In the second scenario, the posture of the torsion spring is adjusted, causing the mechanism to adopt a straight state. In this configuration, the clutch contracts the lower rope, facilitating a bending motion of the patient's knee. This action aids in the later stages of rehabilitation when the patient is able to walk independently.

Overall, this device provides two distinct recovery options based on the stage of rehabilitation. During the early stages, when the patient is in a seated position, the torsion spring directs its force in the forward direction, stretching the upper rope. In the later stages, when the patient is in a standing position, the torsion spring is adjusted to contract the lower rope, enabling a bending motion of the knee.

## 8.3.2  Result Analysis and Discussion

The SRE mechanism has undergone comprehensive design and simulation to ensure its flexibility and adaptability. Our 3D model design and kinematics simulation have shown that the structure closely resembles the human leg, enabling fluid movements without limitations.

Moreover, the optimization process using Adams and MATLAB co-simulation has yielded highly successful results. The final optimized SRE model achieved an impressive accuracy rate of 97.5

The mechanism design of the SRE, along with the optimization results obtained through PSO, confirm that the proposed lower limb exoskeleton rehabilitation structure meets the requirements for stroke patients. Additionally, experimental results indicate that the mechanism operates within the normal working range of human legs during testing, aligning with our expectations.

Furthermore, we conducted an analysis of the resulting curves before and after optimization, as depicted in Fig. 8.10. The comparison reveals a notable improvement in the performance of the optimized mechanism, exhibiting a more stable and precise movement pattern compared to the non-optimized model.

Fig. 8.10 illustrates an analysis of the objective function based on actual simulation and theoretical analysis of the SRE mechanism under three different scenarios. Specifically, when aligning the end-effector of the SRE mechanism with the patient's knee angle, it is essential to ensure that the center of mass of each joint aligns on the same horizontal axis. However, deviations occur due to factors such as gravity, load, and torque of the springs, resulting in variations in the center of mass of the seven revolute joints.

The red line in the figure represents the disparity between the mechanism joint and the non-optimized objective function. Conversely, the blue line depicts the discrepancy between the arbitrarily selected reference value during the optimization process and the objective function. The pink line indicates the distinction between the optimized optimal
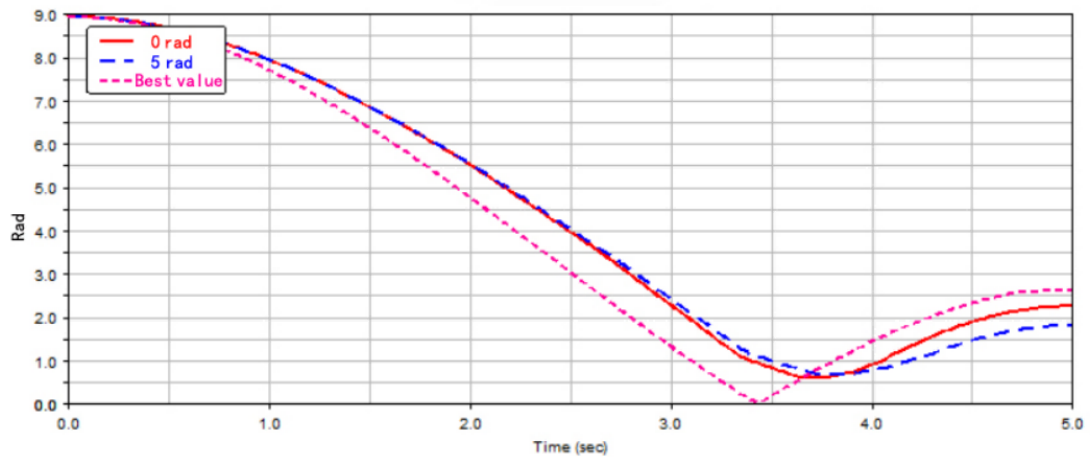
Fig. 8.10 Comparison of the Model Optimization with Different Parameters

solution and the objective function. (It should be noted that the specific parameters for the seven revolute joints were 1.526 radians, 2.586 radians, 0.880 radians, 1.701 radians, 2.888 radians, 7.838 radians, and 9.148 radians).

In the graph, the inflection point of the curve represents the cumulative absolute deviations between the rotational angles and horizontal angles when the end point is in a horizontal state. It is important to note that while the end point may be horizontal, it does not necessarily imply that every rotational joint has reached a horizontal state. Our objective is to attain horizontal alignment for all rotational joints while maintaining a horizontal end point, specifically in the straightened leg position. However, achieving perfect alignment is unattainable, resulting in some degree of deviation in each individual rotational joint. Thus, our aim is to minimize the sum of these absolute value deviations, as illustrated in the graph. Furthermore, when the optimal solution is applied for simulation in the desired state, the optimized state achieves a minimal difference of only 0.0535 radians from the objective function after 3.433 seconds of optimization. This outcome underscores the effectiveness of the optimization approach employed, significantly enhancing the accuracy of the mechanism.

In conclusion, these findings affirm the feasibility of the SRE mechanism and validate the efficacy of the optimization method employed in this study. Overall, our research emphasizes the importance of precise design and optimization of robotic mechanisms in medical applications, opening avenues for future advancements that will enhance patient care and revolutionize the field of medical robotics.

Overall, our study underscores the significance of optimizing robotic mechanisms in the medical field to foster the development and implementation of efficient and dependable technology for patient care. The optimized SRE mechanism holds immense potential to

revolutionize post-stroke rehabilitation by offering a safe and effective solution for patients. Furthermore, this study provides insights into the application of optimization algorithms to enhance the performance of existing robotic mechanisms, driving advancements in the field of medical robotics.

## 8.4 Conclusions

This chapter delves into the application of the PSO genetic algorithm to effectively tackle the challenge of the "S-shaped" curve that arises in the Adams simulation of the knee joint rehabilitation mechanism. By conducting thousands of theoretical calculations, the PSO genetic algorithm successfully identifies the optimal combination and configuration of torsion springs for the knee joint. This optimization process ensures improved performance and enhances the overall functionality of the rehabilitation mechanism.

Furthermore, the implementation of a meticulously designed 3D knee joint model serves as a crucial tool for verifying the accuracy and efficacy of the structural design and optimization outcomes. Through a comprehensive analysis of the 3D model, including stress distribution, range of motion, and mechanical behavior, the validity and reliability of the proposed solution can be thoroughly assessed.

# Chapter 9

# Configuring and Gait-Cycle Analysis of the Overall Lower Limb Rehabilitation Mechanism

## 9.1    Introduction

The synergistic combination of the ankle, knee, and hip joints would be explored to create a comprehensive lower limb rehabilitation exoskeleton. A detailed design analysis will be performed to ensure optimal functionality and compatibility between these components. Additionally, a thorough examination of the bio-mechanics and kinematics of normal human gait will guide the overall motion analysis of the lower limb in the context of rehabilitation.

Furthermore, the rehabilitation movements will be broken down into two main categories: the recovery of normal gait and the rehabilitation of other specific movements. By deconstructing and analyzing these movements, we can better understand the rehabilitation process and tailor the exoskeleton's functionality to meet the specific needs of each movement.

By comprehensively examining the integration, design analysis, motion analysis, and movement decomposition of the lower limb rehabilitation exoskeleton, this chapter aims to provide valuable insights and guidance for the development of effective and functional rehabilitation devices.

## 9.2   Gait-Cycle of Normal Human Movement

### 9.2.1   Overview of Human Anatomy

Through medical anatomy analysis and a review of relevant literature on rehabilitation kinematics, a thorough examination of the lower limb joints in the human body has been conducted. In three-dimensional space, the sagittal plane, coronal plane, and horizontal plane serve as orientation reference planes for human movement. The corresponding reference axes are the sagittal axis, coronal axis, and vertical axis, as depicted in Fig. 9.1.
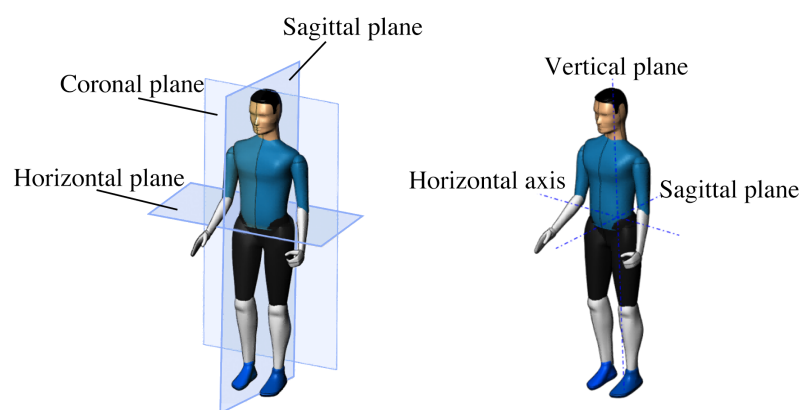


Fig. 9.1 The orientation reference planes based on human anatomy

Understanding these planes and axes is crucial for analyzing human locomotion and developing effective rehabilitative strategies. Each joint in the lower limb exhibits specific movements within these planes, and a comprehensive understanding of these movements is essential for devising successful treatment approaches.

In the sagittal plane, flexion and extension movements occur at the hip, knee, and ankle joints, while adduction and abduction movements take place at the hip joint in the coronal plane. Conversely, the ankle joint demonstrates inversion, eversion, and internal/external rotation movements in the horizontal plane.

Accurate analysis and assessment of lower limb joint movements can greatly contribute to the development of targeted interventions aimed at improving mobility and functional outcomes for individuals with lower limb injuries or neurological impairments. Additionally, factors such as muscle strength, range of motion, balance, and gait patterns must be considered when planning rehabilitation programs. By incorporating a comprehensive understanding of human kinematics and anatomy into rehabilitative strategies, it becomes possible to optimize outcomes and enhance the quality of life for individuals seeking to recover from lower limb impairments.

The definitions of the three anatomical planes are as follows:

Sagittal plane: A plane that passes through the body's central axis of symmetry, dividing the body into two symmetrical halves.

Coronal plane: A plane that passes through the body's central axis of symmetry, dividing the body into anterior and posterior portions.

Horizontal plane: A plane that passes through the body's center of gravity, dividing the body into upper and lower portions.

The intersection of any two of the three anatomical reference planes generates three reference axes:

Sagittal axis: An axis formed by the perpendicular intersection of the sagittal and horizontal planes. It passes through the joint center and has a horizontal anterior-posterior direction.

Horizontal axis: An axis formed by the perpendicular intersection of the coronal and horizontal planes. It passes through the joint center and has a horizontal medial-lateral direction.

Vertical axis: An axis formed by the perpendicular intersection of the sagittal and coronal planes. It passes through the joint center and has a vertical upward direction.

Understanding these anatomical planes and reference axes is crucial for accurately analyzing human movement and designing effective rehabilitation strategies. By considering the specific movements within each plane and the corresponding axes, healthcare professionals can develop targeted interventions to address impaired joint function and facilitate recovery.

This chapter offers a detailed and comprehensive overview of the movement characteristics observed in the hip, knee, ankle, and toe joints of the lower limb. To aid in comprehending the directional movements of these joints, symbol definitions have been provided. Furthermore, the chapter includes an overview of the functional movements associated with each joint, which is illustrated in the accompanying diagram (refer to Fig. 9.2).

The hip joint exhibits flexion/extension movements in the sagittal plane, adduction/abduction movements in the coronal plane, and internal/external rotation movements in the horizontal plane. These movements allow the hip joint to bear weight and maintain stability during locomotion.

The knee joint is a hinge joint primarily responsible for flexion/extension movements in the sagittal plane, which are vital for activities like walking, running, and jumping. While the knee joint has limited rotational and lateral movement capabilities, its primary function is facilitating flexion and extension.

The ankle joint is a complex joint that enables dorsiflexion/plantarflexion movements in the sagittal plane, inversion/eversion movements in the coronal plane, and prona-
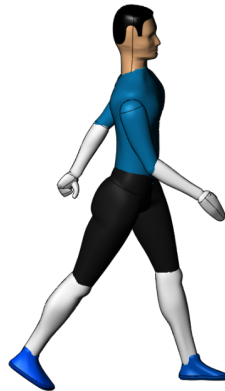
Fig. 9.2 Human Motion Model

tion/supination movements in the horizontal plane. These versatile movements play a crucial role in maintaining balance, stability, and shock absorption during weight-bearing activities.

The toe joints contribute to support and stability during push-off during gait. The metatarsophalangeal joint allows for extension/flexion movements, while the interphalangeal joints enable flexion/extension as well as abduction/adduction movements.

Having an understanding of the movement characteristics and functional roles of the different joints in the lower limb is essential for developing effective rehabilitation programs and preventing injuries. Healthcare professionals can utilize this knowledge to design interventions that target specific weaknesses or imbalances, thereby improving overall mobility and enhancing the quality of life for their patients.

### 9.2.2 Gait-Cycle Experiment and Data Collection

In the preliminary design stage of developing a lower limb exoskeleton for stroke patients, this study incorporated a gait experiment plan. The objective was to gather motion-dynamic data for the hip, knee, and ankle joints during the gait cycle of a healthy individual. This data aimed to provide insights into the geometric parameters and motion dynamics performance targets for the lower limb exoskeleton.

To accomplish this, a motion capture system utilizing multiple optical cameras (Motion-Analysis, USA) was employed [43]. Six high-definition optical cameras were strategically positioned to track markers affixed to the human lower limb. The spatial position data of these markers, captured by the cameras, was transmitted to the computer terminal through the image processing unit. On the computer terminal, information fusion and image data processing techniques were utilized to derive continuous spatial coordinate positions and real-time three-dimensional motions of the measured objects in the time domain.

Table 9.1 Details of Testing

| Equipment | Motion capture system | AMIT | Natrox |
|---|---|---|---|
| Sensor | Labeled Spheres | Force transducer | Myocardial electrode |
| Signal capture | Infrared HD camera | - | - |
| Data transfer | Cable | Cable | Wireless |
| Data processing | Host computer | Synchronization | Synchronization |

The Motion Analysis motion capture system utilizes optical cameras to accurately capture the spatial position changes of fluorescent markers attached to the human body. By tracking these markers, the system is able to calculate essential motion information for each joint involved in the gait cycle, including position, velocity, and acceleration.

Additionally, the AMIT 3D force measurement system employs pressure sensors to measure changes in foot pressure, also known as ground reaction force, during walking. By integrating the joint motion information with foot pressure parameters, this system can calculate the force and torque exerted on each joint during the gait cycle.

Furthermore, the Natrox electromyography (EMG) testing device monitors muscle activity during walking by attaching electrodes to the surface of the muscles. This allows for a direct correlation between joint movement and muscle activity within the human body.

These advanced technologies provide a comprehensive approach to understanding the biomechanics of human gait. By combining data from multiple sources, including joint positions and forces, ground reaction forces, and muscle activity, researchers are able to gain a more complete understanding of the complex relationships between different elements of human movement.

This knowledge serves as a foundation for designing rehabilitation devices, such as lower limb exoskeletons, that are tailored to the specific needs of patients. These devices can provide effective training and support for individuals with various gait-related conditions, improving their mobility and overall quality of life.

The detailed information of the testing equipment used in gait tests is shown in the Tab. 9.1 [43]:

Prior to conducting gait tests, it is crucial to ensure proper placement of markers on the lower limbs. By analyzing the continuous spatial position of these markers during the gait cycle, motion parameters for each joint of the lower limb can be determined.

In the initial stage of the gait experiment, 19 markers are attached to specific positions on the subject's lower limbs. It is important to calibrate the motion capture system before commencing the experiment. The subject remains stationary for 30 seconds within the gait experiment area, allowing the capture of marker data in a static state. This data serves as the reference for the experiment.

During the gait experiment, joint motion data of the subjects is collected and statistically analyzed using the baseline established from the reference static state. To ensure accurate analysis of knee and ankle joint motion data post-gait test, four markers should be removed before beginning the experiment.

By adhering to these procedures, we can obtain reliable and precise data on joint motion during the gait cycle, facilitating a comprehensive understanding of the biomechanics involved.

### 9.2.3   Dynamic Characteristics of Human Lower Limbs

During gait analysis, the motion capture system accurately captures the joint angles of lower limb joints and calculates their range of motion. This information is crucial for assessing the quality of the gait pattern and identifying any abnormal motion characteristics. Additionally, analyzing the spatial position of the body's center of gravity provides insights into the subject's balance control ability.

The stance phase of the gait cycle can be further divided into three sub-phases. First is the initial contact phase, where the heel initially contacts the ground. Next is the loading response phase, where the foot flattens against the ground and the body weight shifts over the stationary foot. Lastly, the mid-stance phase occurs as the body weight moves over the supporting foot in preparation for toe-off. The swing phase commences with toe-off, where the foot lifts off the ground, followed by the acceleration phase as the leg swings forward, and then the mid-swing phase as the knee reaches maximum flexion. Finally, the deceleration phase begins as the knee starts to extend, and the terminal swing phase concludes when the foot makes initial contact with the ground again.

In summary, gait analysis using the motion capture system provides valuable information about lower limb kinematics, as well as the subject's balance control abilities. This data can be utilized for diagnosing and treating gait abnormalities, as well as designing effective rehabilitation programs.

# 9.3 Mechanism Configuration and Gait Analysis of the Overall Lower Limb Exoskeleton Rehabilitation Mechanism

## 9.3.1 Configuration of the Overall Lower Limb Rehabilitation Mechanism

Based on the analysis of human lower limb data, the length of the calf of healthy adult subjects was found to be 375mm, with a cross-sectional width of approximately 150mm. Through gait experiments, data was collected and analyzed to determine the range of motion of the lower limb joints in the sagittal plane, the degrees of freedom of lower limb joint motion, and the range of rotation under normal joint movement conditions, as shown in Fig. 9.3 below:
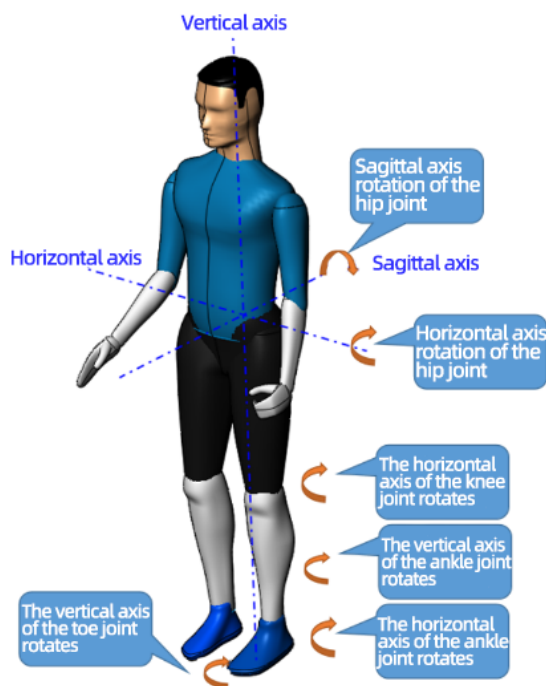


Fig. 9.3 The State of Rotational Joints in Human Lower Limbs

As shown in the Tab. 5.4 below, the degrees of freedom and range of motion for the hip joint, knee joint, and ankle joint in human lower limbs have been clearly identified. These data came from the tests by the motion capture system mentioned in chapter 4. This provides design requirements for the overall structure and kinematics of lower limb exoskeletons in the early stages of rehabilitation training.

Table 9.2 Relative Mass Distribution of Each Part of the Human Body

| Joints | State | Maximum Angle | Testing Angles |
|---|---|---|---|
| Hip | Flexion-Extension | $-100° \sim 20°$ | $-21.55° \sim 22.50°$ |
| | Adduction-Abduction | $-30° \sim 40°$ | $-7.05° \sim 6.10°$ |
| Knee | Internal-External Rotation | $-40° \sim 40°$ | $-3.45° \sim 2.31°$ |
| | Flexion-Extension | $-130° \sim 5°$ | $-69.76° \sim 0.88°$ |
| Ankle | Internal-External Rotation | $-35° \sim 35°$ | $-14.25° \sim 14.25°$ |
| | Dorsiflexion-Plantarflexion | $-40° \sim 45°$ | $-8.87° \sim 14.26°$ |
| Toe | Inversion-Eversion | $-40° \sim 35°$ | $-12.45° \sim 1.02°$ |
| | Flexion-Extension | $-35° \sim 75°$ | $-2.25° \sim 68.12°$ |

This analysis provides valuable information for the design and development of lower limb exoskeletons that aim to emulate human joint movement. By understanding the degrees of freedom and normal range of motion for lower limb joints, designers can ensure that their exoskeleton mechanisms effectively and safely support natural human movement, leading to improved rehabilitation outcomes for people with lower limb injuries or disabilities.

Due to its simple structure and multi-degree-of-freedom motion characteristics, this chapter proposes the use of a series-parallel structure in the design of lower limb exoskeletons. The structure utilizes a two-degree-of-freedom hip joint passive-active interaction system to accommodate the flexion-extension and abduction-adduction movements of the human lower limb hip joint. The knee joint is connected in series with a single degree of freedom rotational structure, while the ankle joint adopts a series three-axis rotational structure with three degrees of freedom, enabling inversion-eversion and dorsiflexion-plantarflexion movements of the ankle joint. Furthermore, the last degree of freedom is provided by the freedom of motion of the toes at the metatarsophalangeal joint, which complements the horizontal axis rotation of the ankle joint during locomotion. The simplified structural diagram is shown in Fig. 9.4.

The following Fig. 9.5 shows the design model of a series-connected lower limb exoskeleton rehabilitation device, which consists of three main components: the hip joint, knee joint, and ankle joint. The hip joint is a series mechanical structure that has two degrees of freedom for flexion-extension and abduction-adduction movements, as well as an active deceleration motor and a passive nitrogen spring energy storage structure for interaction. The knee joint is a segmented rotating degree of freedom structure driven by a linear cable, which can flex and extend to accommodate various leg shapes. Finally, the ankle joint adopts an active motor gear drive and heel spring energy storage structure, which can store energy during the lower limb rehabilitation training of stroke patients and reduce energy consumption.
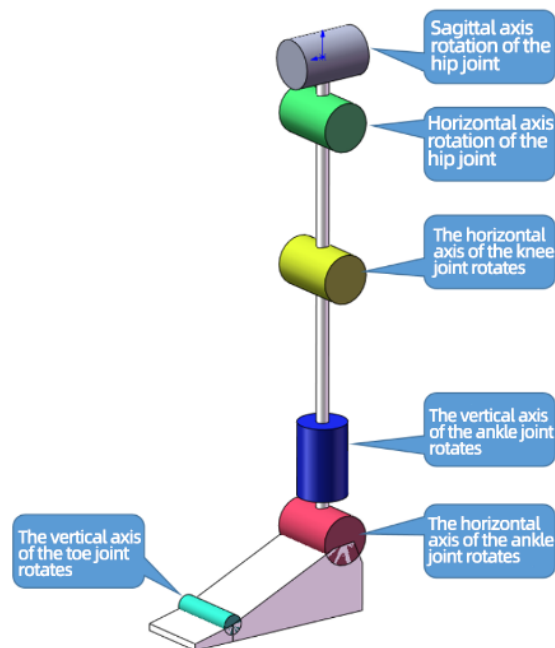
Fig. 9.4 Diagram of the Overall Lower Limb Exoskeleton Rehabilitation Mechanism

By utilizing this series-connected design, the lower limb exoskeleton rehabilitation device can better replicate natural human lower limb biomechanics, thus providing more effective and efficient rehabilitation outcomes for individuals with lower limb injuries or disabilities. The hip joint's active deceleration motor and passive nitrogen spring energy storage structure provide enhanced control and stability during movement, while the knee joint's segmented rotating degree of freedom structure allows for greater adaptability to various leg shapes. The ankle joint's active motor gear drive and heel spring energy storage structure not only enable inversion-eversion, dorsiflexion-plantarflexion movements, but also assist in absorbing shock and reducing energy consumption during locomotion.

This study explores the application of simplified series-connected mechanical structures with multi-degree-of-freedom motion characteristics and high load-bearing capabilities in the design of lower limb exoskeletons. The design also takes into account energy-saving modes of active and passive interaction, allowing for optimal motor performance and reduced energy consumption. To simulate the lower limb exoskeleton's series-connected multi-degree-of-freedom active and passive interaction mechanism, the exoskeleton combined by the three main parts mentioned in chapter 5 was virtually worn on the lateral side of a human leg, as shown in Fig. 9.6 below:

To verify the kinematic design rationality of the multi-degree-of-freedom series-connected structure and its feasibility in lower limb exoskeleton mechanisms, this section establishes a kinematic model and conducts motion characteristic and mechanical performance analysis based on theoretical derivation and simulation.
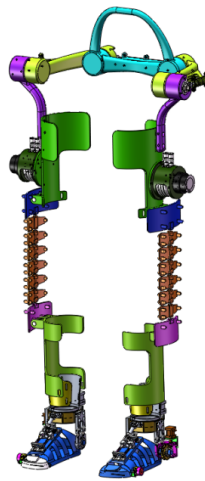
(a) The Overall Lower Limb Exoskeleton Rehabilitation Mechanism
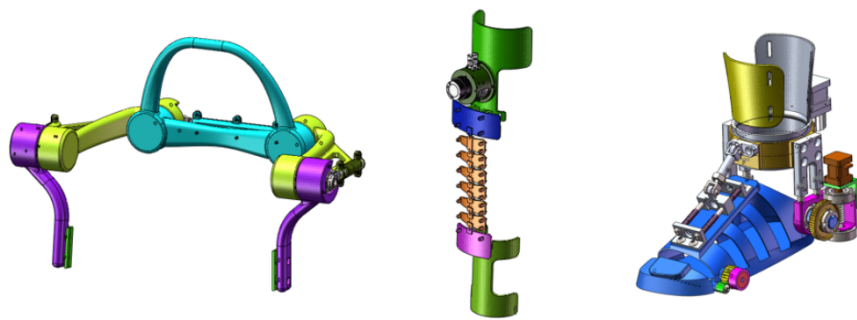


(b) Each Main Part of the Overall Rehabilitatinno Mechanism

Fig. 9.5 Structure of the Overall Rehabilitation Mechanism
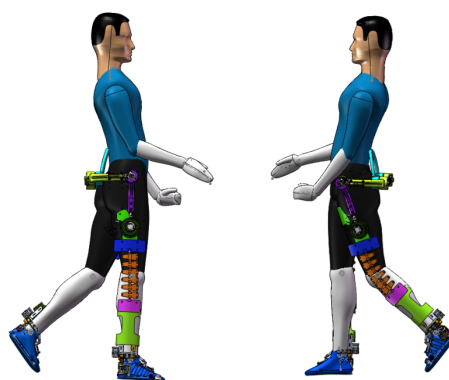


(a) Upright State    (b) Bending State

Fig. 9.6 The Different States of the Exoskeleton Accompanying with the Unilateral Lower Limb

Assuming that the initial position of the end of the joint series-connected structure is identical to the stationary platform, when the moving platform completes arbitrary rotation in space, the final posture can be obtained by the Euler angle representation method to obtain the final rotation matrix. Assuming the position vector $\mathrm{p} = [x_p, y_p, z_p]$ about the fixed coordinate system, the expression for the position vector $A_i$ and $B_i$ with respect to the fixed coordinate system is derived:

$$a_1 = [a \quad 0 \quad 0]^T; \mathrm{b}_1 = [b \quad 0 \quad 0]^T \tag{9.1}$$

The closed-loop equation of the end in this mechanism is:

$$a_i + l_i s_i = p + b_i \tag{9.2}$$

Translation: In the equation, $s_i$ is a unit vector pointing in a certain direction from $a_i$ to $b_i$, $b_i$ is the end vector which can be obtained through derivation $b_i = R_B^A b_i^p$, and $l_i$ is the length of the actuator.

The dexterity of the mechanism based on the multi-degree-of-freedom series-connected structure is evaluated to determine if there are singularity problems that occur in the reachable workspace of the operating end of the mechanism, and the feasibility of using it in the kinematic aspect of lower limb exoskeleton rehabilitation mechanisms is verified. Generally, the dexterity of the series-connected structure can be obtained by calculating the condition number of the Jacobian matrix constructed by the structure, as follows:

$$\mathrm{k}(J) = \frac{\lambda_{max}}{\lambda_{min}} \tag{9.3}$$

In the equation, $\mathrm{k}(J)$ is the condition number, and $\lambda_{max}$ and $\lambda_{min}$ are the maximum and minimum eigenvalues obtained by the Jacobian matrix.

Based on the measured geometric dimensions of the calf, the length of the parallel mechanism was determined to be . Due to the limited use of internal and external rotation of the knee joint in daily movements, the dexterity analysis of the mechanism only refers to one position of the mechanism in humanoid movement, as shown in Fig. 9.7.

Furthermore, the positioning of the mechanism was determined based on the typical gait pattern observed in human level walking. This position takes into account the specific angles of hip joint flexion and abduction, knee joint flexion, and ankle joint dorsiflexion. By accurately setting these joint angles, the mechanism can effectively replicate the natural motion of the lower limb during walking.
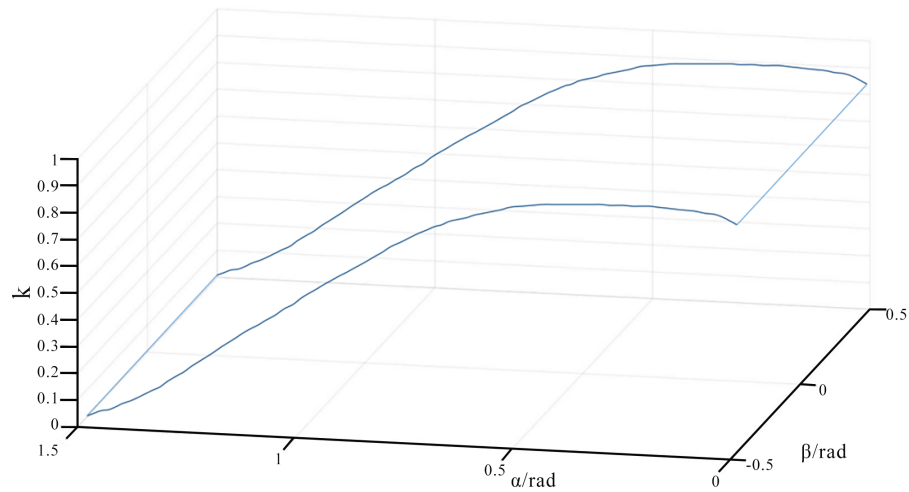
Fig. 9.7 The Dexterity Analysis of the Rehabilitation Mechanism

In addition, through the kinematic verification of the multi-degree-of-freedom series-connected mechanism, it has been established that this mechanism is well-suited for integration into lower limb exoskeleton devices, allowing for the replication of key motion characteristics of the knee and ankle joints. Furthermore, the reachable workspace of the mechanism does not exhibit any singularity phenomena, ensuring smooth and reliable operation. Moreover, when the moving platform rotates within the x-axis and y-axis range, the condition number remains between 0-1, indicating excellent motion dexterity for the parallel mechanism.

The successful validation of these characteristics further supports the applicability and effectiveness of the mechanism in lower limb exoskeletons. Its ability to replicate natural joint motion, combined with its favorable kinematic properties, makes it a suitable choice for enhancing mobility and assisting individuals with lower limb impairments or disabilities.

To conduct a comprehensive performance analysis of the lower limb exoskeleton device, we conducted mechanical performance analysis on the main load-bearing components. By utilizing a series-connected multi-degree-of-freedom exoskeleton structure, the maximum critical load during the heel contact, flat foot and toe off stages were obtained and are summarized in Tab. 9.3, these values could be obtained from different testing points in different stages

The mechanical performance analysis was conducted using advanced simulation tools, taking into account factors such as external forces, frictional forces, and material properties. The results showed that the parallel mechanism has excellent load-bearing capacity and can effectively support the weight of the human body during different stages of gait pattern.

Table 9.3 The Maximum Critical Load during Different Stage

| Stages | Maximum Critical Load |
|---|---|
| Heel Contact | 2815.8$N$ |
| Flat Foot | 2534.7$N$ |
| Toe Off | 2597.4 |

Next, we conducted stress analysis calculation using finite element method, and the deformation trend of each part under critical instability conditions can be displayed as shown in Fig. 9.8 below. The maximum load-bearing capacity of the multi-degree-of-freedom series-connected mechanism is about 2534.7N. Using this structure as the supporting body configuration of the lower limb exoskeleton device, stroke patients can ensure complete and reliable safety performance during the rehabilitation training phase.
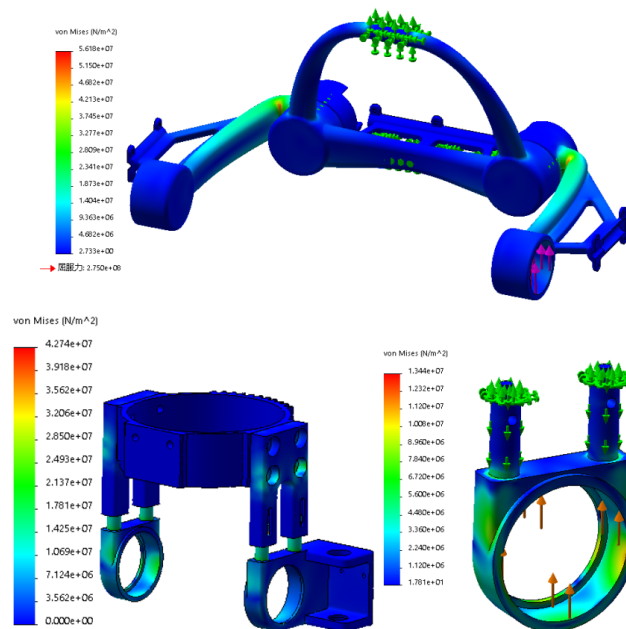


Fig. 9.8 The Stress Analysis of Each Part under Critical Conditions

The stress analysis calculation was performed using advanced simulation tools, taking into account factors such as external forces, frictional forces, and material properties. The results showed that the mechanism has excellent stability and strength, and is capable of withstanding the loads experienced during rehabilitation training.

In addition to the stress analysis calculation, we also conducted a comprehensive evaluation of the safety performance of the lower limb exoskeleton device, evaluating factors such as structural durability and control reliability. Through these analyses, we were able to ensure that the device meets the highest safety standards, providing individuals with lower limb injuries or disabilities with a reliable and effective rehabilitation tool.

## 9.3.2 Gait-Cycle Analysis

Assuming that the lower limb exoskeleton is used for gait training of stroke rehabilitation patients, the flexion-extension motion trajectory of the knee joint in the sagittal plane during one gait cycle can be obtained by curve fitting method. The parameters are as follows:

$$\begin{cases} \alpha_k = \sum_{r=1}^{10} a_r t^{10-r} \\ \beta_k = 0 \end{cases} \tag{9.4}$$

k is the rotational angle of the knee joint during flexion-extension; $\beta_k$ is the rotational angle of the ankle joint during inversion-eversion. The coefficients $a_1 = 39000$, $a_2 = -190000$, $a_3 = 390000$, $a_4 = -400000$, $a_5 = 230000$, $a_6 = -70000$, $a_7 = 8700$, $a_8 = 760$, $a_9 = -280$, and $a_{10} = -5.9$ are used in the mathematical equation with t being the gait cycle time variable, and the gait cycle interval is $\begin{bmatrix} 0, & 1.2 & s \end{bmatrix}$.

The curve fitting method was utilized to accurately model the trajectory of knee joint motion during gait training for stroke rehabilitation patients. Through detailed analysis of the motion trajectory, specific areas for improvement in the design of the lower limb exoskeleton device were identified. This involved adjustments to joint angles and increased support in targeted areas.

To further enhance the biomechanical performance of the knee joint, virtual simulation was conducted using a biomechanical model of a femoral prosthesis. The simulation encompassed various phases of gait, including heel strike, foot flat, heel off, toe off, and swing phase. By employing a multi-degree-of-freedom lower limb exoskeleton mechanism with an active and passive interaction system featuring motor-driven and spring-loaded components, significant advancements were achieved in the biomechanical performance of the knee joint, surpassing that of individuals with amputations. Furthermore, this mechanism helped alleviate the load on the hip joint, thereby enhancing the overall biomechanical performance of the hip joint during gait.

Specifically, during the heel strike and foot flat phases, the stability of the hip joint was strengthened. In the toe off phase, the load-bearing burden was reduced. These improvements contribute to the enhanced stability of stroke patients during rehabilitation training and reduce excessive metabolic energy expenditure during walking, as illustrated in Fig. 9.9.

Through the analysis of the virtual simulation results, we were able to optimize the design of the lower limb exoskeleton device, creating a practical and effective tool for stroke rehabilitation patients. The combination of motor-driven and spring-loaded components in

225

(a) The Adduction-abduction State  (b) The Flexion-extension State



(c) Different Stages in a Gait Cycle
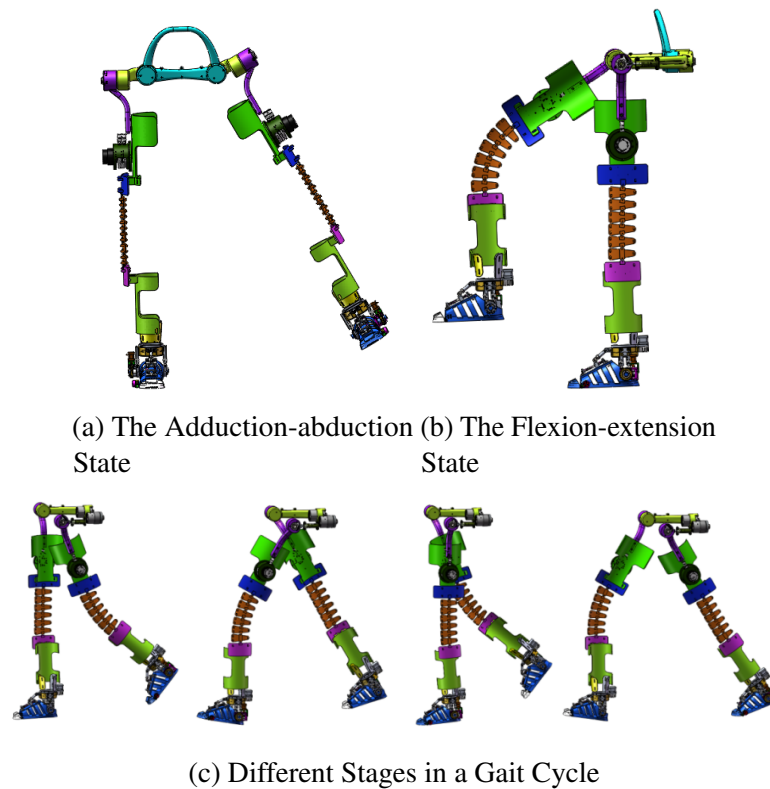
Fig. 9.9 Different Rehabilitation Stages of the Exoskeleton in a Gait Cycle

the exoskeleton mechanism provides a promising solution for the future development of prosthetic devices that improve the quality of life for individuals with lower limb injuries or disabilities.

### 9.3.3 Summary of Performance of the Overall Exoskeleton Rehabilitation Mechanism

Building upon the data collected based on the motion capture system regarding gait experiments as shown in Tab. 5.4, lower limb movements, and kinetic data, this chapter focuses on determining the structural motion and dynamic design requirements of the exoskeleton used in stroke patient rehabilitation training. Through analysis of the configuration of the lower limb exoskeleton mechanism, a multi-degree-of-freedom serial mechanism is proposed for the hip joint, knee joint, ankle joint, and toe joint, which is then validated through kinematic modeling.

In addition to assessing the feasibility of the mechanism's movement, the safe bearing capacity of its key components is evaluated using finite element analysis. Kinematic simulation is conducted to demonstrate that the mechanism effectively replicates the multi-degree-of-freedom motion function of the human knee and ankle joints. The integration

of an active driving system with a passive energy storage system enhances the dynamic characteristics of the joint while reducing the power consumption of the exoskeleton mechanism.

The analysis and simulation results confirm that the proposed exoskeleton structure is well-suited for assisting stroke patients in their rehabilitation training. The multi-degree-of-freedom design of the exoskeleton mechanism expands the range of motion for each joint in the lower limb, ultimately improving the overall performance of the mechanism. The combination of active driving and passive energy storage systems contributes to more efficient and sustainable utilization of the exoskeleton, reducing metabolic energy consumption and enhancing safety and comfort during use. This study serves as a valuable foundation for further research and development of exoskeleton technologies for clinical rehabilitation applications.

## 9.4    Conclusions

By successfully integrating the ankle, knee, and hip joints, this chapter demonstrates the versatility and effectiveness of the proposed lower limb rehabilitation exoskeleton. Each joint component has been shown to perform its intended rehabilitation movements individually, and the modularity of the design allows for seamless integration into a unified system. This comprehensive integration ensures that the exoskeleton can effectively support the rehabilitation needs of the entire lower limb. As shown in the Tab. 5.4, the maximum angle testing angles of each joint could be obtained form the experiments, including the flexion-extension state and adduction-abduction state of the hip joint, internal-external rotational state of knee joint, flexion-extension state, internal-external ratational state and dorsiflesion-plantarflexion state of ankle joint and the flexion-extension state of toes joint. From these values, we can easily compared the difference between the maximum angle and the testing angles. During the experimental process, our focus is on assisting patients in achieving the range of motion angles that can be achieved by normal testers, without necessarily aiming for maximum flexion angles. It is important to ensure that patients can perform movements within a functional and safe range, rather than pushing for extreme angles that may pose unnecessary risks or challenges during the rehabilitation process. By setting realistic goals and working within the boundaries of what is achievable for each individual patient, we can effectively promote their recovery and enhance their overall functional abilities.

Furthermore, the performance analysis of the overall lower limb exoskeleton has been conducted using the foundation of normal human gait. By evaluating the exoskeleton's functionality under the context of typical walking patterns, its ability to mimic natural

movements and provide necessary support during the rehabilitation process has been validated. Additionally, specialized rehabilitation movements have been verified to ensure that the exoskeleton meets the requirements of more specific rehabilitation protocols.

Through the rigorous examination of integration, performance analysis, and verification of specific rehabilitation movements, this chapter establishes the feasibility and effectiveness of the proposed integrated configuration. The findings provide valuable insights for the development of advanced lower limb rehabilitation mechanisms capable of supporting various rehabilitation exercises and enhancing overall recovery outcomes.

# Chapter 10

# Rendering and Prototype Analysis of the Overall Lower Limb Rehabilitation Exoskeleton Mechanism

## 10.1 Introduction

In the field of mechanical engineering, the importance of prototype fabrication, also known as prototyping, cannot be overlooked. A prototype is a functional and physical representation of a design concept or blueprint. Firstly, prototyping plays a crucial role in validating and testing designs. By creating prototypes, engineers can verify the feasibility and accuracy of their designs, as well as examine the coordination and interaction among various components. Prototypes help engineers evaluate the practicality of their design solutions, identify potential issues or flaws, and facilitate timely improvements and optimizations. This, in turn, reduces risks and costs during later stages of development and production. Secondly, prototypes serve as effective tools for showcasing and communication. Through prototypes, designers can visually demonstrate the appearance, functionality, and performance of their products to clients, investors, or other stakeholders. Prototypes enable better conveyance of design intentions and concepts, enabling others to understand the product more intuitively and enhancing their confidence and comprehension. Moreover, prototypes are vital for experimentation and testing purposes. Testing and experimentation involving prototypes provide essential data and feedback, enabling engineers to gather insights into critical aspects such as functionality, durability, and safety. This information serves as the foundation for further product improvement and refinement. Lastly, prototypes contribute significantly to market development and promotion. By producing prototypes, potential customers and market participants can have firsthand experiences with the product, providing valuable feedback and insights.

This aids in market positioning, strategy formulation, pricing determination, and sales planning. In summary, prototypes play a pivotal role in mechanical engineering. They validate designs, facilitate communication, enable testing and experimentation, and support market development. Inclusion of a discussion on the importance of prototype fabrication is necessary and valuable in research papers focused on mechanical design.

This chapter aims to present a complete prototype of the lower limb rehabilitation system based on the elastic ankle joint rehabilitation device model proposed in Chapter 5, the flexible drive knee joint rehabilitation device model proposed in Chapter 6, and the overall lower limb rehabilitation system with a two-degree-of-freedom hip joint device proposed in Chapter 7. The main content of this chapter consists of processing and rendering the established 3D simulation models to better fit the real-life human movement. Subsequently, the functionality of the entire prototype will be verified through actual processing and testing. In addition, this chapter will discuss the advantages of this lower limb rehabilitation device by comparing it with other existing rehabilitation structures. Finally, a summary of the entire prototype processing part will be provided, detailing the outcome of the project and laying out potential future improvements.

## 10.2 Rendering Animated Videos Based on Cinema4D

### 10.2.1 Introduction of Cinema4D

Cinema 4D is a highly versatile software used for 3D modeling, animation, and rendering in various industries such as film, animation, and advertising. Its rendering process encompasses an array of features and options that enable users to generate high-quality output images tailored to the specific requirements of their projects. When it comes to rendering, users have the ability to adjust parameters like lighting, materials, and camera angles within the scene to achieve a realistic representation of the created models. Moreover, Cinema 4D offers multiple rendering engines, including the Standard Renderer and Physical Renderer, which empower users to produce exceptional rendered images while providing precise control over desired effects and styles. With its comprehensive range of features and options, Cinema 4D equips users with a versatile toolkit for effortlessly creating and rendering high-quality 3D animations and still images that cater to diverse project needs.

Hence, the Cinema 4D would be employed to render the model of the lower limb rehabilitation exoskeleton put forth in the preceding chapters. By utilizing the powerful capabilities of Cinema 4D's rendering features and options, we can generate visually stunning and lifelike representations of the proposed exoskeleton model. This will allow us to visualize the design, assess its functionality, and make any necessary refinements before

proceeding with the actual fabrication and implementation stages. Consequently, we can present a comprehensive and compelling visualization of the lower limb rehabilitation exoskeleton, contributing to a better understanding of its potential benefits and aiding in the evaluation of its practicality in clinical rehabilitation settings.

## 10.2.2 Rendering Animated Videos of the Overall Lower Limb Rehabilitation Exoskeleton Mechanism

In addition to selecting materials and surface colors, we also paid close attention to the lighting setup during the rendering process. Lighting is a crucial component of the rendering process as it can have a significant impact on the final output of an image. We experimented with different lighting settings to create a dynamic and immersive environment for the exoskeleton model.

Furthermore, we also utilized motion graphics techniques to simulate the movement process of the exoskeleton during rehabilitation exercises. This involved creating keyframes for the joints and applying smooth transitions between them to create a natural and believable motion. The simulation allowed us to visually showcase the range of motion and capabilities of the exoskeleton, which is essential in the medical field where precise and accurate movements are crucial in rehabilitation exercises.

In addition to the technical aspects of the rendering process, we meticulously considered the overall design and aesthetics of the exoskeleton model. Our aim was to create a design that not only served its functional purpose but also had visual appeal. While drawing inspiration from existing exoskeleton designs, we incorporated unique features to make it distinct. We took care to strike a balance between form and function, ensuring that the exoskeleton not only performed effectively but was also visually captivating. One key element we focused on was the color scheme. The combination of red and gold was carefully chosen for several reasons. Firstly, it pays homage to the iconic Iron Man suit, which symbolizes strength, resilience, and technological advancement. This association helps to create a sense of empowerment and inspiration for the patients who will be utilizing the exoskeleton. Additionally, the red and gold color combination has inherent positive connotations, evoking feelings of determination, motivation, and optimism. By incorporating these colors into the exoskeleton design, we aspire to foster a positive mindset in patients during their rehabilitation journey. Overall, our approach to the exoskeleton design encompassed not only technical functionality but also the emotional and psychological impact on users. Through thoughtful consideration of aesthetics and incorporating elements that inspire and uplift, we aim to enhance the overall rehabilitation experience and contribute to the well-being and motivation of patients.The rendered models in different phases are presented in Fig. 10.1 and Fig. 10.2.
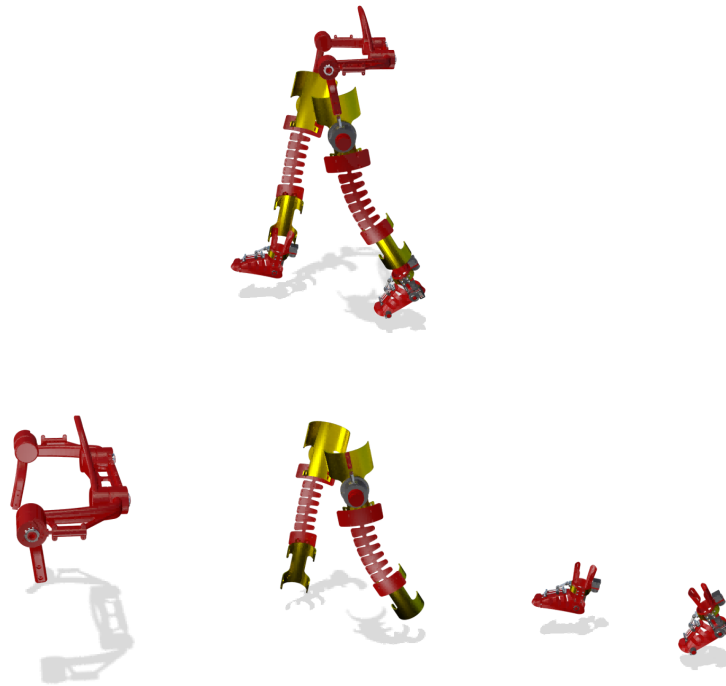
Fig. 10.1 Rendered Model in a Gait-cycle Phase

Once rendered in C4D, the model vividly presents the overall lower limb exoskeleton, highlighting its key joint components such as the hip, knee, ankle, and toe joints, as they seamlessly move through a typical gait cycle. The outcome not only captures the fluidity of each joint's motion but also exemplifies the harmonious coordination among them, perfectly aligning with our initial design vision.

In addition to observing joint movements during a gait cycle, additional capabilities of individual joints are examined.. For instance, in action 1, the knee joint can independently flex; in action 2, the ankle joint can oscillate horizontally around a central axis perpendicular to the ground; and in action 3, the hip joint can perform abduction movements of the lower limb. It's important to highlight that during the normal gait cycle, the hip joint in action 4 passively adapts its movement.

These supplementary actions significantly enhance the range of motion in rehabilitation exercises, surpassing the limitations of mere walking or sitting postures. Each rehabilitation component not only has individual mobility but can also be interconnected and combined with others, allowing for a wider variety in the rehabilitation process.

Overall, the rendering process played a vital role in prominently showcasing the capabilities and design of the exoskeleton, effectively bringing our envisioned model to life and solidifying a strong foundation for the actual prototype. By employing various tools and

(a) Action 1

(b) Action 2



(c) Action 3

(d) Action 4
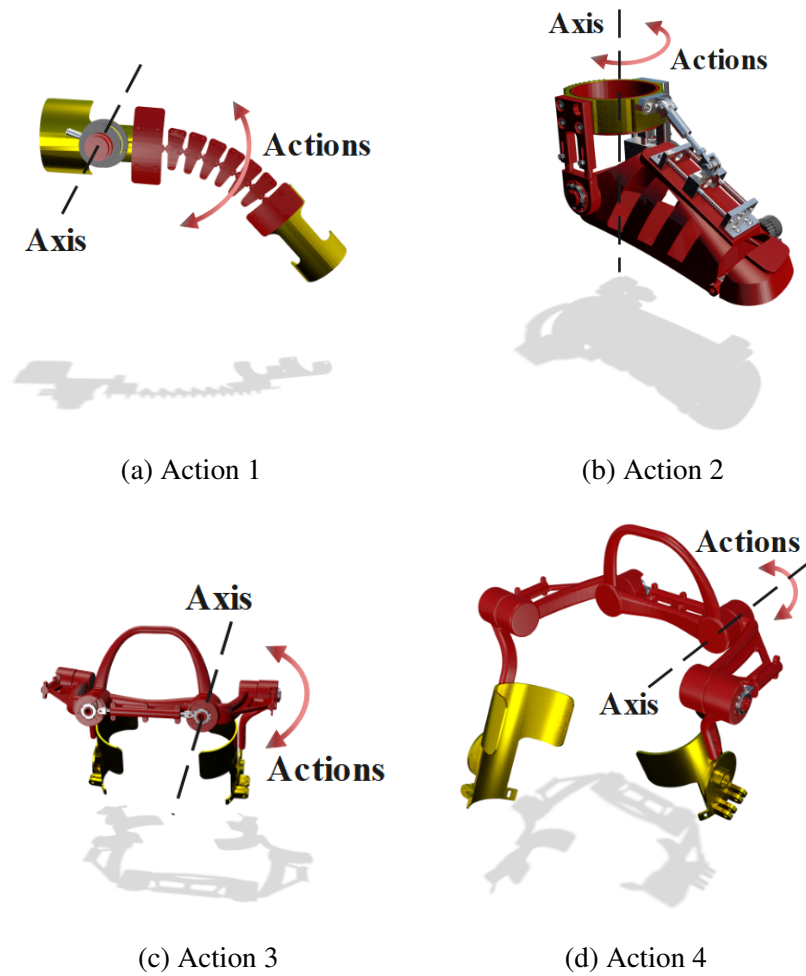
Fig. 10.2 Rendered Model in other Phases

techniques such as lighting, motion graphics, and color selection, we successfully created a high-quality and visually breathtaking output that accurately demonstrated the intended purpose and functionality of the exoskeleton. Furthermore, the rendering process enabled us to highlight key features and capture the intricate details of the exoskeleton, enhancing its visual appeal and facilitating better comprehension among viewers. Thoughtful consideration of lighting and color choices helped to accentuate the form and structure of the exoskeleton, while the incorporation of dynamic graphics added a sense of movement and adaptability.

## 10.3 The prototype of the overall lower limb rehabilitation mechanism

### 10.3.1 The Description of the Prototype

Based on the design and analysis presented in previous sections, this section aims to complete the engineering design and manufacturing process of the entire lower limb exoskeleton rehabilitation mechanism. Furthermore, a fully functional prototype is constructed, as illustrated in Fig. 10.3. The complete prototype comprises a hip joint rehabilitation structure, knee joint rehabilitation structure, and ankle joint rehabilitation structure. In order to evaluate the performance of each component, Fig. 10.4 demonstrates the wearable effect of each part.



Fig. 10.3 The prototype of the Overall Mechanism

(a) The Hip Component          (b) The Knee Component



(c) The Ankle Component
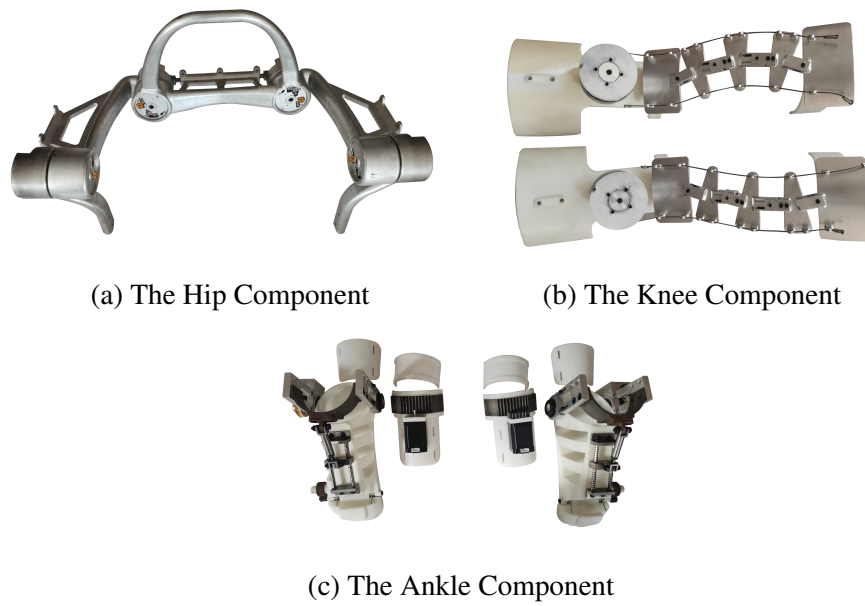
Fig. 10.4 The Prototypes of Each Component

As can be observed from Fig. 10.4, the ankle, knee, and hip joint rehabilitation structures are designed to perfectly align with human joints. Whether they are combined or functioning separately, these structures exhibit a full range of motion within the workspace.

## 10.3.2   The Determination of the Motors



Fig. 10.5 HJ14 Motor

In addition to the mechanical design, the control system and software programming played a crucial role in the engineering process of the exoskeleton. The control system encompasses the motor control system, sensor system, and communication system. These components are responsible for real-time control of the exoskeleton's movements, collection of wearer's movement and force feedback data, and smooth communication with external devices. To facilitate this, software programming was conducted using MATLAB

and Simulink software, enabling the design, testing, and simulation of control algorithms in a virtual environment prior to implementation.The majority of components in the prototype are specifically tailored by the factory, while standardized components are preferred for the connecting parts. This strategic selection facilitates convenient replacements during subsequent phases of development. By utilizing standard components, the prototype ensures compatibility and simplifies the process of swapping out parts as needed in the future.

Taking into account the specific parameters of the human body and considering corresponding dimensional constraints, we have selected the HJ14 motor for our exoskeleton. The physical model of the motor is depicted in Figure 10.5, while the mathematical physics principles underlying its operation are illustrated in Figure 10.6.
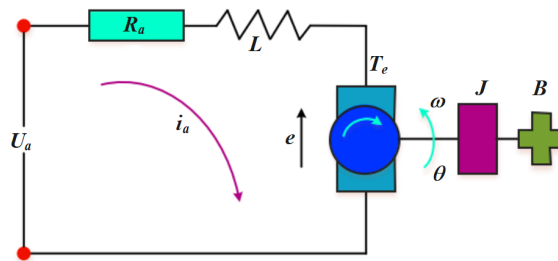


Fig. 10.6 Physical Principle of the Motor

The HJ14 motor is a high-performance, brushless DC motor that is capable of producing precise torque and speed control, making it an ideal choice for powering the exoskeleton mechanism. The HJ14 motor model is produced by TianTai Robotics Co., Ltd., a manufacturing company based in Guangdong, China. Known for their expertise in robotics, TianTai Robotics specializes in the production of high-quality motors for various applications. With their commitment to innovation and advanced manufacturing techniques, the HJ14 motor is a testament to their dedication to delivering reliable and efficient robotic solutions. And this Its compact size and high power-to-weight ratio also make it suitable for use in wearable devices such as exoskeletons. The physical model of the motor shows a cylindrical shape with multiple elements, including a stator, a rotor, and a magnetic field, that interact to produce the desired torque and speed. The mathematical physics model, on the other hand, describes the motor's behavior in terms of its electrical, mechanical, and magnetic properties, allowing us to calculate the appropriate control signals to achieve the desired motion control.

Using this motor, we can establish the following equations for the dynamic control model:

$$
\begin{cases}
U_a = Ri_a + L\frac{di_a}{dt} + e \\
e = k_b \omega_m \\
T_e = k_1 i_a \\
\frac{d\omega_m}{dt} = \frac{T_c - T_t - B\omega_m}{J}
\end{cases}
\tag{10.1}
$$

In the formula, $U_a$ represents the motor voltage; $R$ is the resistance of the motor winding; $i_a$ is the current flowing through the motor winding; $L$ stands for the motor inductance; $e$ is the back electromotive force; $k_b$ is the back electromotive force constant; $k_1$ is the torque constant; $\omega_m$ is the motor speed, which can be measured by an encoder; $T_c$ is the output torque of the motor; $T_t$ is the load torque; and $B$ is the damping coefficient.

By applying the Laplace transform to the above equation, the following equation can be obtained:

$$
\begin{cases}
U_a(s) - U_c(s) = R_a I_a(s) + sL_a I_a(s) \\
T_c(s) - T_c(s) = Js^2\theta(s) + sB\theta(s) \\
T_a(s) = k_1 I_a(s) \\
U_a(s) = ks\theta(s)
\end{cases}
\tag{10.2}
$$

By performing algebraic operations on the above equation, the transfer function of the motor can be obtained as follows:

$$
\frac{\theta(s)}{U_a(s)} = \frac{k_1}{(R_a + sL_a)(Js + B) + k_1 ks}
\tag{10.3}
$$

Overall, the choice of the HJ14 motor was based on a comprehensive analysis of various factors, including performance, size, weight, and cost, as well as consideration of the specific requirements of our exoskeleton design. With this motor and the corresponding dynamic control equations, we can ensure precise and efficient control of the exoskeleton's movements, enabling effective rehabilitation for patients.

### 10.3.3 Function Test of the Prototype

Initially, we undertook preliminary testing focused on sitting rehabilitation. This phase involved patients maintaining a seated position while performing rehabilitation exercises that primarily targeted the movement of the knee joint. Specifically, we assessed the single

degree of freedom movement of the patient's leg, which involved flexion and extension of the knee joint. The findings of these tests are illustrated in Fig 10.7 for bending state and Fig 10.8 for straight state of knee joint.



Fig. 10.7 The Bending State   Fig. 10.8 The Straight State
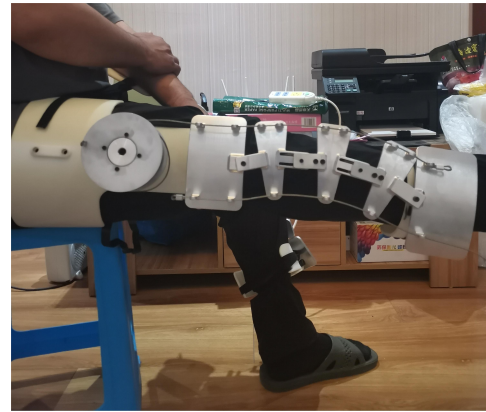
Throughout the testing process, we gathered data on rotational angle, torque, and power output to assess the efficiency and effectiveness of the exoskeleton rehabilitation mechanism. The driving force of knee joint during flexion motion is shown in Fig 10.9. The reference value in this figure came from the data obtained from the motion capture system. From the figure, The blue dashed line represents the baseline values of a participant without wearing an exoskeleton, providing a basis for comparison with the red line. The red line depicts the data recorded when the participant is wearing the exoskeleton prototype. Additionally, we closely monitored the patients' feedback and prioritized factors such as comfort, safety, and compliance during the testing procedure. All of the reference data is obtained through the motion capture system mentioned in chapter 4.

The sitting rehabilitation testing phase carries substantial significance as it offers essential insights into the potential effectiveness of the exoskeleton for patient rehabilitation. By thoroughly analyzing the gathered data and testing outcomes, we can obtain valuable information to refine the control algorithms and mechanical design of the exoskeleton. This iterative process enables us to optimize the performance and usability of the exoskeleton, making it more suitable for patients undergoing lower limb rehabilitation. Through ongoing improvement, our goal is to develop a reliable and effective tool that facilitates the rehabilitation journey and enhances the overall quality of life for individuals in need.

Subsequently, we proceeded with the testing of the exoskeleton mechanism's walking function, the tester with exoskeleton mechanism in standing state is illustrated in Fig 10.7. This testing involved a series of sequential steps:

Heel strike phase: During this phase, the hip gait simulator simulated hip flexion motion. At the maximum flexion position, the prosthetic knee and ankle joints were
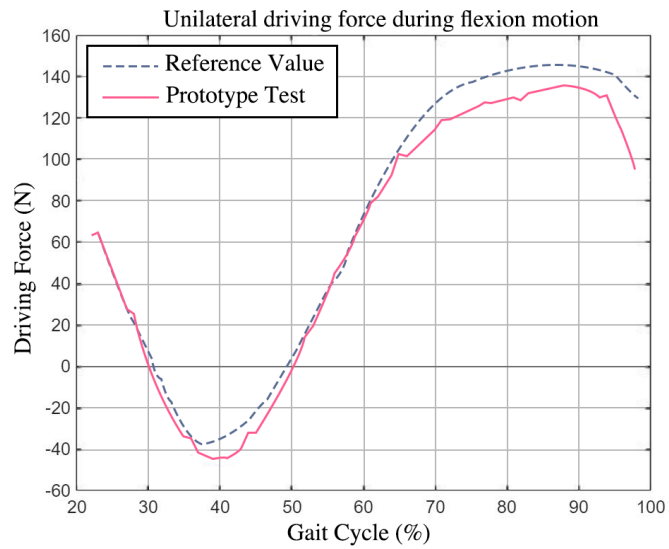
Fig. 10.9 The Driving Force during Flexion Motion



(a) Front View  (b) Side View  (c) Back View

Fig. 10.10 The Bending State of the Knee Joint

slightly flexed and plantarflexed, respectively. This allowed for stability in the lower limbs and optimal contact with the ground.

Flat foot phase: During this phase, the hip flexion angle gradually decreased, and the prosthetic knee and ankle joints returned to their resting positions. In this phase, the movement of the lower limbs resembled that of an inverted pendulum, while the center of gravity of the exoskeleton system moved vertically upward.

Heel lift-off phase: This status depicts the transition of the hip gait simulator from flexion to extension. The center of gravity of the system shifted forward, resulting in flexion of the prosthetic knee and dorsiflexion of the ankle joints due to the ground reaction force.

Toe lift-off phase: In this phase, the hip gait simulator remained in extension and reached its maximum extension angle towards the end of toe lift-off. The prosthetic knee continued to flex, while the plantarflexion angle of the ankle gradually decreased due to dorsiflexion, lifting the calf off the ground.

Swing phase: This phase illustrates the return of the hip gait simulator from extension to its zero position. The prosthetic knee reached its maximum flexion angle and then extended back to its resting position. Through position control, both the prosthetic knee and ankle joints swung freely in the air, preparing for the next gait cycle.

By conducting these walking function tests, we can gain valuable insights into the performance and functionality of the exoskeleton mechanism during different phases of walking. The Fig 10.11 below illustrates the angular variations of the hip joint, knee joint, and ankle joint throughout a gait cycle. The blue dashed line represents the reference values of a participant without wearing an exoskeleton, which serve as a benchmark for the red line. Besides, the reference value in this figure came from the data obtained from the motion capture system. The red line represents the data obtained while wearing the exoskeleton prototype. This information will contribute to further refinements and improvements in the design and control algorithms of the exoskeleton, ultimately enhancing its effectiveness for individuals undergoing lower limb rehabilitation.

Through a comprehensive analysis of the movements of all joints in the lower limb exoskeleton mechanism, we have determined that the prototype successfully completes the entire rehabilitation process. These results validate the accuracy and practicality of the exoskeleton's design and functionality. By offering valuable insights, these findings contribute to further optimization and refinement of the exoskeleton, ensuring its effectiveness in assisting patients throughout the walking rehabilitation process.

(a) Hip Joint                    (b) Knee Joint
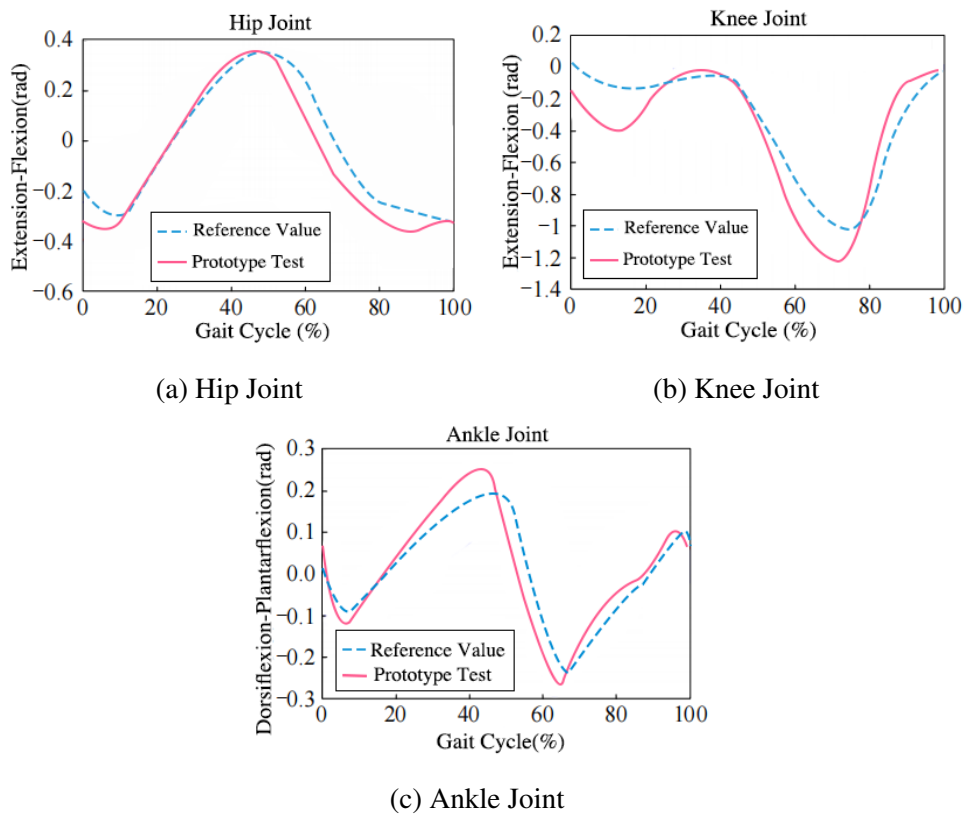
(c) Ankle Joint

Fig. 10.11 The Angle Changes of Each Component during a Gait Cycle

### 10.3.4 Additional Function Test of the Toes and Ankle Joint

In addition to facilitating passive motion for the completion of the entire rehabilitation process, the toe joint and ankle joint also could possess the capability to perform independent active rehabilitation exercises, as demonstrated in Fig 10.12 and Fig 10.14. Then, the result of the rotational angles of each joints of the ankle, including the toes, are shown in Fig 10.13. From the Fig 10.13, the ankle joint 1 represents the rotational action of adduction-abduction, while ankle joint 2 symbolizes dorsiflexion-plantarflexion. These joint movements play vital roles in controlling the side-to-side and up-and-down motions of the ankle, allowing for flexibility and stability in various activities., as shown in Fig 3.1. Besides, it is evident that the training cycles for the toes and the ankle do not align. This is done to demonstrate that each rotational rehabilitation exercise can be independently operated and freely adjusted. It avoids the misconception that the entire foot rehabilitation movement can only be performed synchronously. The ability to customize and perform individual rotational exercises allows for greater flexibility and tailored rehabilitation programs based on specific needs.



Fig. 10.12 Movement of the Toes

This additional function is essential in preventing necrosis and degeneration of the toe joint and ankle joint.

The testing results are shown in below Fig 10.15. As mentioned before, the blue dashed line represents the baseline values of a participant without wearing an exoskeleton, providing a basis for comparison with the red line. The red line depicts the data recorded when the participant is wearing the exoskeleton prototype. The graph depicts a complete cycle, including both inward and outward bending processes. From the graph, it is evident that the maximum amplitudes of the prototype's inward and outward bending movements surpass the reference values. This demonstrates that the prototype is capable of achieving all motions within the reference range. Moreover, the intersection point at 40 percent of the cycle indicates the transition from an outward position to an inward motion. This
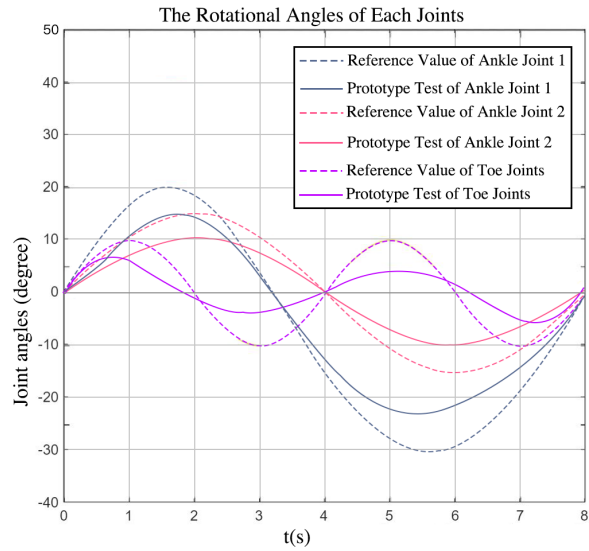
Fig. 10.13 The Rotational Angles of Each Joints



(a) Leftward Rotation　　　(b) Normal State　　　(c) Rightward Rotation
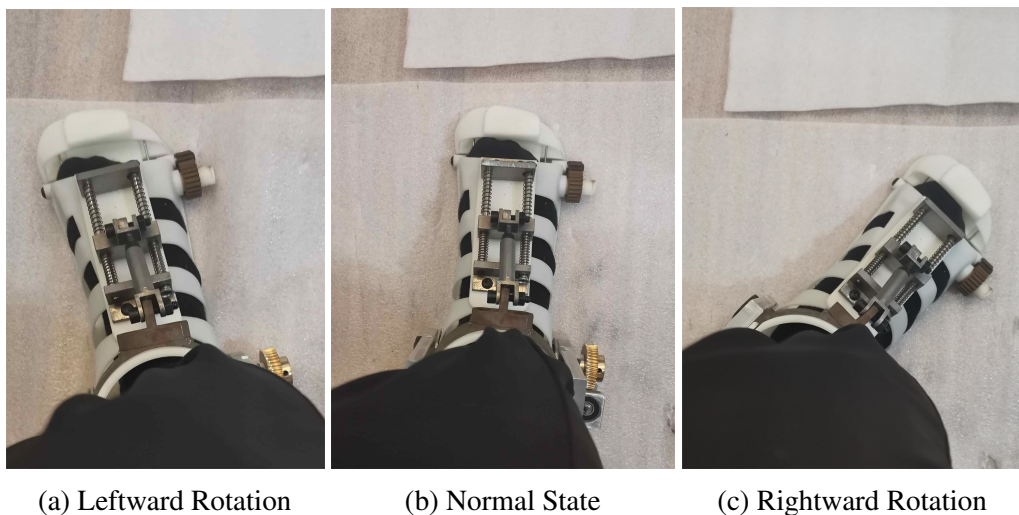
Fig. 10.14 The Additional Rotation States of the Ankle Joint

experimental result confirms the feasibility of the mechanical design and validates that the prototype's maximum range of motion encompasses the entire reference range.
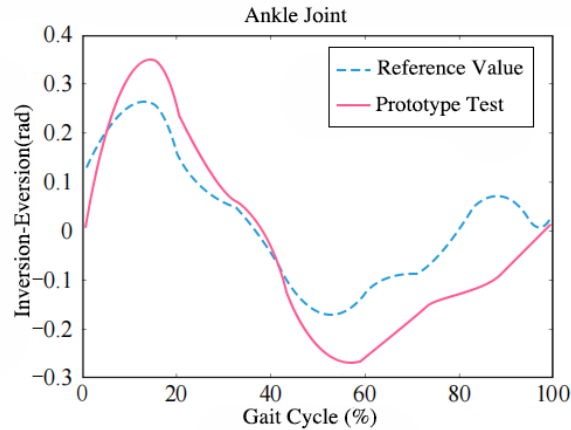


Fig. 10.15 Inversion-Eversion Motion

The experimental results indicate that the innovative design of the toe portion enhances the overall flexibility of the mechanism, enabling it to play a more significant role in diverse rehabilitation processes. The additional toes and ankle rehabilitation exercises hold great importance for several reasons:

1.Prevention of joint stiffness and muscle atrophy: Prolonged immobilization or inactivity can lead to joint stiffness and muscle atrophy. Toe exercises help strengthen muscles and improve the range of motion in the toe joints, effectively preventing these negative outcomes. This promotes joint health and mobility.

2.Restoration of balance and gait: The toes contribute significantly to maintaining balance and stability during walking and standing. Weak or dysfunctional toe muscles can result in gait abnormalities and reduced mobility, significantly impacting an individual's quality of life. Therefore, toe rehabilitation exercises are crucial for restoring proper balance and gait patterns.

3.Aid in the recovery from foot injuries: Common foot injuries such as sprains, strains, and fractures can benefit from toe rehabilitation exercises. Regular exercise promotes blood flow, reduces swelling, and accelerates the healing process, leading to optimized recovery outcomes.

4.Prevention of future injuries: By strengthening muscles, improving flexibility, and increasing the range of motion, toe rehabilitation exercises reduce the risk of future injuries. This proactive approach enhances overall foot health and minimizes the likelihood of recurring injuries.

Incorporating toes and ankle rehabilitation exercises into the rehabilitation process is highly recommended due to their numerous benefits. These exercises not only promote

joint health and mobility but also aid in the restoration of balance, facilitate recovery from foot injuries, and prevent future injuries.

### 10.3.5 Additional Function Test of the Abduction-adduction of the Hip

The exoskeleton structure designed for hip rehabilitation incorporates a waist-mounted cam mechanism, enabling the simulation of not only hip flexion and extension but also hip abduction-adduction movement of the human body, as shown in Fig 10.16.



Fig. 10.16 Abdduction-adduction Movement of the Hip Joint

Experimental results affirm that the innovative design of the hip joint section enhances the overall flexibility of the mechanism, which is shown in Fig 10.17, allowing it to play a more prominent role in a wide range of rehabilitation procedures. The graph depicts the movement of the tester's left leg (L) and right leg (R) during a complete cycle. It is important to note that the y-axis of the graph represents the driving force of the motors. From the graph, it can be observed that the reference curves for both legs exhibit regular patterns. However, when the tester actually wore the prototype, the measured driving forces for the left and right legs were not as regular. This inconsistency is primarily caused by the fact that the weight of the tester's single leg is slightly higher than the predetermined value in the simulation software. As a result, the peak driving forces exceeded those of the reference curves. Additionally, involuntary movements and the influence of gravity during the test also contributed to the irregular motion observed in the actual curves. The upward and downward bending of the curves represent the lifting and lowering processes

of the leg during the lateral leg lift motion. The intersection points between the curves do not hold any specific meaning. However, the intersection points between each curve and the baseline axis indicate changes in the direction of the driving force. Taking any of the curves as an example, an upward curve signifies an increase in the applied force during the leg lifting process, while a downward curve represents a decrease in the applied force while still maintaining the same direction. Furthermore, the intersection point between the curve and the baseline axis indicates a change in the direction of the applied force from lifting to inwardly bringing the leg down. Similarly, the intersection point between the curve and the baseline axis implies that the leg has reached its highest point during the lateral leg lift motion. Subsequently, as the opposing force increases during the downward phase, the decrease in force indicates that the leg is about to return to its initial position. When the leg returns to its initial position, the driving force returns to zero.

The Fig 10.17 mainly demonstrates the variation in driving forces from the motors during the lateral leg lift motion of the prototype. The peak forces reflect the correctness of the motor selection, as they align with the shape of the reference curves, validating the design against expectations. The differences in peak values and shape between the curves primarily stem from the variances of actual leg weight compared to the expected weight and the influence of involuntary movements during the motion, as well as other factors. Therefore, the graph provides a clear visualization of the driving forces generated by the motors during the lateral leg lift process.
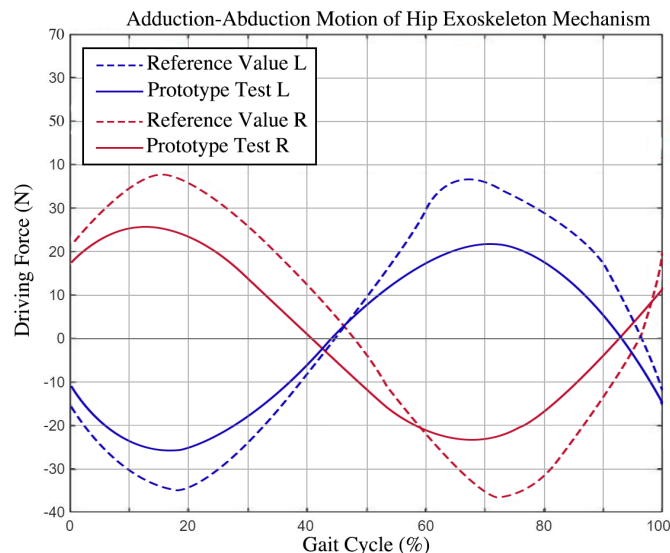


Fig. 10.17 Adduction-Abduction Motion

The hip's abduction-adduction function holds significant importance for several reasons:

Maintenance of balance and stability: Abduction and adduction movements of the hip joint are integral to maintaining balance and stability while standing, walking, or running. The abduction movement moves the leg away from the body's midline, while the adduction movement brings it back towards the midline. These movements facilitate adjustments in the center of gravity while changing directions or shifting weight.

Muscle strengthening: Hip abduction and adduction exercises are effective in strengthening the muscles surrounding the hip joint. The gluteus medius and minimus muscles predominantly perform the abduction movement, while the adductor muscles contribute to the adduction movement. Strengthening these muscles helps improve overall hip joint stability, reduces the risk of injury, and enhances athletic performance.

Rehabilitation for hip joint injuries: Hip abduction-adduction exercises are commonly prescribed as part of rehabilitation protocols for various hip joint injuries. Individuals recovering from hip surgery or dealing with hip joint-related conditions like trochanteric bursitis or hip osteoarthritis can benefit from these exercises. They aid in increasing range of motion, improving muscle strength, and alleviating pain associated with these conditions.

Including hip abduction-adduction exercises in the rehabilitation process is highly recommended due to their multiple benefits. These exercises contribute to the maintenance of balance and stability, strengthen hip muscles, and facilitate recovery from hip joint injuries.

# 10.4 Discussion of the Novelty under the Comparison with the Other Lower Limb Rehabilitation Mechanisms

Compared to existing lower limb exoskeleton rehabilitation robots, exemplified by current models, this prototype exhibits innovative features both at the individual joint level and as a whole. Let's delve into these aspects in detail:

Firstly, the ankle joint incorporates a spring device that introduces flexibility and cushioning into the rehabilitation process, significantly reducing the risk of secondary injuries. This feature sets it apart from current models, addressing the rigidity often associated with conventional devices. The addition of the cushioning function enhances patient comfort and minimizes stress on the joints during rehabilitation.

Secondly, the knee joint utilizes a flexible device that overcomes the limitations of a purely rigid structure. This design allows for arbitrary adjustment of the force direction on the rope, enabling diverse motor positions based on specific requirements. The inclusion of a torsion spring provides additional buffering functions, further enhancing the versatility of the device. Moreover, by modifying the torsion spring installation method, the prototype

enables movement in two distinct rehabilitation states: sitting and standing (walking). This capability differentiates it from existing models, offering greater flexibility and adaptability during the rehabilitation process.

Thirdly, the hip joint incorporates a cam device that transforms the rotation-based motor torque output into radial force output, ensuring optimal force distribution. This unique feature ensures consistent force output and sets it apart from conventional designs. Furthermore, the joint design incorporates two degrees of freedom, expanding the repertoire of movements available during rehabilitation.

Additionally, the entire prototype is designed with modularity in mind. Each module can independently perform specific rehabilitation movements and can be seamlessly assembled into a complete unit. This modular approach enhances adaptability, simplifies maintenance, and allows for customization based on the individual needs of patients.

Furthermore, the rehabilitation process facilitated by this prototype extends beyond a single rehabilitation state. It enables exercises in both sitting and standing (walking) positions. In the sitting state, the machine primarily assists in patient rehabilitation efforts, while in the standing state, the focus shifts to the patient's own movements, supported by the device. This versatility distinguishes it from existing models, broadening the range of therapeutic options available.

In summary, the exoskeleton prototype model distinguishes itself from current lower limb rehabilitation equipment in several aspects. These include innovative features in individual joint designs, overall modularity, and a wide variety of rehabilitation movements. The validation of these features during the prototype stage highlights the potential for significant advancements in the field of rehabilitation through this technology.

## 10.5   Conclusions

In summary, the proposed innovative lower limb exoskeleton rehabilitation system is capable of replicating human-like joint movements, including knee flexion-extension, ankle inversion-eversion, and ankle dorsiflexion-plantarflexion, within the normal gait cycle. This mechanism aids stroke patients in recovering multi-joint mobility in the knee and ankle joints. Additionally, the lower limb exoskeleton rehabilitation system enables multiple degrees of freedom movement during the simulation of human body forward motion, encompassing hip flexion-extension and abduction-adduction. This feature provides natural hip joint functionality as well as toe training capabilities, effectively enriching the patient's rehabilitation program. The inclusion of torsion springs and elastic springs significantly enhances the system's buffering and protective functions, thereby preventing any potential secondary physical damage to amputees during the human-machine interaction process.

Despite the promising outcomes exhibited by the prototype model, there is still room for improvement. As previously mentioned, further optimization of the size and positioning of components can enhance functionality, while the control mechanism should be refined to offer greater precision and accuracy. Additionally, careful consideration should be given to the weight and bulkiness of the device, as these factors can influence patient comfort and mobility during rehabilitation exercises.

Another aspect to consider is the cost-effectiveness of the exoskeleton design. While it holds the potential to revolutionize the rehabilitation process and enhance patient outcomes, maintaining accessibility for those who need it most remains crucial. Consequently, additional research and development efforts are necessary to optimize production processes and reduce manufacturing costs.

Moreover, the development of user-friendly interfaces and intuitive control systems is essential to improve the usability of the exoskeleton, enabling both patients and healthcare professionals to easily navigate its functions. Furthermore, conducting long-term studies and clinical trials becomes imperative to validate the system's effectiveness and gather valuable feedback from patients and medical practitioners.

In conclusion, the exoskeleton prototype model has demonstrated remarkable potential in improving the rehabilitation process, yet further work is required to achieve optimal performance. Through continuous research, meticulous design optimization, cost reduction initiatives, and user-centric enhancements, this technology could bring about a transformative impact on the lives of patients striving to regain mobility and independence.

# Chapter 11

# Conclusions and Future Work

## 11.1 General conclusions for the Thesis

This dissertation is dedicated to providing a comprehensive modular lower limb exoskeleton rehabilitation mechanism that addresses the diverse needs of post-stroke patients. Its primary objective is to restore the active functionality of patients' lower limbs and enable them to regain their ability to walk, ultimately facilitating a return to normal daily life. The general conclusions drawn from this dissertation are outlined below.

Chapter 1 introduces the motivations, aims, and objectives of the research on lower limb rehabilitation exoskeletons.

Chapter 2 presents a comprehensive introduction to continuum robots, covering their origins and development, driving modes and characteristics, modeling and control principles, as well as their advantages and potential applications. Continuum robots exhibit high flexibility and adaptability, making them an ideal choice for performing intricate tasks in constrained environments. Originating from soft robots, continuum robots have undergone notable advancements, particularly in enhancing their driving modes and characteristics. By incorporating active and passive mechanisms along with pneumatic, hydraulic, or cable-driven systems, continuum robots can execute precise and efficient operations. Accurate modeling and precise control are vital for ensuring optimal performance. The benefits of utilizing continuum robots are vast and encompass improved adaptability, precise motion control, and safer operations within confined spaces when compared to traditional rigid-body robots. The potential applications of continuum robots are extensive, spanning various fields such as minimally invasive surgery and space exploration. In the medical field, they enable surgeons to operate with enhanced precision and maneuverability while minimizing damage to healthy tissues. In conclusion, continuum robots represent a significant advancement in robotics, offering unique advantages over traditional rigid-body robots. Through ongoing research and development, they hold tremendous potential

to revolutionize numerous industries and sectors, paving the way for new and exciting applications.

Chapter 3 offers a comprehensive overview of the recent advancements in robotics for rehabilitation systems, with a specific focus on ankle, knee, and hip joint rehabilitation. Each section delves into the working principles, advantages, and limitations of various rehabilitation mechanisms in meticulous detail. The chapter begins with an extensive discussion on ankle joint rehabilitation systems, categorized as either stationary or dynamic. It proceeds to outline knee joint rehabilitation systems, highlighting the distinctions between pure rigid-body and soft-body systems. Additionally, the chapter explores overall rehabilitation systems targeting hip joint structures, emphasizing the significance of selecting appropriate materials to ensure safe and effective rehabilitation. Furthermore, the chapter introduces innovative continuum mechanism designs for rehabilitation systems, drawing comparisons with traditional pure rigid-body designs. Lastly, it summarizes key findings and underscores the potential benefits of robotics in enhancing patient recovery. In summary, this chapter presents valuable insights and resources for patients, healthcare professionals, and researchers who are interested in staying abreast of the latest developments in rehabilitation robotics. It also provides a glimpse into future trends within this field.

Chapter 4 serves as an introductory section to the fundamental theories and methods utilized in this thesis. The chapter commences with an overview of screw theory, encompassing definitions, basic calculation formulas, and parameters such as twist and wrench. It emphasizes the significance of screw system algebra in theory and covers both instantaneous and finite screw systems, elucidating their importance. Subsequently, the chapter transitions to PSO (Particle Swarm Optimization), highlighting their role in optimization problems. It discusses the advantages and disadvantages of genetic algorithms in comparison to traditional mathematical algorithms, along with techniques for optimizing and integrating them with the Matlab language. This integration provides robust optimization support for subsequent mechanical structure design. Furthermore, the chapter introduces the extraction method of human gait data, underscoring the utilization and applicable scope of motion capture systems as well as the analysis method for the extracted data. Overall, this chapter accentuates the practical application and critical importance of screw theory and genetic algorithms in mechanical structure design. It also establishes a theoretical foundation and provides data support for future studies.

Chapter 5 represents the successful development of a novel ankle joint exoskeleton mechanism, encompassing its structural design and simulation. The study demonstrates that integrating active and passive elastic devices during rehabilitation can offer patients more flexible exercise modes, thereby significantly expediting their recovery process. The results of kinematic analysis and motion simulation validate that the experimental design

fulfills the required design standards. However, future research endeavors will focus on investigating force direction and the stability of variable stiffness compression torsion springs. This entails addressing any structural flaws and enhancing the exoskeleton's adaptability to adult feet. The ultimate objective is to mass-produce this rehabilitation robot to effectively assist a larger population of patients in need of rehabilitation treatment. Through continued research and development, the performance and reliability of the exoskeleton mechanism will be optimized, consequently propelling advancements in the realm of rehabilitation robotics.

Chapter 6 presents a comprehensive examination of the design, kinematics, and motion planning for a hybrid active and passive SRE mechanism used in stroke patient rehabilitation. The redesigned mechanism incorporates hybrid active and passive cables, offering impressive rigidity and load capacity that can bring significant benefits to stroke patients. One notable feature of this redesigned system is its capability to constrain the operational arm while moving in a virtually continuous shape. This simplifies the kinematic equations and enhances operational efficiency. Additionally, by implementing the PSO algorithm, the exoskeleton can be optimized to match the lower limb movement of each individual patient, thereby creating a more effective and personalized therapy. Furthermore, the SRE can be upgraded to cater to specific patient needs. By combining motor learning principles with more traditional approaches, exceptional benefits can be provided to patients. Multitouch sensing units also play a crucial role by offering timely feedback on patient-exoskeleton interaction, enabling real-time adjustments. While the development of exoskeletons for rehabilitation is still in its early stages, the utilization of a multitouch robotic device for coordination rehabilitation exhibits tremendous potential. Although challenges lie ahead, this research indicates that integrating a self-matching mechanism with the legs of stroke patients in the SRE system leads to a highly sensitive and flexible mechanism, holding great promise for stroke patient recovery throughout the treatment process. However, further clinical studies involving a larger cohort of patients are necessary to fully validate the effectiveness of the SRE. With continued research, development, and optimization, the SRE mechanism has the potential to revolutionize the field of stroke patient rehabilitation, providing much-needed assistance to countless individuals worldwide.

Chapter 7 mainly focuses on the design and verification of lower limb rehabilitation exoskeletons, with particular emphasis on the development of an innovative active and passive interactive hip joint. The analysis of the gait cycle and human lower limb movement provides a fundamental understanding of the design requirements for the exoskeleton. Moreover, this chapter offers an overview of human anatomy and the dynamic characteristics of lower limbs to guide the design process. The configuration of an active-passive interaction mechanism for a hip exoskeleton is thoroughly examined, including discussions on primary driving structures, energy storage system design, and the passive energy storage

system of the hip joint rehabilitation mechanism. Inverse kinematic analysis of the 2-Dof hip rehabilitation mechanism, along with working space and stiffness analysis, is explored. Additionally, kinematic validation of the 2-Dof hip rehabilitation mechanism is included in this section. Finally, the chapter concludes with a comprehensive performance analysis of the overall lower limb exoskeleton rehabilitation mechanism, providing valuable insights into the design and performance of such exoskeletons for rehabilitation purposes. The study specifically focuses on designing and analyzing lower limb exoskeletons to provide effective assistance in the rehabilitation training of stroke patients. Based on data collected from gait experiments, the motion and dynamic design requirements of the exoskeleton were determined, and the mechanism's configuration was analyzed. The results demonstrate that the proposed exoskeleton design is feasible and effective in assisting stroke patients in their rehabilitation training. The exoskeleton achieves flexible kinematic control over multiple joints, enhancing its overall performance. Furthermore, the active driving system combined with the passive energy storage system improves the dynamic characteristics of the joints while reducing power consumption.

Chapter 8 begins by providing a detailed rendering of the exoskeleton structure design proposed in the preceding chapters. Following that, the chapter focuses on the design of basic control theories and the selection of appropriate motors. Additionally, it discusses the prototyping process of the overall mechanism, which involves precision machining, including the rational layout of motors and appropriate configuration of electrical wiring. Finally, the chapter presents the experimental testing conducted on the prototype. During the tests, the prototype's motion under normal walking patterns is examined to assess its functionality and synchronization with natural human gait. Additionally, specific rehabilitation movements are conducted to evaluate the device's ability to facilitate targeted joint recovery exercises while the user is in a seated position. These experimental tests provide valuable insights into the prototype's effectiveness in assisting stroke patients with lower limb rehabilitation. The results contribute to the validation of the proposed design's capability to support targeted movements, promoting the recovery of specific joint functions and ultimately enhancing the rehabilitation process. The experimental results confirm the validity of the proposed design approach, as demonstrated through the validation of the prototype. This design has the potential to assist stroke patients in achieving lower limb training and rehabilitation goals, thereby alleviating the financial burden on patients and reducing the time pressure on therapists. Moreover, the successful implementation of this exoskeleton design holds promise for improving the overall quality of life for stroke patients.

# 11.2 Main Contribution and Achievements of the Dissertation

The research work presented in this dissertation has yielded a range of original research outcomes, with the following main contributions/achievements:

1.Proposal of a novel self-adaptive ankle rehabilitation exoskeleton incorporating elastic buffering modules. It is designed to adapt to the specific needs and conditions of individual patients through self-alignment capabilities. The modules enhance the effectiveness and safety of the rehabilitation process. This innovative mechanism provides targeted support, improves range of motion, muscle strength, and overall recovery outcomes. It also ensures patient comfort, minimizes the risk of injuries, and offers personalized rehabilitation experiences.

2.The study focuses on kinematic and stiffness analysis using the Zero Moment Position (ZMP) during the gait cycle of a normal individual. It examines joint angles, movements, and overall body motion to gain insights into the biomechanics of walking. This helps understand the coordination and sequencing of movements in different phases of the gait cycle. Additionally, it analyzes stiffness distribution and changes across joints and muscles, providing crucial information about mechanical properties related to walking. These analyses shed light on the complex mechanisms involved in normal gait, serving as a reference for identifying deviations, abnormalities, and designing interventions for gait rehabilitation.

3.This study presents simulation analysis and performance evaluation of an innovative ankle rehabilitation mechanism, providing valuable insights into its functionality and effectiveness. Through empirical testing and objective measurements, it validates the mechanism's ability to enhance range of motion, muscle strength, and overall recovery outcomes. The findings contribute to optimizing rehabilitation outcomes and improving care quality for ankle injuries or impairments.

4.This study significantly contributes through the design of a novel knee rehabilitation exoskeleton model for stroke patients. The model utilizes self-matching segmented redundant elements (SRE) and a continuous body structure to provide precise and customizable support to the knee joint during rehabilitation exercises. This innovative design addresses specific needs and challenges, improving functionality, comfort, and adaptability. This approach highlights the advantages of a continuous body structure compared to The pure rigid structure.

5.The utilization of the Motion Capture System to capture lower limb movement data during the gait cycle is a significant contribution. It provides precise measurements of joint angles, muscle activations, and ground reaction forces. This information enhances our

254

understanding of human locomotion and improves assessments, treatment strategies, and patient outcomes in gait disorders and rehabilitation programs.

6.The combination of a genetic algorithm and MATLAB to address the issue of the "S-shape" curve is an innovative solution. It optimizes parameters and variables, improving performance and accuracy in various applications. These findings have the potential to enhance optimization algorithms, particularly in dealing with complex curves and improving efficiency in fields like data analysis and decision-making processes.

7.The analysis of the knee joint rehabilitation mechanism model based on continuum mechanics provides valuable insights into its kinematics. This analysis improves our understanding of knee joint motion during rehabilitation and enhances the design of rehabilitation mechanisms. The findings have the potential to improve the effectiveness of knee joint rehabilitation interventions and enhance patient outcomes.

8.The introduction of a novel 2-DOF hip joint exoskeleton mechanism with combined active and passive functions is exhibited in this research. This innovative design improves the versatility and efficiency of hip joint exoskeletons. The integration of active and passive elements provides muscle assistance, natural joint movement, and energy conservation. This expands the possibilities of exoskeleton technology in rehabilitation, assistive devices, and mobility enhancement, ultimately benefiting stroke patients and improving their quality of life.

9.The compilation and listing of various reference data based on human anatomy is a valuable contribution. It serves as a comprehensive resource for researchers, educators, and healthcare professionals, facilitating accurate anatomical references in their work. This data enhances understanding and analysis in fields like medical imaging, surgical planning, biomechanics, and education.

10.The presentation of a complete set of lower limb exoskeleton structures, along with performance analysis throughout a full gait cycle using three assemble parts, is a significant contribution. These modular components allow for targeted rehabilitation for different types of patients, whether it's rehabilitating a specific joint such as the hip, knee, or ankle individually, or any combination of these three parts. This paves the way for more personalized designs in the future, breaking away from the notion of non-detachable systems and providing a theoretical foundation for individualized rehabilitation.

11.The exhibition of the lower limb exoskeleton prototype in the laboratory highlights the crucial role of a physical prototype in the development process. This showcase not only presents theoretical concepts but also provides a tangible embodiment of the lower limb exoskeleton. The presence of a physical prototype adds credibility to the research and showcases the successful translation of ideas into practical solutions.

12.The comparison between the proposed lower limb exoskeleton in this thesis and previous designs highlights its advantages. This analysis showcases unique features, func-

tionalities, and improvements, providing valuable insights for researchers and engineers. It contributes to the advancement of lower limb exoskeleton technology by identifying areas of excellence and potential for further innovation.

## 11.3 The Novelty in Comparison to Existing Lower Limb Rehabilitation Systems

As mentioned in the previous chapters, there are inevitable issues associated with the currently available lower limb exoskeleton rehabilitation robots. Here are the summaries below:

1.High cost: Lower limb exoskeleton rehabilitation devices are often priced at a premium, making them unaffordable for many individuals in need of rehabilitation. This poses a significant barrier, particularly for those from economically disadvantaged backgrounds, who are unable to bear the financial burden associated with these devices.

2.Weight and discomfort: Present-day lower limb exoskeletons tend to be bulky and uncomfortable to wear, causing users to experience significant physical exertion while walking. Additionally, some exoskeletons lack flexibility, failing to adapt to the specific movement patterns and needs of individual users.

3.Power supply issues: Lower limb exoskeleton rehabilitation devices typically rely on battery power. However, the limited battery capacity restricts their usage duration for extended rehabilitation training. This necessitates frequent recharging, which limits the time and space in which users can incorporate exoskeletons into their daily lives.

4.Individual variations in rehabilitation requirements: Each individual's rehabilitation needs vary, but the current lower limb exoskeleton rehabilitation devices lack personalization capabilities. They fail to cater to unique requirements, resulting in an inability to fully address patients' specific rehabilitation needs.

5.Technological limitations: Despite progress in the development of lower limb exoskeleton rehabilitation devices, technological limitations persist. For example, some devices lack precise sensor technology, while control systems may exhibit slow response times, impeding user convenience and flexibility in operation.

To address the these drawbacks, I proposed a novel lower limb exoskeleton rehabilitation system specifically targeting stroke patients in this thesis. Compared to existing designs, it incorporates the following key advantages:

1.Customized Design: The proposed system allows for a high degree of customization to accommodate the individual needs and remaining abilities of stroke patients. It can apply different rehabilitation strategies based on the varying levels of stroke severity and can switch between active and passive rehabilitation modes. In the active mode, mechanical

assistance is the primary focus while patient participation is secondary. In the passive mode, the motors can be turned off, and the patient takes the lead with mechanical assistance as a secondary support.

2.Wearable and Lightweight Design: Emphasizing portability and ease of use, the proposed system is designed to be lightweight and ergonomic. It prioritizes user comfort while minimizing the burden of wearing the exoskeleton, enabling longer and more frequent usage throughout the day. The compact motors selected for the system ensure that it does not impose a significant burden on the patients. Additionally, the portable nature of the system allows patients to engage in rehabilitation exercises not only within hospitals or indoor settings but also in flat outdoor environments. This not only facilitates physical rehabilitation but also promotes psychological well-being.

3.Cost-effectiveness: An important consideration in the design process was ensuring affordability. By utilizing cost-effective materials and manufacturing techniques, the system aims to provide an accessible and reasonably priced solution for stroke patients in need of lower limb rehabilitation. While some major components require customized manufacturing, the remaining connecting parts are chosen as standard components as much as possible. This reduces production costs and enables easy replacement, avoiding situations where the entire system becomes inoperable due to damage or loss of a single part.

4.Combination of Rigidity and Flexibility: Due to the flexible-driven and the collaboration of elastic modules, the entire system possesses a combination of rigidity and flexibility. This helps avoid excessive force exerted on the patients by the motors, preventing secondary injuries caused by excessive torque or improper use.

5.Self-alignment: As mentioned in the previous designing chapters, the rotational centers of ankle joints, knee joints, and hip joints are not fixed during actual movements. Through special structural design in these three parts, the system achieves real-time matching between the rotation centers of the mechanism and the human body's actual condition. This enhances the effectiveness of rehabilitation while preventing secondary injuries.

6.Toes joint rehabilitation: For stroke patients, lower limb rehabilitation should not be limited to ankle joints, knee joints, and hip joints. Training for toe joint movement is also necessary to prevent muscle atrophy and necrosis. In addition, in the normal gait cycle of a human body, the toe joint is not stationary. Coordinated toe movements contribute to stability during the gait cycle, effectively preventing falls.

7.Modular Design: The three main modules mentioned in this paper are divided into five parts: two exoskeletons for foot rehabilitation, two for leg rehabilitation, and one for hip rehabilitation. This design allows for targeted repairs of specific areas or assembly for

comprehensive lower limb rehabilitation training. It ensures both targeted rehabilitation effects and flexibility in the system structure.

Although these features provide certain advantages compared to other existing rehabilitation systems, there are still areas that need improvement. The future work plans would be outlined in the following section.

## 11.4 Future Work and Potential Applications

### 11.4.1 Future Research for the Rehabilitation Exoskeleton based on this Thesis

This dissertation introduced an innovative overall lower limb rehabilitation mechanism that holds significant potential for assisting stroke patients in their journey towards a normal life. However, there are still some unresolved issues that merit further investigation. The research topics/directions for future study are as follows:

1.The prototype of the designed lower limb exoskeletons requires further refinement to accommodate different rehabilitation modes, and the study of modular control algorithms is worthwhile: To enhance the effectiveness of lower limb exoskeleton rehabilitation, researchers should continuously optimize the design of exoskeletons for various rehabilitation modes. The implementation of modular control algorithms is a valuable area of research, as it facilitates easy reconfiguration and adaptation of exoskeletons to meet diverse rehabilitation requirements.

2.Control system optimization is necessary to achieve a more natural human-like motion in the exoskeleton: The ultimate objective of lower limb exoskeletons is to provide a walking experience that closely emulates natural human motion. To accomplish this, researchers must further optimize the exoskeleton's control system to ensure synchronized movement with the user's own gait pattern, resulting in a more realistic walking experience.

3.Motion analysis of the exoskeleton mechanism should consider scenarios beyond flat and level ground, such as uphill, downhill, stairs, and uneven terrain, necessitating further investigation: To enhance the adaptability of lower limb exoskeletons in real-world environments, researchers need to conduct comprehensive studies on various terrain conditions beyond flat and level ground. This includes analyzing exoskeleton motion patterns on inclines, stairs, and uneven surfaces, as well as developing control systems capable of accommodating these diverse scenarios.

4.Establishing a more accurate human-machine interaction model is crucial to determine the compatibility between the rehabilitation exoskeleton and human body movements, facilitating design updates and iterations: A significant challenge in the development of lower limb exoskeletons lies in achieving seamless integration between humans and

machines. To enhance this integration, researchers must establish a more precise human-machine interaction model that can accurately assess and respond to user movements. This requires further research into machine learning and artificial intelligence algorithms capable of adapting to individual differences in body type, injury severity, and rehabilitation needs.

5.Further research in continuum mechanics and flexible control knowledge is necessary to enhance the exoskeleton system: Continuum mechanics and flexible control knowledge are crucial areas of study for improving the performance and functionality of lower limb exoskeletons. By conducting further research in these domains, researchers can deepen their understanding of the mechanical properties of human joints, tendons, and muscles. This knowledge will enable the development of more advanced control strategies that allow exoskeletons to respond flexibly to the user's movements.

6.Perform additional physical tests on the prototype, compare the resulting motion data with theoretical calculation models, and identify factors influencing the physical prototype for troubleshooting: Physical testing is essential for validating the performance and safety of lower limb exoskeletons. Researchers should conduct additional physical tests on prototypes, comparing the resulting motion data with theoretical calculation models. This process will help to identify any potential issues or factors that may influence the performance of the exoskeleton. By doing so, researchers can address these issues early in the design process.

7.Optimize the toe joint rotation function based on foot conditions and structural layout to improve toe rehabilitation capabilities: The toe joint plays a critical role in walking and balance, making it an important focus for lower limb exoskeletons. To enhance toe rehabilitation capabilities, researchers need to optimize the function of the toe joint rotation based on foot conditions and structural layout. This optimization process involves analyzing the mechanical properties of the foot and developing specialized control algorithms that target specific muscle groups and joints.

8.Gain a more accurate understanding of the pain and needs of stroke patients, distinct from other lower limb disabled patients, by exploring interdisciplinary fields beyond engineering, such as human engineering and biology. This will aid in proposing reliable mechanism models, designing appropriate rehabilitation plans, and implementing tailored control strategies: To design effective lower limb exoskeletons, it is crucial to have a comprehensive understanding of the human body and the specific needs of different patient populations. This requires collaboration across various disciplines, including engineering, biology, and medical sciences. By engaging in interdisciplinary research, researchers can gain a more accurate understanding of the pain and needs encountered by stroke patients and other lower limb disabled patients. This knowledge will enable them to propose

reliable mechanism models, design appropriate rehabilitation plans, and implement control strategies that are customized to individual requirements.

9.Broaden the scope of lower limb exoskeletons beyond rehabilitation and medical domains, integrating knowledge of morphogenesis to enable multifunctional usage that can adapt to different environments. This includes capabilities such as lifting the knee during sitting or standing, and extension and flexion during walking: Lower limb exoskeletons have the potential to be utilized in various settings beyond just medical and rehabilitation domains. To enhance their applicability, researchers should incorporate knowledge of morphogenesis into the exoskeleton design process. This integration will enable the exoskeletons to seamlessly transition between different environments and perform multiple functions, such as lifting the knee while sitting or standing, as well as extension and flexion during walking.

10.Expand the application of lower limb exoskeletons to fields beyond rehabilitation and medical sectors, such as labor-intensive work and military applications: As the technology behind lower limb exoskeletons advances, there is a tremendous opportunity to extend their application beyond just medical and rehabilitation sectors. These exoskeletons could potentially assist laborers who engage in physically demanding tasks, as well as provide additional support for military personnel in the field. However, further research and development is necessary to optimize the design of exoskeletons for different use cases and environments.

## 11.4.2   Potential Application of the Exoskeleton Robot

Exoskeleton robots have extensive applications beyond rehabilitation and medical care, finding utility in various domains. For example, exoskeletons can assist in heavy lifting activities, bolster soldiers' readiness for combat, enhance industrial production efficiency, aid in space exploration, and enhance athletic training performance, among other uses.

1. In the realm of heavy lifting activities, exoskeletons play a crucial role in alleviating the physical burden on workers. By providing mechanical support to the human body, they reduce the risk of occupational-related injuries and accidents. Furthermore, exoskeletons can improve workers' productivity and precision across industries such as logistics, manufacturing, construction, and more.

2. In military operations, exoskeletons significantly enhance soldiers' physical abilities, including strength, endurance, and agility. This empowers them to perform with greater effectiveness on the battlefield, navigate challenging terrain, and successfully achieve mission objectives.

3. When it comes to space exploration, exoskeletons offer astronauts additional support and mobility. This is particularly important during extended space missions where

prolonged exposure to zero gravity can cause bone and muscle degeneration. Exoskeletons mitigate these effects, enabling astronauts to carry out their duties more effectively.

4. Additionally, exoskeletons hold potential applications in athletics by enhancing training outcomes and reducing the risk of injuries. Across various sports, exoskeleton technology can assist athletes in improving their strength, stamina, and overall performance while minimizing the likelihood of overexertion or injury.

Overall, exoskeleton technology exhibits diverse applications across multiple domains. However, further research and innovation are necessary to fully harness its capabilities. The wide-ranging utilization of exoskeletons provides a glimpse into the vast potential impact of this technology.

# List of Publications

[1]  **Meng Gao**, Junpeng Chen, Mi Li, Jiansheng Dai, "Design and Evaluation of a Novel Self-Adaptive Ankle Rehabilitation Exoskeleton with Elastic Modules", *2023 International Conference on Advanced Robotics and Mechatronics (ICARM). IEEE,* 2023: 900-905.

[2] **M. Gao**, T. Wang, E. Spyrakos-Papastavridis, and J. S. Dai, 2023, "Self-matching Segmented Redundant Lower Limb Exoskeleton for Stroke Patients: Design, Kinematics and Planning." (To be submitted)

[3] Chen J., Pan Y., Li M., Zhu R. **Gao M**., Wang K., Xiao X., Deng L. and Dai J., Analysis of the obstacle-crossing capability for a coupled parallelogram leg, *Advances in Mechanism and Machine Science: Proceedings of the 16th IFToMM World Congress on Mechanism and Machine Science 16.* Springer International Publishing, 2023.

# References

[1] Alabdulkarim, S. and Nussbaum, M. A. (2019). Influences of different exoskeleton designs and tool mass on physical demands and performance in a simulated overhead drilling task. *Applied ergonomics*, 74:55–66.

[2] Alatorre, D., Axinte, D., and Rabani, A. (2021). Continuum robot proprioception: the ionic liquid approach. *IEEE Transactions on Robotics*, 38(1):526–535.

[3] Ali, T., Gulzar, S., Khan, S. U., et al. (2021). A literature survey on particle swarm optimization. *Swarm and Evolutionary Computation*, 59:100879.

[4] Allemand, Y. and Stauffer, Y. (2009). Overground gait rehabilitation: first clinical investigation with the walktrainer. In *Proceedings of the European Conference on Technically Assisted Rehabilitation,(TAR'09)*.

[5] Amiri, M. S., Ramli, R., and Ibrahim, M. F. (2019). Hybrid design of pid controller for four dof lower limb exoskeleton. *Applied Mathematical Modelling*, 72:17–27.

[6] Anderson, J. et al. (2019). Passive interventions for improved range of motion in toe joint rehabilitation. *Physical Therapy Review*, 21(2):89–95.

[7] Anderson, L. A. and Peters, C. L. (2010). Anatomy and biomechanics of the adult hip. *Clinical Orthopaedics and Related Research®*, 468(3):540–545.

[8] Andersson, S. B. (2008). Discretization of a continuous curve. *IEEE Transactions on Robotics*, 24(2):456–461.

[9] Ansari, Y., Manti, M., Falotico, E., Mollard, Y., Cianchetti, M., and Laschi, C. (2017). Towards the development of a soft manipulator as an assistive robot for personal care of elderly people. *International Journal of Advanced Robotic Systems*, 14(2):1729881416687132.

[10] Association, A. P. M. (2021). Footwear for toe joint rehabilitation. Retrieved from https://www.apma.org/Patients/FootHealth.cfm?ItemNumber=988.

[11] Aurand, A. M., Dufour, J. S., and Marras, W. S. (2017). Accuracy map of an optical motion capture system with 42 or 21 cameras in a large measurement volume. *Journal of biomechanics*, 58:237–240.

[12] Bacek, T., Moltedo, M., Langlois, K., Prieto, G. A., Sanchez-Villamañan, M. C., Gonzalez-Vargas, J., Vanderborght, B., Lefeber, D., and Moreno, J. C. (2017). Biomot exoskeleton—towards a smart wearable robot for symbiotic human-robot interaction. In *2017 International Conference on Rehabilitation Robotics (ICORR)*, pages 1666–1671. IEEE.

[13] Bai, S. (2010). Optimum design of spherical parallel manipulators for a prescribed workspace. *Mechanism and Machine Theory*, 45(2):200–211.

[14] Baker, J. E. (1978). On the investigation of extreme in linkage analysis, using screw system algebra. *Mechanism and Machine Theory*, 13(3):333–343.

[15] Baker, J. E. (1980). Screw system algebra applied to special linkage configurations. *Mechanism and Machine Theory*, 15(4):255–265.

[16] Balaguer, C. and Abderrahim, M. (2008). *Robotics and automation in construction*. BoD–Books on Demand.

[17] Ball, R. S. (1998). *A Treatise on the Theory of Screws*. Cambridge university press.

[18] Baltrusch, S., Van Dieën, J., Bruijn, S., Koopman, A., Van Bennekom, C., and Houdijk, H. (2019). The effect of a passive trunk exoskeleton on metabolic costs during lifting and walking. *Ergonomics*, 62(7):903–916.

[19] Baltrusch, S. J., Van Dieën, J., Koopman, A. S., Näf, M., Rodriguez-Guerrero, C., Babič, J., and Houdijk, H. (2020). Spexor passive spinal exoskeleton decreases metabolic cost during symmetric repetitive lifting. *European Journal of Applied Physiology*, 120(2):401–412.

[20] Bär, M., Steinhilber, B., Rieger, M. A., and Luger, T. (2021). The influence of using exoskeletons during occupational tasks on acute physical stress and strain compared to no exoskeleton–a systematic review and meta-analysis. *Applied Ergonomics*, 94:103385.

[21] Barus, C. (1900). A treatise on the theory of screws. by sir robert stawell ball, ll. d., frs, lowndean professor of astronomy and geometry in the university of cambridge. cambridge, the university press; new york, the macmillan company. 1900. pp. xix+ 544, quarto. *Science*, 12(313):1001–1003.

[22] Beil, J., Perner, G., and Asfour, T. (2015). Design and control of the lower limb exoskeleton kit-exo-1. In *2015 IEEE International Conference on Rehabilitation Robotics (ICORR)*, pages 119–124. IEEE.

[23] Beyl, P., Van Damme, M., Van Ham, R., Versluys, R., Vanderborght, B., and Lefeber, D. (2008). An exoskeleton for gait rehabilitation: prototype design and control principle. In *2008 IEEE International Conference on Robotics and Automation*, pages 2037–2042. IEEE.

[24] Bharadwaj, K., Hollander, K. W., Mathis, C. A., and Sugar, T. G. (2004). Spring over muscle (som) actuator for rehabilitation devices. In *The 26th Annual International Conference of the IEEE Engineering in Medicine and Biology Society*, volume 1, pages 2726–2729. IEEE.

[25] Bian, H., Liu, Y., Liang, Z., and Zhao, T. (2010a). A novel 2-rrr/uprr robot mechanism for ankle rehabilitation and its kinematics. *Robot*, 32(1):6–12.

[26] Bian, H., Zhao, T., and Tian, X. (2010b). Biological fusion rehabilitation institution and its application. *Robot*, 32(04):470–477.

[27] Bishop, C., Russo, M., Dong, X., and Axinte, D. (2022). A novel underactuated continuum robot with shape memory alloy clutches. *IEEE/ASME Transactions on Mechatronics*, 27(6):5339–5350.

[28] Bissolotti, L., Orizio, C., Ometto, M., Legnani, G., Gobbo, M., Chiari, S., Calabretto, C., Lussignoli, D., Baruzzi, E., Gaffurini, P., et al. (2010). Gait training on lokohelp after stroke: analysis of the benefits in chronic patients. In *17TH ESPRM EUROPEAN CONGRESS OF PHYSICAL AND REHABILITATION MEDICINE*, pages 133–135.

[29] Black, C. B., Till, J., and Rucker, D. C. (2017). Parallel continuum robots: Modeling, analysis, and actuation-based force sensing. *IEEE Transactions on Robotics*, 34(1):29–47.

[30] Blaya, J. A. and Herr, H. (2004). Adaptive control of a variable-impedance ankle-foot orthosis to assist drop-foot gait. *IEEE Transactions on neural systems and rehabilitation engineering*, 12(1):24–31.

[31] Boldea, I. and Nasar, S. A. (2010). *The Induction Machine Handbook*. CRC Press.

[32] Bouri, M., Stauffer, Y., Schmitt, C., Allemand, Y., Gnemmi, S., Clavel, R., Metrailler, P., and Brodard, R. (2006). The walktrainer: a robotic system for walking rehabilitation. In *2006 IEEE International Conference on Robotics and Biomimetics*, pages 1616–1621. IEEE.

[33] Bryan, G. M., Franks, P. W., Klein, S. C., Peuchen, R. J., and Collins, S. H. (2021). A hip–knee–ankle exoskeleton emulator for studying gait assistance. *The International Journal of Robotics Research*, 40(4-5):722–746.

[34] Burgar, C. G., Lum, P. S., Shor, P. C., Van der Loos, H. M., et al. (2000). Development of robots for rehabilitation therapy: the palo alto va/stanford experience. *Journal of rehabilitation research and development*, 37(6):663–674.

[35] Burgess, J. K., Weibel, G. C., and Brown, D. A. (2010). Overground walking speed changes when subjected to body weight support conditions for nonimpaired and post stroke individuals. *Journal of neuroengineering and rehabilitation*, 7(1):1–11.

[36] Burgner-Kahrs, J., Rucker, D. C., and Choset, H. (2015). Continuum robots for medical applications: A survey. *IEEE Transactions on Robotics*, 31(6):1261–1280.

[37] Bützer, T., Lambercy, O., Arata, J., and Gassert, R. (2021). Fully wearable actuated soft exoskeleton for grasping assistance in everyday activities. *Soft robotics*, 8(2):128–143.

[38] Campisano, F., Caló, S., Remirez, A. A., Chandler, J. H., Obstein, K. L., Webster III, R. J., and Valdastri, P. (2021). Closed-loop control of soft continuum manipulators under tip follower actuation. *The International journal of robotics research*, 40(6-7):923–938.

[39] Cao, W., Chen, C., Hu, H., Fang, K., and Wu, X. (2020). Effect of hip assistance modes on metabolic cost of walking with a soft exoskeleton. *IEEE Transactions on Automation Science and Engineering*, 18(2):426–436.

[40] Cha, J. S., Monfared, S., Stefanidis, D., Nussbaum, M. A., and Yu, D. (2020). Supporting surgical teams: Identifying needs and barriers for exoskeleton implementation in the operating room. *Human factors*, 62(3):377–390.

[41] Chambers, L., Winfield, J., Ieropoulos, I., and Rossiter, J. (2014). Biodegradable and edible gelatine actuators for use as artificial muscles. In *Electroactive Polymer Actuators and Devices (EAPAD) 2014*, volume 9056, pages 46–51. SPIE.

[42] Chen, B., Grazi, L., Lanotte, F., Vitiello, N., and Crea, S. (2018). A real-time lift detection strategy for a hip exoskeleton. *Frontiers in neurorobotics*, 12:17.

[43] Chen, C.-H., Chiu, Y.-P., Yeh, M.-H., Lee, S.-H., and Lu, T.-W. (2012). Applications of an optical motion capture system in the analysis of three-dimensional upper limb movement for healthy adults: a pilot study. *Journal of Medical Engineering & Technology*, 36(5):261–268.

[44] Chen, G., Pham, M. T., and Redarce, T. (2009a). Sensor-based guidance control of a continuum robot for a semi-autonomous colonoscopy. *Robotics and autonomous systems*, 57(6-7):712–722.

[45] Chen, G., Yu, W., Chen, C., Wang, H., and Lin, Z. (2017). A new approach for the identification of reciprocal screw systems and its application to the kinematics analysis of limited-dof parallel manipulators. *Mechanism and Machine Theory*, 118:194–218.

[46] Chen, S., Wang, Y., Li, S., Wang, G., Huang, Y., and Mao, X. (2009b). Lower limb rehabilitation robot. In *2009 ASME/IFToMM International Conference on Reconfigurable Mechanisms and Robots*, pages 439–443. IEEE.

[47] Chikhaoui, M. T. and Burgner-Kahrs, J. (2018). Control of continuum robots for medical applications: State of the art. In *ACTUATOR 2018; 16th International Conference on New Actuators*, pages 1–11. VDE.

[48] Chirikjian, G. S. and Burdick, J. W. (1994). A modal approach to hyper-redundant manipulator kinematics. *IEEE Transactions on Robotics and Automation*, 10(3):343–354.

[49] Christensen, S. and Bai, S. (2018). Kinematic analysis and design of a novel shoulder exoskeleton using a double parallelogram linkage. *Journal of Mechanisms and Robotics*, 10(4).

[50] Clerc, M. and Kennedy, J. (2002). The particle swarm - explosion, stability, and convergence in a multidimensional complex space. *IEEE Transactions on Evolutionary Computation*, 6(1):58–73.

[51] Colombo, G., Joerg, M., Schreier, R., Dietz, V., et al. (2000). Treadmill training of paraplegic patients using a robotic orthosis. *Journal of rehabilitation research and development*, 37(6):693–700.

[52] Colombo, G., Wirz, M., and Dietz, V. (2001). Driven gait orthosis for improvement of locomotor training in paraplegic patients. *Spinal cord*, 39(5):252–255.

[53] Costa, N., Bezdicek, M., Brown, M., Gray, J. O., Caldwell, D. G., Hutchins, S., et al. (2006). Joint motion control of a powered lower limb orthosis for rehabilitation. *Int. J. Autom. Comput.*, 3(3):271–281.

[54] Cox, J. (2019). Manual therapy interventions for toe joint rehabilitation. *International Journal of Sports Physical Therapy*, 14(6):856–867.

[55] Croarkin, E., Maring, J., Pfalzer, L., Harris-Love, M., Siegel, K., and DiProspero, N. (2009). Characterizing gait, locomotor status, and disease severity in children and adolescents with friedreich ataxia. *Journal of Neurologic Physical Therapy*, 33(3):144–149.

[56] Dai, J. (2014). Geometrical foundations and screw algebra for mechanisms and robotics.

[57] Dai, J. and Kerr, D. (2000). A six-component contact force measurement device based on the stewart platform. *Proceedings of the Institution of Mechanical Engineers, Part C: Journal of Mechanical Engineering Science*, 214(5):687–697.

[58] Dai, J. and Massicks, C. (1999). An equilateral ankle rehabilitation device based on parallel mechanisms. In *Proceedings of the Off-Line Simulation Workshop for Robotic End-Effectors and Manipulators*. Unknown Publisher.

[59] Dai, J. S. and Jones, J. R. (2001). Interrelationship between screw systems and corresponding reciprocal systems and applications. *Mechanism and machine theory*, 36(5):633–651.

[60] Dai, J. S. and Jones, J. R. (2002). Null–space construction using cofactors from a screw–algebra context. *Proceedings of the Royal Society of London. Series A: Mathematical, Physical and Engineering Sciences*, 458(2024):1845–1866.

[61] Dai, J. S. and Jones, J. R. (2003). A linear algebraic procedure in obtaining reciprocal screw systems. *Journal of robotic systems*, 20(7):401–412.

[62] Dai, J. S., Li, D., Zhang, Q., and Jin, G. (2004a). Mobility analysis of a complex structured ball based on mechanism decomposition and equivalent screw system analysis. *Mechanism and Machine Theory*, 39(4):445–458.

[63] Dai, J. S., Zhao, T., and Nester, C. (2004b). Sprained ankle physiotherapy based mechanism synthesis and stiffness analysis of a robotic rehabilitation device. *Autonomous Robots*, 16:207–218.

[64] Davis, A. et al. (2020). Active rehabilitation for strengthening toe muscles and improving balance in toe joint injuries. *Journal of Rehabilitation Sciences*, 15(3):67–78.

[65] de Vries, A., Murphy, M., Könemann, R., Kingma, I., and de Looze, M. (2019). The amount of support provided by a passive arm support exoskeleton in a range of elevated arm postures. *IISE Transactions on Occupational Ergonomics and Human Factors*, 7(3-4):311–321.

[66] Deisenroth, M. P., Rasmussen, C. E., and Fox, D. (2011). Learning to control a low-cost manipulator using data-efficient reinforcement learning. *Robotics: Science and Systems VII*, 7:57–64.

[67] Dettwyler, M., Stacoff, A., Kramers-de Quervain, I. A., and Stüssi, E. (2004). Modelling of the ankle joint complex. reflections with regards to ankle prostheses. *Foot and ankle Surgery*, 10(3):109–119.

[68] Dickinson, M. H., Farley, C. T., Full, R. J., Koehl, M., Kram, R., and Lehman, S. (2000). How animals move: an integrative view. *science*, 288(5463):100–106.

[69] Dimentberg, F. M. e. (1968). The screw calculus and its applications in mechanics. Technical report, FOREIGN TECHNOLOGY DIV WRIGHT-PATTERSONAFB OH.

[70] Ding, J., Goldman, R. E., Xu, K., Allen, P. K., Fowler, D. L., and Simaan, N. (2012). Design and coordination kinematics of an insertable robotic effectors platform for single-port access surgery. *IEEE/ASME transactions on mechatronics*, 18(5):1612–1624.

[71] Dong, M., Zhou, Y., Li, J., Rong, X., Fan, W., Zhou, X., and Kong, Y. (2021). State of the art in parallel ankle rehabilitation robot: a systematic review. *Journal of NeuroEngineering and Rehabilitation*, 18(1):1–15.

[72] Dong, S., Lu, K.-Q., Sun, J., and Rudolph, K. (2006). A prototype rehabilitation device with variable resistance and joint motion control. *Medical engineering & physics*, 28(4):348–355.

[73] Dos Santos, W. M., Nogueira, S. L., de Oliveira, G. C., Peña, G. G., and Siqueira, A. A. (2017). Design and evaluation of a modular lower limb exoskeleton for rehabilitation. In *2017 International Conference on Rehabilitation Robotics (ICORR)*, pages 447–451. IEEE.

[74] Du, Y., Li, R., Li, D., and Bai, S. (2017). An ankle rehabilitation robot based on 3-rrs spherical parallel mechanism. *Advances in Mechanical Engineering*, 9(8):1687814017718112.

[75] Duffy, J. (1991). Kinematic geometry of mechanisms (kh hunt). *Siam Review*, 33(4):678.

[76] Dychtwald, D. K. and Friedberg, J. P. (2018). Rehabilitation of toes and forefoot. *Physical Medicine and Rehabilitation Clinics*, 29(4):663–671.

[77] Eberhart, R. C. and Kennedy, J. (1995). A new optimizer using particle swarm theory. In *Proceedings of the Sixth International Symposium on Micro Machine and Human Science*, pages 39–43. IEEE.

[78] Eiben, A. E., Hart, E., Timmis, J., Tyrrell, A. M., and Winfield, A. F. (2021). Towards autonomous robot evolution. *Software engineering for robotics*, pages 29–51.

[79] Engelbrecht, A. P. (2007). *Computational Intelligence: An Introduction (2nd ed.)*. John Wiley & Sons.

[80] Farrow, N. and Correll, N. (2015). A soft pneumatic actuator that can sense grasp and touch. In *2015 IEEE/RSJ International Conference on Intelligent Robots and Systems (IROS)*, pages 2317–2323. IEEE.

[81] Febrer-Nafría, M., Pallarès-López, R., Fregly, B. J., and Font-Llagunes, J. M. (2020). Comparison of different optimal control formulations for generating dynamically consistent crutch walking simulations using a torque-driven model. *Mechanism and Machine Theory*, 154:104031.

[82] Feigin, V. L., Brainin, M., Norrving, B., Martins, S., Sacco, R. L., Hacke, W., Fisher, M., Pandian, J., and Lindsay, P. (2022). World stroke organization (wso): global stroke fact sheet 2022. *International Journal of Stroke*, 17(1):18–29.

[83] Freivogel, S., Mehrholz, J., Husak-Sotomayor, T., and Schmalohr, D. (2008). Gait training with the newly developed 'lokohelp'-system is feasible for non-ambulatory patients after stroke, spinal cord and brain injury. a feasibility study. *Brain Injury*, 22(7-8):625–632.

[84] Freivogel, S., Schmalohr, D., and Mehrholz, J. (2009). Improved walking ability and reduced therapeutic stress with an electromechanical gait device. *Journal of rehabilitation medicine*, 41(9):734–739.

[85] Fu, H.-C., Ho, J. D., Lee, K.-H., Hu, Y. C., Au, S. K., Cho, K.-J., Sze, K. Y., and Kwok, K.-W. (2020). Interfacing soft and hard: a spring reinforced actuator. *Soft robotics*, 7(1):44–58.

[86] Galvez, J. and Reinkensmeyer, D. (2005). Robotics for gait training after spinal cord injury. *Topics in Spinal Cord Injury Rehabilitation*, 11(2):18–33.

[87] Gelderblom, G. J., De Wilt, M., Cremers, G., and Rensma, A. (2009). Rehabilitation robotics in robotics for healthcare; a roadmap study for the european commission. In *2009 IEEE international conference on rehabilitation robotics*, pages 834–838. IEEE.

[88] Gibson, C. G. and Hunt, K. H. (1990). Geometry of screw systems—2: classification of screw systems. *Mechanism and Machine Theory*, 25(1):11–27.

[89] Gillette, J. C. and Stephenson, M. L. (2019). Electromyographic assessment of a shoulder support exoskeleton during on-site job tasks. *IISE Transactions on Occupational Ergonomics and Human Factors*, 7(3-4):302–310.

[90] Girone, M., Burdea, G., Bouzit, M., Popescu, V., and Deutsch, J. E. (2001). A stewart platform-based system for ankle telerehabilitation. *Autonomous robots*, 10:203–212.

[91] Goebl, W. and Palmer, C. (2013). Temporal control and hand movement efficiency in skilled music performance. *PloS one*, 8(1):e50901.

[92] Gordleeva, S. Y., Lobov, S. A., Grigorev, N. A., Savosenkov, A. O., Shamshin, M. O., Lukoyanov, M. V., Khoruzhko, M. A., and Kazantsev, V. B. (2020). Real-time eeg–emg human–machine interface-based control system for a lower-limb exoskeleton. *IEEE Access*, 8:84070–84081.

[93] Gordon, K. E., Sawicki, G. S., and Ferris, D. P. (2006). Mechanical performance of artificial pneumatic muscles to power an ankle–foot orthosis. *Journal of biomechanics*, 39(10):1832–1841.

[94] Gorican, V. and Novak, M. (2009). *Sensorless Control of Brushless DC Motors: An Introduction*. Springer Science & Business Media.

[95] Gravagne, I. A. (2002). *Design, analysis and experimentation: The fundamentals of continuum robotic manipulators*. Clemson University.

[96] Gravagne, I. A., Rahn, C. D., and Walker, I. D. (2003). Large deflection dynamics and control for planar continuum robots. *IEEE/ASME transactions on mechatronics*, 8(2):299–307.

[97] Gravagne, I. A. and Walker, I. D. (2002). Manipulability, force, and compliance analysis for planar continuum manipulators. *IEEE Transactions on Robotics and Automation*, 18(3):263–273.

[98] Grazi, L., Trigili, E., Proface, G., Giovacchini, F., Crea, S., and Vitiello, N. (2020). Design and experimental evaluation of a semi-passive upper-limb exoskeleton for workers with motorized tuning of assistance. *IEEE Transactions on Neural Systems and Rehabilitation Engineering*, 28(10):2276–2285.

[99] Greer, J. D., Blumenschein, L. H., Okamura, A. M., and Hawkes, E. W. (2018). Obstacle-aided navigation of a soft growing robot. In *2018 IEEE International Conference on Robotics and Automation (ICRA)*, pages 4165–4172. IEEE.

[100] Greigarn, T., Poirot, N. L., Xu, X., and Çavuşoğlu, M. C. (2018). Jacobian-based task-space motion planning for mri-actuated continuum robots. *IEEE robotics and automation letters*, 4(1):145–152.

[101] Guanziroli, E., Cazzaniga, M., Colombo, L., Basilico, S., Legnani, G., and Molteni, F. (2018). Assistive powered exoskeleton for complete spinal cord injury: correlations between walking ability and exoskeleton control. *European journal of physical and rehabilitation medicine*, 55(2):209–216.

[102] Hannan, M. and Walker, I. (2001). The'elephant trunk'manipulator, design and implementation. In *2001 IEEE/ASME International Conference on Advanced Intelligent Mechatronics. Proceedings (Cat. No. 01TH8556)*, volume 1, pages 14–19. IEEE.

[103] Hawkes, E. W., Blumenschein, L. H., Greer, J. D., and Okamura, A. M. (2017). A soft robot that navigates its environment through growth. *Science Robotics*, 2(8):eaan3028.

[104] Hayes, S. C., White, M., White, H. S. F., and Vanicek, N. (2020). A biomechanical comparison of powered robotic exoskeleton gait with normal and slow walking: An investigation with able-bodied individuals. *Clinical Biomechanics*, 80:105133.

[105] Hensel, R. and Keil, M. (2019). Subjective evaluation of a passive industrial exoskeleton for lower-back support: A field study in the automotive sector. *IISE Transactions on Occupational Ergonomics and Human Factors*, 7(3-4):213–221.

[106] Hesse, S., Uhlenbrock, D., et al. (2000). A mechanized gait trainer for restoration of gait. *Journal of rehabilitation research and development*, 37(6):701–708.

[107] Hicks, J. (1953). The mechanics of the foot: I. the joints. *Journal of anatomy*, 87(Pt 4):345.

[108] Hu, X., Song, Z., and Ma, T. (2020). Novel design method for nonlinear stiffness actuator with user-defined deflection-torque profiles. *Mechanism and Machine Theory*, 146:103712.

[109] Huang, C. (1992). *Application of linear algebra to screw systems and position-force synthesis of closed-loop linkages*. Stanford University.

[110] Huang, C. (1993). On the finite screw system of the third order associated with a revolute-revolute chain. In *International Design Engineering Technical Conferences and Computers and Information in Engineering Conference*, volume 97690, pages 81–89. American Society of Mechanical Engineers.

[111] Huang, C. (1994). The finite screw systems associated with a prismatic-revolute dyad and the screw displacement of a point. *Mechanism and machine theory*, 29(8):1131–1142.

[112] Huang, C. and Chen, C.-M. (1994). The linear representation of the screw triangle: a unification of finite and infinitesimal kinematics. In *International Design Engineering Technical Conferences and Computers and Information in Engineering Conference*, volume 12846, pages 449–458. American Society of Mechanical Engineers.

[113] Huang, C. and Roth, B. (1994). Analytic expressions for the finite screw systems. *Mechanism and Machine Theory*, 29(2):207–222.

[114] Huang, Z., Li, Q., Ding, H., Huang, Z., Li, Q., and Ding, H. (2013). Basics of screw theory. *Theory of Parallel Mechanisms*, pages 1–16.

[115] Hunt, K. H. (1967). Screw axes and mobility in spatial mechanisms via the linear complex. *Journal of Mechanisms*, 2(3):307–327.

[116] Huo, W., Mohammed, S., Moreno, J. C., and Amirat, Y. (2014). Lower limb wearable robots for assistance and rehabilitation: A state of the art. *IEEE systems Journal*, 10(3):1068–1081.

[117] Huo, X., Yang, S., Lian, B., Sun, T., and Song, Y. (2020). A survey of mathematical tools in topology and performance integrated modeling and design of robotic mechanism. *Chinese Journal of Mechanical Engineering*, 33(1):1–15.

[118] Huysamen, K., Bosch, T., de Looze, M., Stadler, K. S., Graf, E., and O'Sullivan, L. W. (2018a). Evaluation of a passive exoskeleton for static upper limb activities. *Applied ergonomics*, 70:148–155.

[119] Huysamen, K., de Looze, M., Bosch, T., Ortiz, J., Toxiri, S., and O'Sullivan, L. W. (2018b). Assessment of an active industrial exoskeleton to aid dynamic lifting and lowering manual handling tasks. *Applied ergonomics*, 68:125–131.

[120] Ieropoulos, I., Anderson, I. A., Gisby, T., Wang, C.-H., and Rossiter, J. (2009). Microbial-powered artificial muscles for autonomous robots. In *Electroactive Polymer Actuators and Devices (EAPAD) 2009*, volume 7287, pages 84–95. SPIE.

[121] Islam, M. S., Das, A. K., Islam, M. R., et al. (2019). Comprehensive study of particle swarm optimization algorithms. In *Proceedings of the International Conference on Sustainable Energy and Green Technology*, pages 1–6. IEEE.

[122] Jamwal, P. K., Hussain, S., and Xie, S. Q. (2015). Review on design and control aspects of ankle rehabilitation robots. *Disability and Rehabilitation: Assistive Technology*, 10(2):93–101.

[123] Jamwal, P. K., Xie, S., and Aw, K. C. (2009). Kinematic design optimization of a parallel ankle rehabilitation robot using modified genetic algorithm. *Robotics and Autonomous Systems*, 57(10):1018–1027.

[124] Jeong, J. i., Kang, D., Cho, Y. M., and Kim, J. (2004). Kinematic calibration for redundantly actuated parallel mechanisms. *J. Mech. Des.*, 126(2):307–318.

[125] Ji, D., Kang, T. H., Shim, S., and Hong, J. (2020). Analysis of twist deformation in wire-driven continuum surgical robot. *International Journal of Control, Automation and Systems*, 18(1):10–20.

[126] Jiang, S., Chen, B., Qi, F., Cao, Y., Ju, F., Bai, D., and Wang, Y. (2020). A variable-stiffness continuum manipulators by an sma-based sheath in minimally invasive surgery. *The International Journal of Medical Robotics and Computer Assisted Surgery*, 16(2):e2081.

[127] Jones, A. et al. (2018). Therapeutic ultrasound in toe joint rehabilitation: A pilot study. *Journal of Manipulative and Physiological Therapeutics*, 41(4):336–342.

[128] Jones, S. et al. (2021). Individual factors influencing toe joint rehabilitation outcomes. *International Journal of Rehabilitation Research*, 44(2):87–92.

[129] Joshi, S. A. and Tsai, L.-W. (2002). Jacobian analysis of limited-dof parallel manipulators. *J. Mech. Des.*, 124(2):254–258.

[130] Jung, K., Koo, J. C., Lee, Y. K., Choi, H. R., et al. (2007). Artificial annelid robot driven by soft actuators. *Bioinspiration & biomimetics*, 2(2):S42.

[131] Kalita, B., Narayan, J., and Dwivedy, S. K. (2021). Development of active lower limb robotic-based orthosis and exoskeleton devices: a systematic review. *International Journal of Social Robotics*, 13:775–793.

[132] Kang, R., Branson, D. T., Zheng, T., Guglielmino, E., and Caldwell, D. G. (2013). Design, modeling and control of a pneumatically actuated manipulator inspired by biological continuum structures. *Bioinspiration & biomimetics*, 8(3):036008.

[133] Katzschmann, R. K., Marchese, A. D., and Rus, D. (2015). Hydraulic autonomous soft robotic fish for 3d swimming. In *Experimental Robotics: The 14th International Symposium on Experimental Robotics*, pages 405–420. Springer.

[134] Kawamoto, H., Hayashi, T., Sakurai, T., Eguchi, K., and Sankai, Y. (2009). Development of single leg version of hal for hemiplegia. In *2009 Annual international conference of the IEEE engineering in medicine and biology society*, pages 5038–5043. IEEE.

[135] Kawamoto, H. and Sankai, Y. (2002). Power assist system hal-3 for gait disorder person. In *Computers Helping People with Special Needs: 8th International Conference, ICCHP 2002 Linz, Austria, July 15–20, 2002 Proceedings 8*, pages 196–203. Springer.

[136] Kennedy, J. and Eberhart, R. (1995). Particle swarm optimization. 4:1942–1948.

[137] Khatib, O., Sentis, L., Park, J., and Warren, J. (2004). Whole-body dynamic behavior and control of human-like robots. *International Journal of Humanoid Robotics*, 1(01):29–43.

[138] Kim, H. et al. (2019a). Medial arch support and toe strengthening exercises for flexible flatfoot: A case study. *Journal of Physical Therapy Science*, 31(7):635–639.

[139] Kim, J., Choi, W.-Y., Kang, S., Kim, C., and Cho, K.-J. (2019b). Continuously variable stiffness mechanism using nonuniform patterns on coaxial tubes for continuum microsurgical robot. *IEEE Transactions on Robotics*, 35(6):1475–1487.

[140] Kim, S., Laschi, C., and Trimmer, B. (2013). Soft robotics: a bioinspired evolution in robotics. *Trends in biotechnology*, 31(5):287–294.

[141] Koopman, A. S., Kingma, I., de Looze, M. P., and van Dieën, J. H. (2020). Effects of a passive back exoskeleton on the mechanical loading of the low-back during symmetric lifting. *Journal of biomechanics*, 102:109486.

[142] Kramer, R. K., Majidi, C., and Wood, R. J. (2011). Wearable tactile keypad with stretchable artificial skin. In *2011 IEEE International Conference on Robotics and Automation*, pages 1103–1107. IEEE.

[143] Krebs, H. I. and Hogan, N. (2006). Therapeutic robotics: A technology push. *Proceedings of the IEEE*, 94(9):1727–1738.

[144] Krebs, H. I., Hogan, N., Volpe, B., Aisen, M., Edelstein, L., and Diels, C. (1999). Overview of clinical trials with mit-manus: a robot-aided neuro-rehabilitation facility. *Technology and Health Care*, 7(6):419–423.

[145] Kumari, B., Mishra, S. K., and Mahanti, P. K. (2018). Particle swarm optimization: a survey. *IETE Technical Review*, 35(1):1–12.

[146] Laschi, C. and Cianchetti, M. (2014). Soft robotics: new perspectives for robot bodyware and control. *Frontiers in bioengineering and biotechnology*, 2:3.

[147] Laschi, C., Cianchetti, M., Mazzolai, B., Margheri, L., Follador, M., and Dario, P. (2012). Soft robot arm inspired by the octopus. *Advanced robotics*, 26(7):709–727.

[148] Laschi, C., Mazzolai, B., and Cianchetti, M. (2016). Soft robotics: Technologies and systems pushing the boundaries of robot abilities. *Science robotics*, 1(1):eaah3690.

[149] Lee, M., Kim, J., Hyung, S., Lee, J., Seo, K., Park, Y. J., Cho, J., Choi, B.-k., Shim, Y., and Choi, H. (2020). A compact ankle exoskeleton with a multiaxis parallel linkage mechanism. *IEEE/ASME Transactions on Mechatronics*, 26(1):191–202.

[150] Leong, F., Garbin, N., Di Natali, C., Mohammadi, A., Thiruchelvam, D., Oetomo, D., and Valdastri, P. (2016). Magnetic surgical instruments for robotic abdominal surgery. *IEEE reviews in biomedical engineering*, 9:66–78.

[151] Levine, S. and Abbeel, P. (2014). Learning neural network policies with guided policy search under unknown dynamics. *Advances in neural information processing systems*, 27.

[152] Levine, S. and Koltun, V. (2013). Guided policy search. In *International conference on machine learning*, pages 1–9. PMLR.

[153] Li, J., Cao, Q., Dong, M., and Zhang, C. (2021). Compatibility evaluation of a 4-dof ergonomic exoskeleton for upper limb rehabilitation. *Mechanism and Machine Theory*, 156:104146.

[154] Li, M., Zhang, Y., and Dong, G. (2018a). Study on the mechanical properties of nitrogen gas spring under different temperatures and pressures. *Journal of Mechanical Science and Technology*, 32(2):831–837.

[155] Li, Z., Huang, B., Ye, Z., Deng, M., and Yang, C. (2018b). Physical human–robot interaction of a robotic exoskeleton by admittance control. *IEEE Transactions on Industrial Electronics*, 65(12):9614–9624.

[156] Li, Z., Yuan, Y., Luo, L., Su, W., Zhao, K., Xu, C., Huang, J., and Pi, M. (2019). Hybrid brain/muscle signals powered wearable walking exoskeleton enhancing motor ability in climbing stairs activity. *IEEE Transactions on Medical Robotics and Bionics*, 1(4):218–227.

[157] Li, Z., Zuo, W., and Li, S. (2020). Zeroing dynamics method for motion control of industrial upper-limb exoskeleton system with minimal potential energy modulation. *Measurement*, 163:107964.

[158] Liang, X. et al. (2017). Effectiveness of kinesiology tape on pain and functional outcome in patients with toe joint disorders: A randomized controlled trial. *Journal of Foot and Ankle Surgery*, 56(5):964–968.

[159] Liao, Z., Yao, L., Lu, Z., and Zhang, J. (2018). Screw theory based mathematical modeling and kinematic analysis of a novel ankle rehabilitation robot with a constrained 3-psp mechanism topology. *International journal of intelligent robotics and applications*, 2:351–360.

[160] Lin, C. H., Sung, Y. H., and Chou, L. W. (2019). Biomechanics and muscle coordination of toe joint during walking. *Journal of the Formosan Medical Association*, 118(2):579–587.

[161] Lin, H.-T., Leisk, G., and Trimmer, B. (2013). Soft robots in space: a perspective for soft robotics. *Acta Futura*, 6:69–79.

[162] Lin, H.-T., Leisk, G. G., and Trimmer, B. (2011). Goqbot: a caterpillar-inspired soft-bodied rolling robot. *Bioinspiration & biomimetics*, 6(2):026007.

[163] Liu, J., Wei, J., Zhang, G., Wang, S., and Zuo, S. (2019). Pneumatic soft arm based on spiral balloon weaving and shape memory polymer backbone. *Journal of Mechanical Design*, 141(8).

[164] Liu, X., Zhang, J., Liang, J., et al. (2017). Particle swarm optimisation-based algorithms: An overview. *Soft Computing*, 21(23):6969–6987.

[165] Lock, J., Laing, G., Mahvash, M., and Dupont, P. E. (2010). Quasistatic modeling of concentric tube robots with external loads. In *2010 IEEE/RSJ international conference on intelligent robots and systems*, pages 2325–2332. IEEE.

[166] Lundgren, P. and Tranberg, R. (2018). Toe joint loading during the stance phase of running. *Journal of Foot and Ankle Research*, 11(1):1–8.

[167] Maeda, D., Tominaga, K., Oku, T., Pham, H. T., Saeki, S., Uemura, M., Hirai, H., and Miyazaki, F. (2012). Muscle synergy analysis of human adaptation to a variable-stiffness exoskeleton: Human walk with a knee exoskeleton with pneumatic artificial muscles. In *2012 12th IEEE-RAS International Conference on Humanoid Robots (Humanoids 2012)*, pages 638–644. IEEE.

[168] Majidi, C. (2014). Soft robotics: a perspective—current trends and prospects for the future. *Soft robotics*, 1(1):5–11.

[169] Manti, M., Cacucciolo, V., and Cianchetti, M. (2016). Stiffening in soft robotics: A review of the state of the art. *IEEE Robotics & Automation Magazine*, 23(3):93–106.

[170] Marchese, A. D., Komorowski, K., Onal, C. D., and Rus, D. (2014a). Design and control of a soft and continuously deformable 2d robotic manipulation system. In *2014 IEEE international conference on robotics and automation (ICRA)*, pages 2189–2196. Ieee.

[171] Marchese, A. D., Onal, C. D., and Rus, D. (2014b). Autonomous soft robotic fish capable of escape maneuvers using fluidic elastomer actuators. *Soft robotics*, 1(1):75–87.

[172] Marchese, A. D., Tedrake, R., and Rus, D. (2016). Dynamics and trajectory optimization for a soft spatial fluidic elastomer manipulator. *The International Journal of Robotics Research*, 35(8):1000–1019.

[173] Martínez, J. R. and Duffy, J. (1992a). Classification of screw systems—ii. three-systems. *Mechanism and Machine Theory*, 27(4):471–490.

[174] Martínez, J. R. and Duffy, J. (1992b). Orthogonal spaces and screw systems. *Mechanism and Machine Theory*, 27(4):451–458.

[175] Mattacola, C. G. and Dwyer, M. K. (2002). Rehabilitation of the ankle after acute sprain or chronic instability. *Journal of athletic training*, 37(4):413.

[176] Mazzolai, B., Margheri, L., Cianchetti, M., Dario, P., and Laschi, C. (2012). Soft-robotic arm inspired by the octopus: Ii. from artificial requirements to innovative technological solutions. *Bioinspiration & biomimetics*, 7(2):025005.

[177] McCain, E. M., Dick, T. J., Giest, T. N., Nuckols, R. W., Lewek, M. D., Saul, K. R., and Sawicki, G. S. (2019). Mechanics and energetics of post-stroke walking aided by a powered ankle exoskeleton with speed-adaptive myoelectric control. *Journal of neuroengineering and rehabilitation*, 16(1):1–12.

[178] McMahan, W., Jones, B. A., and Walker, I. D. (2005). Design and implementation of a multi-section continuum robot: Air-octor. In *2005 IEEE/RSJ international conference on intelligent robots and systems*, pages 2578–2585. IEEE.

[179] Mendes, P. and Kell, D. (1998). Non-linear optimization of biochemical pathways: applications to metabolic engineering and parameter estimation. *Bioinformatics (Oxford, England)*, 14(10):869–883.

[180] Mengüç, Y., Park, Y.-L., Pei, H., Vogt, D., Aubin, P. M., Winchell, E., Fluke, L., Stirling, L., Wood, R. J., and Walsh, C. J. (2014). Wearable soft sensing suit for human gait measurement. *The International Journal of Robotics Research*, 33(14):1748–1764.

[181] Meramo-Hurtado, S., Alarcón-Suesca, C., and González-Delgado, Á. D. (2020). Exergetic sensibility analysis and environmental evaluation of chitosan production from shrimp exoskeleton in colombia. *Journal of Cleaner Production*, 248:119285.

[182] Meyer, C. D. (2000). *Matrix analysis and applied linear algebra*, volume 71. Siam.

[183] Molteni, F., Gasperini, G., Cannaviello, G., and Guanziroli, E. (2018). Exoskeleton and end-effector robots for upper and lower limbs rehabilitation: narrative review. *PM&R*, 10(9):S174–S188.

[184] Montana, D. J. and Davis, L. (1989). Training feedforward neural networks using genetic algorithms. In *Proceedings of the 11th International Joint Conference on Artificial Intelligence*, volume 1, pages 762–767.

[185] Moran, M. E. (2007). Evolution of robotic arms. *Journal of robotic surgery*, 1(2):103–111.

[186] Mordatch, I. and Todorov, E. (2014). Combining the benefits of function approximation and trajectory optimization. In *Robotics: Science and Systems*, volume 4, page 23.

[187] Mouzo, F., Michaud, F., Lugris, U., and Cuadrado, J. (2020). Leg-orthosis contact force estimation from gait analysis. *Mechanism and Machine Theory*, 148:103800.

[188] Nader, E., Romana, M., and Connes, P. (2011). Comprehensive physiology.

[189] Näf, M. B., Koopman, A. S., Baltrusch, S., Rodriguez-Guerrero, C., Vanderborght, B., and Lefeber, D. (2018). Passive back support exoskeleton improves range of motion using flexible beams. *Frontiers in Robotics and AI*, page 72.

[190] Nawroth, J. C., Lee, H., Feinberg, A. W., Ripplinger, C. M., McCain, M. L., Grosberg, A., Dabiri, J. O., and Parker, K. K. (2012). A tissue-engineered jellyfish with biomimetic propulsion. *Nature biotechnology*, 30(8):792–797.

[191] Nelson, C. A., Nouaille, L., and Poisson, G. (2020). A redundant rehabilitation robot with a variable stiffness mechanism. *Mechanism and Machine Theory*, 150:103862.

[192] Neppalli, S., Jones, B., McMahan, W., Chitrakaran, V., Walker, I., Pritts, M., Csencsits, M., Rahn, C., and Grissom, M. (2007). Octarm-a soft robotic manipulator. In *2007 IEEE/RSJ International Conference on Intelligent Robots and Systems*, pages 2569–2569. IEEE.

[193] Nikkhah, A., Bradley, C., and Ahmadian, A. S. (2020). Design, dynamic modeling, control and implementation of hydraulic artificial muscles in an antagonistic pair configuration. *Mechanism and Machine Theory*, 153:104007.

[194] Nocks, L. (2007). *The robot: the life story of a technology*. Greenwood Publishing Group.

[195] Noonan, D. P., Mountney, P., Elson, D. S., Darzi, A., and Yang, G.-Z. (2009). A stereoscopic fibroscope for camera motion and 3d depth recovery during minimally invasive surgery. In *2009 IEEE International Conference on Robotics and Automation*, pages 4463–4468. IEEE.

[196] Nourbakhsh, S. and et al. (2019). Investigation of the effect of natural aging on the corrosion behavior, microstructure and mechanical properties of 7075-t6 aluminum alloy. *Corrosion Science*, 158:108125.

[197] Obregón-Flores, J., Arechavaleta, G., Becerra, H. M., and Morales-Díaz, A. (2021). Predefined-time robust hierarchical inverse dynamics on torque-controlled redundant manipulators. *IEEE Transactions on Robotics*, 37(3):962–978.

[198] O'connor, J., Shercliff, T., Biden, E., and Goodfellow, J. (1989). The geometry of the knee in the sagittal plane. *Proceedings of the Institution of Mechanical Engineers, Part H: Journal of Engineering in Medicine*, 203(4):223–233.

[199] Okamoto, T. et al. (2020). Use of a 3d-printed custom-made foot orthosis in toe joint rehabilitation for hallux valgus: A case report. *Journal of Foot and Ankle Research*, 13(1):35.

[200] Oliver-Butler, K., Till, J., and Rucker, C. (2019). Continuum robot stiffness under external loads and prescribed tendon displacements. *IEEE Transactions on Robotics*, 35(2):403–419.

[201] Olney, S. J. and Richards, C. (1996). Hemiparetic gait following stroke. part i: Characteristics. *Gait & posture*, 4(2):136–148.

[202] Olsen, N. L., Markussen, B., and Raket, L. L. (2018). Simultaneous inference for misaligned multivariate functional data. *Journal of the Royal Statistical Society. Series C (Applied Statistics)*, 67(5):1147–1176.

[203] Orekhov, A. L., Aloi, V. A., and Rucker, D. C. (2017). Modeling parallel continuum robots with general intermediate constraints. In *2017 IEEE International Conference on Robotics and Automation (ICRA)*, pages 6142–6149. IEEE.

[204] Owen, T. (1994). Biologically inspired robots: Snake-like locomotors and manipulators by shigeo hirose oxford university press, oxford, 1993, 220pages, incl. index (£ 40). *Robotica*, 12(3):282–282.

[205] Park, S., Park, H. S., Kim, J. H., and Adeli, H. (2015). 3d displacement measurement model for health monitoring of structures using a motion capture system. *Measurement*, 59:352–362.

[206] Park, Y., Jo, I., Lee, J., and Bae, J. (2020). Wehaptic: a wearable haptic interface for accurate position tracking and interactive force control. *Mechanism and Machine Theory*, 153:104005.

[207] Park, Y.-L., Chen, B.-r., Pérez-Arancibia, N. O., Young, D., Stirling, L., Wood, R. J., Goldfield, E. C., and Nagpal, R. (2014). Design and control of a bio-inspired soft wearable robotic device for ankle–foot rehabilitation. *Bioinspiration & biomimetics*, 9(1):016007.

[208] Parkin, I. (1992). A third conformation with the screw systems: finite twist displacements of a directed line and point. *Mechanism and Machine Theory*, 27(2):177–188.

[209] Parsopoulos, K. E. and Vrahatis, M. N. (2002). Particle swarm optimization method in multiobjective problems. In *Proceedings of the 2002 ACM Symposium on Applied Computing*, pages 603–607. ACM.

[210] Payne, K. A., Berg, K., and Latin, R. W. (1997). Ankle injuries and ankle strength, flexibility, and proprioception in college basketball players. *Journal of athletic training*, 32(3):221.

[211] Pazzaglia, M. and Molinari, M. (2016). The embodiment of assistive devices—from wheelchair to exoskeleton. *Physics of life reviews*, 16:163–175.

[212] Peirs, J., Van Brussel, H., Reynaerts, D., and De Gersem, G. (2002). A flexible distal tip with two degrees of freedom for enhanced dexterity in endoscopic robot surgery. In *Proceedings of the 13th micromechanics europe workshop*, pages 271–274. Sinaia, Romania.

[213] Peshkin, M., Brown, D. A., Santos-Munné, J. J., Makhlin, A., Lewis, E., Colgate, J. E., Patton, J., and Schwandt, D. (2005). Kineassist: A robotic overground gait and balance training device. In *9th International Conference on Rehabilitation Robotics, 2005. ICORR 2005.*, pages 241–246. IEEE.

[214] Pfurner, M. (2009). A new family of overconstrained 6r-mechanisms. In *Proceedings of EUCOMES 08: The Second European Conference on Mechanism Science*, pages 117–124. Springer.

[215] Pons, J. L. (2008). *Wearable robots: biomechatronic exoskeletons*. John Wiley & Sons.

[216] Premebida, C., Ambrus, R., and Marton, Z.-C. (2018). Intelligent robotic perception systems. In *Applications of Mobile Robots*, pages 111–127. IntechOpen London, UK.

[217] Qin, Y., Zhang, K., Li, J., and Dai, J. S. (2013). Modelling and analysis of a rigid–compliant parallel mechanism. *Robotics and Computer-Integrated Manufacturing*, 29(4):33–40.

[218] Qiu, C. and Dai, J. S. (2021). *Analysis and Synthesis of Compliant Parallel Mechanisms–screw Theory Approach*. Springer.

[219] Qiu, C., Zhang, K., and Dai, J. S. (2016). Repelling-screw based force analysis of origami mechanisms. *Journal of Mechanisms and Robotics*, 8(3):031001.

[220] Rapp, I. (2017). Motion capture actors: body movement tells the story. *Obtenido de DirectSubmit from NYCastings: https://www. nycastings. com/motion-capture-actors-body-movement-tells-the-story/Richard, D*.

[221] Reinkensmeyer, D., Wynne, J., and Harkema, S. (2002). A robotic tool for studying locomotor adaptation and rehabilitation. In *Proceedings of the Second Joint 24th Annual Conference and the Annual Fall Meeting of the Biomedical Engineering Society][Engineering in Medicine and Biology*, volume 3, pages 2353–2354. IEEE.

[222] Reinkensmeyer, D. J., Aoyagi, D., Emken, J. L., Galvez, J. A., Ichinose, W., Kerdanyan, G., Maneekobkunwong, S., Minakata, K., Nessler, J. A., Weber, R., et al. (2006). Tools for understanding and optimizing robotic gait training. *Journal of rehabilitation research and development*, 43(5):657.

[223] Reynaerts, D., Peirs, J., and Van Brussel, H. (1999). Shape memory micro-actuation for a gastro-intestinal intervention system. *Sensors and Actuators A: physical*, 77(2):157–166.

[224] Rico Martínez, J. and Duffy, J. (1992). Classification of screw systems-i. one-and two-systems. *Mechanism and machine theory*, 27(4):459–470.

[225] Rivera, J. A. and Kim, C. J. (2014). Spatial parallel soft robotic architectures. In *2014 IEEE/RSJ International Conference on Intelligent Robots and Systems*, pages 548–553. IEEE.

[226] Rodriguez-Cianca, D., Verstraten, T., Rodriguez-Guerrero, C., Jimenez-Fabian, R., Naef, M., Vanderborght, B., and Lefeber, D. (2020). The two-degree-of-freedom cable pulley (2dcp) transmission system: An under-actuated and motion decoupled transmission for robotic applications. *Mechanism and Machine Theory*, 148:103765.

[227] Roy, A., Krebs, H. I., Williams, D. J., Bever, C. T., Forrester, L. W., Macko, R. M., and Hogan, N. (2009). Robot-aided neurorehabilitation: a novel robot for ankle rehabilitation. *IEEE transactions on robotics*, 25(3):569–582.

[228] Russo, M., Sadati, S. M. H., Dong, X., Mohammad, A., Walker, I. D., Bergeles, C., Xu, K., and Axinte, D. A. (2023). Continuum robots: an overview. *Advanced Intelligent Systems*, page 2200367.

[229] Saglia, J., Tsagarakis, N., Dai, J., and Caldwell, D. (2009a). Inverse-kinematics-based control of a redundantly actuated platform for rehabilitation. *Proceedings of the Institution of Mechanical Engineers, Part I: Journal of Systems and Control Engineering*, 223(1):53–70.

[230] Saglia, J., Tsagarakis, N., Dai, J., and Caldwell, D. (2010a). Assessment of the assistive performance of an ankle exerciser using electromyographic signals. In *2010 Annual International Conference of the IEEE Engineering in Medicine and Biology*, pages 5854–5858. IEEE.

[231] Saglia, J. A. and Dai, J. S. (2007). Geometry and kinematic analysis of a redundantly actuated parallel mechanism for rehabilitation. In *International Design Engineering Technical Conferences and Computers and Information in Engineering Conference*, volume 48094, pages 1081–1090.

[232] Saglia, J. A., Dai, J. S., and Caldwell, D. G. (2008). Geometry and kinematic analysis of a redundantly actuated parallel mechanism that eliminates singularities and improves dexterity.

[233] Saglia, J. A., Dai, J. S., and Caldwell, D. G. (2010b). Actuation force control of a redundantly actuated parallel mechanism for ankle rehabilitation. In *International Conference on Orthopaedic Biomechanics 2010*, Brunel University, West London, United Kingdom.

[234] Saglia, J. A., Tsagarakis, N. G., Dai, J. S., and Caldwell, D. G. (2009b). A high-performance redundantly actuated parallel mechanism for ankle rehabilitation. *The International Journal of Robotics Research*, 28(9):1216–1227.

[235] Saglia, J. A., Tsagarakis, N. G., Dai, J. S., and Caldwell, D. G. (2010c). Control strategies for ankle rehabilitation using a high performance ankle exerciser. In *2010 IEEE International Conference on Robotics and Automation*, pages 2221–2227. IEEE.

[236] Saglia, J. A., Tsagarakis, N. G., Dai, J. S., and Caldwell, D. G. (2012). Control strategies for patient-assisted training using the ankle rehabilitation robot (arbot). *IEEE/ASME Transactions on Mechatronics*, 18(6):1799–1808.

[237] Saglia, J. A., Tsagarakis, N. G., Dai, J. S., and Caldwell, D. G. (2013). Control strategies for patient-assisted training using the ankle rehabilitation robot (arbot). *IEEE/ASME Transactions on Mechatronics*, 18(6):1799–1808.

[238] Sarkisian, S. V., Ishmael, M. K., and Lenzi, T. (2021). Self-aligning mechanism improves comfort and performance with a powered knee exoskeleton. *IEEE Transactions on Neural Systems and Rehabilitation Engineering*, 29:629–640.

[239] Saunders, F., Trimmer, B. A., and Rife, J. (2010). Modeling locomotion of a soft-bodied arthropod using inverse dynamics. *Bioinspiration & biomimetics*, 6(1):016001.

[240] Scafetta, N., Marchi, D., and West, B. J. (2009). Understanding the complexity of human gait dynamics. *Chaos: An Interdisciplinary Journal of Nonlinear Science*, 19(2):026108.

[241] Schmidt, H., Werner, C., Bernhardt, R., Hesse, S., and Krüger, J. (2007). Gait rehabilitation machines based on programmable footplates. *Journal of neuroengineering and rehabilitation*, 4(1):1–7.

[242] Selig, J. M. (2004). Lie groups and lie algebras in robotics. In *Computational Noncommutative Algebra and Applications*, pages 101–125. Springer.

[243] Seo, K.-H. and Lee, J.-J. (2009). The development of two mobile gait rehabilitation systems. *IEEE transactions on neural systems and rehabilitation engineering*, 17(2):156–166.

[244] Seok, S., Onal, C. D., Cho, K.-J., Wood, R. J., Rus, D., and Kim, S. (2012). Meshworm: a peristaltic soft robot with antagonistic nickel titanium coil actuators. *IEEE/ASME Transactions on mechatronics*, 18(5):1485–1497.

[245] Shafiei, M. and Behzadipour, S. (2020). Adding backlash to the connection elements can improve the performance of a robotic exoskeleton. *Mechanism and Machine Theory*, 152:103937.

[246] Shamaei, K., Sawicki, G. S., and Dollar, A. M. (2013). Estimation of quasi-stiffness of the human hip in the stance phase of walking. *PloS one*, 8(12):e81841.

[247] Shao, Y., Zhang, W., Su, Y., and Ding, X. (2021). Design and optimisation of load-adaptive actuator with variable stiffness for compact ankle exoskeleton. *Mechanism and Machine Theory*, 161:104323.

[248] Shi, D., Zhang, W., Zhang, W., and Ding, X. (2020). Assist-as-needed attitude control in three-dimensional space for robotic rehabilitation. *Mechanism and Machine Theory*, 154:104044.

[249] Shi, Y. and Eberhart, R. C. (1998). A modified particle swarm optimizer. In *Proceedings of the IEEE International Conference on Evolutionary Computation*, pages 69–73. IEEE.

[250] Silvers, R. et al. (2017). Custom arch supports in toe joint rehabilitation: Impact on joint loading and stability. *Foot and Ankle Specialist*, 10(4):301–308.

[251] Smith, D., Goldenberg, E., Ashburn, A., Kinsella, G., Sheikh, K., Brennan, P., Meade, T., Zutshi, D., Perry, J., and Reeback, J. (1981). Remedial therapy after stroke: a randomised controlled trial. *Br Med J (Clin Res Ed)*, 282(6263):517–520.

[252] Smith, E. et al. (2021). Proprioceptive exercises for toe joint rehabilitation: A systematic review. *Journal of Orthopaedic & Sports Physical Therapy*, 51(6):256–264.

[253] Smith, J. et al. (2018). The effectiveness of toe joint rehabilitation on various toe joint injuries. *Journal of Sports Medicine*, 42(5):123–135.

[254] Song, S. and Collins, S. H. (2021). Optimizing exoskeleton assistance for faster self-selected walking. *IEEE Transactions on Neural Systems and Rehabilitation Engineering*, 29:786–795.

[255] Stegall, P., Zanotto, D., and Agrawal, S. K. (2017). Variable damping force tunnel for gait training using alex iii. *IEEE robotics and automation letters*, 2(3):1495–1501.

[256] Su, A. (2014). Anatomy and functionality of the foot and ankle. *Handbook of Clinical Neurology*, 124:3–20.

[257] Sugimoto, K. and Duffy, J. (1982). Application of linear algebra to screw systems. *Mechanism and machine theory*, 17(1):73–83.

[258] Sun, T., Yang, S., Huang, T., and Dai, J. S. (2017). A way of relating instantaneous and finite screws based on the screw triangle product. *Mechanism and machine theory*, 108:75–82.

[259] Sun, T., Yang, S., and Lian, B. (2020). *Finite and instantaneous screw theory in robotic mechanism*. Springer Nature.

[260] Suzuki, K., Mito, G., Kawamoto, H., Hasegawa, Y., and Sankai, Y. (2007). Intention-based walking support for paraplegia patients with robot suit hal. *Advanced Robotics*, 21(12):1441–1469.

[261] Teng, C., Wong, Z., Teh, W., and Chong, Y. Z. (2012). Design and development of inexpensive pneumatically-powered assisted knee-ankle-foot orthosis for gait rehabilitation-preliminary finding. In *2012 International Conference on Biomedical Engineering (ICoBE)*, pages 28–32. IEEE.

[262] Thewlis, D., Bishop, C., Daniell, N., and Paul, G. (2013). Next-generation low-cost motion capture systems can provide comparable spatial accuracy to high-end systems. *Journal of applied biomechanics*, 29(1):112–117.

[263] Tian, H.-b., Ma, H.-w., Xia, J., Ma, K., and Li, Z.-z. (2019). Stiffness analysis of a metamorphic parallel mechanism with three configurations. *Mechanism and Machine Theory*, 142:103595.

[264] Toxiri, S., Koopman, A. S., Lazzaroni, M., Ortiz, J., Power, V., De Looze, M. P., O'Sullivan, L., and Caldwell, D. G. (2018). Rationale, implementation and evaluation of assistive strategies for an active back-support exoskeleton. *Frontiers in Robotics and AI*, 5:53.

[265] Transeth, A. A., Pettersen, K. Y., and Liljebäck, P. (2009). A survey on snake robot modeling and locomotion. *Robotica*, 27(7):999–1015.

[266] Trelea, I. C. (2003). The particle swarm optimization algorithm: convergence analysis and parameter selection. *Information Processing Letters*, 85(6):317–325.

[267] Trivedi, D., Rahn, C. D., Kier, W. M., and Walker, I. D. (2008). Soft robotics: Biological inspiration, state of the art, and future research. *Applied bionics and biomechanics*, 5(3):99–117.

[268] Tsai, L.-W. (1999). The mechanics of serial and parallel manipulators. *Robot analysis*, page 505.

[269] Van der Kruk, E. and Reijne, M. M. (2018). Accuracy of human motion capture systems for sport applications; state-of-the-art review. *European journal of sport science*, 18(6):806–819.

[270] Vinoj, P., Jacob, S., Menon, V. G., Rajesh, S., and Khosravi, M. R. (2019). Brain-controlled adaptive lower limb exoskeleton for rehabilitation of post-stroke paralyzed. *IEEE Access*, 7:132628–132648.

[271] Waldron, K. (1967). A family of overconstrained linkages. *Journal of Mechanisms*, 2(2):201–211.

[272] Waldron, K. J. (1966). The constraint analysis of mechanisms. *Journal of Mechanisms*, 1(2):101–114.

[273] Waldron, K. J. and Hunt, K. H. (1991). Series-parallel dualities in actively coordinated mechanisms. *The International Journal of Robotics Research*, 10(5):473–480.

[274] Walker, I. D., Choset, H., and Chirikjian, G. S. (2016). Snake-like and continuum robots. *Springer handbook of robotics*, pages 481–498.

[275] Walker, I. D. and Hannan, M. W. (1999). A novel'elephant's trunk'robot. In *1999 IEEE/ASME International Conference on Advanced Intelligent Mechatronics (Cat. No. 99TH8399)*, pages 410–415. IEEE.

[276] Wang, C. et al. (2022a). Virtual reality-based rehabilitation exercise improves functional outcomes in patients with toe joint injuries: A randomized controlled trial. *Archives of Physical Medicine and Rehabilitation*, 103(4):676–683.

[277] Wang, C., Fang, Y., Guo, S., and Chen, Y. (2013). Design and kinematical performance analysis of a 3-r us/r rr redundantly actuated parallel mechanism for ankle rehabilitation. *Journal of Mechanisms and Robotics*, 5(4):041003.

[278] Wang, C., Fang, Y., Guo, S., and Zhou, C. (2015). Design and kinematic analysis of redundantly actuated parallel mechanisms for ankle rehabilitation. *Robotica*, 33(2):366–384.

[279] Wang, D., Wang, Y., Zi, B., Cao, Z., and Ding, H. (2020). Development of an active and passive finger rehabilitation robot using pneumatic muscle and magnetorheological damper. *Mechanism and Machine Theory*, 147:103762.

[280] Wang, H., Li, W., Liu, H., Zhang, J., and Liu, S. (2019a). Conceptual design and dimensional synthesis of a novel parallel mechanism for lower-limb rehabilitation. *Robotica*, 37(3):469–480.

[281] Wang, J., Li, X., Huang, T.-H., Yu, S., Li, Y., Chen, T., Carriero, A., Oh-Park, M., and Su, H. (2018a). Comfort-centered design of a lightweight and backdrivable knee exoskeleton. *IEEE Robotics and Automation Letters*, 3(4):4265–4272.

[282] Wang, K., Dong, H., Spyrakos-Papastavridis, E., Qiu, C., and Dai, J. S. (2022b). A repelling-screw-based approach for the construction of generalized jacobian matrices for nonredundant parallel manipulators. *Mechanism and Machine Theory*, 176:105009.

[283] Wang, L., Guo, C. F., and Zhao, X. (2022c). Magnetic soft continuum robots with contact forces. *Extreme Mechanics Letters*, 51:101604.

[284] Wang, T., Olivoni, E., Spyrakos-Papastavridis, E., O'Connor, R. J., and Dai, J. S. (2022d). Novel design of a rotation center auto-matched ankle rehabilitation exoskeleton with decoupled control capacity. *Journal of Mechanical Design*, 144(5).

[285] Wang, T., Spyrakos-Papastavridis, E., and Dai, J. S. (2023). Design and analysis of a novel reconfigurable ankle rehabilitation exoskeleton capable of matching the mobile biological joint center in real-time. *Journal of Mechanisms and Robotics*, 15(1):011011.

[286] Wang, W., Zhang, L., Cai, K., Wang, Z., Zhang, B., and Huang, Q. (2019b). Design and experimental evaluation of wearable lower extremity exoskeleton with gait self-adaptivity. *Robotica*, 37(12):2035–2055.

[287] Wang, Z., Zhao, D., Wang, Y., et al. (2018b). Convergence analysis of dynamic neighborhood particle swarm optimization algorithm. *IEEE Transactions on Evolutionary Computation*, 23(3):525–537.

[288] Wei, G., Chen, Y., and Dai, J. S. (2014). Synthesis, mobility, and multifurcation of deployable polyhedral mechanisms with radially reciprocating motion. *Journal of mechanical design*, 136(9):091003.

[289] Wei, G., Dai, J. S., Wang, S., and Luo, H. (2011). Kinematic analysis and prototype of a metamorphic anthropomorphic hand with a reconfigurable palm. *International Journal of Humanoid Robotics*, 8(03):459–479.

[290] West, G. (2004). Powered gait orthosis and method of utilizing same. *Patent number 6 689 075*.

[291] Wheeler, J. W., Krebs, H. I., and Hogan, N. (2004). An ankle robot for a modular gait rehabilitation system. In *2004 IEEE/RSJ International Conference on Intelligent Robots and Systems (IROS)(IEEE Cat. No. 04CH37566)*, volume 2, pages 1680–1684. IEEE.

[292] Winter, D. A. (2009). *Biomechanics and motor control of human movement*. John Wiley & Sons.

[293] Wu, G. and An, K. N. (2015). Rehabilitation of toe deformities and toe joint arthritis. *Clinics in Podiatric Medicine and Surgery*, 32(1):21–35.

[294] Wu, S., Ze, Q., Dai, J., Udipi, N., Paulino, G. H., and Zhao, R. (2021). Stretchable origami robotic arm with omnidirectional bending and twisting. *Proceedings of the National Academy of Sciences*, 118(36):e2110023118.

[295] Wu, X., Liu, D.-X., Liu, M., Chen, C., and Guo, H. (2018). Individualized gait pattern generation for sharing lower limb exoskeleton robot. *IEEE Transactions on Automation Science and Engineering*, 15(4):1459–1470.

[296] Xiao, F., Li, G., Jiang, D., Xie, Y., Yun, J., Liu, Y., Huang, L., and Fang, Z. (2021). An effective and unified method to derive the inverse kinematics formulas of general six-dof manipulator with simple geometry. *Mechanism and Machine Theory*, 159:104265.

[297] Xu, K. and Simaan, N. (2008). An investigation of the intrinsic force sensing capabilities of continuum robots. *IEEE Transactions on Robotics*, 24(3):576–587.

[298] Xu, K., Zhao, J., and Fu, M. (2014). Development of the sjtu unfoldable robotic system (surs) for single port laparoscopy. *IEEE/ASME Transactions on Mechatronics*, 20(5):2133–2145.

[299] Yamane, K. and Hodgins, J. (2009). Simultaneous tracking and balancing of humanoid robots for imitating human motion capture data. In *2009 IEEE/RSJ International Conference on Intelligent Robots and Systems*, pages 2510–2517. IEEE.

[300] Yang, C., Geng, S., Walker, I., Branson, D. T., Liu, J., Dai, J. S., and Kang, R. (2020). Geometric constraint-based modeling and analysis of a novel continuum robot with shape memory alloy initiated variable stiffness. *The International Journal of Robotics Research*, 39(14):1620–1634.

[301] Yang, C., Kang, R., Branson, D. T., Chen, L., and Dai, J. S. (2019). Kinematics and statics of eccentric soft bending actuators with external payloads. *Mechanism and Machine Theory*, 139:526–541.

[302] Yang, K., Qin, N., Zhou, C., Wang, B., Yu, H., Li, H., Yu, H., and Deng, H. (2022a). The study of mechanical behaviors of caprinae horn sheath under pendulum impact. *Polymers*, 14(16):3272.

[303] Yang, S., Dai, J. S., Jin, Y., and Fu, R. (2022b). Finite displacement screw-based group analysis of 3prs parallel mechanisms. *Mechanism and Machine Theory*, 171:104727.

[304] Yang, S., Sun, T., Huang, T., Li, Q., and Gu, D. (2016). A finite screw approach to type synthesis of three-dof translational parallel mechanisms. *Mechanism and machine theory*, 104:405–419.

[305] Yang, Y., Li, Y., and Chen, Y. (2018). Principles and methods for stiffness modulation in soft robot design and development. *Bio-Design and Manufacturing*, 1(1):14–25.

[306] Yano, H., Tamefusa, S., Tanaka, N., Saitou, H., and Iwata, H. (2010). Gait rehabilitation system for stair climbing and descending. In *2010 IEEE Haptics Symposium*, pages 393–400. IEEE.

[307] Yin, G., Zhang, X., Chen, D., Li, H., Chen, J., Chen, C., and Lemos, S. (2020). Processing surface emg signals for exoskeleton motion control. *Frontiers in Neurorobotics*, 14:40.

[308] Yin, Y., Li, Y.-F., Wei, L.-Y., et al. (2016). An improved pso algorithm for residential energy-efficient scheduling considering occupant behavior. *Energies*, 9(1):15.

[309] Yip, M. C., Sganga, J. A., and Camarillo, D. B. (2017). Autonomous control of continuum robot manipulators for complex cardiac ablation tasks. *Journal of Medical Robotics Research*, 2(01):1750002.

[310] Yoon, J., Novandy, B., Yoon, C.-H., and Park, K.-J. (2010). A 6-dof gait rehabilitation robot with upper and lower limb connections that allows walking velocity updates on various terrains. *IEEE/ASME Transactions on Mechatronics*, 15(2):201–215.

[311] Yu, H., Cruz, M. S., Chen, G., Huang, S., Zhu, C., Chew, E., Ng, Y. S., and Thakor, N. V. (2013). Mechanical design of a portable knee-ankle-foot robot. In *2013 IEEE International Conference on Robotics and Automation*, pages 2183–2188. Ieee.

[312] Zhang, K. and Dai, J. S. (2015). Screw-system-variation enabled reconfiguration of the bennett plano-spherical hybrid linkage and its evolved parallel mechanism. *Journal of Mechanical Design*, 137(6):062303.

[313] Zhang, T. and Huang, H. (2018). A lower-back robotic exoskeleton: Industrial handling augmentation used to provide spinal support. *IEEE Robotics & Automation Magazine*, 25(2):95–106.

[314] Zhang, T., Tran, M., and Huang, H. (2018). Design and experimental verification of hip exoskeleton with balance capacities for walking assistance. *IEEE/ASME Transactions on mechatronics*, 23(1):274–285.

[315] Zhang, T., Yang, L., Yang, X., Tan, R., Lu, H., and Shen, Y. (2021). Millimeter-scale soft continuum robots for large-angle and high-precision manipulation by hybrid actuation. *Advanced Intelligent Systems*, 3(2):2000189.

[316] Zhao, B., Zhang, W., Zhang, Z., Zhu, X., and Xu, K. (2018). Continuum manipulator with redundant backbones and constrained bending curvature for continuously variable stiffness. In *2018 IEEE/RSJ International Conference on Intelligent Robots and Systems (IROS)*, pages 7492–7499. IEEE.

[317] Zhao, C., Chen, Z., Song, J., Wang, X., and Ding, H. (2020a). Deformation analysis of a novel 3-dof parallel spindle head in gravitational field. *Mechanism and Machine Theory*, 154:104036.

[318] Zhao, T. S., Dai, J. S., and Huang, Z. (2002). Geometric analysis of overconstrained parallel manipulators with three and four degrees of freedom. *JSME International Journal Series C Mechanical Systems, Machine Elements and Manufacturing*, 45(3):730–740.

[319] Zhao, Y., Song, X., Zhang, X., and Lu, X. (2020b). A hyper-redundant elephant's trunk robot with an open structure: design, kinematics, control and prototype. *Chinese Journal of Mechanical Engineering*, 33(1):1–19.

[320] Zhou, L., Chen, W., Chen, W., Bai, S., Zhang, J., and Wang, J. (2020a). Design of a passive lower limb exoskeleton for walking assistance with gravity compensation. *Mechanism and Machine Theory*, 150:103840.

[321] Zhou, Q., Yang, Z., Li, X., et al. (2020b). An enhanced particle swarm optimization algorithm based on chaotic local search and genetic operators. *IEEE Access*, 8:1036–1048.

[322] Zhu, M., Sun, Z., Chen, T., and Lee, C. (2021). Low cost exoskeleton manipulator using bidirectional triboelectric sensors enhanced multiple degree of freedom sensory system. *Nature communications*, 12(1):2692.